

UNITED STATES AIR FORCE

ADA248774

SUMMER RESEARCH PROGRAM -- 1991

HIGH SCHOOL APPRENTICESHIP PROGRAM (HSAP) REPORTS

VOLUME 11

PHILLIPS LABORATORY  
CIVIL ENGINEERING LABORATORY

RESEARCH & DEVELOPMENT LABORATORIES

5800 Uplander Way  
Culver City, CA 90230-6608

Program Director, RDL  
Gary Moore

Program Manager, AFOSR  
Lt. Col. Claude Cavender

Program Manager, RDL  
Claude Baum

Program Administrator, RDL  
Gwendolyn Smith

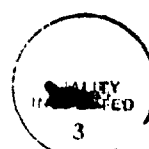
Submitted to:

AIR FORCE OFFICE OF SCIENTIFIC RESEARCH

Bolling Air Force Base

Washington, D.C.

December 1991



Accession For	ITIS CRA&I
STIC TAB	Announced
Justification	
y	Distribution /
Availability Co.	
Dist	Avail and/or Special
A-1	



# REPORT DOCUMENTATION PAGE

Form Approved  
OMB No 0704-0188

Public reporting burden for this collection of information is estimated to average 1 hour per response, including the time for reviewing instructions, searching existing data sources, gathering and maintaining the data needed, and completing and reviewing the collection of information. Send comments regarding this burden estimate or any other aspect of this collection of information, including suggestions for reducing this burden, to Washington Headquarters Services, Directorate for Information Operations and reports, 1215 Jefferson Davis Highway, Suite 1204, Arlington, VA 22202-4302 and to the Office of Management and Budget Paperwork Reduction Project (0704-0188), Washington, DC 20503.

<b>1. AGENCY USE ONLY (Leave blank)</b>			<b>2. REPORT DATE</b> 9 January 1992	<b>3. REPORT TYPE AND DATES COVERED</b> 30 Sep 90-30 Sep 91	<b>4. TITLE AND SUBTITLE</b>  1991 High School Apprenticeship Program (HSAP) Volumes 10-13  <i>Vol 11</i>	<b>5. FUNDING NUMBERS</b>  F49620-90-C-0076
<b>6. AUTHOR(S)</b>  Mr Gary Moore			<b>7. PERFORMING ORGANIZATION NAME(S) AND ADDRESS(ES)</b>  Research Development Laboratories (RDL) 5800 Uplander Way Culver City CA 90230-6608  <i>AFOSR-TR-92 0178</i>			<b>8. PERFORMING ORGANIZATION REPORT NUMBER</b>
<b>9. SPONSORING/MONITORING AGENCY NAME(S) AND ADDRESS(ES)</b>  AFOSR/NI Bldg 410 Bolling AFB DC 20332-6448  Lt Col V. Claude Cavender			<b>10. SPONSORING/MONITORING AGENCY REPORT NUMBER</b>			
<b>11. SUPPLEMENTARY NOTES</b>						
<b>12a. DISTRIBUTION/AVAILABILITY STATEMENT</b>  UNLIMITED			<b>12b. DISTRIBUTION CODE</b>			
<b>13. ABSTRACT (Maximum 200 words)</b>  High school students who live in communities where Air Force laboratories are located have an opportunity to spend eight weeks during the summer doing scientific research at the laboratory. Each student is assigned a mentor from the laboratory. During the summer of 1991 132 students participated in the program. Each student was required to submit a report on their accomplishments. Those student reports were consolidated and bound into this annual report.						
<b>14. SUBJECT TERMS</b>					<b>15. NUMBER OF PAGES</b>	<b>16. PRICE CODE</b>
<b>17. SECURITY CLASSIFICATION OF REPORT</b>  UNCLASSIFIED	<b>18. SECURITY CLASSIFICATION OF THIS PAGE</b>  UNCLASSIFIED	<b>19. SECURITY CLASSIFICATION OF ABSTRACT</b>  UNCLASSIFIED	<b>20. LIMITATION OF ABSTRACT</b>  UL			

## PREFACE

Reports in this document are numbered consecutively beginning with number 1. Each report is paginated with the report number followed by consecutive page numbers, e.g., 1-1, 1-2, 1-3; 2-1, 2-2, 2-3.

This document is one of a set of 13 volumes describing the 1991 AFOSR Summer Research Program. The following volumes comprise the set:

<u>VOLUME</u>	<u>TITLE</u>
1	Program Management Report
<i>Summer Faculty Research Program (SFRP) Reports</i>	
2	Armstrong Laboratory, Wilford Hall Medical Center
3	Phillips Laboratory, Civil Engineering Laboratory
4	Rome Laboratory, Arnold Engineering Development Center, Frank J. Seiler Research Laboratory
5	Wright Laboratory
<i>Graduate Student Research Program (GSRP) Reports</i>	
6	Armstrong Laboratory, Wilford Hall Medical Center
7	Phillips Laboratory, Civil Engineering Laboratory
8	Rome Laboratory, Arnold Engineering Development Center, Frank J. Seiler Research Laboratory
9	Wright Laboratory
<i>High School Apprenticeship Program (HSAP) Reports</i>	
10	Armstrong Laboratory
11	Phillips Laboratory, Civil Engineering Laboratory
12	Rome Laboratory, Arnold Engineering Development Center
13	Wright Laboratory

# 1991 HIGH SCHOOL RESEARCH REPORTS

## Phillips Laboratory, Civil Engineering Laboratory

<u>Report Number</u>	<u>Report Title</u>	<u>Author</u>
<u><i>Phillips Laboratory</i></u>		
<b>Astronautics Laboratory (ASTRO)</b>		
1	Nitinol, Shape Memory, and Space Applications	Jessica Gardner
2	Specific Impulse Calculations for Clean Solution Propellant Compositions	Jacqualynn Hearne
3	The Synthesis of Aminopropyltriethoxysilane-Terminated Poly Imides	Debra Meyer
4	LEAP into Engineering	Diane Monaghan
5	Using the I-DEAS' Automatic Mesher	Steven Olkowski
6	WLF Shift Programs	Joseph Padilla
7	Liquid Crystal Polymers	Jason Phillips
8	Study of HX-4000 and Tensile Testing of Liquid Crystal Polymers	Tracy Reed
<b>Geophysics Laboratory (GEO)</b>		
9	Analysis of Model Output Statistics Thunderstorm Prediction Model	Frank Lasley
10	Equatorward Boundaries of Nightside Aurorae	Jeremy Liebowitz
11	Solar Terrestrial Interactions	Galen McKinley
12	Temperature, Kinetic Energy, and Internal Energy Dependences and Isotopic Effect for the Reaction of Cl- with CH <sub>3</sub> Br	John Paschkewitz
13	Ionospheric Effects on Radio Signals	Jeffrey Roth
14	Final Report 1991	Paul Swietek
<b>Weapons Laboratory (WL)</b>		
15	Polarization of Laser Light in a Double Conjugate Mirror Experiment	Mara Collins
16	Interfacing Neural Network Programs with KHOROS Environment	Eric Eidson
17	Experimenting with Fractals and Careers	Eric Engberg
18	Summer Apprenticeship in the Chief Geologic Response Section	Matthew Firstenburg

<u>Report Number</u>	<u>Report Title</u>	<u>Author</u>
<i><u>Phillips Laboratory (cont.)</u></i>		
19	TEM Stage Collectors, LDEF Samples, and a Summer at Kirtland AFB	Russell Grubbs
20	Adventures in High Energy	Brad Karmiol
21	Comparison of Seismic Refraction and Borehole Data with Different Computer Interpretation Programs to Determine a Suitable Site for Pile Testing	Kerim Martinez
22	Experiment Versus Theory - Marauder and Mach 2	Brian Rizzoli
23	Holography	Dawn Vernooy
24	Surface Quenching of Singlet Delta Oxygen on a 90% Nickel/10% Copper Alloy	Evan Werkema

*Civil Engineering Laboratory*

Engineering & Services Center (ESC)		
25	Kinetics of Hydroxyl Radical Photodegradation of 2-Butanone (Methyl Ethyl Ketone) Under Simulated Atmospheric Conditions	Jennifer Brewer
26	Working at Tyndall Air Force Base	Nirmala Darmarajah
27	Compugraphic Integrator's Capability	Philip Dorsch
28	HSAP Final Report	Richard Hartzler
29	Long Range Agent Delivery System: Summer 1991 Development	Thor Johnson
30	Plasmids	Jerome Lindsay
31	HSAP Final Report	Brent Miller
32	Finite Element Pre-Processing, Analysis, and Post-Processing on a 3-Dimensional Graphics Workstation	Johnathan Protz
33	High Heat Effects Resulting from Auxiliary Propulsion Unit	David Summey
34	Not Available at this Time	Amy Thomas

NITINOL, SHAPE MEMORY, AND SPACE APPLICATIONS

Jessica Gardner

ABSTRACT

Shape memory describes the ability of certain metal alloys to be deformed at low temperatures and return to their original shapes upon heating. This phenomenon is not a new technology, however, since its discovery in 1962 by scientists at the Naval Ordnance Research Laboratory, applications have not yet reached their full potential. To date, the nickel-titanium alloy, which best demonstrates shape memory, has been used in eyeglass frames, as an implant material in orthopedics, and in the brackets used for orthodontic therapy. Missile guiding systems and airplane systems have also utilized the shape memory effect.

Because of their unique properties, amazing strengths, and extremely light weights, shape memory alloys also have many applications in space. These include a ball and socket system to assemble composite tubing and a latching system for assembling cross-types of structures in composite tubing. Shape memory alloys can also be used as actuators to erect folding protective shells.<sup>1</sup> This paper describes a novel application of nitinol, a shape memory alloy, as the primary power source in a direct current motor.

## INTRODUCTION

The ability of the nickel-titanium shape memory alloy to be trained to "remember" a specific shape has led to the development of a nitinol motor. The nitinol motor utilizes the shape memory effect to create continuous motion without the use of a conventional motor. The concept of a nitinol motor is appealing because it limits not only weight, but complexity. The nitinol motorless motor is much simpler than the everyday electromagnetic motor. No longer is there a need for permanent magnets, brushes, and commutators.

The design of the motorless motor is very simple. A nickel-titanium wire can be trained to remember the shape of a spring. The same wire, after being deformed (pulled straight), can be heated and forced to remember and return to its previous shape, a spring. The force the wire exerts as it contracts back to the shape of a spring is enough to extend an opposing stainless steel spring (see Figure 1). When the nickel-titanium wire is allowed to cool, the stainless steel spring takes control, pulling the shape memory wire straight. These events are the basis of the design of the nitinol motor.

## THEORY

Nickel-titanium alloys, commonly referred to as nitinol, have a unique ability to "remember" a shape, even after undergoing severe deformations. When deformed at low temperatures, they stay deformed until heated, when they spontaneously return to their original form.

The basis for this shape memory effect is that these materials can easily transform to and from martensite. 2

At the microscopic level, there are two types of solid state transformations: diffusional and displacive. Diffusional transformations involve random atomic migration. Displacive transformations are merely cooperative rearrangements of atoms, creating a new, more stable crystal structure. Most importantly, displacive transformations do not change the chemical nature of the matrix. Displacive transformations are also called athermal transformations because the phase change is dependent only on temperature, and not the length of time at a certain temperature. It is important to note that martensitic transformations are displacive, or athermal.

The transformation from austenite to martensite happens in two parts: Bain strain and lattice-invariant shear. The Bain strain, often called lattice deformation, includes the entire series of movements needed to form a new structure. It usually consists of several small atomic shuffles or sidesteps. The second step, lattice-invariant shear, involves either twinning, a folding of the atoms, or slipping of the atoms to accommodate volume and shape changes. Twinning is not able to accomodate significant changes in volume, but it does support reversible shape changes unlike the slipping process, which is a permanent deformation. Consequently, for shape memory to occur, twinning must be the principal process of accomodation. 3

As previously stated, shape memory requires that a martensitic phase change occur. When a shape memory metal is deformed in the low temperature state (martensite), the strain is stored through the twinning process. The new twinned structure is not very stable and

functions only to allow the transformation. When the metal is heated and transformed to austenite, the deformation is reversed because the austenite cannot support any twinned structure (see Figure 2). Thus, any deformation of the martensite that can be accommodated by the twinning process is reversible.

It is this reversibility that supports the concept of a motorless motor. A nitinol wire can be shaped into a spring and heated past its transformation temperature, causing the alloy to "remember" the spring shape. When the spring shape of the nitinol is distorted, the wire can be reheated, forcing it to assume its austenite structure, in this case, a spring shape. This reversibility from distortion to spring shape is an essential process in the design of the motorless motor.

There are many different types and sizes of nitinol wire. For the purposes of this experiment, five mil diameter wire was found to have the required range of activating force. The nitinol motor requires that the nitinol spring, when heated, overcomes the force of the stainless steel spring. However, after the nitinol spring has pulled and reached its maximum deflection, the stainless steel spring must be able to pull the nitinol spring straight. For this to happen, the nitinol wire must cool fairly rapidly so the opposing spring will be able to deform it. It is for this reason that a thin wire was chosen over a thicker one.

The length and diameter of the nitinol spring are also very important factors contributing to the action of the nitinol motor. It is obvious that longer springs will pull more because they have more coils, but how does the diameter of the spring affect its pull? This question is easily answered by Castigliano's Theorem as follows. Strain energy is defined as  $U$ , and  $U_1$  is the tension/compression component of

strain energy. The torsional component,  $U_2$ , will be neglected due to the fact that the mean diameter of the spring is much greater than the diameter of the wire (about 100 times as large). In addition, the nitinol is prestrained so that it never approaches a coil-bound configuration.

According to the equations shown below, it is apparent that a spring with a relatively large coil diameter will deflect more than a spring with a smaller diameter.

$$U_T = U_1 + U_2 \quad (1)$$

$$U_1 = F^2 L / 2AE \quad (2)$$

In equation (2), A is cross-sectional area, while E is the Young's Modulus, and L is the length of the coiled spring. The deflection of a spring due to an applied force is given as:

$$y = dU/dF \quad (3)$$

Equations 1, 2, and 3 combine to give the following equation for deflection, where again the  $U_2$  torsional component is neglected:

$$y = 8FD^3N/d^4G, \quad (4)$$

where N is the number of coils in the spring, L is the mean diameter, G is the shear modulus, F is force, and d is the diameter of the wire.<sup>5</sup>

From equation 4, it can be seen that the deflection of the spring is heavily dependent on the coil diameter, which is to the third power. By changing this parameter, we can get different deflections.

#### EXPERIMENTAL PROCEDURE

The experimental part of this project began with discovering an effective method of nitinol training. Eventually, a procedure developed

and was followed for each new piece of nitinol. The piece of nitinol, five mils in diameter and approximately 60 inches long, was wrapped around the threads of a brass bolt with a half inch diameter. Both ends of the nitinol wire were clamped tight between two nuts. Then, at each end of the nitinol, the bolt was heated with a propane torch for seven minutes. Next, the hot bolt, with the nitinol still attached, was placed under running water until it was cool enough to touch. This caused a "freezing" of the austenite molecular configuration. The nitinol wire was then unwound from the bolt and stretched lightly.

To insure that the wire remembered the shape of a spring, it was heated using a triple output power supply. Each end of the wire was attached to a lead from the power supply, which was set at zero volts. After the power supply was turned on, the voltage was gradually increased until it reached eighteen volts and the nitinol coiled to its spring shape. The power supply was then turned off and the nitinol was allowed to cool. At this time, the nitinol was lightly stretched again. The nitinol wire went through this cyclic process of heating, cooling, and stretching seventy-five times to rid it of any hysteresis.

The assembly of the actual mechanism began with a 12" x 7" plexiglass base plate. Then, a plexiglass block (3" x 1" x 1") was prepared. A groove was cut into the middle of the top of the block (.5" deep x .5" wide) and a composite bushing was press fitted across it. The block was then glued to the end of the base plate, in the middle. The switch and the bearing were placed at the other end of the base plate, in alignment with the plexiglass block.

Two inches from the end of the plate and two and a half inches from its side, a hole was tapped for the bearing. The bearing was

supported by a three inch bolt which was screwed into the plate and tightened with a nut (see Figure 3). Two washers were placed under the nut to clamp one end of the nitinol and keep the threads of the bolt from cutting the wire. The bearing had an aluminum arm attached to it with a screw for activating the switch and clamping the other end of the nitinol. There was a separate screw on the other side of the bearing where the stainless steel spring attached.

Next, a two and a half inch tall copper contact post was press-fitted to the plate. It was placed one inch from the end and four and three tenths inches from the same side as the bearing. Attached to the contact post was a wire spring that acted as the on/off switch for the current. The wire spring was simply soldered to the contact post and hand-shaped until it made acceptable contact with the gate (see Figure 4).

Finally, the gate was attached to the plate, two inches from the end and four and a half inches from the same side as the bearing. The gate was made from a quarter inch diameter composite rod that was three inches tall. The upper inch of the rod was made into a bushing so the gate could pivot. A very thin aluminum plate was glued to the rotating piece of composite and was bent to form a "V" shape. One end of a conductive wire was attached to the back of the aluminum plate, and the other end was attached to the screw holding the arm on the bearing. The other end of the stainless steel spring was attached to the composite rod, about an inch and a half from the base.

After all the pieces were attached to the base plate, the nitinol wire was connected. First, it was fastened with the screw holding the

arm on the bearing. Then, it was strung to the block on the opposite side of the plate and looped around the horizontal bushing. It was pulled from the bushing down to the base of the bearing bolt and slipped between the two washers. The nut above the washers was tightened so the wire was taut, but the arm was still making contact with the gate and the contact post.

When all assembly had been completed, the leads from the power supply were attached. One lead was clamped to the bottom of the contact post, and the other lead was attached to the nitinol wire just before it went between the two washers, making a circuit through the nitinol when the gate was closed. The power supply was set for eighteen volts.

#### RESULTS

When the power supply was turned on, the current ran up the contact post and passed through the wire spring to the gate. The current passed through the conductive wire to the screw holding the arm and the nitinol on the bearing. The nitinol wire heated up and pulled, turning the bearing. When the bearing rotated far enough, the arm pushed the other side of the gate, causing it to break contact with the wire spring. Since the nitinol wire was no longer receiving any current, it cooled.

As the nitinol was cooling, the stainless steel spring took control and deformed the nitinol spring while it pulled the bearing back to its starting position. When the bearing reached its starting position, the gate made contact with the wire spring, and the path for

the current was completed once again. These events are repeated until the power supply is turned off and no more current is flowing.

#### CONCLUSION

Even though the nitinol motor is not perfect, it is functional and it shows great promise. Further research and development might benefit from the following suggestions. The stainless steel spring attachments should be made permanent, along with the gate, the contact post, and the wire spring. The gate, the bearing, and the contact post could be shortened to provide for more stability. The bearing could be attached to something other than a threaded bolt to ensure the safety of the nitinol wire. Finally, the motor could be run on two nine volt batteries in series instead of the power supply. This would enable the motor to travel as a demo.

References

1. Stoekel, Dieter : Tinel Shape Memory Alloys, 2-13 (1990)
2. Duerig, T.W.; Melton, K.N.: Systematizing the Application of Shape Memory, 1-3 (1990)
3. Wayman, C.M.; Duerig, T.W.: An Introduction to Martensite and Shape Memory, 3-5 (1990)
4. Shigley, Joseph; Mischke, Charles R.: Mechanical Engineering Design, 415-418 (1989)

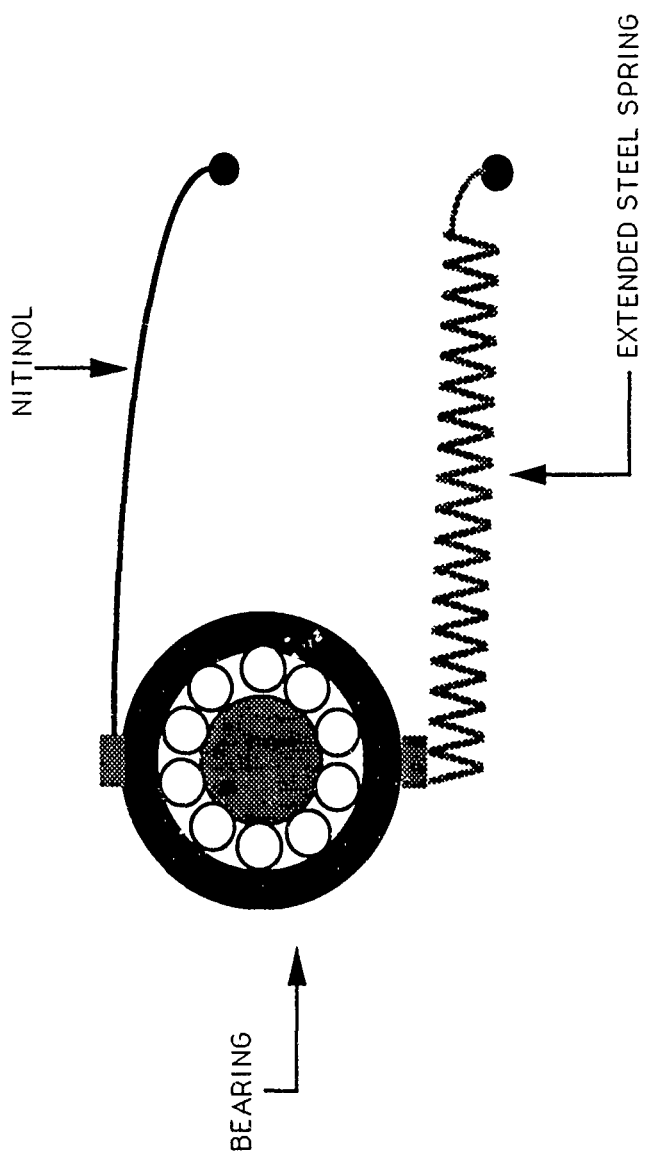


FIGURE 1

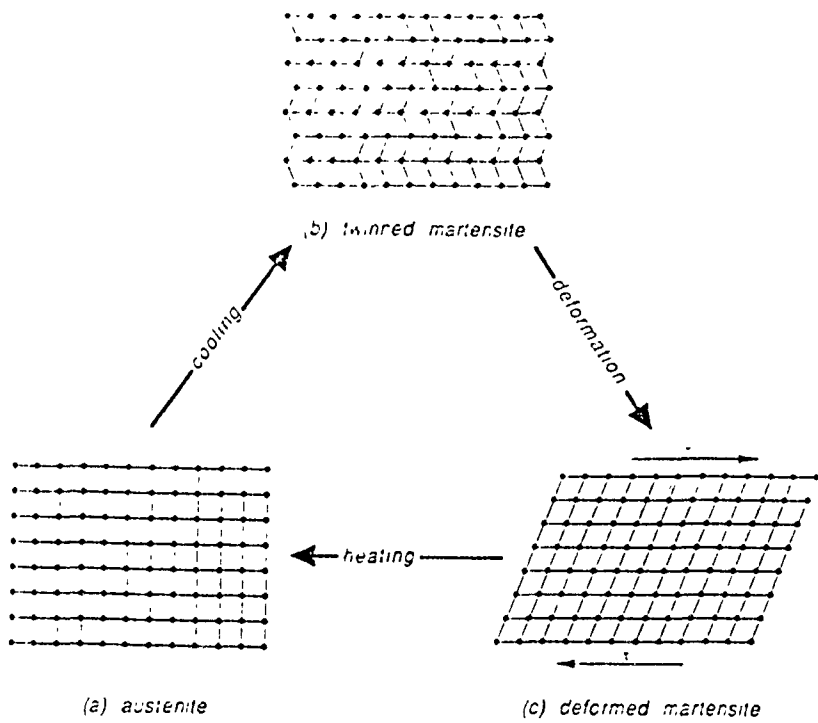


FIGURE 2

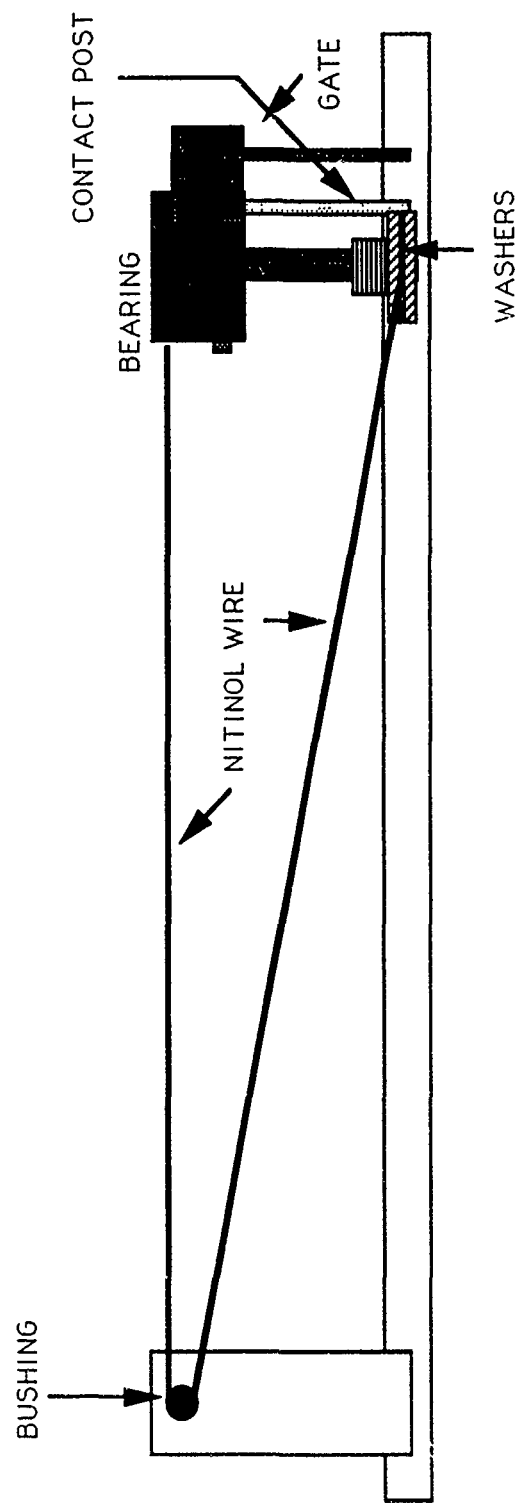


FIGURE 3

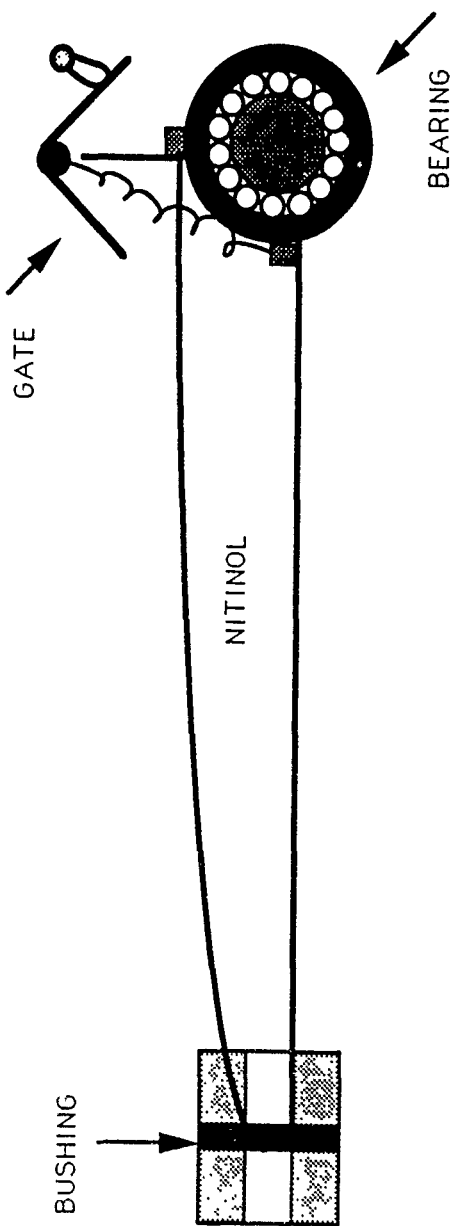


FIGURE 4

**SPECIFIC IMPULSE CALCULATIONS FOR  
CLEAN SOLUTION PROPELLANT COMPOSITIONS**

**Jacqualynn Leilani Hearne  
ID# 699  
AFOSR / HSAP  
July 12, 1991**

## SPECIFIC IMPULSE CALCULATIONS FOR CLEAN SOLUTION PROPELLANT COMPOSITIONS

Specific Impulse Calculations For Clean Solution Propellant Compositions  
Jacqualynn L. Hearne

### **ABSTRACT**

During my work at Phillips Laboratory, I examined theoretical specific impulses of potential clean solution propellant compositions. The data that I came up with, would help to determine which oxidizer and polymer/matrix would work best to make a good, clean solution propellant.

### **INTRODUCTION**

A clean solution propellant is prepared by using a liquified oxidizer and a high molecular weight polymer, the polymer should be capable of swelling in the presence of an oxidizer. During this process, the substance ultimately undergoes a physical process of gellation to form a cured solid propellant. The clean propellant contains no metals or halogens. This type of propellant is a good idea because it is environmentally safer than conventional solid propellant.

The metals, which occur in other propellants, cause particulate matter to flow into the atmosphere. The halogens act to eliminate ozone and also make acid rain. With both of these components in a propellant, they increase the performance of the propellant, which is nice, but we are more concerned with a clean type of propellant that would help the environment. Theoretically finding a beneficial clean solution propellant has been the basis for my project this summer.

Current clean solution propellant compositions that are being examined by Aerojet and Phillips lab contain polyvinyl-alcohol (PVA) and stabilized hydroxylammoniumnitrate (S-HAN5). This system has an Isp of 245, which is below that of typical solid propellant (Advanced Solid Rocket Motor-ASRM- has an Isp of 264).

#### **PROCEDURES**

Before I began my theoretical calculations, I found out that not many clean solution propellants had been made. This meant that I had to do some research to find out what types of polymers and oxidizers would make the best solution. I found out, from my mentor that I should use polymers that could swell in a liquid oxidizer (an aqueous or salt solution). Then we chose a variety of oxidizers which may be used to prepare a liquid composition. (The best oxidizers are ones with low melting points).

After acquiring this information, I started doing the calculations on a computer program called Theoretical Isp Program. I read about the program in a pamphlet, Theoretical Isp Program Documentation. This pamphlet is the Beckman and Acree Microcomputer Version by Christopher E. Gazze.

First of all, I had to create input files for the different combinations of polymers and oxidizers. In these files I had to include the chemical's names, heat of formation, density and chemical formula, under a library heading. Then I selected the ingredients, from the list in the library heading, that I was going to use for the first calculation. Having selected the ingredients, I had to tell Isp how much of each ingredient to

use.

I did optimizations of the polymer/oxidizer combinations. I did this to find out the optimum for each combination without running the program over and over again. With this optimization technique all I had to do was tell the computer how much of each ingredient to use and at what increments to change the amounts of each ingredient.

For example, I would use PVA (a polymer) and S-HAN5 (an oxidizer). I would start off with PVA at 98% and S-HAN5 at 2% and go by increments of 2, so that PVA would go to 96%, 94%, and so on until it got to 2%.

After these calucations were finished, I would write down the theoretical specific impulses (Isp) and make plots to show each polymer/oxidizer combination at each increment. These plots gave my mentor and I a pretty good idea of which combinations of ingredients would theoretically make the best clean solution propellants.

## RESULTS

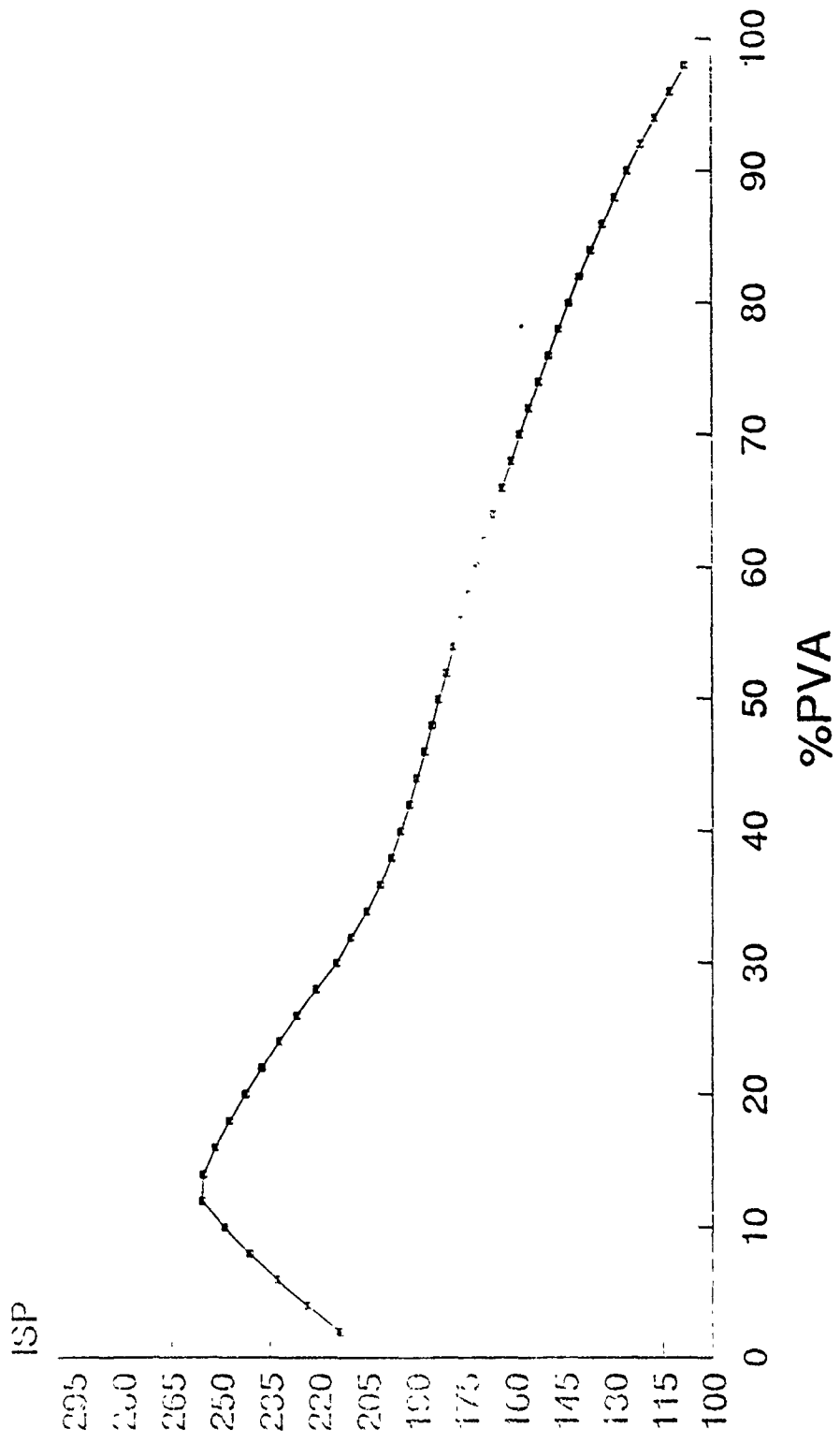
<u>Polymer/Matrix</u>	<u>Oxidizer</u>	<u>Polymer/Oxidizer (ratio)</u>	<u>Isp</u>
PVA at-61 Delta hf	S-HAN5	34/66	254
PVA at-49 Delta hf	S-HAN5	14/86	245
PVA at-39 Delta hf	S-HAN5	14/86	247.5
PVA at-29 Delta hf	S-HAN5	14/86	250.1
PVA at-19 Delta hf	S-HAN5	14/86	252.6
PVA at-09 Delta hf	S-HAN5	14/86	255.2
PVA at-49 Delta hf	GDN	2/98	237.5
" " "	HNF	8/92	270
" " "	ONDO	4/96	268.8
" " "	ADN	12/88	255.8
ETHOCEL	ADN	8/92	257.3
" " "	GDN	2/98	234.3
" " "	HMX	2/98	261.7
" " "	HNF	4/96	270

"	"	"	S-HAN5	8/92	238.1
PAM			ADN	14/86	257.4
"	"	"	GDN	2/98	238
"	"	"	S-HAN5	16/84	241.3
PEG			ADN	14/86	260.1
"	"	"	GDN	2/98	236.4
"	"	"	S-HAN5	14/86	246.7
PEI			ADN	10/90	262.2
"	"	"	GDN	2/98	237.3
"	"	"	HNF	6/94	273.3
"	"	"	ONDO	4/96	270.5
"	"	"	S-HAN5	12/88	245.7
PVAM			ADN	10/90	262.8
"	"	"	GDN	2/98	237.4
"	"	"	HNF	6/94	273.6
"	"	"	S-HAN5	12/88	246.5

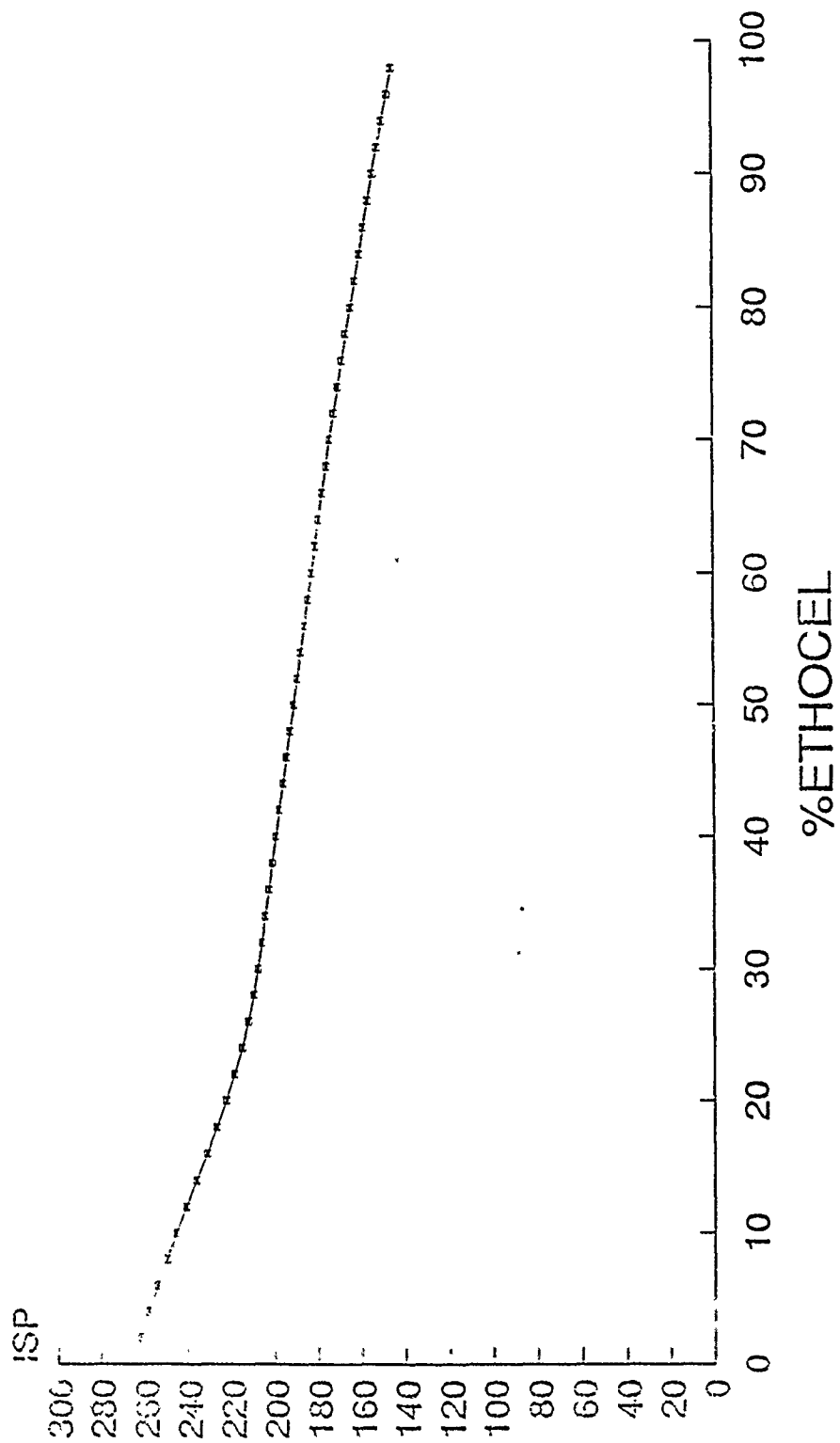
### CONCLUSION

My results have led me to believe that HNF mixed with PVA, PVAM, PEI, or ETHOCEL would give a theoretical first rate clean solution propellant. In my opinion, I think that HNF is a good oxidizer to react with polymers. Maybe my mentor can go on with this study.

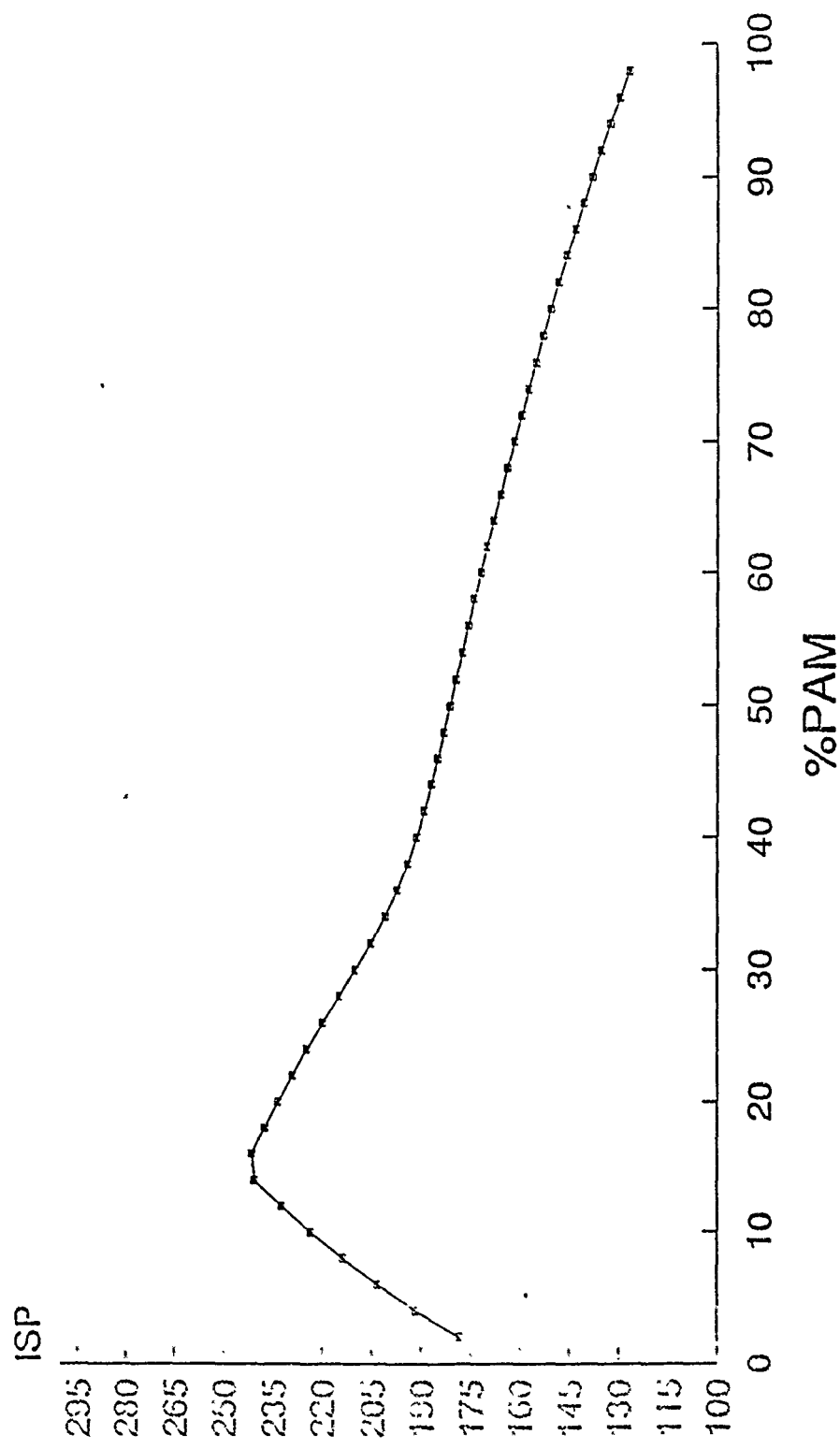
# ADN / PVA



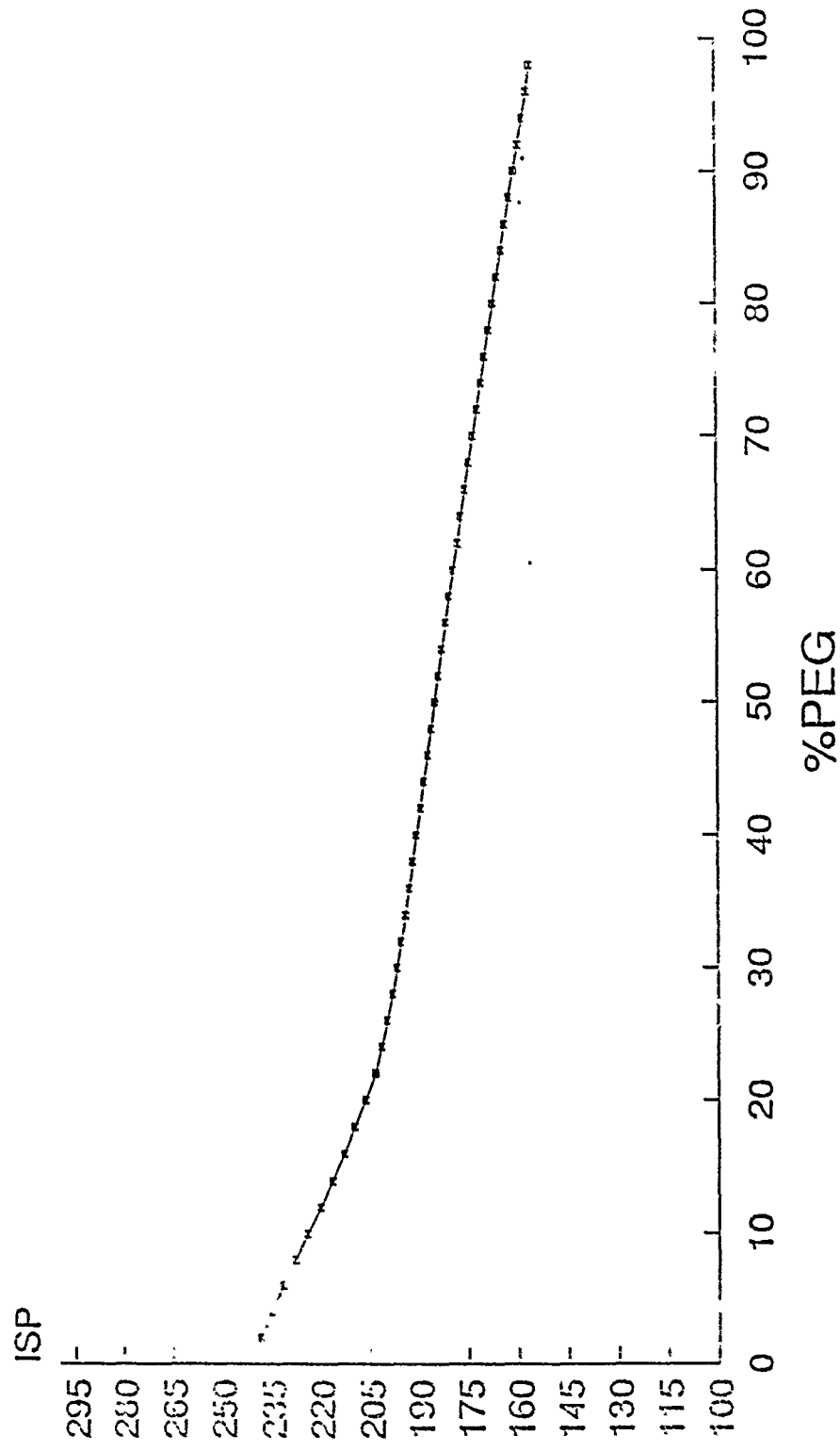
# HMX / ETHOCEL



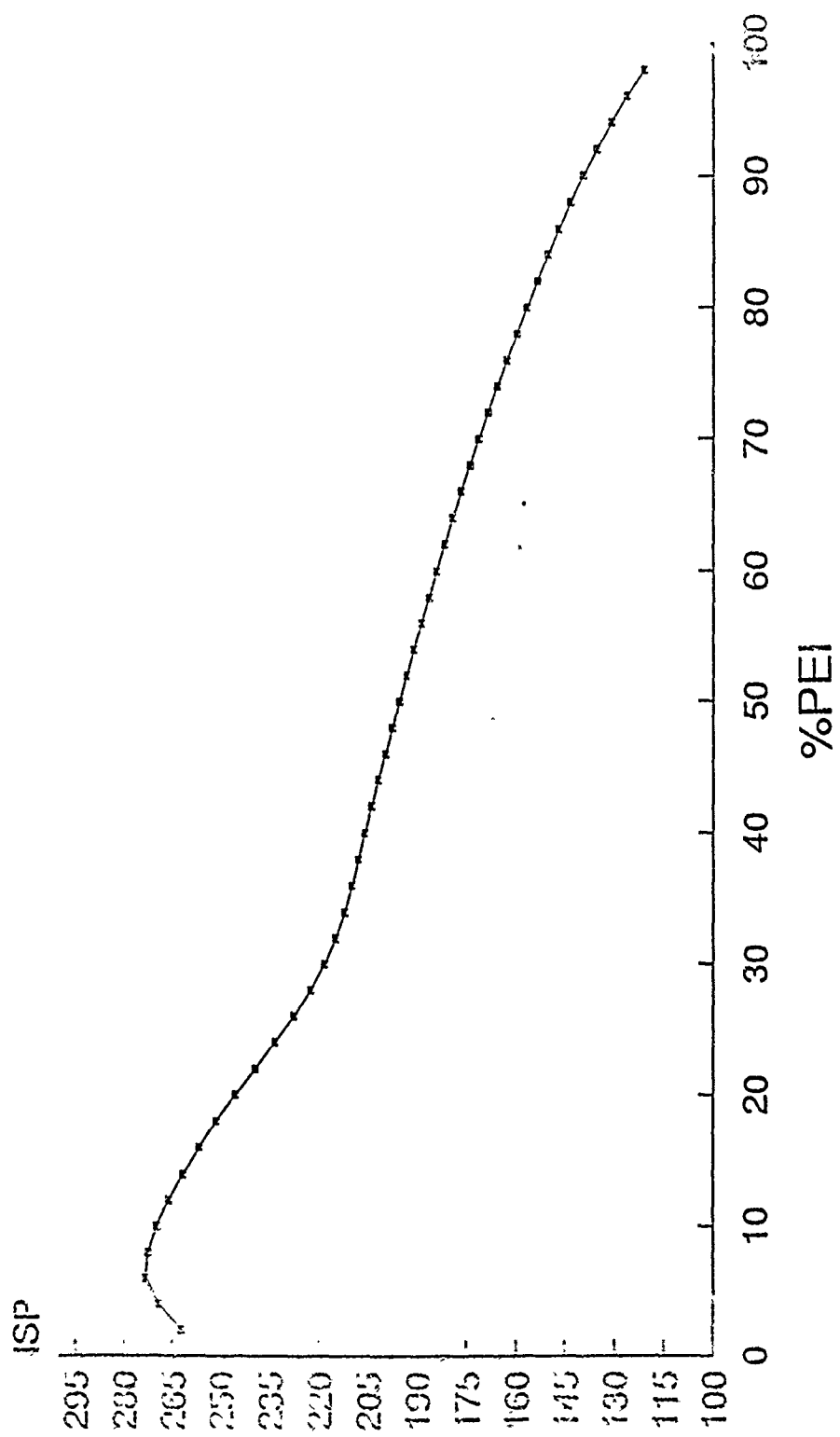
# S-HAN5 / PAM



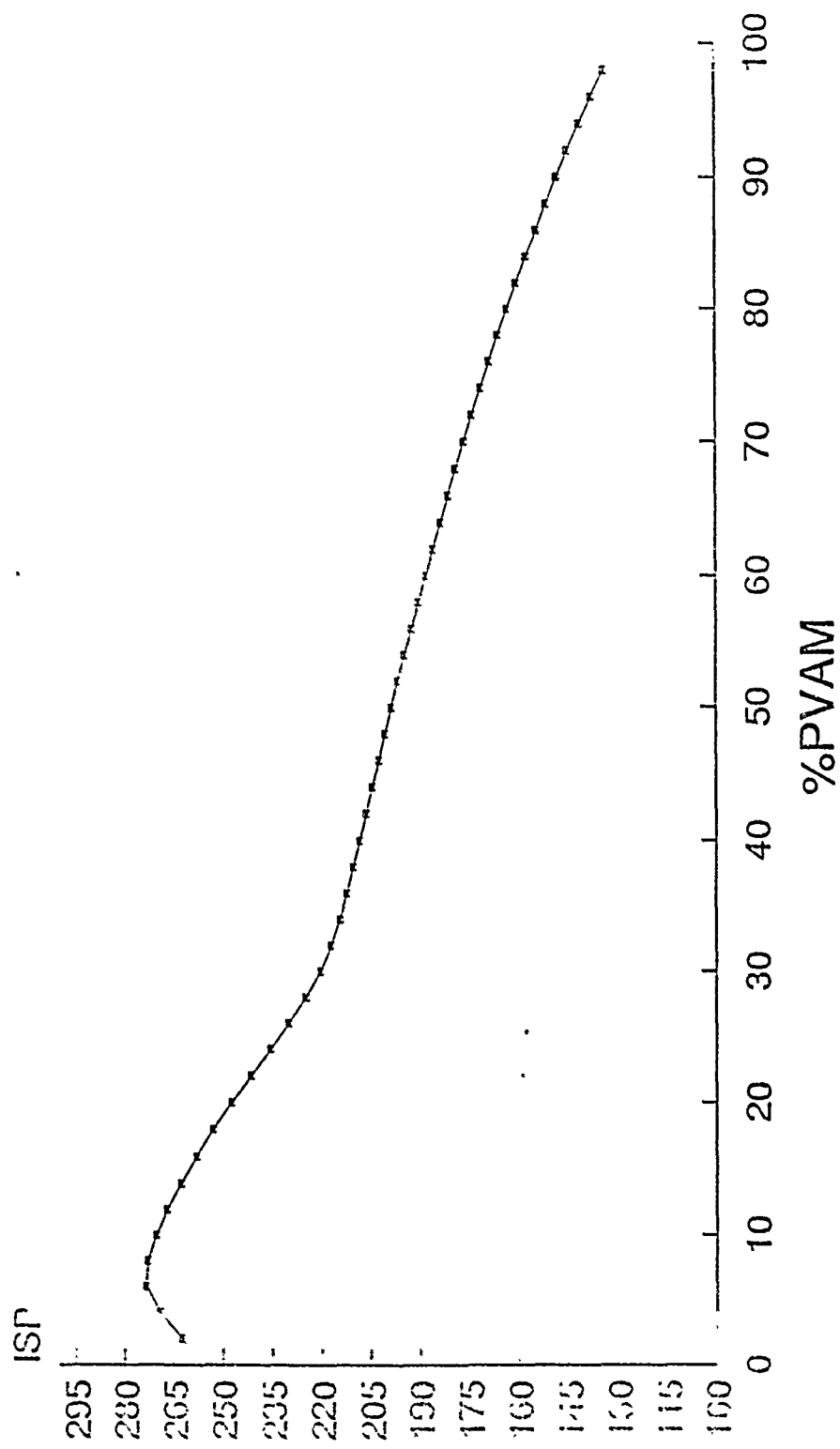
# GDN / PEG



# HNF / PEI



# HNFE / PVAM



## 1991 SUMMER RESEARCH PROJECT AT PHILLIPS LABORATORY

Debra Meyer

### SUMMARY

over the past eight weeks, I have been studying the synthesis of aminopropyltriethoxysilane-terminated poly imides. This had two parts. First, a simple monomeric model compound was synthesized to test the synthetic methods planned to use for the polymer synthesis. Secondly, a small molecular weight polymer was synthesized to further investigate these synthetic methods and characterization parameters. In order to characterize the compounds synthesized, I learned to operate the fourier-transform nuclear magnetic resonance spectrometer (FT-NMR) and fourier-transform infrared spectrophotometer (FTIR).

## INTRODUCTION

Studies have shown that the low earth orbit (LEO) atmosphere at altitudes between 200 and 600 km consists mostly of atomic oxygen. Recent Space Shuttle flights have shown that interactions between spacecraft surfaces and high velocity oxygen atoms within the low earth orbital environment can produce significant changes in surface properties of many materials resulting in surface degradation. Future long-term missions in the low earth environment will require atomic oxygen stable coatings/materials.

Polymers coatings and materials have been investigated for their atomic oxygen resistance. Polymers must be capable of sustaining high loads and stresses over long periods of time and broad ranges of temperature to be acceptable materials for advanced structures. Good environmental stability, fatigue, and impact resistance are very important. Many of the organic polymers experience rapid erosion in the low earth orbit environment encountered in space missions. This effect is particularly damaging for materials facing the direction of flight. Fluorinated polymers and silicon polymers have shown good resistance to oxygen atom degradation. Poly(imide siloxane) polymers have recently been shown to exhibit excellent atomic oxygen resistance.

Advancing science has attempted to combine the physical properties of polymeric and ceramic systems to develop a new class of materials. By incorporating the hardness of an inorganic glass and the flexibility of a polymer into one material, the resulting organic/inorganic material may have good impact resistance in addition to being transparent, scratch, and atomic oxygen resistant.

Earlier this summer, the synthesis of a new poly(imide siloxane) polymer which has aminopropyltriethoxysilane end groups was attempted in this lab. This polymer will eventually be reacted with tetraethoxyorthosilicate to tie it into an organic glass network. Standard methods for poly(imide siloxane) synthesis were used. The resulting product could not be characterized due to the complicated nature of the target poly(imide siloxane). Not only were several monomers involved, but these monomers react to form the polymer chain by different reactions which occur in one pot. It was not at all clear what the structure of the final polymer was. It was uncertain whether the ethoxy groups of the aminopropyltriethoxysilane end groups had survived the synthetic steps to the final imide.

The objective of this project was to better understand the synthesis of a poly(imide siloxane) polymer with aminopropyltriethoxysilane end groups and to investigate the chemistry of much simpler, "model" compounds which can easily be characterized. This could also help determine whether the ethoxy groups of the aminopropyltriethoxysilane would survive the variety of reaction conditions they would be subjected to in the poly(imide siloxane) polymer synthesis.

#### REFERENCES

1. H. Schmidt, H. Scholze, and G. Tunker, Journal of Non-Crystalline Solids, 80, 557 (1986).
2. A. Garton, P.D. MacLean, W. Wiebe, and J. Densley, J. Appl. Polym. Sci., 32, 3941 (1986).

3. L.J. Leger, J. Visentine, and B. Santos-Mason, Proc. 18th International SAMPE Technical Conference, 1015 (1986).
4. A. Garton, W.T.K. Stevenson, and P.D. McLean, Materials and Design, 7, 319 (1986).
5. G.S. Arnold, D.R. Peplinski, and F.M. Cascarano, J. Spacecraft, 24, 454-458 (1987).
6. A. Garton, P. McLean, and WTK Stevenson, Polym. Prepr., 29, 104-105 (1988).
7. L.J. Leger, "Oxygen Atom Reaction with Shuttle Materials at Orbital Altitudes", NASA TM-58246 (1982).
8. L.J. Leger, I.K. Spiker, J.F. Kuminecz, T.J. Ballentine, and J.T. Visentine, "STS Flight 5 LEO Effects Experiment - Background Description and Thin Film Results", AIAA Paper 83-2631, Oct. 1983.

## EXPERIMENTAL

The instruments used for characterization were the Bruker AMX-300 FT-NMR spectrometer, Mattson Galaxy 4020 FT-IR spectrophotometer, DuPont 910 Differential Scanning Calorimeter (DSC), and the DuPont 951 Thermogravimetric Analyzer (TGA). The DSC and TGA were conducted by Paul Jones and Robert F. Cohn.

Starting materials were used without further purification unless indicated. The Tetrahydroendo-furan (THF) was distilled from Na/K/benzophenone and dimethyl acetamide (DMAC) was distilled from calcium hydride.

1. Synthesis of the imide from phthalic anhydride (PA) and aminopropyltriethoxysilane (APTES).

A. synthesis of amic acid

procedure:

The first step of this reaction was to purge the system with nitrogen. Then 4.036g of PA was put into the flask. At first 6ml of THF was added, but this was not enough to dissolve the PA, so an additional 5ml was added. In the addition funnel 6.025g of APTES and 3ml of THF were added. Nitrogen was sent into the addition funnel to relieve the vacuum created as the fluid level dropped. This solution was stirred at room temperature overnight.

B. synthesis of imide

procedure:

In the second step of this reaction 3.95ml of TFAA was added. This refluxed in THF for 4 hours. Then the solution was rotavaped and put on the high vacuum to remove the solvent.

2. Synthesis of the poly imide from 4, 4' hexafluoroisopropylidene and 3-aminophenyl.

A. synthesis of amic acid  
procedure:

The first step of this reaction was to purge the system with nitrogen. 7.820g of 6F was then dissolved in 50ml of DMAc. The DDS solution was slowly added to a stirred solution of 6F. The solution turned a bright yellow color when the DDS was added. This was allowed to stir for 2 hours at room temperature.

The next step was to slowly add 4.1ml of APTES to the reaction mixture and slowly rinse the addition funnel with 2ml of THF. This was allowed to stir overnight.

33.75% of the reaction mixture was removed leaving 66.25%, 5.84mmol.

B. synthesis of imide  
procedure:

The second step of this reaction was to take the existing mixture and add 5.22ml of TFAA. When TFAA was added the color turned yellow and the flask became warmer. It refluxed for approximately 4 hours and as time passed the color became darker. At this point it was rotavaped and then put on the high vacuum to remove the solvent.

## RESULTS AND DISCUSSION

NMR spectra for Amic Acid A, Imide A, Amic Acid B, and Imide B

Amic Acid A: Analysis of the  $^1\text{H}$ -NMR of the amic acid shows it to be impure, containing the amic acid, residual THF solvent, and unreacted APTES starting material. The numerous resonances in the aromatic region also suggest that more than one type of aromatic structure is present.

The product needs to be further purified.

Imide A:  $^1\text{H}$ -NMR of the imide product shows it to be impure. Possible peak assignments are as indicated. The imidization of the amic acid would result in about the same spectrum with the aromatic region, but analysis of the aromatic region shows basically two peak areas, the largest being very asymmetric. Imidization has occurred to either no extent or some small extent. Peaks at 4.40 ppm (q) and 1.29 (tr) indicate an ethoxy group, which is consistent with the ethoxy resonances of ethyl trifluoroacetate. We believe that the trifluoroacetic anhydride used as a water scavenger in the imidization reaction reacts with the ethoxy groups of the aminopropyltriethoxysilane.

These results show that another method for the imidization reaction should be used. Trifluoroacetic anhydride appears to decompose the amic acid.

Amic Acid B:  $^1\text{H}$ -NMR shows that the product sample is not pure. It contains substantial amounts of the reaction solvent dimethylacetamide (d 1.94 ppm (s, 3H), 2.77 (s, 3H), 2.93 (s, 3H)).

Many other peaks are also present but are not identifiable due to the low concentration in the sample tube.

Product needs to be further purified by room temperature, high vacuum distillation to residual dimethylacetamide solvent.

Imide B:  $^1\text{H-NMR}$  shows that the product sample contains a significant amount of the reaction solvent dimethylacetamide. Also, the absence of peaks in the aromatic region (approx. 7-9 ppm) indicates that the product contains no phenyl protons, which is not at all expected (the target imide contains several phenyl protons). Resonances at  $\delta$  1.042 ppm (tr, 3H) and 3.43 (q, 2H) indicate an ethoxy group, but the peaks for the aminopropyltriethoxysilane IU are absent. This would indicate that the ethoxy groups are no longer connected to the silicon. Peaks at  $\delta$  1.75 ppm (m, 4H) and 3.59 (m, 4H) are possibly residual THF.

Based on the  $^1\text{H-NMR}$  of this product, it is not clear what exactly went on with the reaction. It should be run again.

### NMR Spectra for Starting Materials

These spectra were taken to make sure that the starting materials were pure and then to later compare with the products' spectra. This would help in determining if all the starting materials reacted.

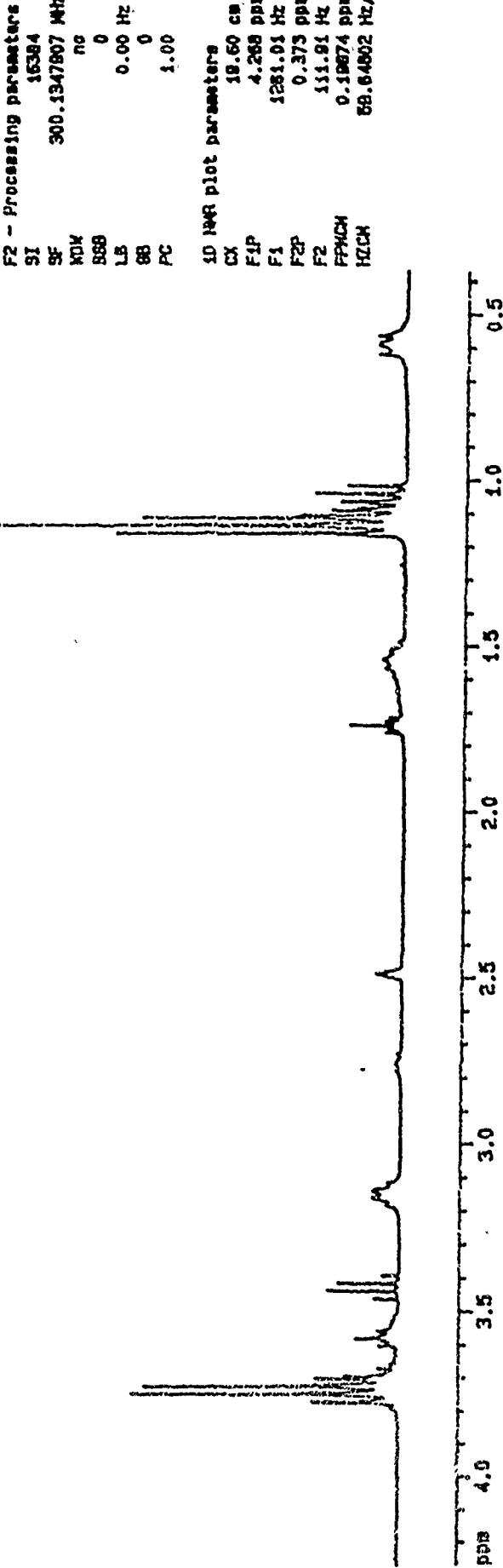
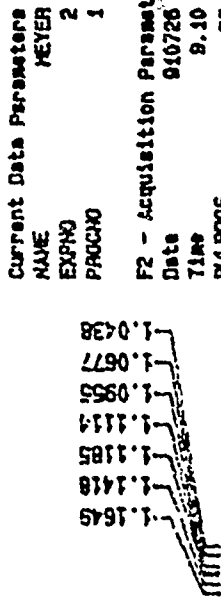
## CONCLUSIONS

1. The amic acid A was a successful synthesis.
2. The method used for imide A was unsuccessful. TFAA was used to absorb the water biproduct, but it reacted with the ethyl trifluoroacetate.
3. The method used for amic acid B was unsuccessful. It needs further purification.
4. The method used for imide B was unsuccessful. It needs further purification.

ppm

-3.7778  
-3.7547  
-3.7315  
-3.7084  
-3.4420

### Amide A in DMSO



Imide  $\Delta$  in DMSO

ppm

4.1014  
4.3775  
3.5608  
3.4237  
3.4006

ppm

7.3007  
7.182  
1.2774  
1.2530  
1.0481  
0.0250

Current Data Parameters

NUCLEUS: H1  
EXPGO: 3  
PROCED: 1

F2 - Acquisition Parameters

Date: 8/10/26  
T1INE: 14.08  
PULPROG: zg3h  
NUCLEUS: 1H  
SOLVENT: CDCl3  
A9: 2.1626880 sec  
FDRES: 0.231194 Hz  
DR: 60.0 usec  
F2: 512  
H1: 1 us  
D1: 5.0000000 sec  
P1: 3.3 usec  
FD: 0.0000000 sec  
PW: 0.0 usec  
DE: 82.5 usec  
SF01: 300.1358497 Hz  
SH1: 7676.76 Hz  
T2: 32768  
HS: 128  
DS: 0

3-12

F2 - Processing parameters

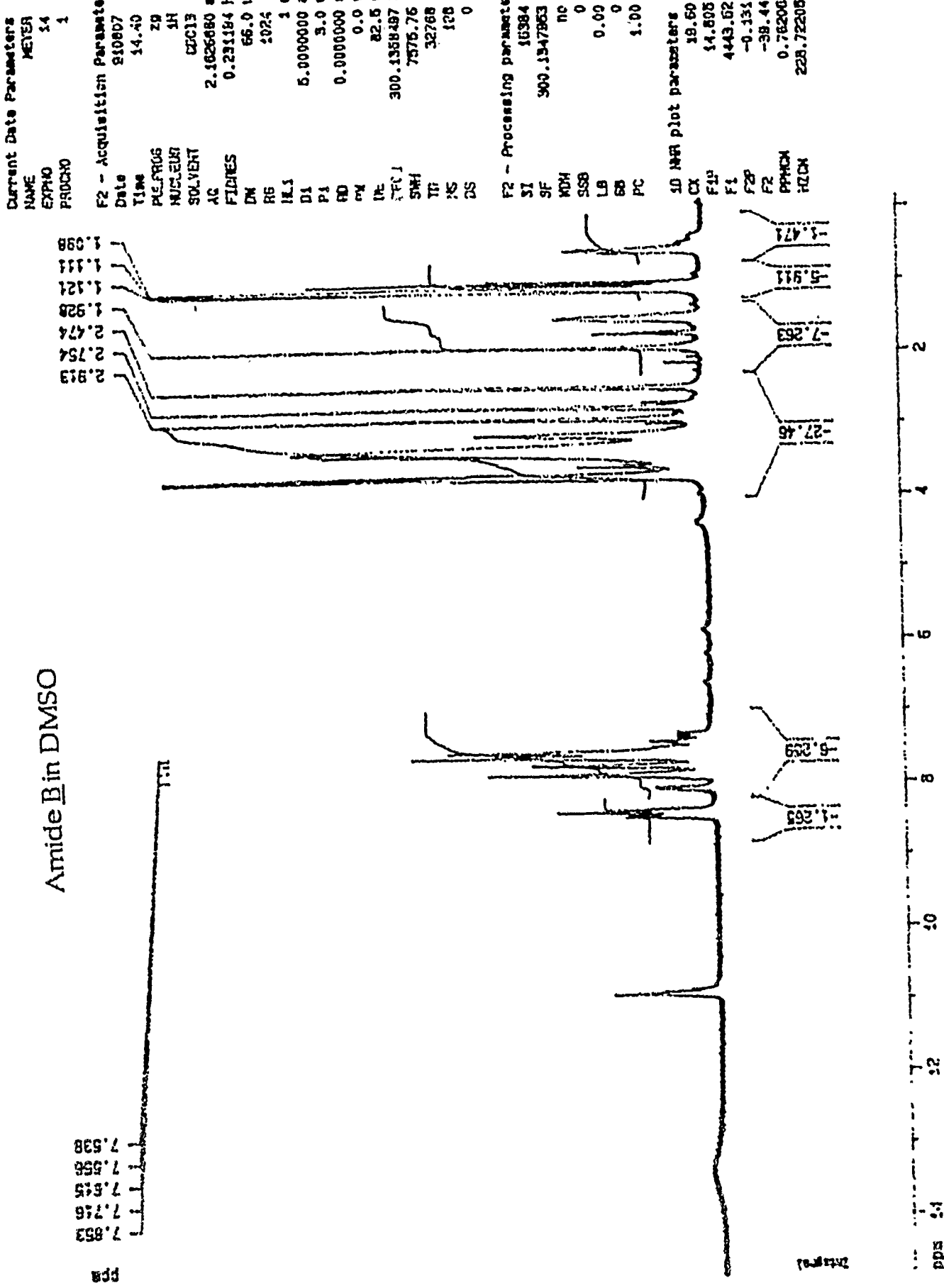
ST: 16384  
SF: 300.1357803 Hz  
WDW: no  
SSB: 0  
LB: 0.00 Hz  
RR: 0  
PC: 1.00

1D NMR plot parameters

CX: 19.60 CR  
F1P: 6.018 ppm  
F1: 1655.96 Hz  
F2P: -0.040 ppm  
F2: -23.84 Hz  
PPMCK: 0.26207 ppm/cm  
HZCM: 78.05599 Hz/cm



Amide B in DMSO



Imide B in DMSO

Current Data Parameters

NAME	MEYER
EXPNO	15
FRACTION	1

F2 - Acquisition Parameters

Date	210809
Time	8.22
PULPROG	Z9
NUCLEUS	1H
SOLVENT	CDC13
ACQ	2.16255600 sec
TDRES	0.231184 Hz
DW	86.0 usec
R6	1024
TE,1	1.00
SI	65000000 sec
P1	3.0 usec
RD	0.0000000 sec
PR	0.8 1.0sec
DE	82.6 usec
RF01	300.1398497 MHz
SWH	7675.75 Hz
TJ	82768
IS	128
DS	0
PC	0

3.14

F2 - Processing parameters

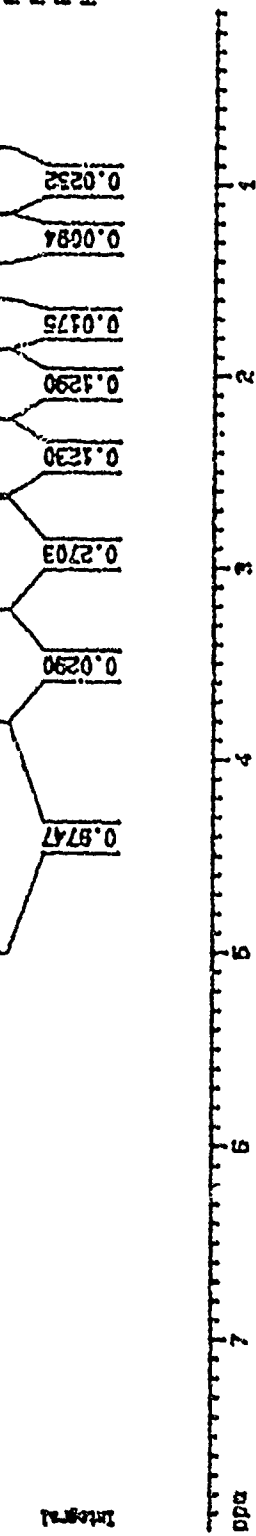
SI	16384
SF	300.1397912 Hz
TCW	72
SWB	0
WD	0.00 Hz
BB3	9
PC	1.00

2D NMR plot generation

CX	18.60 ppm
F1P	7.884 ppm
F1	2398.54 Hz
F2P	0.081 ppm
F2	27.29 Hz
PPM	0.40258 ppm/cm
HZ	120.46876 Hz/cm



ppm

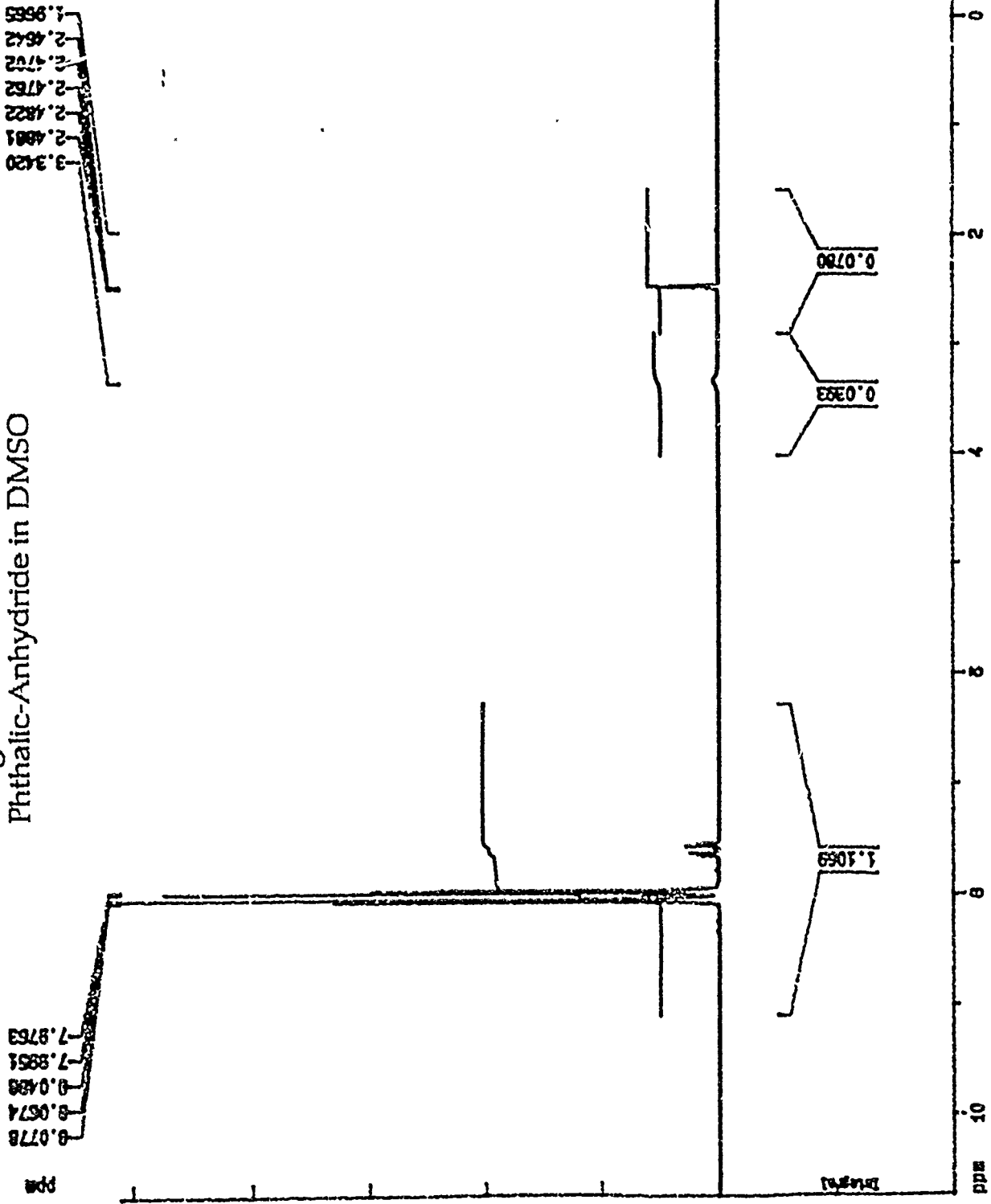


Intensity

### NMR Spectra for Starting Materials

These spectra were taken to make sure that the starting materials were pure and then to later compare with the products' spectra. This would help in determining if all the starting materials reacted

staring material for first reaction  
Phthalic-Anhydride in DMSO



**Current Data Parameters**

P2 - Acquisition Parameters	
Date	9/10/99
Time	14:13
PULPROG	79
NUCLEUS	1H
SOLVENT	CDCl3
A4	2.1624800 sec
FIDRES	0.281194 Hz
D1	63.0 usec
T9	2048
H4	4.08
D1	6.0000000 sec
F1	3.0 usec
RQ	0.0000000 sec
PW	0.0 usec
DE	82.5 usec
SP01	399.1380487 Hz
SIH	7676.76 Hz
T1	32768
H3	128
DP	0

3-16

starting material for first reaction  
APTES in DMSO

Current Data Parameters  
NAME HEYER  
EXPOD 6  
PROCED 1

F2 - Acquisition Parameters  
Date 9/10/98  
Time 15:30  
PULPROG NUCLEUS  
SCN.YCFT 1H  
TD 2048  
T1 2.1623600 sec  
TDRES 0.233184 Hz  
DW 68.0 usec  
RG 128  
HL 1  
D1 6.0000000 sec  
P1 3.0 usec  
P0 0.0000000 sec  
PW 0.0 usec  
DE 82.5 usec  
SF(0) 300.1358497 Hz  
SSB 7676.76 Hz  
TJ 32768  
NS 128  
D1 0



3.17

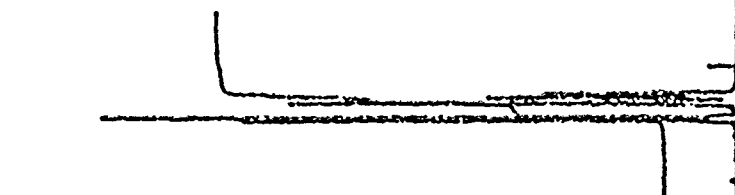
F2 - Processing parameters  
SI 16384  
SF 300.1358497 Hz  
WDW no  
SSB 0  
LB 0.00 Hz  
RR 0  
HC 1.00

1D NMR plot parameters  
CX 25.60 cm  
F1P 4.721 ppm  
F1 1416.80 Hz  
F2 -0.212 ppm  
F2 -53.68 Hz  
PPM/Hz 0.28170 ppm/ca  
HZ/CA 75.54369 Hz/ca





starting material for second reaction  
6F in DMSO



17 NMR parameters

NAME	HEYER
EXPNO	16
PROCNO	1
F2 - Acquisition parameters	
TD	31000
T1	1.00
FL	4096
SWH	16384
SC	32768
DS	1
TE	1.00000 sec.
R1	0.233194 Hz
TM	0.0 sec
TR	20.0 sec
TMJ	1.0 sec
D1	6.000000 sec
P1	3.0 usec
RD	0.000000 sec
PH	0.0 usec
DE	82.6 usec
DPF1	300.1438497 MHz
SPH	7376.76 Hz
TD1	32768
NS	128
DS1	0

18 NMR parameters

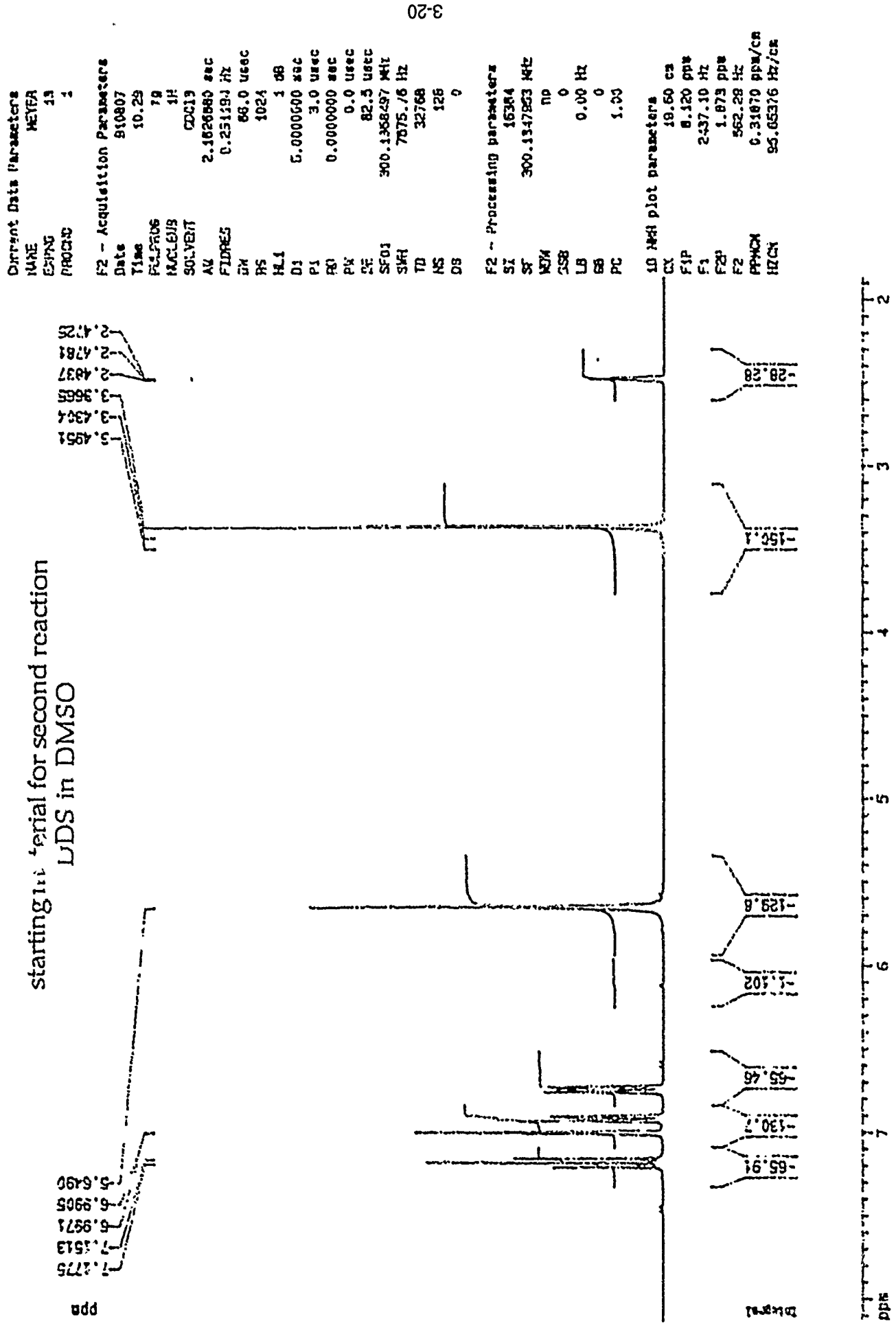
NAME	F2
EXPNO	16334
PROCNO	300.1437612 Hz
F2 - Processing parameters	
RT	10.0 sec
SF	10.0 sec
WDW	0
SSB	0
L5	0.00 Hz
LS	0
PC	1.00

19 NMR parameters

NAME	19.60
EXPNO	9.837
PROCNO	230.241 Hz
F2 - Processing parameters	
RT	-2.763 ppm
SF	-835.42 Hz
WDW	5.43351 ppm/cr
SSB	15.23612 Hz/cr



starting material for second reaction  
UDS in DMSO



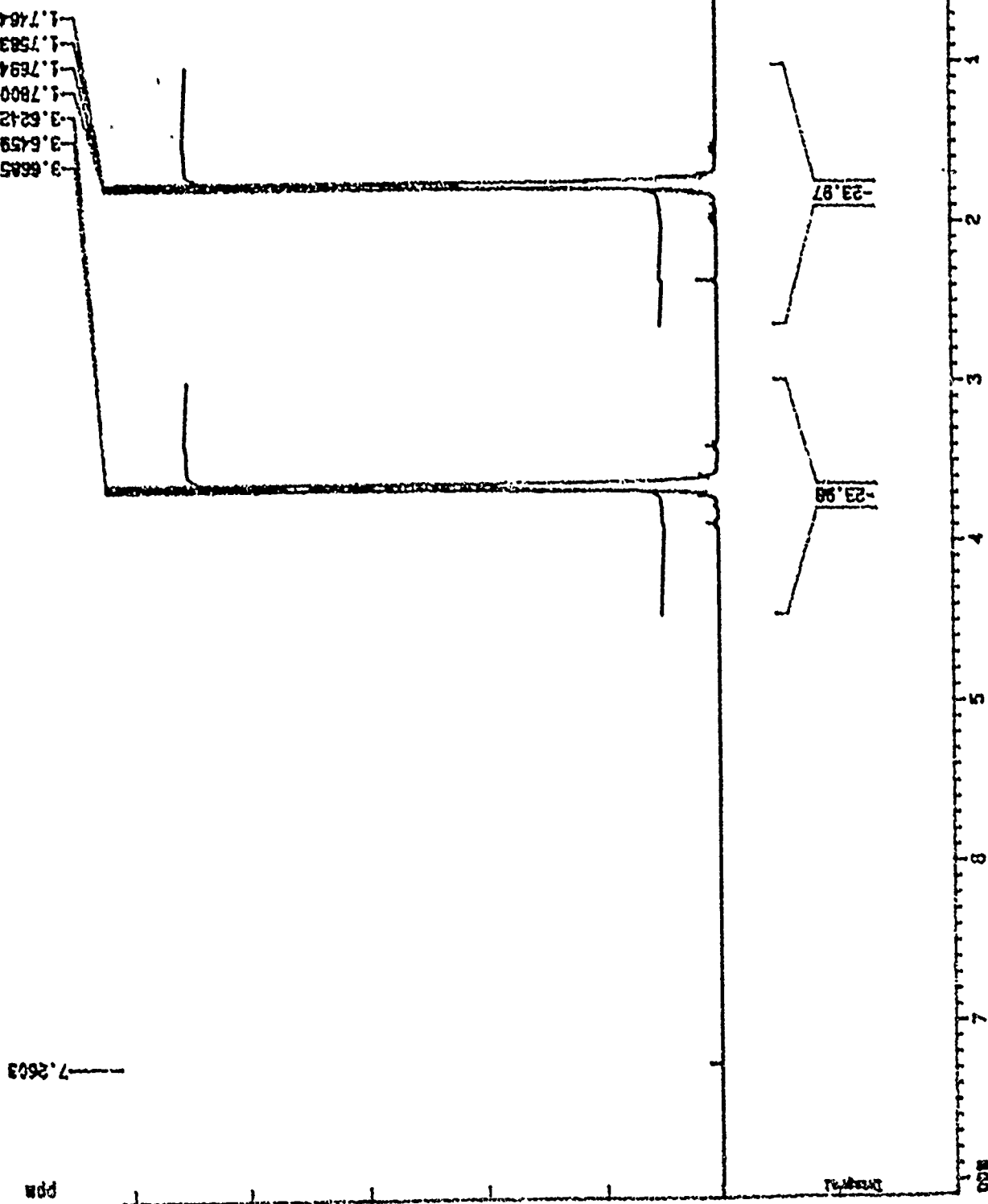
solvent used in reactions  
THF in chloroform

Current Data Parameters  
NAME: MEYER  
EXPGO: 7  
PPHCHO: 1

F2 - Acquisition Parameters  
Date: 5/10/93  
Time: 13:46  
P1/FIDN: 28  
NUCLEUS: 1H  
SOLVENT: CDCl<sub>3</sub>  
A2: 2.162880 sec  
FIRES: 9.231194 Hz  
IM: 128  
P2: 68.0 usec  
H1: 1.00  
D1: 5.000000 sec  
P1: 3.0 usec  
RD: 0.000000 sec  
PR: 0.0 usec  
DC: 82.0 usec  
SF: 300.1333674 Hz  
SM: 7675.76 Hz  
TU: 32768  
HS: 128  
ZSP: 0

F2 - Processing parameters  
ST: 10384  
SF: 300.1333674 Hz  
KEM: 79  
SSB: 0  
LB: 0.00 Hz  
GS: 0  
PC: 1.00

2D NMR plot parameters  
CX: 29.60 ppm  
F1P: 8.996 ppm  
F1: 2429.93 Hz  
F2P: 0.464 ppm  
F2: 1361.12 Hz  
PPHCHO: 0.36003 ppm/cm  
H2CN: 117.03604 Hz/cm



## CONCLUSIONS

1. The amic acid A was a successful synthesis
2. The method used for imide A was unsuccessful. TFAA was used to absorb the water biproduct, but it reacted with the ethyl trifluoroacetate.
3. The method used for amic acid B was unsuccessful. It needs further purification.
4. The method used for imide B was unsuccessful. It needs further purification.

## LEAP INTO ENGINEERING

### LEAP into Engineering by Diane Monaghan

My name is Diane Monaghan and I have been currently working under the High School Apprenticeship Program (HSAP) at the Phillips Laboratory at Edwards Air Force Base, Ca.. I walked in to my first day of work with little knowledge of the field of engineering, but as I leave I take with me my introduction to everything from civil and mechanical engineering to electronical and aeronautical engineering. Through this job I learned about computers, simulations, safety operations, electronical concepts, mechanical concepts, solid propellants, chemical properties, and much more, but my main focus was on liquid propellants.

This summer I worked on writing procedures to fill the LEAP (Lightweight Exo-Atmospheric Projectile) vehicle with oxidizer (NTO) and fuel (Hydrazine). This vehicle will eventually be flown in space as part of the Strategic Defense Initiative Operation (SDIO), but for the time being the vehicle is undergoing a series of simulation tests on computer and hover tests here in the facility.

The LEAP Program itself is very complex. The basic idea of this program is to develop a reliable vehicle having the capability to intercept an unfriendly target in the upper atmosphere without leaving debris behind. This was basically a safer, and more accurate way to intercept a target. As Werner von Braun said, "The object of the missile business is to make the target site more hazardous than

the launch site." In order to eliminate the debris the vehicle was designed to intercept the target using kinetic energy at high velocities, causing the debris to be very tiny, and virtually harmless if it should so happen to fall back to the earth. In order to do this the vehicle was designed with a propulsion system, to position the vehicle, and a seeker, which has the capability of tracking a heat source and finding the body from which the heat is emerging.

The original LEAP vehicle weighed over 200 pounds, but new technology was developed to cut the size down. As the vehicle grew smaller and more lightweight its speed and accuracy increased greatly. New nozzles and motors were built to provide the same thrust as the larger ones, but in a smaller package. The vehicle now weighs about twelve to fourteen pounds and has better capabilities than the original design.

The LEAP program is quite different from other Air Force operations. A policy of "build a little, test a little," is applied to assure that the project will be successful. Before any LEAP vehicle is strapped to a booster and shot off into space for testing it must first come here to the Phillips Laboratory and complete through a successful hover test. After that is accomplished, it will be sent to WSMR (White Sands Missile Range) in New Mexico, where it will be strapped to a ARIES Booster, and shot off in the same package as a target. In this test, the target will detach from the booster, and move away from the LEAP Vehicle. Then the LEAP will detach and track the target, then destroy it. After WSMR, the Vehicle will be sent to the Pacific, where another booster shot off from a different site will

become its target. These tests have not been completed yet, and are still in processing, but they look to be very exciting.

Shortly after my arrival at the Phillips Laboratory, the LEAP vehicle was put through one of the many successful hover tests. I learned a great deal from this test but I still had no idea just how much effort had to be put into one flight. I soon found out that there was a lot more to it than just counting down to lift-off.

First a contractor has to design and build an improved version of the LEAP vehicle. Then the Contractor and the Facility go through a complex process of integration. This is where the technology of the Facility and that of the Contractor are put together to hopefully produce a successful test. One of the beginning steps in this procedure is the loading of the LEAP vehicle with propellants. The contractor supplies the general guidelines of how they want their vehicle filled, and the facility integrates these guidelines with their own equipment to produce operating procedures for this operation.

This was my project this summer. With the help of my mentor, Glenn Yanagi, I wrote the technical operating procedure to fill the vehicle, using the guidelines provided by the contractor, and a pin game chart of the LEAP vehicle. A pin game chart is a diagram of the Contractor's Vehicle, the Facility's loading equipment, called a propellant cart, and any other associated hardware used in the actual operation.

The facility has two sets of propellant carts to service the contractor's vehicle, the PSS (Propellant Servicing System) and the HAPC (High Accuracy Propellant Carts). Each set has its own benefits and drawbacks. For instance while the procedure to load using the

PSS Carts only takes about three hours, the carts contain no vacuum system and no coolant system. Because the carts are without a cooling system, the operation to load must be conducted in the early morning when the temperature is still cool enough to keep the propellant in liquid form. The HAPC carts do have both a coolant system and a vacuum system, but the procedure to load takes about five to six hours to complete. In the procedures I wrote the HAPC carts were used to load the LEAP vehicle.

The pin game diagram of the propellant carts themselves, as shown in diagram 1 , takes the complex wiring and piping inside the actual cart and represents it in a schematic way on paper, showing each individual valve and its location on the hardware. During an actual operation red and green pins are placed in these represented valves to show if the valves are open or closed, or if ports are capped or not. This lets the Red Crew, the crew which performs the operation, and the control room verify that the path through the hardware is clear and safe for either propellant, pressure, or vacuum. These pin game charts are also used to write the procedures themselves. Red and green pins are used in the same way, to open or close a valve, or to open ports and connect extra hardware.

But writing the procedures is more than just typing in commands to open some valve and close another. There are pressure checks, leak checks, vacuum checks and valve verifications to worry about before the contractor's guidelines are even considered. After these are completed the object is to follow the original guidelines in the most efficient way possible. There are many things to consider in this efficiency, safety, the people performing the operation who

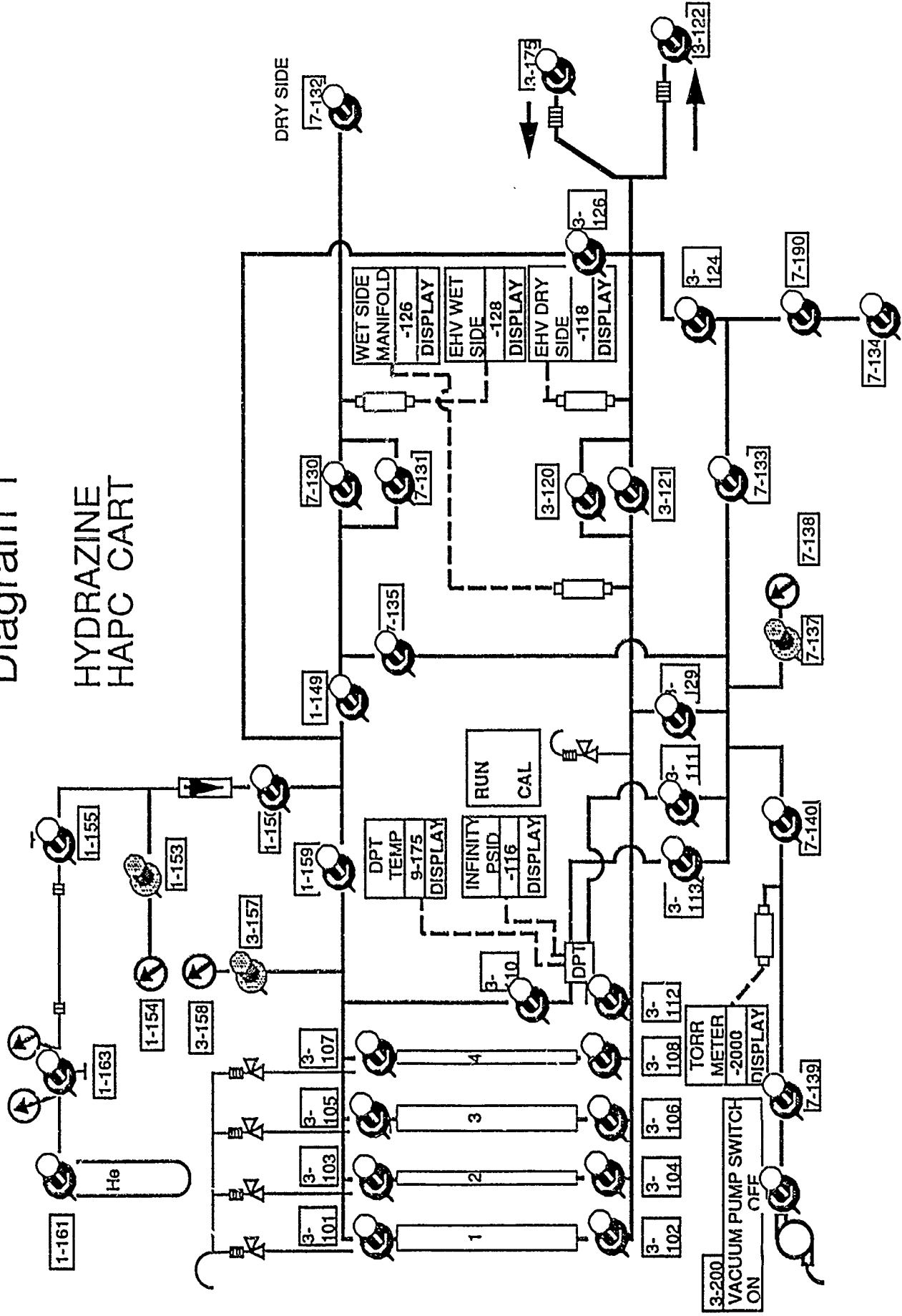
have to wear heavy protective equipment, the possibility of passivation problems, and many others as well. After a lot of thought, work, and repining, the procedures are printed out complete with warnings, pressure checks, and calculations following the contractor's guidelines. But the procedures are not ready to be thrown into operation just yet. The preliminary procedure is given to the contractor, where it is gone through with a fine toothed comb. The suggestions and comments are discussed and the appropriate changes are made. When the contractor is pleased with the procedures, they are then sent to safety for more evaluation. Finally after the necessary people are pleased with the product, the procedures are closely reviewed by the TEC's (Technical Evaluation Committee) and approved for use in real time testing.

This is only a small part of the integration process. The facility and the contractor together have to make sure that the test will be a success by doing everything from writing the countdown procedures to actually transporting the vehicle to the facility. When everything has been done and integration is complete, the procedures which I helped write will be used to fill the vehicle, and it will hover.

While my main focus was on procedures and liquid propellants, I now know more about all types of engineering. This job has shown me that engineering is not just about numbers and figures, but that it involves a little bit of everything, including excitement. I learned a lot through this experience and it has really helped me to decide what career I wish to pursue. I hope to continue my studies in engineering, and this experience has really educated me in a way that could never be accomplished in a classroom. I will keep with

me always the things I have learned and the possibilities that lay ahead.

Diagram 1



## USING THE I-DEAS' AUTOMATIC MESHER

S. Olkowski, Engineer Technician  
Research & Development Laboratories  
Under Contract Number F49620-90-C-0076 For AFOSR

### ABSTRACT

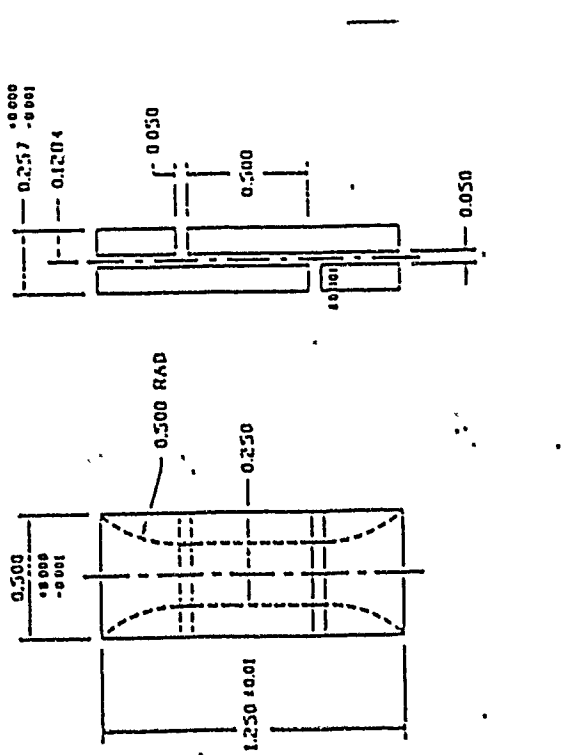
This report takes a look at the I-DEAS' automatic mesher. Models were created using the automatic mesher and then solved, so they could be compared to a hand-meshed model made in PATRAN by PDA, and which was solved using the P/STRESS Linear solver also by PDA. In this comparison, the three things looked at were the accuracy of the results, the time it took for the model to be meshed, and the cpu time to solve each model.

### INTRODUCTION

The Finite Element Modeling and Analysis program is a part of SDRC's I-DEAS package. The Finite Element Module includes geometry modeling, beam section modeling, mesh creation, adaptive meshing, post processing, and other tasks. The focus of this report is on the automatic mesher, which is found in the mesh creation task. The automatic mesher will take a solid object ported from SDRC's Solid Modeler and automatically mesh the solid with tetrahedral elements after applying mesh areas, mesh volumes, and nodes to the model. The effectiveness of the automatic mesher on a single geometric model will be explored, as well as some of the problems that were ran into while using the automatic mesher. Analysis results will be compared between a model which was meshed by hand using Patran by PDA, and models that were meshed by using the I-DEAS' automatic mesher. The analysis was ran on the VAX 8650, under VMS 5.4.

A double notch shear test specimen (Figure 1) was used for this analysis, because there was already data available on the double notch, which had been ran using the P/STRESS solver. The P/STRESS solver was also ran on the same VAX 8650, under an earlier version of VMS. The solver used for the automatically meshed models was Model Solution, SDRC's static linear solver. The model ran in Patran had carbon carbon material properties, and was meshed by hand using 1290, 8 noded hexagonal elements (Figure 2). The model was to be used as a basis of comparison for the models meshed with tetrahedral elements by the automatic mesher.

Figure 1



FREE FACE ELEMENT CHECK

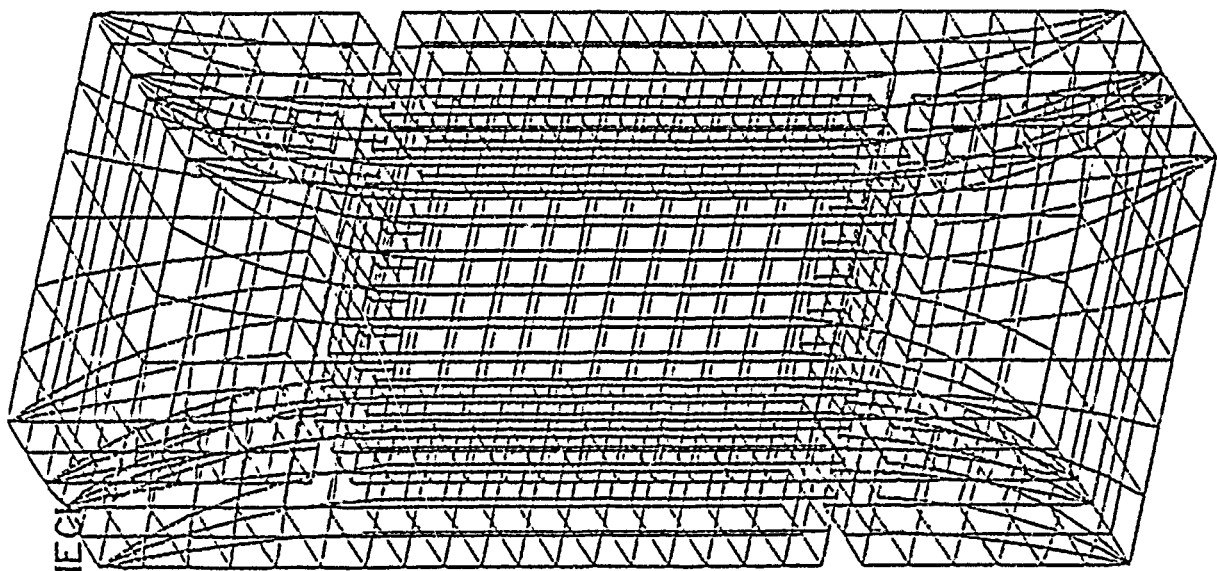


Figure 2

## CREATING A MODEL

When entering I-DEAS, the measurement system was set for British Grav (mod-in). The double notch shear test specimen was then read into I-DEAS through a universal file. It was a solid model of the double notch, that had been created by using the SDRC's Solid Modeler. The solid model was then sent to the Mesh Creation task under the Finite Element Modeling and Analysis family. In the first mesh run, the goal was to get as close to 1290 elements as possible, since this was the number of hexagonal elements in the hand-meshed model. The difference in the two models will be that I-DEAS automatically meshes using tetrahedral elements and the hand-meshed model was made using hexagonal elements.

Once in the Mesh Creation task, the global element length was changed to .095 and the curvature based size was turned on. Under mesh generation, input was asked for global element length, percent deviation, and coincident point tolerance with defaults given for all options. All defaults were accepted except for global element length. The element length was changed in order to vary the total number of elements in the model. The default value for percent deviation was 20% and coincident point tolerance was equal to .00027412036. With the global element length set at .095, the automatic mesher created a mesh with 1294 elements, in order to compare with the model meshed by hand with 1290 elements.

After the mesh was created, an element distortion check was ran to find any elements with a stretch value under .01 (.01 was used, because that is what the FINITE ELEMENT MODELING AND ANALYSIS, GETTING STARTED book used). SDRC defines stretch for a tetrahedral element as the radius of the largest sphere that will fit inside the element, divided by the longest distance between corner nodes, and is normalized by multiplying the inverse of the above value for the ideal target element, which is the square root of 24.

$$\text{Stretch} = (R/L_{\max}) * \sqrt{24}$$

There were three elements with stretch values of .0091, .0062, and .0062. So to see if these values could be improved, Tetra Fixes was ran on all the elements. Tetra Fixes will fix elements with a 0 or negative distortion by either straightening edges or by moving mid nodes. Fixing elements with these kind of distortions can also improve the element's stretch value. The computer reported that no elements required modification. No changes were made to the elements even though there were some with stretch values under .01. A typical acceptable value for stretch in tetrahedral elements is .5, and what is an acceptable value is dependant upon the geometry and the problem. Since the distorted elements were not near the center of the gauge section or at the notches, it was decided to accept the model as meshed.

The next step was to assign the elements material properties that matched those of the carbon-carbon in the hand-meshed model. So an orthotropic material property table was created. All the values for modulus of elasticity, Poissons ratio, and shear modulus were changed to match those of the hand-meshed model. The values put in for each were as follows:

MODULUS OF ELASTICITY	X =	2.40 E6	PSI
MODULUS OF ELASTICITY	Y =	1.60 E6	PSI
MODULUS OF ELASTICITY	Z =	0.49 E6	PSI
POISSONS RATIO	XY =	0.1000	
POISSONS RATIO	YZ =	0.1730	
POISSONS RATIO	XZ =	0.0429	
SHEAR MODULUS	XY =	0.806 E6	PSI
SHEAR MODULUS	YZ =	0.680 E6	PSI
SHEAR MODULUS	XZ =	0.680 E6	PSI

All the elements were then modified to take on the material properties of the new table.

Next, boundary conditions were applied to the model to match those used in the hand-meshed model. This was done in the Boundary Conditions task. A restraint set was made to fully restrain the bottom from moving in any direction. The load set was made to apply a face pressure of 100 PSI on top of the model. Both the restraint and load set were then put into a case set so it could be solved by SDRC's Model Solution.

Once in the Model Solution task, the case set containing the restraint and load set was made the active set, and the displacements and stresses were picked for the output selection. The model was then solved.

#### OTHER MODELS

Three more models were created using the same steps. The global element lengths were all changed to vary the amount of elements. The number of elements were varied to show the difference in the analysis results.

On one of the new models the default value of .079134050 was accepted as the global element length. Using this value the computer created a mesh with 2547 tetrahedral elements. No elements with a stretch value under .01 were found. The most distorted element in the whole model had a stretch value of .1215.

The goal for the next model was to have as close to 1900 elements as possible, since it was in the middle of the two models already created. This was to see how the accuracy changed with the number of elements. A problem arose while trying to get this many elements, the computer was not able to process a mesh when certain values for the global element length were entered. If it did not like a certain length it would stop processing the mesh and give an error message which read: "Due to high concavity no further subdivision can be made. This can be caused by a global element length, which is too coarse. Manual splitting of the mesh-volume on high concave curves might help. Another possibility is just-touching geometry in a mesh-volume." This message did not appear to apply to the geometry since there were no areas of high concavity and one of the global element lengths entered was .086, which is not as coarse as the .095 value that was used in creating the mesh with 1294 elements. Using the process of trial and error, different values were entered for the global element length, to see if the mesher would accept any of them. Going through this process it was discovered that the automatic mesher is very specific in the values it will accept. For example, the values of .087 and .088 were rejected by the computer and the value of .0875 was accepted, creating a mesh with 1600 elements. The value of .0835 was rejected and the value of .083 was accepted.

SDRC gave two possible suggestions for the problem.

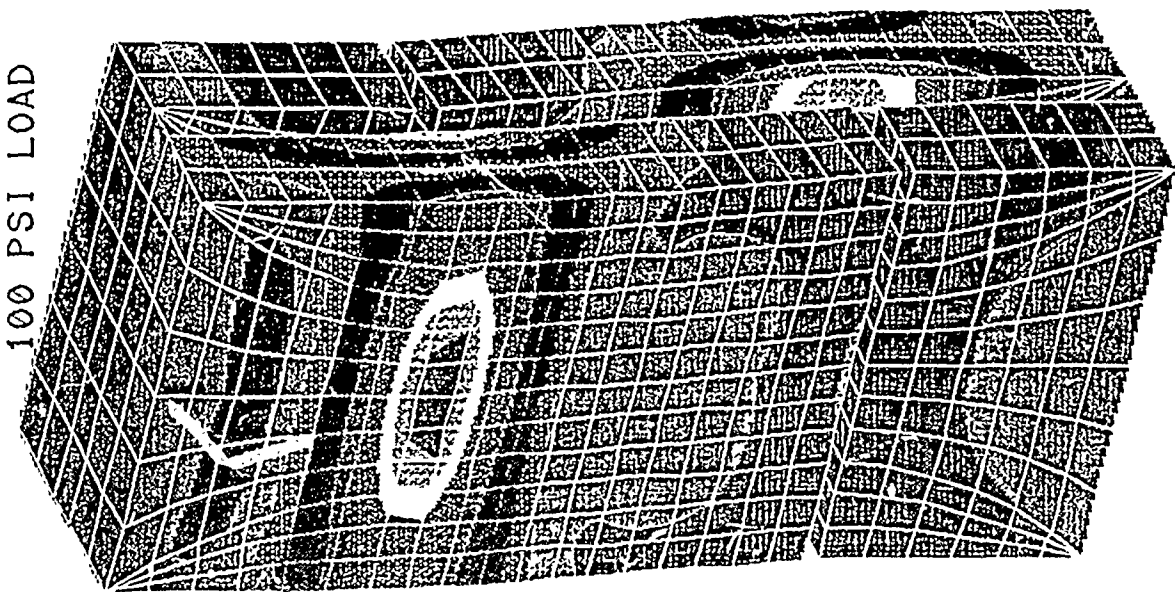
Suggestion 1: The automatic mesher tries to break a line into segments equal to the global element length, plus or minus a certain percentage. What might be the problem is that with certain global element lengths the automatic mesher is not able to split one of the lines into a whole number of segments. This means that some of the line is left over and the global element length is too big to split it again. This could result in an error.

Suggestion 2: The automatic mesher takes an area and starts splitting it into sections while maintaining angles that are of multiples of 60 degrees. Once a section is made which has dimensions equal or a little smaller than the global element length, it is left alone. It is possible that a section which is equal to the global element length is next to a section which is bigger than the global element length. The bigger section is split again, and this leaves two elements together sharing the same side of one element. In other words a node is created between two other nodes, so they are not being shared. This would result in an error.

The problem was circumvented by slightly increasing or decreasing the global element length.

The global element size of .0875 was finally used for the model. The mesh created contained 1600 elements, with none of them having a stretch value under .01, and 4 elements having stretch values under .1.

MAXIMUM SHEAR STRESS DISTRIBUTION  
100 PSI LOAD



PSI

544.  
508.  
472.  
436.  
400.  
364.  
329.  
293.  
257.  
221.  
185.  
149.  
113.  
77.6  
41.8  
5.96

Figure 9

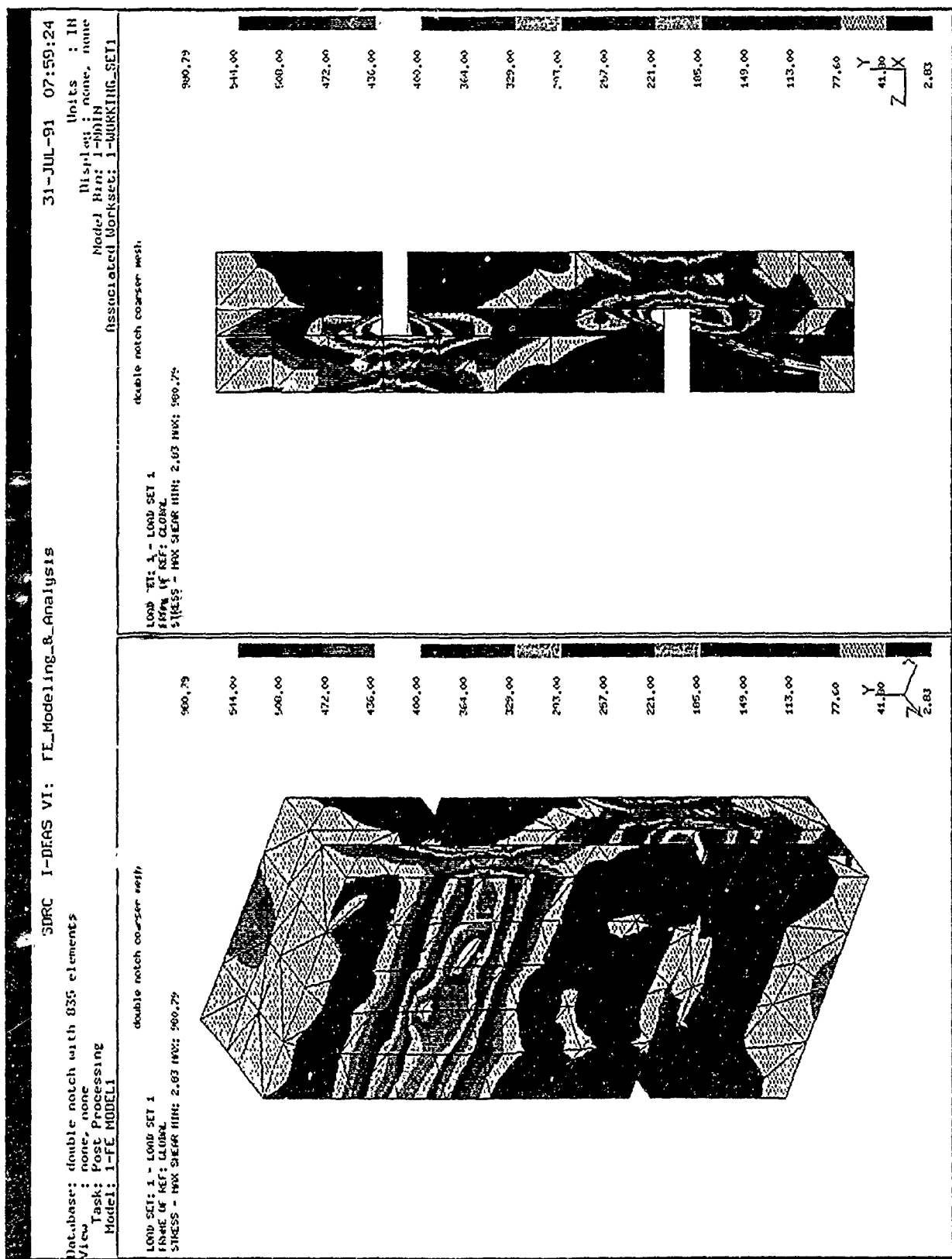
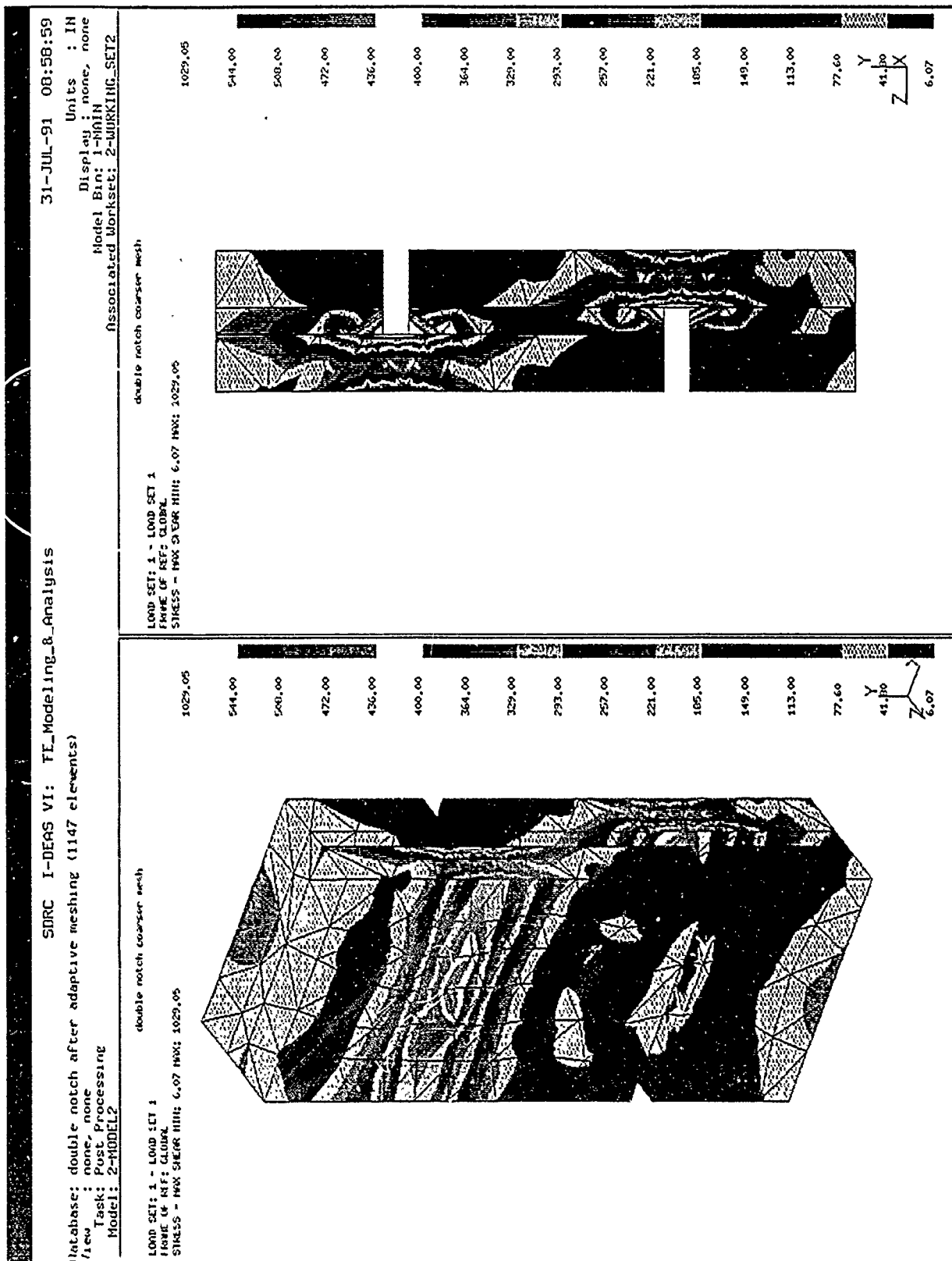


Figure 10



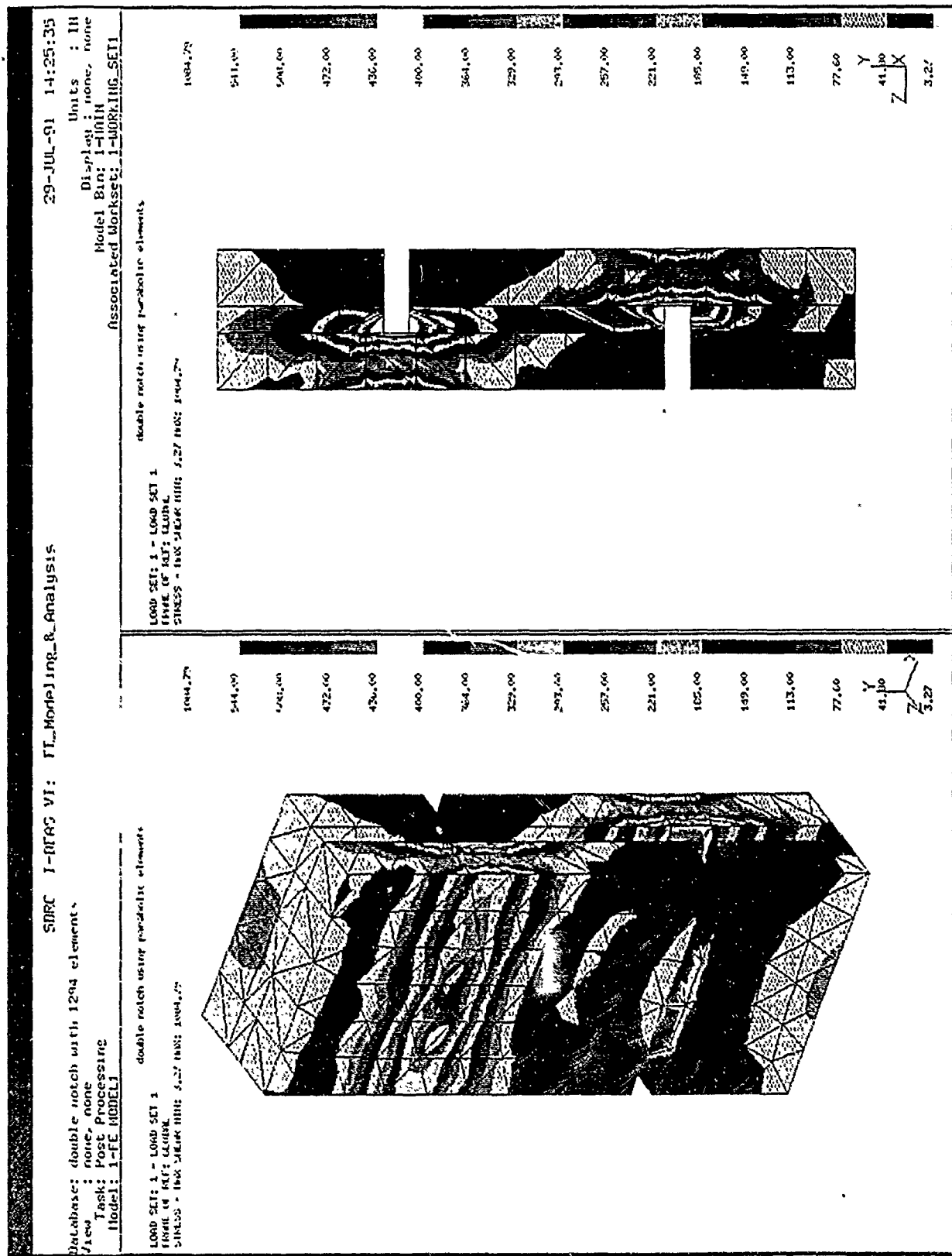


Figure 12

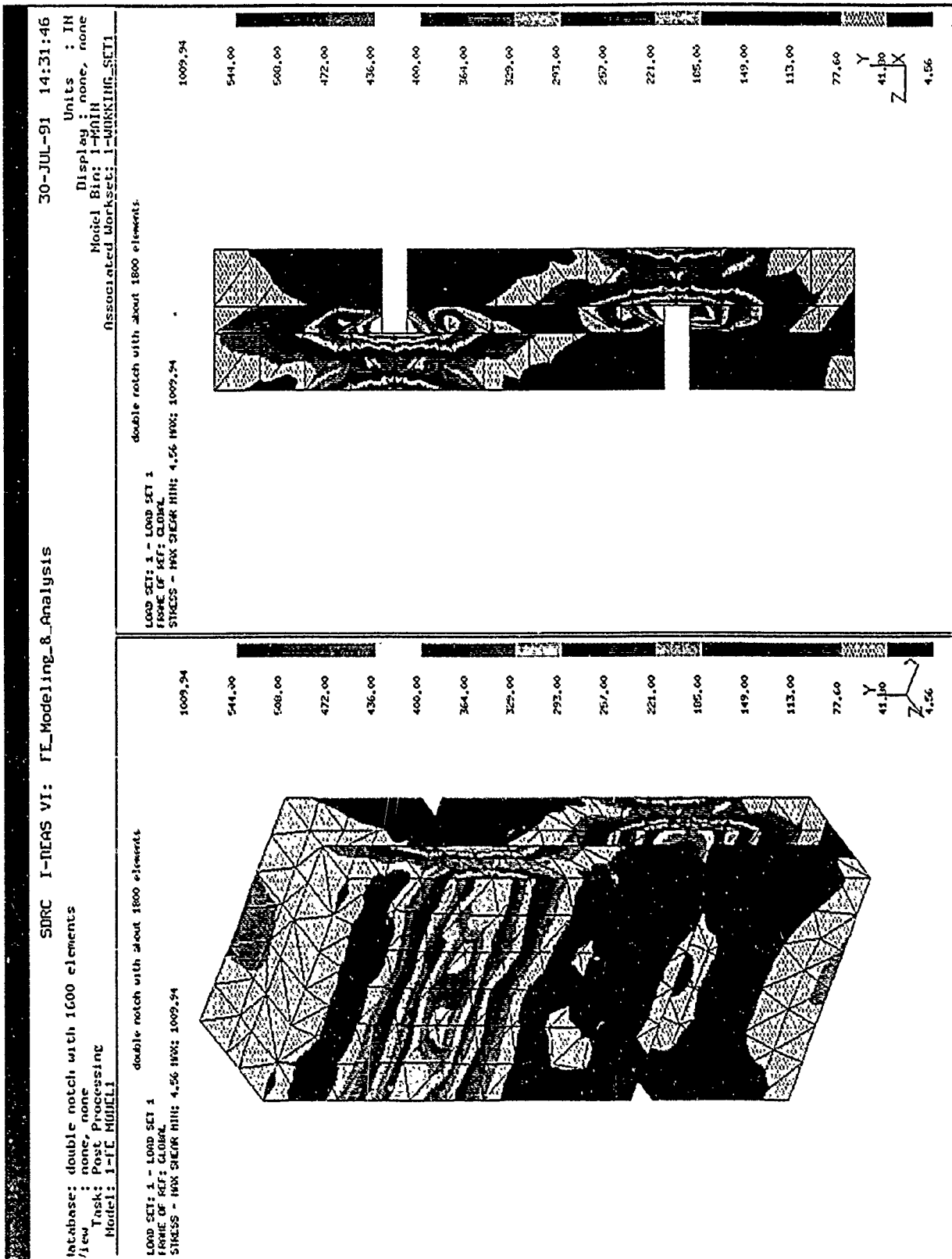


Figure 13

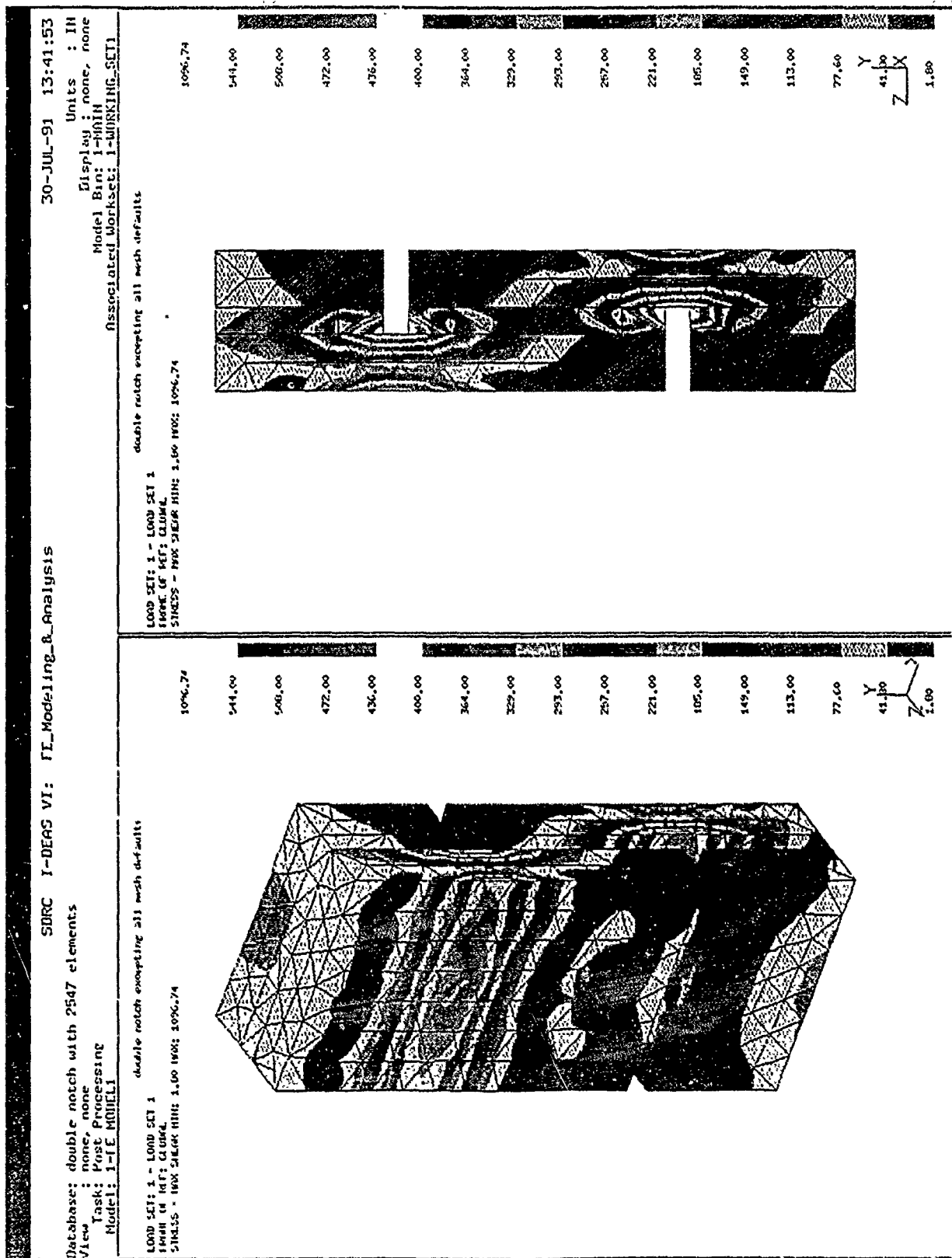


Figure 14

In the last model made, a global element length of .113 was used to create a mesh with 835 elements. This model was made to see if the cpu time could be cut down without giving up accuracy. In the model none of the elements had a stretch value under .01, and 5 elements had stretch values under .1.

#### ADAPTIVE MESH

The adaptive meshing capability was tested out on the model with 835 elements. The basis for modification was set at analysis results, so it would increase the number of elements where the greatest stress occurred. The method of modification was set on remesh, so it would be able to both move nodes and change the shape of elements. After adaptive meshing was ran on the model, it created a new mesh containing 1147 elements, with none of them having stretch values under .01. The most distorted stretch value in the model was .1133.

#### POST PROCESSING

The model's results were displayed in the I-DEAS Post Processing task. Maximum shear stress was the data component used in the comparison. To make the results easier to compare, both the contour colors and labels were changed to match those used in the hand-meshed model.

#### RESULTS

When making an eye comparison between the models created in I-DEAS to that of the hand-meshed model ran in Patran (Figures 9-14), the results appear similar, in that the same stress concentrations occur in the same locations. The most obvious difference seems to be that the hexagonal elements yield a much smoother stress distribution, than does the tetrahedral elements. The contours of the hand-meshed model are smooth, unlike those in the tetrahedral models, which are more distorted. It seems that by raising the number of tetrahedral elements the smoothness of the contours are slightly improved.

Another noticeable difference between the models is that the maximum stresses recorded in the I-DEAS' models are higher than the maximum stress in the hand-meshed model. The reason for the higher stresses in the I-DEAS' models is that in the inside corners of the notches the stresses are infinite, so the more points that are in these areas the higher the reported maximum stress should be. When using tetrahedral elements there are more points in these infinite stress areas, so a higher maximum stress is expected. When hexagonal elements are used, there are less points in these areas, so a lower maximum stress is expected.

A comparison of stresses on the face of the gauge was made to see if, in the center of the gauge, the tetrahedral models' results came close to those in the hand-meshed model. In using the double notch shear specimen, the stresses on the face of the gauge should equal the applied load on top of the model, in this case 100 PSI. When trying to cut the tetrahedral models with the volume clipping to get the same cutaway view of the gauge section as that in the hand-meshed model, the display looked distorted. The reason the hand-meshed model did not look distorted (figure 15), was because with hexagonal elements, it is easy to make a cut at the nodes to avoid interpolating data between the nodes, which would result in a distorted display. When the same cut is made on a tetrahedral model, elements get cut in half, and a distorted display is the result. In order to get the results wanted, a cutting plane display of the gauge section was made in all the tetrahedral models. Then a point in the middle was picked to see what stresses were recorded. The results found were as follows:

Number of elements in model	Stress in center of gauge
1290 (hand-meshed)	89.5-131.0 *
835	89.0
1147	105.1
1294	112.1
1600	113.9
2547	96.9

\* A range had to be used for the hand-meshed model, because a single data point was not available.

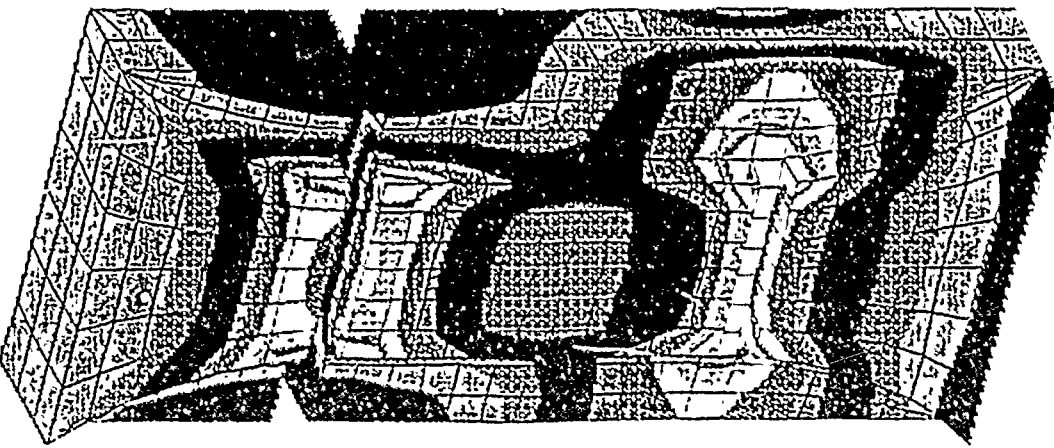
The following table shows the meshing times for the models.

Number of elements in model	Time
1290 (hand-meshed)	5 days
835	5 minutes
1147 (adaptive remesh)	11 minutes
1294	6 minutes
1600	9 minutes
2547	11 minutes

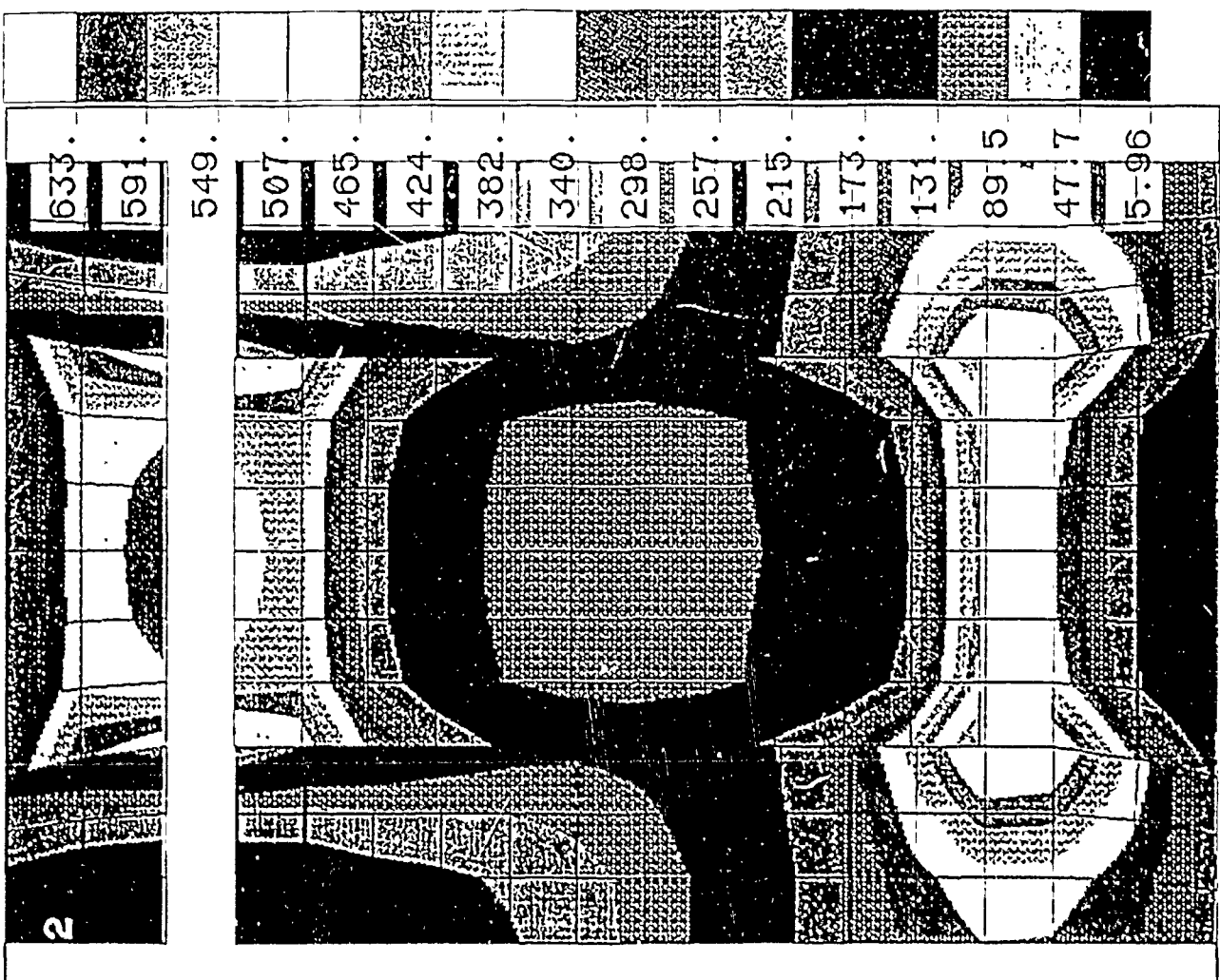
The last comparison made, was the cpu time to solve each model. The hand-meshed model was ran under P/STRESS. The I-DEAS' models were ran in the linear statics solver, SDRC's Model Solution. The cpu times were as follows:

Number of elements in model	CPU Time
1290 (hand-meshed)	36 minutes
835	11 minutes
1147 (adaptive remesh)	19 minutes
1294	30 minutes
1600	45 minutes
2547	105 minutes

MAXIMUM SHEAR STRESS DISTRIBUTION  
100 PSI LOAD CUTAWAY VIEW



BOTTOM CONSTRAINT ONLY



2

Figure 15

## CONCLUSIONS

Using tetrahedral elements, the I-DEAS automatic mesher seemed to give reasonable results for this model. Many man-hours were saved by meshing this specific model using the automatic mesher rather than to mesh it by hand. If the distorted elements in the automatically meshed models were in areas of interest, a significant amount of time could have been required to move nodes to eliminate the distortion. The hand-meshed model and the automatically meshed model's solution cpu times are comparable, 36 min. vs 30 min. The gauge stresses between the models are also in the same order. In this model the automatic mesher seemed to create elements with low stretch values, this could cause problems if very accurate results are required. For this simple geometry model, the results were valid.

## CONCLUSIONS

Using tetrahedral elements, the I-DEAS automatic mesher seemed to give reasonable results for this model. Many man-hours were saved by meshing this specific model using the automatic mesher rather than to mesh it by hand. If the distorted elements in the automatically meshed models were in areas of interest, a significant amount of time could have been required to move nodes to eliminate the distortion. The hand-meshed model and the automatically meshed model's solution cpu times are comparable, 36 min. vs 30 min. The gauge stresses between the models are also in the same order. In this model the automatic mesher seemed to create elements with low stretch values, this could cause problems if very accurate results are required. For this simple geometry model, the results were valid.

calculates the statistical variation and bias relative to the WLF Curve. Once a reasonable-looking master curve has been obtained, the user selects four points with an on screen cursor, and the program calculates the dual power law function which passes through these four points. The program output consists of plots of the WLF function, the relaxation modulus data, and the calculated relaxation modulus function with the data superimposed. In addition, the calculated WLF constants, dual power law constants, and other pertinent results are printed out.

#### DISCUSSION

The EREL programs consist of three modules on the HP 85/87; EREL\_IN, EREL\_SHIFT, and EREL\_MFIT. The EREL\_IN program inputs the data to be shifted. The program creates a simple three level data base. The first level is the directory of the data set names. The second level is a list of data subset names consisting of a signed temperature and a sequence number allowing for more than one data subset for a given temperature. A separate list of data subset names is created for each data set. The third level is the actual data stored in a separated disk file for each data subset. The sample data used for checking the code is "TP-H1011". The user inputs the temperature before beginning the input of each data set; the rest of the data set name is created by the program.

The EREL\_SHIFT program is the module used for actually shifting the data. To use EREL\_SHIFT the data must be stored as data files using the EREL\_IN module. The EREL\_SHIFT program allows the data to be shifted using the WLF Shifting routines or hand shifting to achieve a smoother curve fit.

The EREL\_MFIT program fits a four-constant mathematical function (a "dual power law" equation of the form  $E = E1 + t^{n1} + E2 * t^{n2}$ ) to the shifted modulus data. The fitting process actually forces the equation to go through the four control points graphically input by the user to represent the data. The user inputs each of these control points by moving the cursor to the desired location on a screen plot of the data.

## RESULTS

The New WLF Shifting Programs on the Amiga 2000 computers consist of two main programs which utilize the Amiga's mouse and graphic capability. The Amiga code is written in about 2000 lines of AC BASIC.

EREL\_SHIFT on the Amiga computer reads in file SHF\_FILES.DAT located under a subdirectory titled DATA. The file SHF\_FILES.DAT contains a list of the names of the data sets and the number of temperature subsets within the subdirectory DATA. After reading the file SHF\_FILES.DAT the program then prompts the user for the data set to shift and reads temperature subsets. If the data is correctly read into the right arrays the program asks the user for engineering or true stress, reference temperature, vertical shift parameter (none/true), and if the modulus values have been shifted.

The plot of the unshifted data is drawn on the screen and the user is asked to WLF shift the data, hand shift the data, generate a final report of the constants generated, make a final data plot, or terminate program execution. In WLF shifting of the data, the top data set is shifted horizontally using the mouse. The program reads the mouse values and shifts the first data set left or right. Using the new position of the first data set and the WLF functions and constants, the program draws the plot on the screen by searching for the maximum and minimum values in the data arrays, scaling the plotting region, and converting data coordinates to plotting coordinates. The plotting coordinates are stored in a separate arrays and are plotted using the LINE function in Amiga Basic.

After a reasonable looking curve has been obtained using the WLF shift the user has the option to hand shift the individual data sets. In hand shifting the user selects which data set to shift by cycling through the data sets. The program will read mouse values as the pointer is clicked, dragged and released. It will then shift the highlighted data set with respect to the mouse values.

Once a reasonable looking master curve has been created, the user may generate a report of the shifting or plot the final data set. The report contains the WLF constants and values of  $T_s$ ,  $T_g$ , and  $T_0$ . The report also prints out hand shifting results, Mean Bias, and Standard Error. Reports can also be saved to the disk for later printing or to parameter files with names SHFxxx\_CONST.DAT or SHFxxx\_SHF.DAT. Parameter files are used by other programs such as EREL\_MFIT. The

parameter file SHFxxx\_CONST.DAT contains values for Ts, the reference temperature, WLF constants (C1,C2), flags for stress and vertical shift parameters, and the hand shift results. The parameter file SHFxxx\_SHF.DAT contain arrays on the number of points within each temperature set, temperature values and time-vs-modulus arrays.

In creating the final plot the program will draw a grid on the screen and plot the current data set using special symbols for each of the temperature subsets. The plotting screen is then displayed and the user has the option of saving the screen to a bit map file that can be printed using Deluxe Paint III.

EREL\_MFIT on the Amiga computer serves the same purpose as the HP 85/87 version of SREEL\_MFIT. MFIT uses the parameter files SHFxxx\_SHF.DAT and SHFxxx\_CONST.DAT to plot the curve created from EREL\_SHIFT. MFIT allows the user to select the position of four control points on the screen using the mouse. The program performs calculations to determine the Dual Power Law Equation for the curve upon request of the user. It will also plot the curve and allow the user to save the bitmap of the screen for later printing.

## CONCLUSION

Programs EREL\_SHIFT and EREL\_MFIT work well on the Amiga 2000 computers. The programs which I have translated offer features similar to the older HP 87/85 computer code. There are a few enhancements that can be made to streamline the code and generate professional plots, but the graphic routines and calculations work well. I have learned to program on the Amiga operating system and I am confident that my efforts in translating the EREL programs have been successful. Attached are reports and plots generated from programs EREL\_SHIFT and EREL\_MFIT. 16 Aug 1991.

RESULTS OF WLF SHIFTING FOR DATA SET TP-H1011

(Temperatures are in degrees Kelvin except as noted)

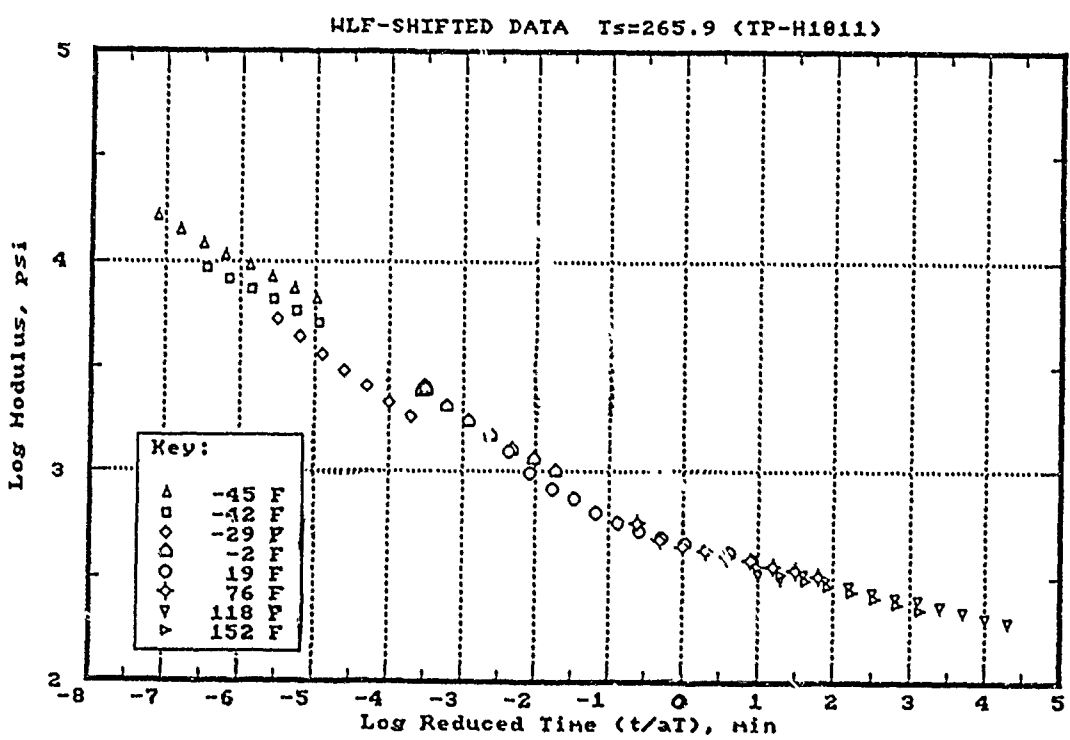
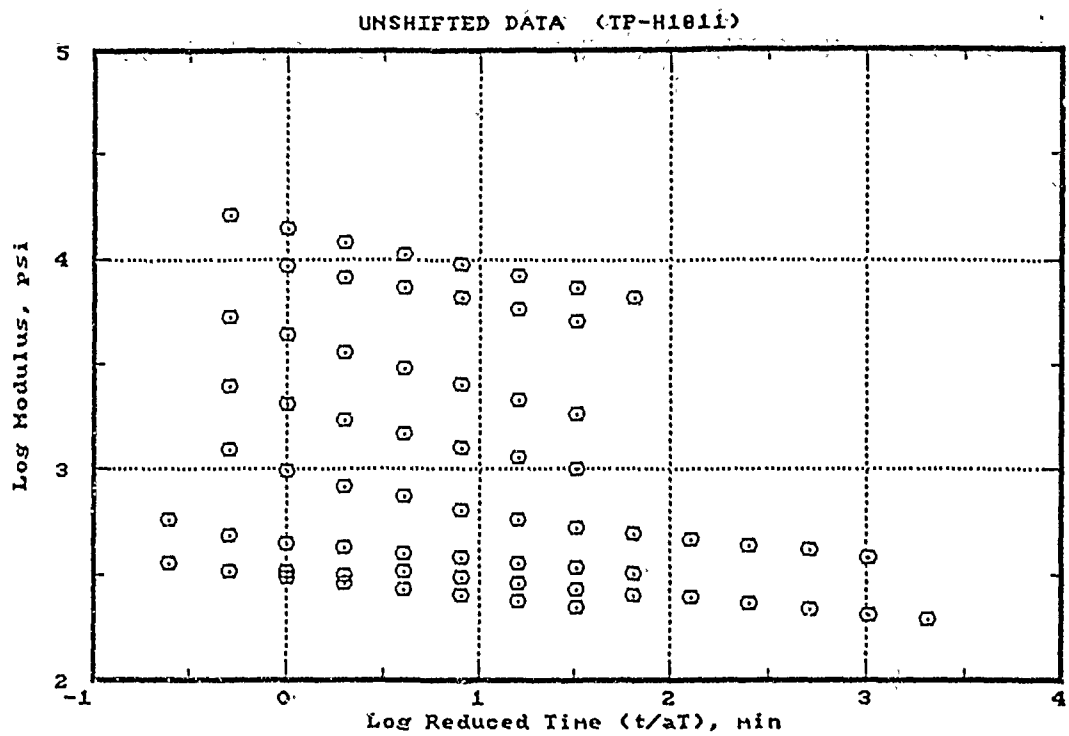
T<sub>s</sub> = 265.9999  
Approx T<sub>g</sub> = 215.9999  
(-70.96024 deg F)

T<sub>0</sub> = 297.6445  
( 76.00002 deg F)  
C<sub>1</sub> = 6.755817  
C<sub>2</sub> = 133.2446

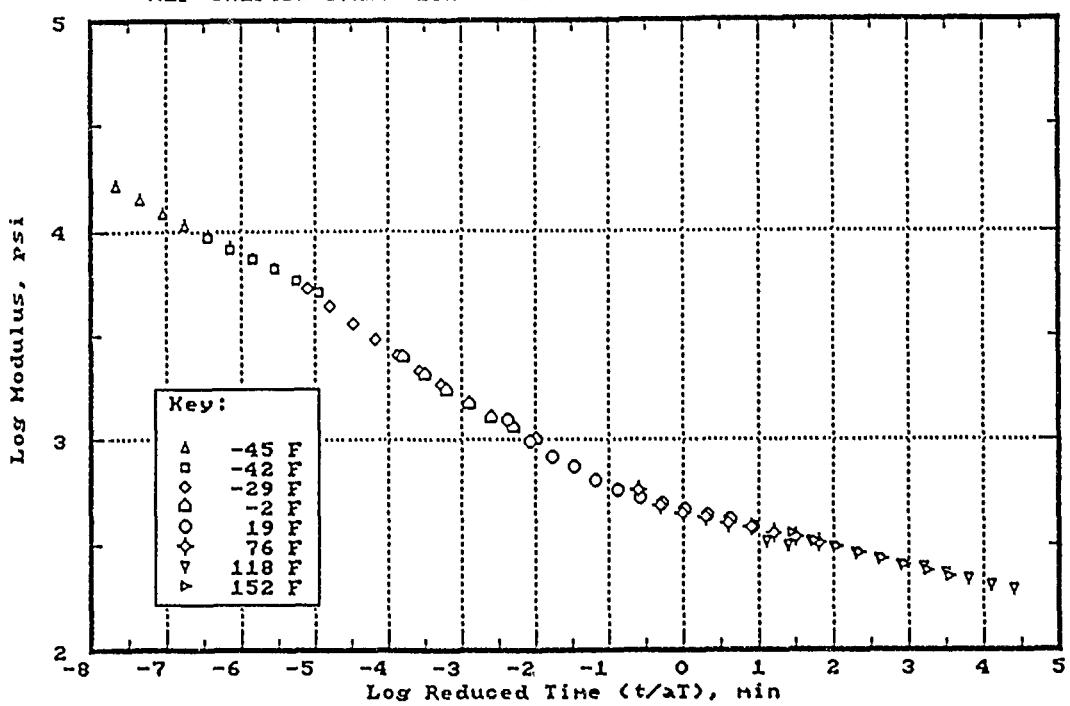
Additional hand shifting results:  
File Name Log (aT)

-45.000	0.5519
-42.000	0.0000
-29.000	-0.4097
-2.000	0.3615
19.000	0.0000
76.000	0.0000
118.000	-0.0966
152.000	-0.4130

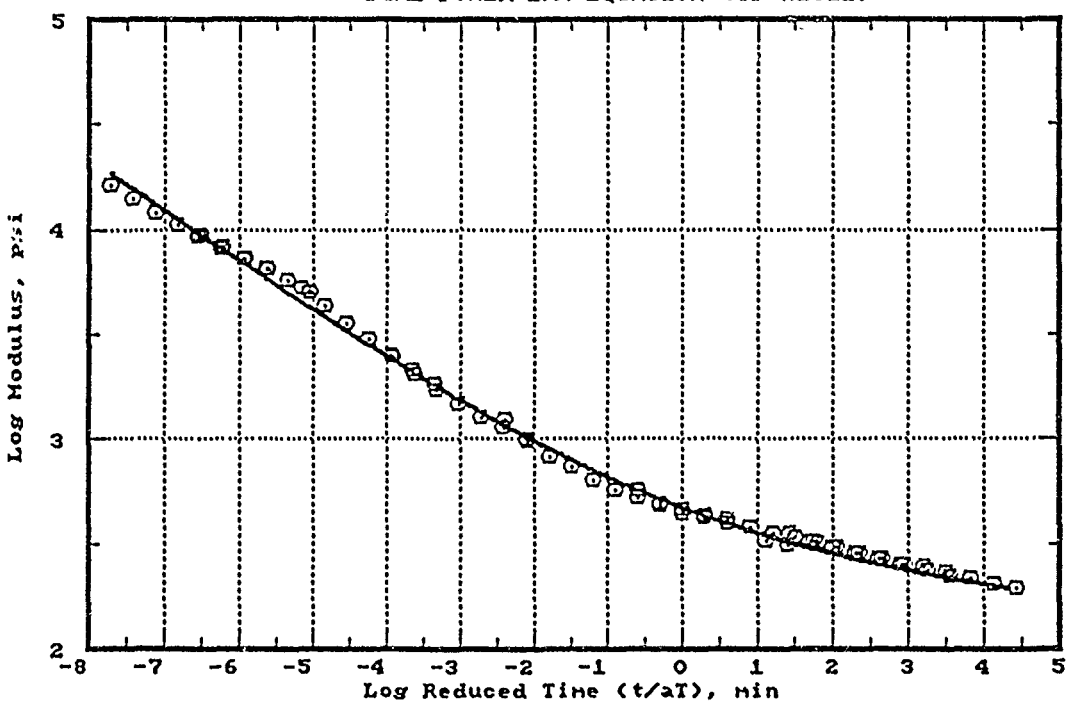
Mean Bias = -5.58123E-03  
Std Error = .2971068



WLF-SHIFTED DATA WITH ADDITIONAL HAND SHIFTING (TP-H1011)



DUAL POWER LAW EQUATION (TP-H1011)



Dual Power Law Equation Through 4 Points

INPUT DATA:

RESULTS:

E1 = 229.4424 n1 = -.2388419  
E2 = 251.1053 n2 = -3.655263E-02

Converged in 20 iterations.

RMS error = 4.745293E-07

Biggest error is 4.692195E-07 at Point No. 2.

Log t	Log Er	Log Er (calc)
-7.731	4.220	4.2201
-3.683	3.318	3.3183
0.366	2.635	2.6346
4.415	2.286	2.2865

Error Analysis:

At control points:

Log (t/aT)	Rel. Error
-7.7315	0.0000
-3.6828	0.0000
0.3659	0.0000
4.4146	0.0000

Relative to data:

Coeff of variation = 0

RDL Mentor Program  
Final Report



Jason Phillips  
OLAC/RCC  
Phillips Laboratory

As a high school student, the future of my chosen field is directly in my hands. What I and thousands like me do, has a profound effect on the future of American science. With that in mind I chose to endure an eight week summer apprenticeship at Phillips Lab, Edwards Air Force Base. This has resulted in a variety of different benefits that if used to their full potential could help immensely in the near future.

### **Computers**

My knowledge of computers drastically increased during my stay here. Before entering this program I was fairly proficient with most Apple computers and I could meander thru most of the other standard personal computers (PCs). Now I am fully competent with a Macintosh and can move through any other with practiced ease. This will most definitely help me in the future, as my knowledge now far surpasses that of my peers.

In the everyday world people see PCs as little more than high powered type-writers. At Phillips Laboratory I learned to see computers as an advanced all-purpose tool. A tool so talented it can do things thousands of miles away. It's this mode of thinking that separates your average PC user from the professional.

### **College Application**

Not all that I learned was expected. I found a surprising number of engineers had recently gone back to college for one reason or another and their advice will hopefully prove to be very helpful. The college co-ops also working here for the summer have proven to be

invaluable. They possess knowledge of the college experience from the eyes of someone closer to my own age. The information they imparted to me was found to be both interesting and helpful.

## **Engineering**

Engineering, especially the actual development of working pieces, is a team effort. Learning this was probably the most important part of my apprenticeship. This is something that the colleges don't teach. Engineers are not the only vital link of the scientific work force. Mechanics and secretaries are easily as important and without draftsmen nothing could ever get off the drawing board.

## **Scientific Research**

This is not to say that I totally avoided any actual scientific research. I worked on a project that involved work on Liquid Crystal Polymers (LCPs). LCPs are the future of the space program, they are light weight, with a high strength to weight ratio, and possess an even greater strength in colder environments. LCPs are highly anisotropic fluids that exist between the boundaries of solid and conventional isotropic liquid phase.

These LCPs are to be used sometime in the future in a turbopump that will be used later in space related activities. The ideal material would be extremely strong and light, yet capable of withstanding cryogenic temperatures. Other factors like compatibility with various chemicals have been taken into account before any actual materials for testing were decided upon.

The test specimens will be injection molded into hollow right cylindrical shapes (See Diagram #1). Due to the nature of the injection molding process all LCPs will have a slight 1.15° taper. The specimens will then be placed onto a specially designed test rig (see Appendix A). Then the pressure inside the polymer casing will be increased until the material ruptured. Testing will be done in both ambient and cryogenic environments. The cryogenic testing will be done using liquid nitrogen. In this environment the LCP will be expected to be approximately twice as strong.

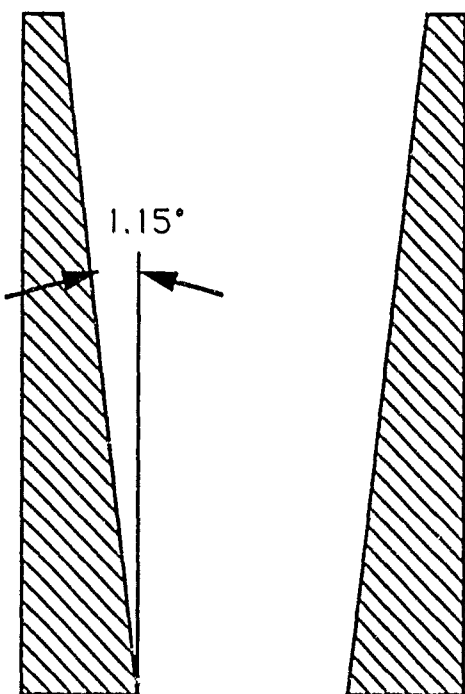
The testing will utilize an on-site pressurization facility to pressurize the LCP case, using gaseous helium. The test-rig has been equipped with an inlet pressurization line and a ventline. The whole device will then be placed inside a stainless steel box. This is done in order to contain both the exploding LCP and the cryogenic material.

During the cryogenic testing the LCP will be pre-pressurized to 300 PSIG before the test rig is submerged in the cryogens. This pre-pressurization stage will assure that the seals seat properly. Also thermocouples will be installed in order to determine when the 2X4 casing has reached equilibrium.

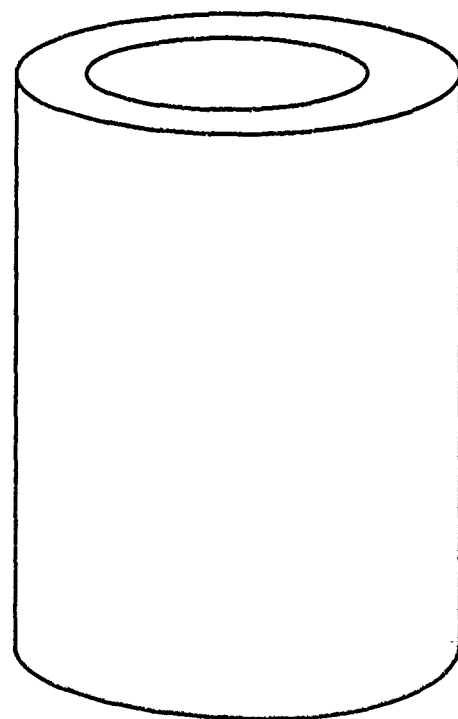
After reaching thermal equilibrium, a pressure build up to 2000 psi will be initiated, with possibilities for higher pressures should the LCP prove to be stronger than expected. Although the maximum pressure is not expected to exceed 2500 psi, the hardware is rated to

**Liquid Crystal Polymer 2X4 Perspectives**

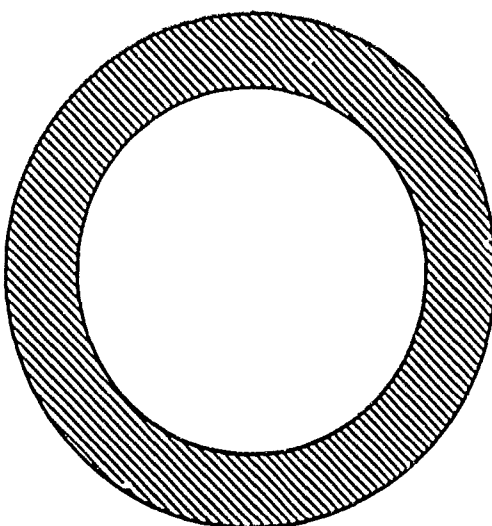
Cross Sectional View:



Front View

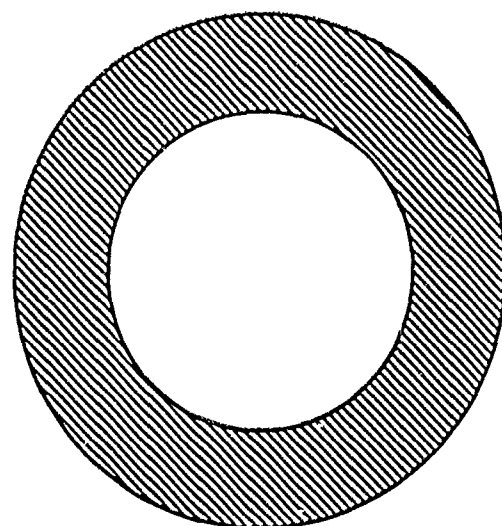


Thin End:



Average Dimensions:  
Wall Thickness: 0.1297  
Inner Diameter: 2.2286  
Outer Diameter: 2.4895

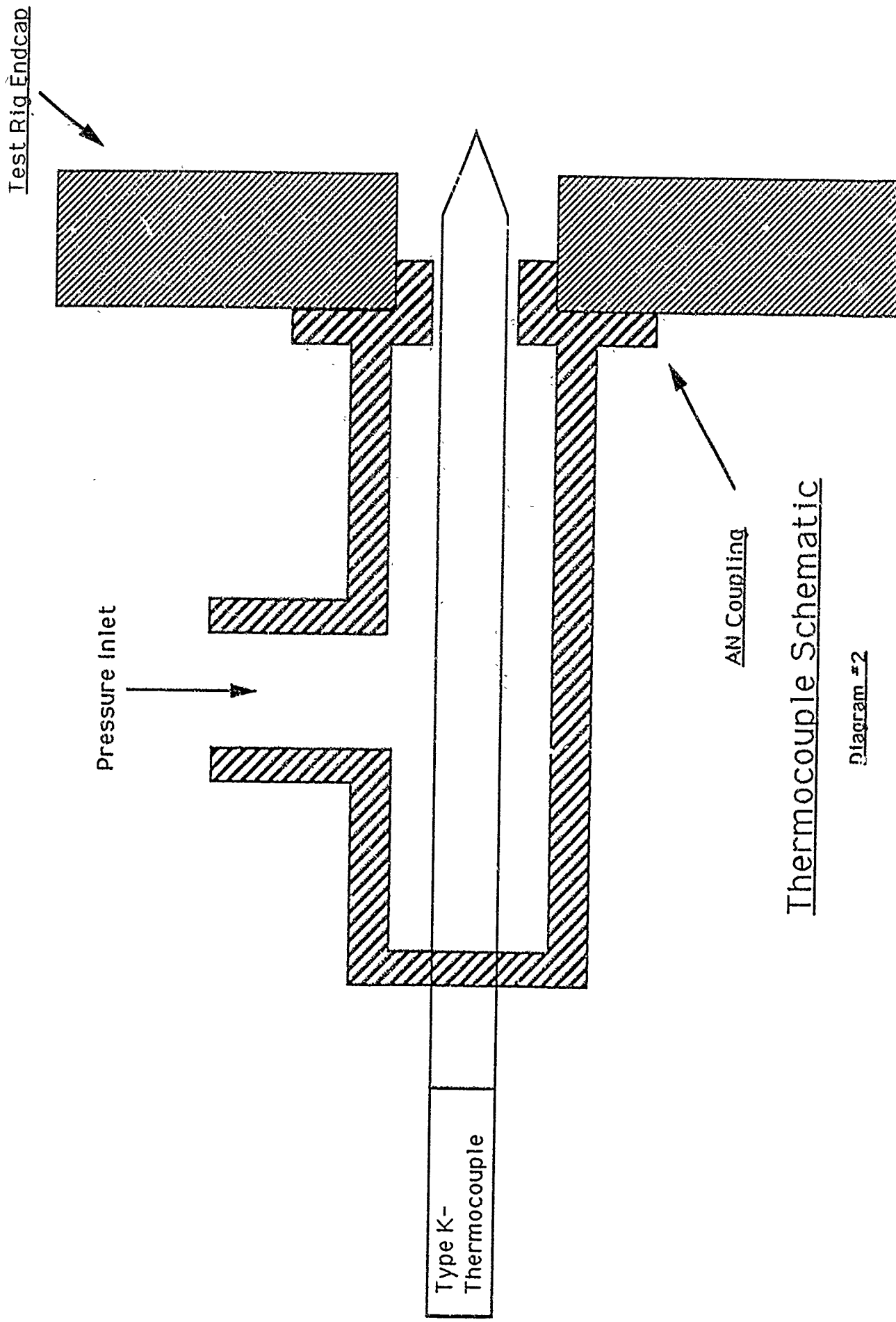
Thick End:



Average Dimensions:  
Wall Thickness: 0.2095  
Inner Diameter: 2.0545  
Outer Diameter: 2.4895

4000 psi.

A pressure transducer is part of the necessary instrumentation. A back-up transducer will also be in place to back-up in case of failure. The transducers will be placed upstream of the 2X4 LCP. All thermocouple data will be taken with two thermocouples that will be ported through a "T" connector at either end of the test rig. The thermocouples will be located at the ends of the "T" (also known as the inlet/thermocouple manifold) allowing them direct access to the 2X4 case chamber. The pressure inlet and the ventline outlet will both use the other "T" port (see Diagram 2). Data acquisition will be taken to provide 100 samples a second, no higher rates are necessary.



Thermocouple Schematic

Diagram #2

## Appendix A

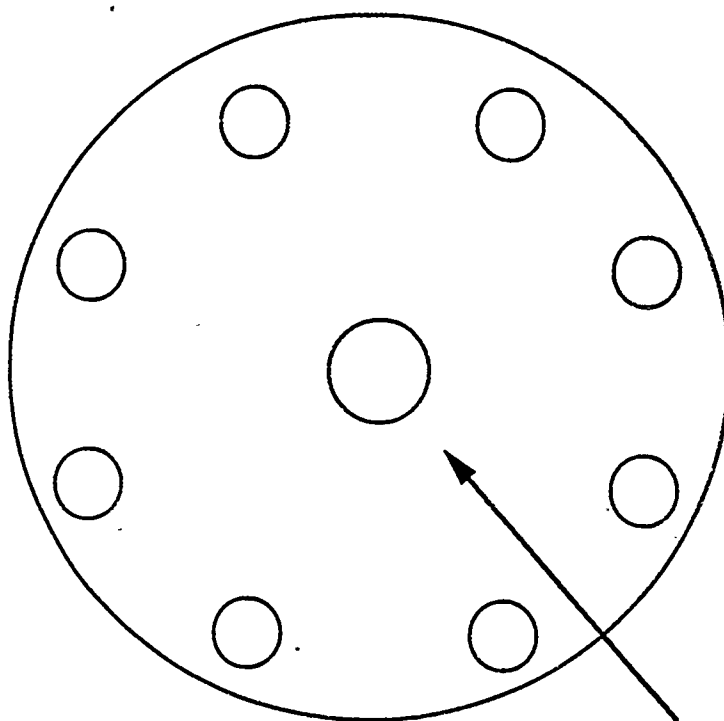
The LCP casing will be tested in a specially designed test rig. The test rig is made of stainless steel. The stainless steel is of the 300 series, which is noted for it's ability to withstand the necessary cryogenic temperatures.

The test rig consists primarily of two end caps (see Diagram#3). These end caps go both above and below the LCP (see Diagram #4). The LCP will be fitted around the inner flange of the test rig end cap. The pressure will be retained via a pressure seal also placed around the flange. The entire structure will be held together by a set of 6 bolts, that run from one end cap to the other.

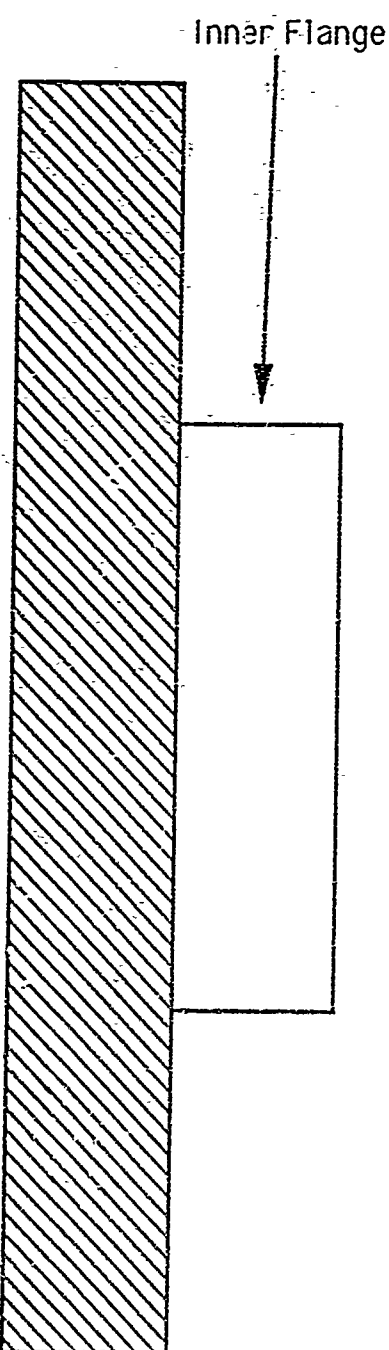
Diagram #3

Test Rig Endcap

Bottom View



Side View



Top View

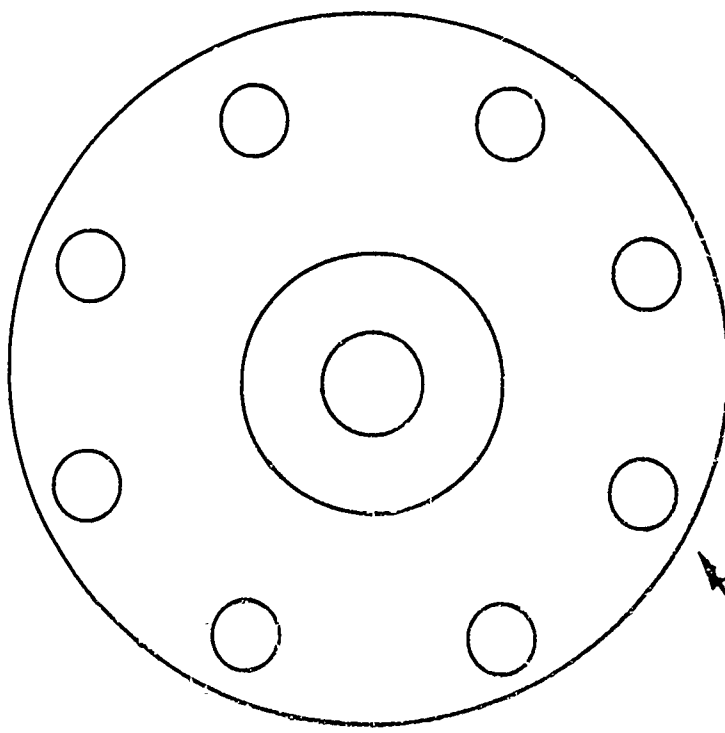
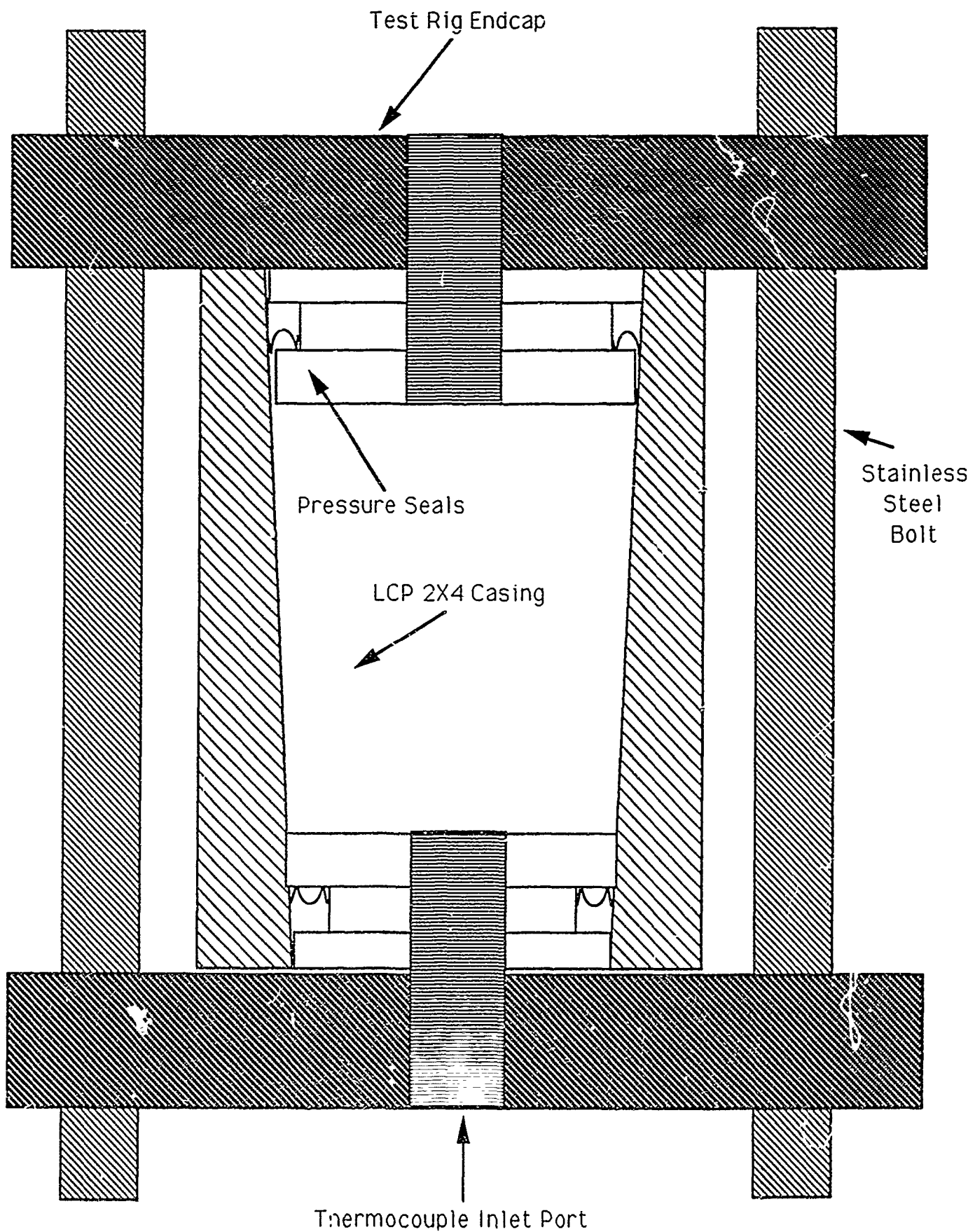


Diagram #4



Final Report

Tracy Reed

I had two main tasks to accomplish at Phillips Laboratory over the summer. I had to do an annealing study on HX-4000, and the tensile testing of several liquid crystal polymers. The object of the annealing study was to find the optimum time and temperature for annealing, find the effects of annealing on HX-4000, and to confirm the already known melting point of the polymer. The object of the tensile testing was to discover the tensile properties of the liquid crystal polymers.

In order to increase the melting temperature and possibly the tensile strength of certain liquid crystal polymers, they can be annealed. In order to anneal a specimen, one must put it in an oven at a certain temperature for a certain length of time and then be allowed to cool to room temperature. This time varies, depending on the material the specimen is made of. The time and temperature necessary to properly anneal HX-4000 was unknown. I set up a test matrix in order to determine this.

In order to anneal the HX-4000 I needed an oven with a nitrogen purge. There were none available so I had to modify one of the ovens on hand. When I started the oven on a test run, the temperature rose and then fluctuated wildly. The cool nitrogen was entering the oven and then carrying off heat with it through the cracks around the unsealed door. The temperature controller could not handle this. Many things were tried to solve this problem. The only one that really worked was to put a rotometer in the nitrogen line to slow the nitrogen flow. The standard valve in the hood could not limit the flow well enough.

After a five minute purge, the nitrogen flow was cut down to nearly nothing. Just enough to keep the oxygen out of the oven. Once the temperature fluctuations were under control, it was time to implement my test matrix. The matrix called for me to run the dogbones in the oven at temperatures varying from 200 to 320 degrees Fahrenheit. The time was varied from four hours to twenty-four hours. It was predicted that the dogbones would turn brown once they reached the approximate annealing temperature. This was not noticed until they reached a temperature of at least 300 degrees. The dogbones were dark green when we put them in the oven. As the specimens were heated for longer times at 300 degrees, they got darker. After 24 hours at this temperature, they were very brown. As the experiment continued, it was determined that HX-4000 melts at a temperature of 320 degrees Fahrenheit.

After the HX-4000 dogbones had been annealed they were tested for any change in mechanical or thermal prop. Each of the dogbones underwent Thermo Mechanical Analysis (TMA) and Dynamic Mech. Analysis (DMA). These tests were to find out if the melting point had increased. After obtaining the results of these tests, we concluded that there had been no significant change in the thermal properties of the material. More study is needed on the annealing of HX-4000.

My second task was to test the mechanical properties of several liquid crystal polymers. I was trained to use an Instron tensile testing machine with a 10,000 pound load cell. I then began testing of the liquid crystal polymers. The dogbones to be tested were instrumented with an extensometer to determine the strain characteristics of each dogbone. The dogbones were to be pulled until they broke. Approximately six of each of the five different types of dogbones were tested. Occasionally, a specimen would break in the grips of the machine. This would yield unreliable data and the experiment would have to be done again. Annealed and unannealed HX-4000 was tested also. Some of the dogbones had exceptionally high tensile strengths. One particular type, RC-500, reached a tensile strength of 24,000.

As stated above, annealed and unannealed HX-4000 dogbones were tested. These specimens were tested just like the others were as described above. The unannealed HX-4000 and the annealed HX-4000 showed no significant difference in tensile strength or strain properties. My mentor and I were both disappointed in these findings, however we remain confident that HX-4000 is annealable. More research will be done on this subject.

The HX-4000 annealing experiments will be continued in an effort to increase the melting point of the material and its tensile strength. The tensile testing of the other liquid crystal polymers turned out well. I found some of them to be quite strong. Already, some of the materials have been used to make 2x4 inch rocket motor casings for test firing and hydroburst testing.

ANALYSIS OF MODEL OUTPUT STATISTICS THUNDERSTORM  
PREDICTION MODEL

High School Apprentice GL/LYS Hanscom AFB

Frank A. Lasley

Abstract

Model Output Statistics (MOS) Thunderstorm prediction information and Service A weather observations collected for the past two years were studied in an effort to validate the predictions generated by MOS. Predictions from the same three month period from 1990 and 1991 were analyzed. The major conclusion was that MOS overestimated the majority of the thunderstorm probabilities for 1991.

Introduction

The focus of this research project was to compare the thunderstorm (TRW) predictions for Boston to the actual observations at sites around Massachusetts for the spring and early summer of the past two years. FOUS (Forecast - United States) MOS (Model Output Statistics) is a meteorological tool which provides predictions and probabilities for the occurrence of various weather events. Temperature, rain, thunderstorm occurrence, quantitative precipitation, and dewpoint, are among the parameters predicted by the MOS statistical model. See figure 1 for an example of Mos Output.

MOS Forecast  
 BOS , 72509  
 BOSTON/LOGAN INTL &  
 31-JUL-1991 00:00Z

DAY/GMT	31/06	31/12	31/18	1/00	1/06	1/12	1/18	2/00	2/12
POP06		20	10	10	0	0	0	5	
POP12				20		0		5	10
QPF06	000/1	000/1	000/1	000/1	000/1	000/1			
QPF12				0000/1		0000/1		0000/1	
TSTORM				14		9		17	
MIN/MAX				80		68		90	71
TEMP	67	66	68	74	76	76	73	83	88
DEWPT	62	62	63	65	66	65	65	64	87
WINDS	0604	3305	1908	2410	2507	2407	2312	2310	
CLOUDS	2214/3	1324/3	0432/3	4411/1	6211/1	4411/1	2621/2	3421/2	
CIG	000153	011224	000227	000019	000009	010008	000018	000018	
VIS	000117	002224	000118	000118	000117	001225	000118	000118	
CV	5/6	4/5	6/6	6/6	6/6	6/6	6/6	6/6	
OBVIS	70X2/1	41X4/4	82X0/1	82X0/1	71X2/1	52X3/1	82X0/1	82X0/1	

Figure 1. Example of Mos Output.

Service A observations provide the meteorologist with hourly weather information from observation stations throughout the United States. Observed parameters include temperature, dewpoint, wind, visibility, and cloud layer information. Specific types of precipitation or weather conditions, such as haze, rain, fog, thunder, and snow are also indicated. See figure 2 for an example of Service A observation output.

By combining the MOS predictions with observations and other forecasting tools a meteorologist can make the predictions upon which people's lives and property depend.

30-JUN-1991 13:00Z													
ID	HH	T	TD	PRE	WIND	VIS	WX	LYR1	LYR2	LYR3	LYR4	dPR	PTT
ACK	13	64	62	1009.5*	1005		15		010S	0400			
EWB	13	64	M	1009.5*	0705		10		0400				
MVY	13	66	M	1010.2*	0905		15		0400				
HYA	13	67	54	1009.1*	0000		15		040B	1500			
BVY	13	M	M	1011.2*	0000		5R-		015S	0400			
BOS	13	61	57	1011.0	2006		5R--		043B	0950			
ORH	13	53	50	1010.8	0411		4RW-		003S	015S	0310		
NZW	13	60	55	1009.9	1004		7TRW-		025S	0350			
OWD	13	57	M	1010.5*	0704		3R-		008S	0200			
RED	13	59	57	1011.2*	2706		21/2R-F		007S	030B	0500		
LWM	13	M	M	1010.5*	0505		15R-		015S	1500			
AYE	13	55	55	1011.6	0000		23/4R-F		-X	007S	025B	0390	
CEF	13	58	55	1010.7	0305		5RW-		008S	0280			
BAF	13	57	M	1010.5*	0110		5F		006B	0400			
FMH	13	66	56	1009.8	0000		15R-		044B	0750			

Figure 2. Example of Service A observation output for Massachusetts.

#### Observation and Prediction Specifics

MOS information is available to forecasters nationwide and is widely used by operational meteorologists. MOS generates weather predictions by applying statistical prediction techniques to the output of numerical weather forecast models. MOS forecasts are made for more than 100 geographical locations throughout the US. Boston MOS predictions are localized for Boston and its immediate surroundings. This study investigates the accuracy of the daily thunderstorm predictions for 24, 36, and 48 hours after 00UTC (Universal Time Coordinated), which corresponds to 8pm Eastern daylight time.

Service A observations provide information from surface weather observation sites every hour on the hour. Included in the reports is a weather remarks section, specifically describing the precipitation and/or weather condition, i.e. rain, fog, and thunder.

#### Methodology for Analysis of Model

The MOS prediction model was validated by comparing the thunderstorm predictions and the weather observations for the same time period. MOS predictions for Boston were compared to observations for all of Massachusetts. Observations for within 1 hour (in either direction) of 00UTC were studied, narrowing the scope of the inquiry. The MOS and OBS data for 1990-1991 were retrieved from a tape archive (please see the Appendix for detailed information regarding programs and specific procedures). MOS makes thunderstorm predictions for 24, 36 and 48 hours every 12 hours. So for a given 00UTC time, three forecasts are valid, one each for 24, 36, and 48 hours into the future. If a thunderstorm was reported by any of the stations during the 3 hour time period (one hour before, at, and one hour after 00UTC), the prediction was considered accurate. For each prediction time, data was subdivided by percent, ranging from 1-5%, 6-10%, 11-15%, all the way to 100%, with a separate category for 0%. Data was stored in bins yielding frequencies of observed and predicted (Good forecasts), observed but not predicted (Missed events),

predicted but not observed (False positives), and not observed and not predicted (Valid negatives). See the key for figure five for an example.

#### Results and Concluding remarks

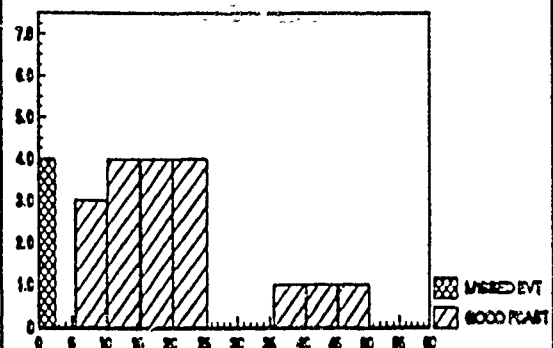
Six months of weather data were analyzed, 13-May-1990 to 29-July-1990 and 12-May-1991 to 28-Jul-1991. MOS predictions for Boston were directly compared to the observations for all of Massachusetts. All available reports were collected, although more stations reported and more predictions were available for the 1990 time period than the 1991 for reasons that are not apparent.

Some definite patterns were observed in the data. The MOS model gives generally low probability percentages for thunderstorms. For example, it is uncommon to witness probabilities higher than 30%. As a result, probabilities of 20 percent or greater have been considered to be cases of near certainty. The 1991 results show a high frequency of poor forecasts - the number of thunderstorm predictions without accompanying occurrences was high (See figure four). Also, many more thunderstorms occurred in 1990 than in 1991. The 1990 data shows a higher percentage of good forecasts, yet also a larger percentage of predictions without occurrences (See figure three). In 1990 predictions were most frequent for the 1 to 5% range and the 11 to 15% range (See figure three). In 1991, predictions were most frequent in the 6 to 10% range

(See figure four). In 1991 the 48 hour model predicted significantly more thunderstorms than at either 24 or 36 hours. In 1990 however, at the 24 hour valid time, the model predicted more thunderstorms than either the 36 or the 48 (See figure three). There seems to be no relationship between good forecasts and percent probability. However there is a relationship between false positive forecasts and percent probabilities. The lower the probability, the more likely the forecast is a false positive forecast.

**GOOD FCAST OCCURENCES OF TRW  
BY % FORECAST**

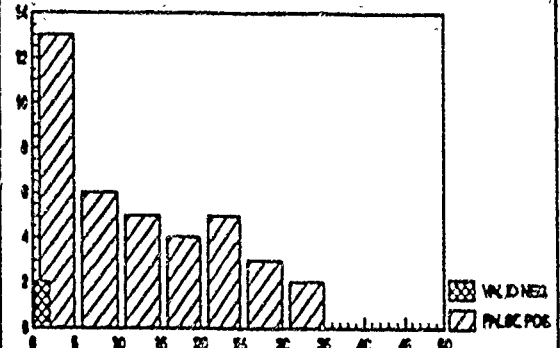
1990 24 hr.



**FALSE POSITIVE FCSTS OF TRW**

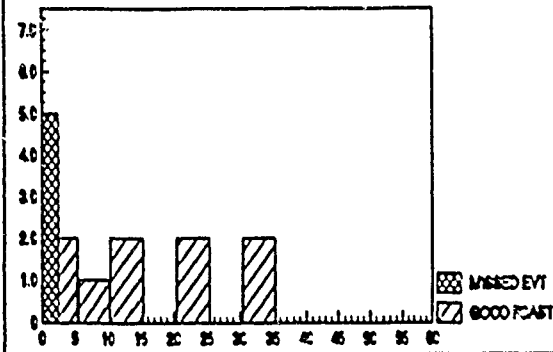
BY % FCAST

1990 24 hr.



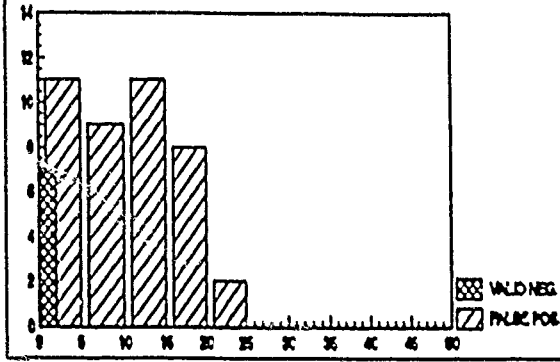
**GOOD FCAST OCCURENCES OF TRW  
BY % FORECAST**

1990 36 hr.



**FALSE POSITIVE FCSTS OF TRW  
BY % FCAST**

1990 36 hr.



**GOOD FCAST OCCURENCES OF TRW  
BY % FCAST**

1990 48 hr.



**FALSE POSITIVE FCSTS OF TRW  
BY % FCAST**

1990 48 hr.

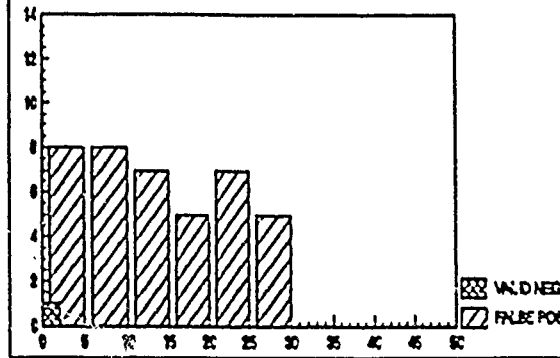
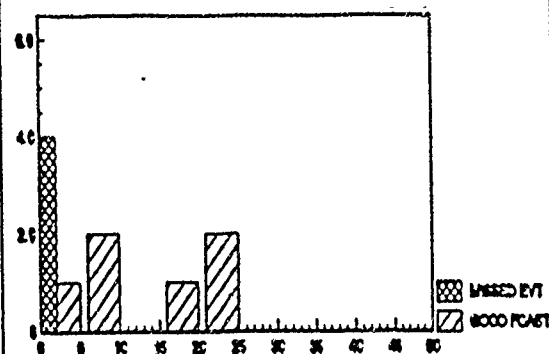
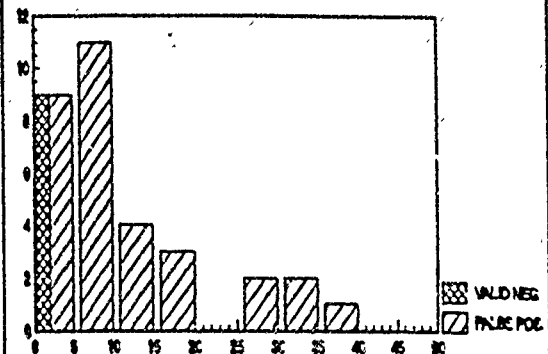


**Figure 3. Graphs showing good forecasts (occurrences that were predicted) and false positive forecasts (predictions without any TRW occurrence ). Graphs represent data for 24, 36 and 48UTC for 1990.**

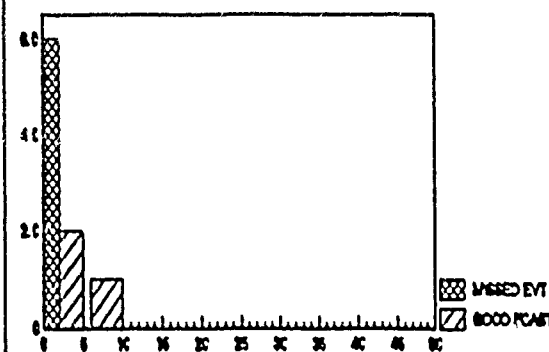
GOOD FCAST OCCURENCES OF TRW  
BY % FCAST  
199124 hr.



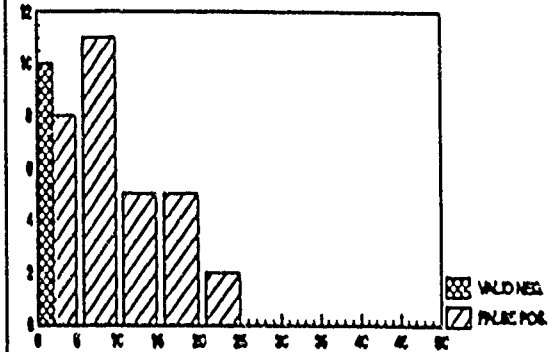
FALSE POSITIVE FCASTS OF TRW  
BY % FCAST  
199124 hr.



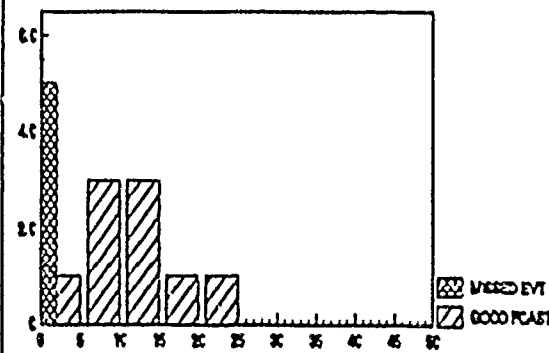
GOOD FCAST OCCURENCES OF TRW  
BY % FCAST  
199136 hr.



FALSE POSITIVE FCASTS OF TRW  
BY % FCAST  
199136 hr.



GOOD FCAST OCCURENCES OF TRW  
BY % FCAST  
199148 hr.



FALSE POSITIVE FCASTS OF TRW  
BY % FCAST  
199148 hr.

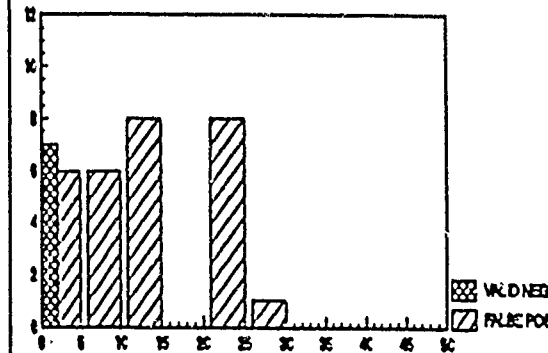


Figure 4. Graphs showing good forecasts (occurrences that were predicted) and false positive forecasts (predictions without any TRW occurrence ). Graphs are for 24, 36 and 48UTC for 1991.

24h FCST

		F	
		Y	N
Ob	Y	18	4
	N	38	2
		1990	

36h FCST

		F	
		Y	N
Ob	Y	9	5
	N	41	7
		1990	

48h FCST

		F	
		Y	N
Ob	Y	16	5
	N	40	1
		1990	

		F	
		Y	N
Ob	Y	6	4
	N	32	9
		1991	

		F	
		Y	N
Ob	Y	3	6
	N	31	10
		1991	

		F	
		Y	N
Ob	Y	9	5
	N	29	7
		1991	

		F	
		Y	N
Ob	Y	24	8
	N	70	11
		Combined 90-91	

		F	
		Y	N
Ob	Y	12	11
	N	72	17
		Combined 90-91	

		F	
		Y	N
Ob	Y	25	10
	N	69	8
		Combined 90-91	

Key for contingency tables.

Y	Good Fcst	Missed Events
N	False Pos	Valid Neg

## Appendix

### Files - Programs

The files/programs encompassed by the project are intended to be used to gather and process the data involved in the analysis of the prediction model. The programs gather data directly from the FOUS/MOS forecast output and the OBS histories. This data is archived offline to free the system of excess data. It is therefore necessary to recover the FOUS and OBS from the 8mm FAA\_02 backup tape in order to process data. Recovery may be achieved by using a routine called `Faa_recover.com` contained within the `FAA_DATA` directory. `Faa_recover` will allow you to place recovered data files to a specified directory. The recover program will check to see that the user has a sufficiently large disk quota (usually on the order of 36000 blocks) to recover the entire save-set for a given week. The programs are designed to operate on one week of data at a time. When the data have been recovered, the `wx_filter.com` procedure is executed. This runs two DCL (Digital Command Language) routines to restore the recovered data to ASCII format, facilitating filtering and sorting processes. Two C programs, `mos_filter.c` and `obs_filter.c` then take over to remove extraneous data from both the MOS and OBS outputs. When filtering has terminated, the status of the output files should be verified. It is then necessary to run `Wx_output.com`, a DCL routine which runs two c programs. `Combo.c`, a C program which sorts the data and writes to output files is executed first, then `Prt_gph.c` merges the output

files and writes to a text file, displaying the data in easy to read chart format.

The steps involved in processing the data are as follows;

1. Login on a node with an 8mm tape-drive. Set the default to Faa\_root (Faa\_recover.com is contained in this directory) and run faa\_recover to recover the data files, placing them in a data directory.
2. Be certain that the logical "FAA\_DATA" is defined to be the directory to which the recovered data is to be located.  
Example: \$ Define faa\_data user\$disk\_1:[lasley.fiddle.wxdata]
3. Edit getmos.com, specifically the day initialization, and the mostime (DCL variable). Also, be sure to set the last day of the month.
4. Edit getobs.com, specifically the day initialization, and the obstime (DCL variable) Also, be sure to set the last day of the month.
5. Run Wx\_filter.com. Contained in [lasley.fiddle], this DCL routine runs getobs, getmos, mos\_filter, and obs\_filter. Getobs and Getmos will output to obs.lis and fous.lis respectively. Notice that getobs uses an output qualifier - this means that a new file will not be created each time the program is executed. Therefore, the file obs.lis must be deleted or renamed after each week is completed. Mos\_filter and obs\_filter take input from obs.lis and fous.lis and write output to record\_p.lis and record\_o.lis.

6. If this is the first time that the set is being run, then run initcomb, a program which will create the necessary files and initialize all values in the files to zero ensuring the validity of any initial data.
7. Finally, execute Wx\_output.com, which will run combo.c, redefine sys\$output and run prt\_gph.c, writing the output to a file name stuff.jnk.
8. Assign fous.lis, obs.lis, record\_p.lis, and record\_o.lis appropriate file names.

Summary of all programs involved in process;

faa\_recover.com - Backup Recovery routine

readme.doc - Information about the programs included in the project.

WX\_filter.com - Executes getmos.com, getobs.com, mos\_filter.c, and obs\_filter.c.

getmos.com - Recovers MOS output from system, returning formatted text.

getobs.com - Recovers OBS output from system, Returning formatted text.

mos\_filter.c - filters MOS output for necessary information only.

obs\_filter.c - filters OBS output for pertinent information only.

wx\_output.com - runs combo, prt\_gph

combo.c - Combines and sorts data into bins (main program)

prt\_gph.c - Prints the stored output from combo.c

Storage Files;

fous.lis - output of getmos.com

obs.lis - output of getobs.com

record\_p.lis - output from mos\_filter.c

record\_o.lis - output from obs\_filter.c

stuff.ink - output from wxoutput.com.

## EQUATORWARD BOUNDARIES OF NIGHTSIDE AURORAE

Jeremy Liebowitz

Finding the equatorward boundary of auroral image data recorded by the Polar Bear satellite can help determine the approximate southern edge of aurorae and where aurorae will appear as a function of solar activity. I have used the current image processing software to locate exact boundaries for specific aurorae and then compared these radii of the auroral oval to the  $K_p$  index in order to find an algorithm which can relate  $K_p$  to the location of the aurora.

The aurora borealis, or northern lights, was a fascinating mystery for many years and is only just now beginning to be understood. The way the aurora is explained at the present time begins with solar activity. Protons and electrons are carried by the solar wind towards the magnetosphere (magnetic field of the earth). A magnetic field in the solar wind may connect with the magnetic field in the earth, thus creating a current along the field lines of the earth's magnetosphere. Under certain conditions the electrons form a sheetlike structure between 10,000 and 20,000 kilometers above the earth which accelerates particles (the electrons), giving them enough energy to penetrate the atmosphere up to an altitude of 50 km above the earth. These particles then collide with other

particles, either ionizing or exciting them. The ionized or excited particles give off light as they sink to a lower energy level or gain electrons. This light is what we see when we observe the aurora, although often the light isn't in the visible spectrum and is impossible to detect without infrared or ultraviolet sensors. Polar Bear carried an ultraviolet sensor which was designed to detect aurorae which occur at a height of greater than 100 km.

In the winter of 1986-87 the Polar Bear satellite recorded some of the best data taken by a satellite due to the fact that the satellite was functioning properly. However, even in the best of times the data from a satellite requires a good deal of careful processing. In finding the boundary there are a large number of possible sources of error which can interfere with getting a complete, clear image. Also, when trying to create an algorithm relating radius of the aurora and the amount of solar activity problems can arise, as the aurorae are recorded at exact times and the  $K_p$ , a measure of activity in the magnetosphere (currents), is recorded as three-hour averages.

Many sources of error have to be taken into account when examining auroral data. The first error occurs in the satellite itself. The satellite may move in one of three ways; pitching is the up and down movement of the front and back ends of the satellite, rolling is the rotating of the satellite around its axis from the front to

the back, and yawing is the rotating of the satellite in a plane parallel to the image. All three create errors in placement of the image, but the yawing is the only one which usually occurs in a magnitude greater than 3 or 4 degrees. The software I used can correct errors caused by yawing, pitching, and rolling if the attitude data (position of the satellite) is present, but for many times attitude data simply does not exist (see appendix 1 for how much error yawing can cause in the position of an image). The most important thing to remember is that if you stay close to the center of an image the yawing, pitching, and rolling will not make as much of a difference. Concentrating on the center of the image will greatly reduce the risk of finding an incorrect boundary.

Other problems encountered while trying to find the equatorward boundary of an image include "noise" in the image. "Noise" is basically very bright points in an image which apparently have nothing to do with the aurora. The noise on a particular image could be particles hitting the detector, in which case it would probably not be a problem, creating only a few bright spots not on the aurora. However, if enough particles hit the detector to make certain bright spots on the edge of the aurora indistinguishable from the aurora itself, this can cause problems. Usually an image will not have enough noise to make the entire boundary fuzzy, but there are exceptions

(which sometimes can be solved by smoothing pixels, assuming the noise will be bright but scattered) that can't be cleaned up and must be discarded.

Finally, there is the problem that the images will contain "dayglow." Dayglow is when the sun sends photons into the earth's atmosphere and causes atoms or molecules in the earth's atmosphere to become excited. This excitation brings about the same effect as an aurora-- the giving off of light. This light is not related to the aurora but it still shows up on the detector and is sometimes as bright or brighter than the aurora itself. The problem of dayglow can be solved by limiting the processing steps to a certain part of the image, but often it is very complicated. It's just more sensible to discard the images cluttered with dayglow.

Despite the above problems, if one follows the rules I give above for avoiding the many pitfalls, a boundary can be found with an accuracy of approximately a tenth of a degree for most images (with attitude data) and between a third and a fifth for some of the more "messy" images. In the beginning of processing, it is a good idea to take a careful look at the image and its raw data. If there is no attitude data, the image may or may not be accurate, and if you try to find the boundary you must keep near the center of the image and realize that the results may not be too accurate. If the roll is almost nonexistent, it is probably not such a good idea to use roll adjustment

derived by the computer as this can distort the image and its boundary. Some images may prove on first glance that they have too much noise or dayglow to be deciphered and are worth putting away for another time.

After the initial glance at the raw image, the aim is to change the image so it can be plotted on a sphere with the pole at the magnetic pole. The final image should have a clearly defined boundary between the aurora and the area around it. There are several steps along the way. First, the adjustments for correcting yawing, rolling, and pitching must be made. If there is no data, they won't be made-- it is best to avoid roll adjustment except in cases of serious roll as it can distort the image. Then the image must be smoothed, a very complex process which can often create errors in the boundary, as it is along this boundary where smoothing doesn't work as well. This smoothing, or filtering, works in the following way: it takes the average of the number in its own pixel (each pixel contains a number representing its brightness) and the pixels closest by and uses the average in itself. For example, if five-pixel smoothing were being used, the program would take the average of the pixel and two pixels on each side of it and place it in the original pixel. The process above is done horizontally and then vertically and then the whole thing is repeated. The reason smoothing doesn't work so well is that computer uses a different smoothing for the aurora and for

what it thinks is not the aurora. The program decides that a certain percentage of the image is aurora and it uses very little smoothing in order to keep the areas of brightness in an aurora; it uses a large-pixel smoothing, such as 25, in the non-aurora, in order to eliminate noise and dayglow. The problem with this is that points on the edge of the aurora which are not aurora will be averaged in with values that are extremely high (13 pixels in for 27 pixel smoothing is often into the brightest part of the aurora) and will appear to become part of the aurora, thus pushing the boundary too far to the south. This can be eliminated by optioning to make the computer accept more of the image as aurora and use small smoothing on the aurora. This will create a reasonably consistent boundary without changing the actual location. If there are noise points which have not been properly smoothed out that can be "fixed" later.

The final step, once the image is plotted on magnetic coordinates, is to find the boundary of the aurora using a program which selects a series of points along the boundary that have a certain brightness or greater. Since the program depends on the counts in the pixels, it requires that you know what values to enter for the threshold. Values for the threshold are based on the smoothing and the amplification-- during the previous processing each pixel is multiplied by a constant to make the brighter points easier to distinguish. For example, if the constant multiplier

(amplification) were 15 and the smoothing was 5 or less, you could assume that any point under 7.5 was definitely not on the aurora, because even with smoothing no point which was originally outside the aurora and not surrounded by very bright noise couldn't possibly have a value of more than half the original amplification. If the smoothing has been kept very small on the border of the aurora then it would be safe to assume that 7.5 would be a reasonable threshold for this example. However, if the aurora got very bright very quickly or if there was a little noise or slightly larger smoothing it could be wise to choose a threshold higher than 7.5 (but not larger than 15) in order to keep the boundary from being set too far out. Thus, any threshold between half the amplification and slightly less than the amplification would find the border with an accuracy of at least a half of a degree. If there is almost no noise and no smoothing, a threshold of half the amplification should be able to find the exact boundary. Also note that it is important to not try to find the boundary too close to the edges of the image.

When the boundaries of a sample group of aurorae have been found then their radii (distance from magnetic pole) can be compared to the  $K_p$  index. The one problem with the  $K_p$  index is that it is very inexact and although a high  $K_p$  should indicate a good deal of current, how long does this current last and how much can it change in its three-

hour measuring range? This index is a good general guideline but it does not have an exact relationship to the auroral radius. The reason that we can use the  $K_p$  index to compare is that it measures the amount of disturbance (or current/energy) and the radius of an aurora will have to get larger to sustain more energy, because the excess current needs to be in contact with more area to release more energy. If the current got too great at a certain radius to release all its electrons it would seek a larger path for the current to run in. Thus an increase in  $K_p$  should bring about an increase in radius of the aurora.

The data I got seems to corroborate this theory. Although there are a few stray points, the data basically forms a line with a positive slope. Most of the data is from the winter of 1986-87, but there are some points from the winter of 1987-88 to show that graphs of  $K_p$ -radius (including higher values of  $K_p$ ) from other years follow the same pattern. Three marks ( $(K_p=1.67, \text{ radius}=24.12), (2.33, 27.67), (2.33, 25.54)$ ) were left off the calculation for the line as they are so far off-- their difference is probably just caused by erroneous attitude data. Several of the stray marks may be attributed to the fact that they occurred in especially noisy times and there was a great deal more disturbance still floating around, although the  $K_p$  may have been low for those three hours.

Overall, the results indicate that  $K_p$  is directly

Overall, the results indicate that  $K_p$  is directly proportional to radius of the aurora and that the approximate algorithm relating the two is radius(degrees)= $16.89+1.47(K_p)$ , assuming that the center of the aurora lies at magnetic latitude 85.6 degrees and magnetic local time 0.8 hours. This can be made use of by using  $K_p$  to determine where the aurora will appear, helping people to keep it from interfering with their communications, tracking systems, or satellite pictures.

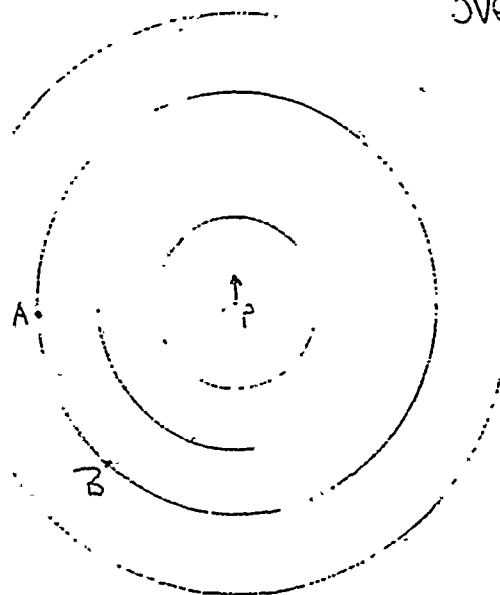
## APPENDIX 1: CORRECTING ERRORS IN IMAGE PROCESSING

Images produced by a satellite are often distorted, bent, or turned. If the satellite was completely stable and the earth were completely flat the image would be much more true, but unluckily this is not the case. Due to the curvature of the earth and the yawing, pitching, and rolling of the satellite, the images are often incorrectly placed or proportioned. Yawing, the rotating of a satellite, is one of the most prominent problems associated with the Polar Bear satellite flight. Correcting the error caused by yawing can lead to much greater accuracy of data processing.

It is important to understand how yawing changes the data before going farther into the problem. If a satellite were directly over the pole and focusing on a pixel at 70 degrees latitude, yawing would reposition the pixel at 70 degrees latitude to different longitudes. If the satellite yawed 360 degrees it would view all pixels at 70 degrees latitude. However, if it was not directly over the pole yawing would also produce changes in latitude. However, the distance between the real and erroneous latitudes will always be measured by a circular arc, assuming that the aurora forms a concentric shell around the

earth. The direction of the error coincides with movement along a circular path in the opposite direction of the yawing.

Figure 1 View of Earth from Satellite directly over Magnetic Pole



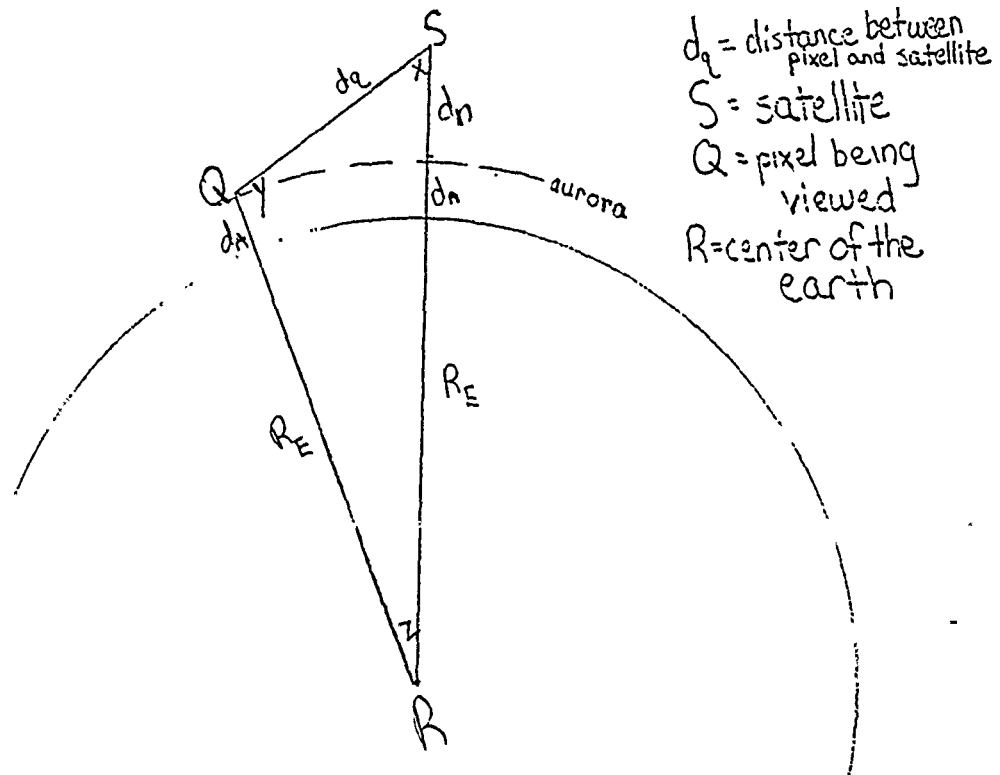
P=magnetic pole  
↑=direction satellite is heading

A=pixel being viewed

B=appearance of pixel if satellite yaws 45° to right

The procedure for determining exact error can be determined by a series of geometric and trigonometric operations which can be combined into a fairly simple equation for determining how many kilometers error the yawing caused. First, however, a set of variables must be introduced in case certain adjustments need to be made.  $R_e$  will stand for the radius of the earth, normally about 6370 km except when taking polar shrinkage into account.  $D_n$  will stand for the distance between the satellite and the part of the aurora directly under it.  $D_a$  will stand for the distance between the aurora and the earth. Angle  $x$  will be

the angle between the line perpendicular to the aurora and the line pointing to the point being viewed, while angle  $\epsilon$  will be the angle of error. Angle  $\gamma$  will be the angle between the line drawn to the point on the aurora and angle  $\alpha$  will designate the central angle shown in the diagram.



$d_s$  = distance between pixel and satellite  
S = satellite  
Q = pixel being viewed  
R = center of the earth

The equation is generated in the following way.

First, the law of sines is used to generate angle y (which must be made into a quadrant II angle in order by subtracting it from  $180^0$ ) and then angles x and y are subtracted from  $180^0$  in order to find angle z.

$$y = \pi - \sin^{-1} \left[ \frac{(d_n + d_A + R_E) \sin X}{d_A + R_E} \right]$$

$$Z = \pi - x - y$$

Then the law of sines can be used again in order to find the distance between the satellite and the viewing point on the aurora,  $d_q$ .

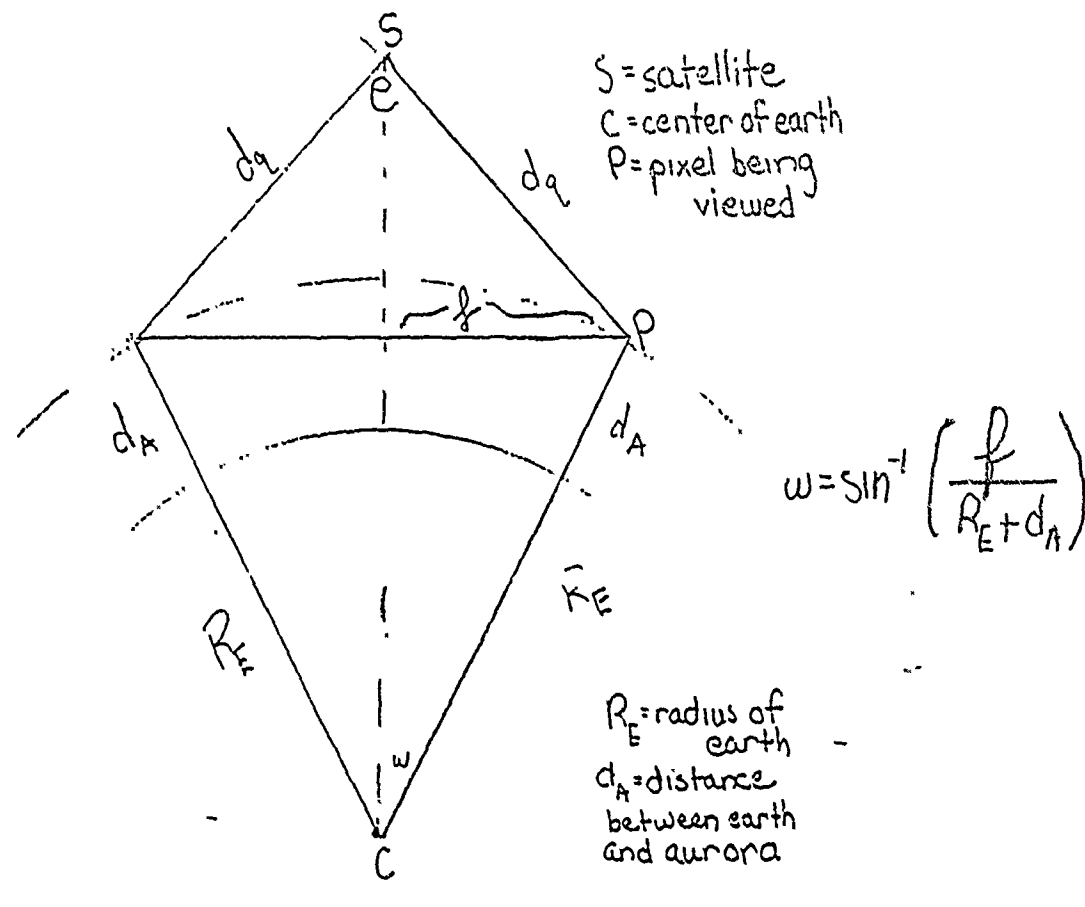
$$d_q = \frac{\sin Z (d_A + R_E)}{\sin X}$$

This segment can be duplicated and the angle e can be placed in between the two segments as in our example of a satellite directly over the pole-- that is, we have the right to create an isosceles triangle because this example shows the segments will be the same lengths. The length of

half the base of the isosceles triangle can then be found using the definition of sine.

$$f = \sin\left(\frac{1}{2}\theta\right) \cdot d_q$$

Creating a triangle like the one in the figure below, with the center of the earth as one vertex, the central angle of the earth can be found using inverse sine.



After doubling this angle and converting it to radian measure, the formula for arclength of a sector,  $s=r(\theta)$ , we can multiply the angle by the quantity  $R_e + d_a$  in order to find the actual distance error.

$$\text{Actual Distance Error} = 2w (R_e + D_a)$$

Therefore, the final equation would be, with c=actual distance error:

$$c = 2(r_e + d_a) \arcsin\left(\frac{\sin(\frac{e}{2})}{\sin[\arcsin\frac{([d_a + d_n + R_e] [\sin x]) - x}{d_a + r_e}] \sin x]}\right)$$

Note: The above equation is slightly simplified, as the pi's subtract out and the "d<sub>a</sub> + R<sub>e</sub>"'s cancel out by division.

## DATA RESULTS SECTION

Figure 1: Images before and after processing.

Figure 2: Image containing dayglow.

Figure 3: Chart of sample yaw calculations.

Figure 4: Table of images used in data.

Figure 5: Graph of 1987 images ( $K_p$ -radius).

Figure 6: Graph of 1988 images ( $K_p$ -radius).

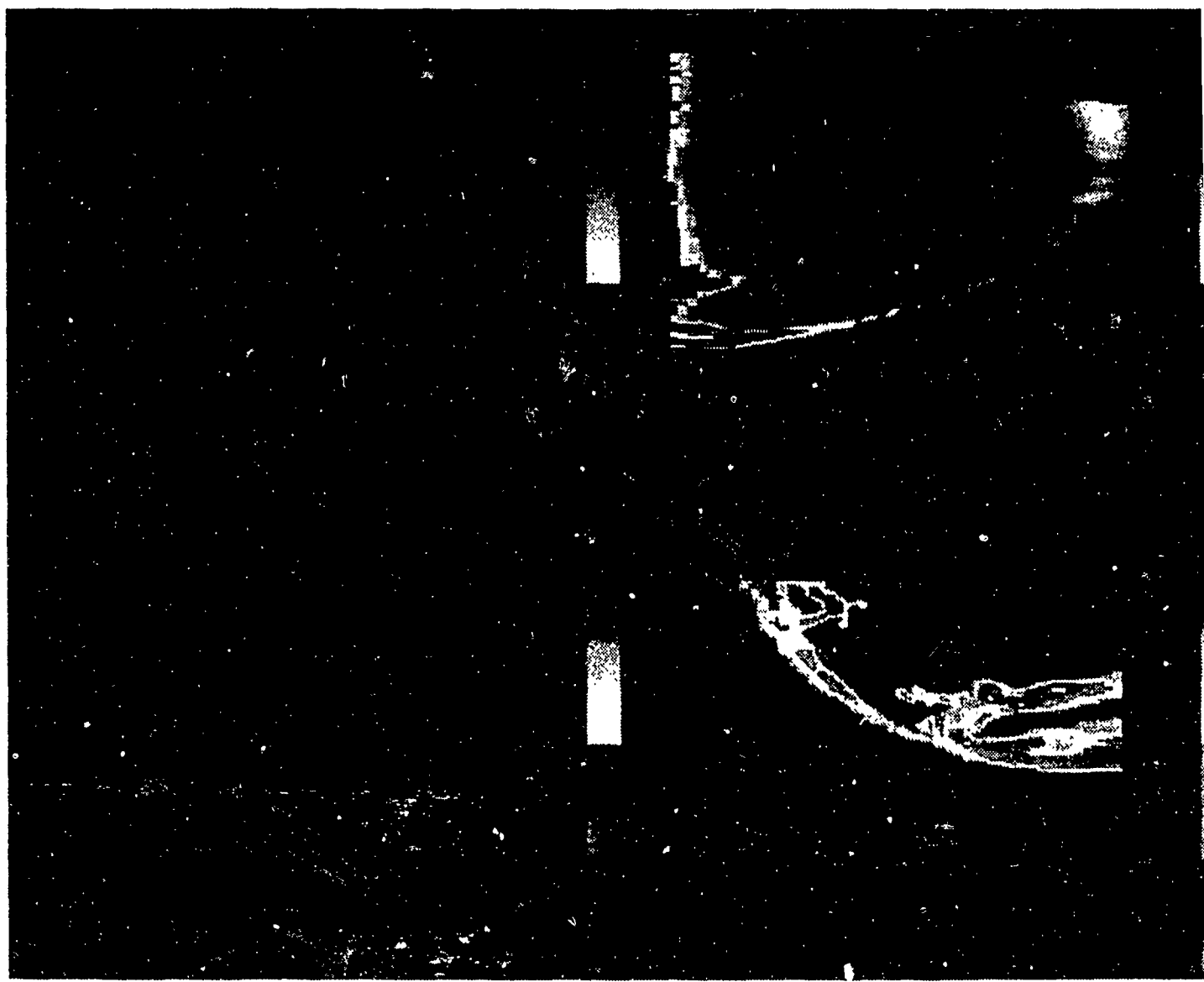
Figure 7: Graph of 1987-1988 images ( $K_p$ -radius).

Figure 8: Chart of how points from graph above fit onto the line relating all the points.

Figure 1

Image before processing

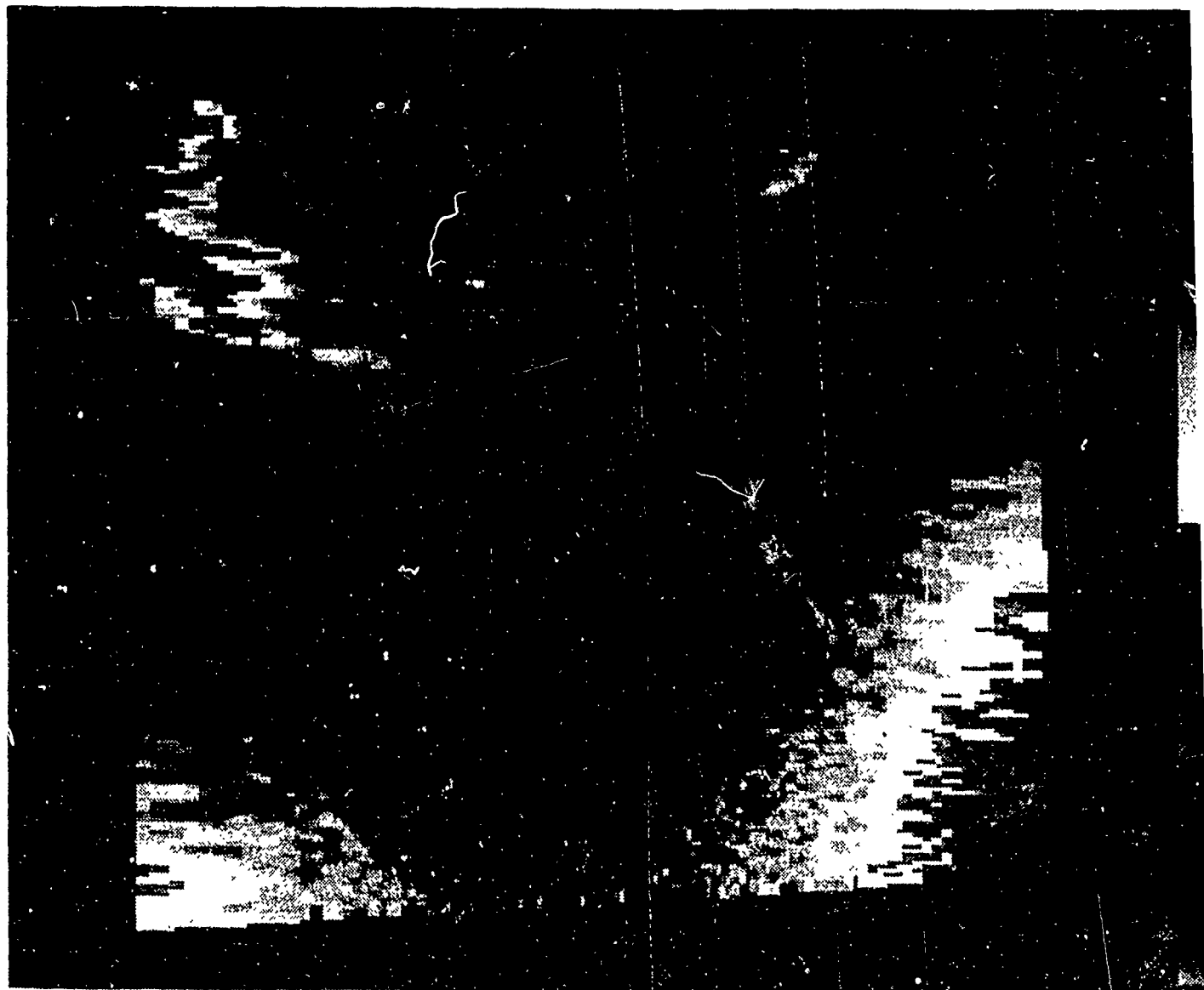
Image after processing



PL/GPIM UV DATA

Figure 2

Image with dayglow



PL/GPIM UV DATA

Figure 3

Error caused by yawing

The following table contains specific examples of calculating the error caused by a known degree of yaw using the final equation from appendix 1. They are not actual calculations used in the data set but they give a good idea of how well you can rely on imageds without attitude data and how specific degrees of yaw affect the image. The viewing angle is angle x, the angle between the satellite and the pixel being viewed.

VIEWING ANGLE	DEGREES YAW	KM ERROR	DGR ERROR
30	2.5	41.5	.37
30	5.0	90.25	.81
30	7.5	135.73	1.22
50	2.5	61.17	.55
50	5.0	152.3	1.36
50	7.5	202.9	1.82
15	2.5	36.5	.33
15	5.0	78.66	.71
15	7.5	119.7	1.08
7.5	2.5	35.5	.32
7.5	5.0	76.40	.69
7.5	7.5	116.24	1.04

Note: In the equation radians must be used as a unit of measure, and the answer is in kilometers, but I used degrees on the table because it is easier to visualize angles in degrees and distance on the earth in degrees latitude.

Figure 4

DATE	TIME (UT)	K <sub>p</sub>	RADIUS (degrees)
2/28/87	9:12 AM	2.33	25.54
2/28/87	12:24 AM	2.00	20.88
1/29/87	2:54 AM	4.67	21.07
2/28/87	7:24 AM	2.33	27.67
2/22/87	7:54 AM	4.00	26.92
1/25/87	4:24 AM	2.67	18.81
1/30/87	1:42 AM	1.67	19.47
2/28/87	7:24 PM	1.67	23.86
2/22/87	7:54 AM	4.33	24.67
2/6/87	1:06 AM	1.33	18.70
2/19/87	11:54 PM	2.33	17.74
1/27/87	1:54 AM	1.00	17.97
1/27/87	12:12 AM	1.00	18.20
2/2/87	10:24 PM	0.33	18.53
1/14/88	3:48 AM	4.00	22.40
1/14/88	2:06 AM	4.00	22.34
1/14/88	7:36 PM	6.33	28.01
1/14/88	11:06 PM	7.00	30.94
1/24/87	12:30 AM	2.67	20.19
1/23/87	10:42 PM	3.00	21.73
1/24/87	12:30 AM	2.33	20.84
1/26/87	10:24 PM	0.33	17.79
2/24/87	7:18 PM	4.00	22.13
2/11/87	9:42 PM	1.67	20.79
2/19/87	10:12 PM	2.33	19.00
2/19/87	10:12 PM	2.33	18.75
2/19/87	9:06 AM	2.33	17.61
2/6/87	7:12 PM	1.33	19.48
2/7/87	3:54 AM	1.67	18.07
2/9/87	5:12 PM	2.67	20.79
2/9/87	6:54 PM	1.00	19.10
1/23/87	10:42 PM	3.00	21.38
1/28/87	9:42 AM	3.00	22.38
1/28/87	11:24 PM	3.33	22.01
2/9/87	11:12 PM	3.33	22.63
1/28/87	6:12 PM	3.33	23.57
2/8/87	4:24 AM	3.33	20.80
1/27/87	7:30 PM	0.67	18.09
1/31/87	7:42 PM	0.67	18.70
2/3/87	11:00 PM	0.67	17.18
2/4/87	9:42 PM	0.67	19.02
2/4/87	11:24 PM	0.67	18.50
2/5/87	6:42 PM	0.67	18.54
1/25/87	1:00 AM	0.33	17.98
1/25/87	2:42 AM	0.33	17.10
1/26/87	10:24 PM	0.33	17.71
1/29/87	10:12 PM	0.33	17.48
1/29/87	12:00 AM	0.33	16.06
1/30/87	3:42 AM	0.33	17.48
2/2/87	10:24 PM	0.33	18.40
2/4/87	4:12 AM	0.33	17.60
2/5/87	1:12 AM	0.33	16.93

DATE	TIME (UT)	K <sub>p</sub>	RADIUS (degrees)
2/5/87	2:54 AM	0.33	16.85
1/4/88	9:36 PM	5.33	22.66
1/4/88	11:18 PM	5.33	26.18
1/6/88	8:48 PM	6.00	26.09
1/11/88	4:06 AM	4.00	20.18
1/14/88	12:18 AM	4.00	21.32
1/7/88	3:48 AM	4.33	22.50
1/7/88	9:18 PM	4.00	23.19
1/7/88	11:06 PM	4.00	21.27
2/21/88	1:42 AM	4.00	18.26
1/2/88	8:18 PM	2.00	22.14
1/4/88	4:06 AM	2.00	17.81
1/13/88	7:06 AM	2.00	20.08
1/13/88	8:48 AM	2.00	19.82
1/10/88	3:36 AM	0.00	15.39
1/11/88	7:48 PM	0.33	17.66
1/13/88	1:36 AM	0.33	18.07
1/4/88	7:36 AM	1.00	20.36
1/9/88	6:54 AM	1.00	18.08
1/9/88	8:36 PM	1.00	19.03
1/9/88	10:18 PM	1.00	18.29
1/10/88	12:06 AM	0.67	18.07

Figure 5

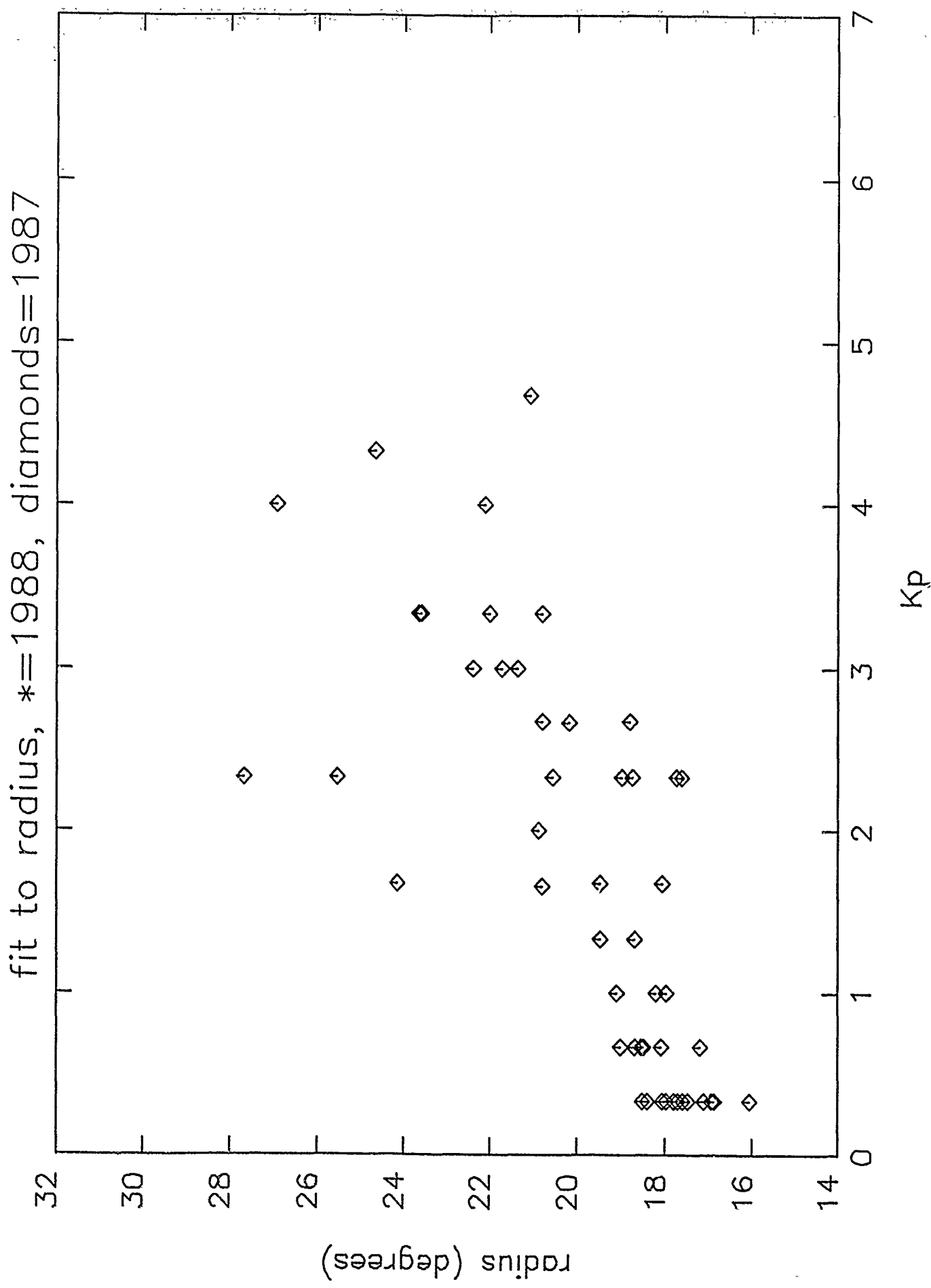


Figure 6

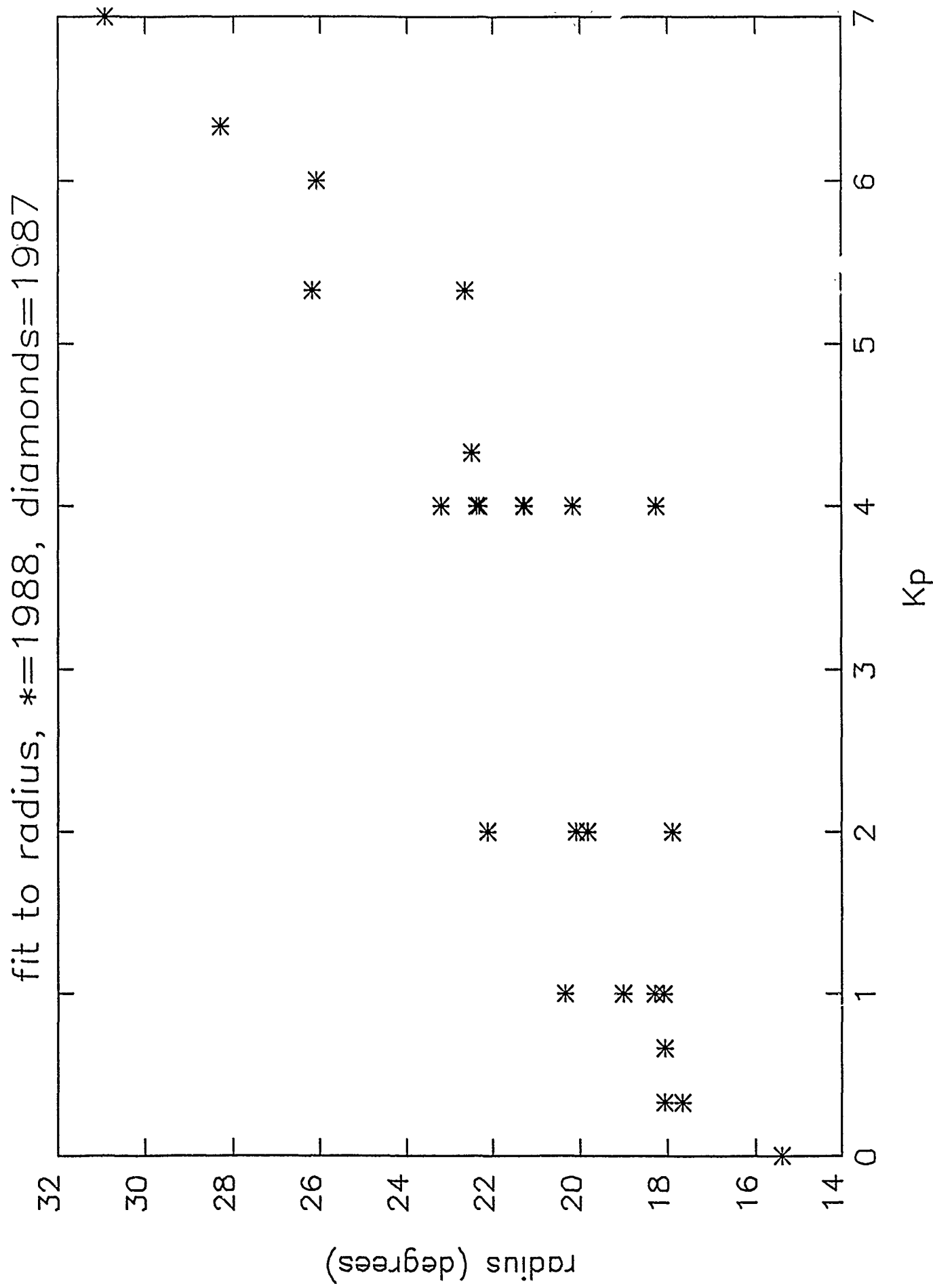
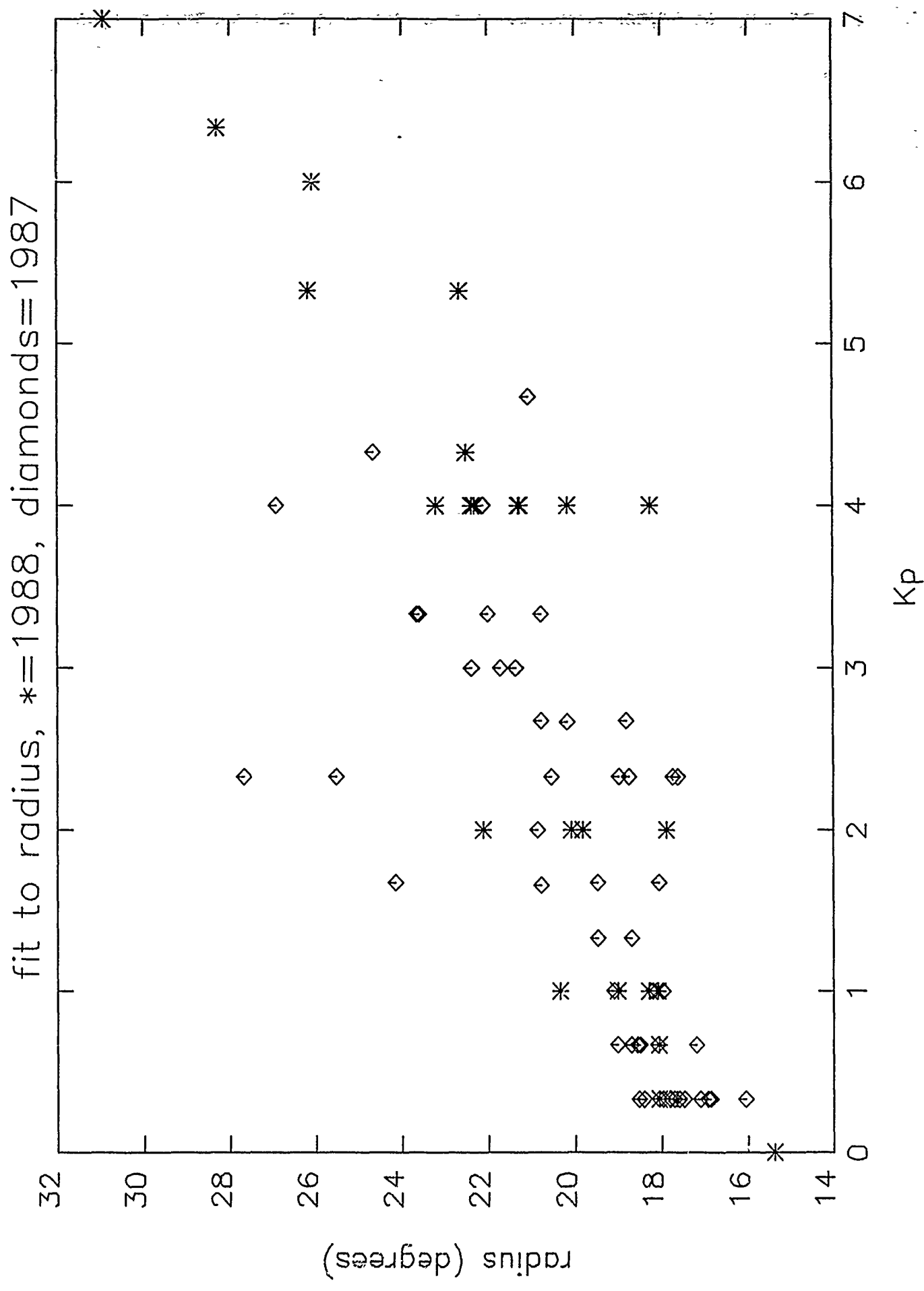


Figure 7



1  
INPUT THE DEGREE OF THE POLYNOMIAL (=<9)

1  
A( 1) = 0.1688913E+02  
A( 2) = 0.1470254E+01

X,	Y FIT,	Y - (Y FIT) DIFFERENCE	
2.0000	20.8800	19.8296	1.0504
4.6700	21.0700	23.7552	-2.6852
4.0000	26.9200	22.7701	4.1499
2.6700	18.8100	20.8147	-2.0047
1.6700	19.4700	19.3445	0.1255
4.3300	24.6700	23.2553	1.4147
1.3300	18.7000	18.8446	-0.1446
2.3300	17.7400	20.3148	-2.5748
1.0000	17.9700	18.3594	-0.3894
1.0000	18.2000	18.3594	-0.1594
0.3300	18.5300	17.3743	1.1557
4.0000	22.4000	22.7701	-0.3701
4.0000	22.3400	22.7701	-0.4301
2.6600	20.1900	20.8000	-0.6100
3.0000	21.7300	21.2999	0.4301
2.3300	20.5600	20.3148	0.2452
0.3300	17.7900	17.3743	0.4157
4.0000	22.1300	22.7701	-0.6402
1.6600	20.7900	19.3298	1.4602
2.3300	19.0000	20.3148	-1.3148
2.3300	18.7500	20.3148	-1.5648
2.3300	17.6100	20.3148	-2.7048
1.3300	19.4800	18.8446	0.6354
1.6700	18.0700	19.3445	-1.2745
2.6700	20.7900	20.8147	-0.0247
1.0000	19.1000	18.3594	0.7406
3.0000	21.3800	21.2999	0.0801
3.0000	22.3800	21.2999	1.0801
3.3300	22.0100	21.7851	0.2249
3.3300	23.6300	21.7851	1.8449
3.3300	23.5700	21.7851	1.7849
3.3300	20.8000	21.7851	-0.9851
0.6700	18.0900	17.8742	0.2158
0.6700	18.7000	17.8742	0.8258
0.6700	17.1800	17.8742	-0.6942
0.6700	19.0200	17.8742	1.1458
0.6700	18.5000	17.8742	0.6258
0.6700	18.5400	17.8742	0.6658
0.3300	17.9800	17.3743	0.6057
0.3300	17.1000	17.3743	-0.2743
0.3300	17.7100	17.3743	0.3357
0.3300	17.4800	17.3743	0.1057
0.3300	18.0600	17.3743	0.6857
0.3300	16.0600	17.3743	-1.3143
0.3300	18.4000	17.3743	1.0257
0.3300	17.6000	17.3743	0.2257
0.3300	16.9300	17.3743	-0.4443
0.3300	16.8500	17.3743	-0.5243
7.0000	30.9400	27.1809	3.7591
6.3300	28.2900	26.1958	2.0942
5.3300	22.6600	24.7256	-2.0656
5.3300	26.1800	24.7256	1.4544
6.0000	26.0900	25.7107	0.3793
4.0000	20.1800	22.7701	-2.5901
1.0000	21.3200	22.7701	-1.4501
4.3300	22.5000	23.2553	-0.7553
4.0000	23.1900	22.7701	0.4199
4.0000	21.2700	22.7701	-1.5001
4.0000	18.2600	22.7701	-4.5101
2.0000	22.1400	19.8296	2.3104

2.0000	17.8700	19.8296	-1.9596
2.0000	20.0800	19.8296	0.2504
2.0000	19.8200	19.8296	-0.0096
0.0000	15.3900	16.8891	-1.4991
0.3300	17.6600	17.3743	0.2857
0.3300	18.0700	17.3743	0.6957
1.0000	20.3600	18.3594	2.0006
1.0000	18.0800	18.3594	-0.2794
1.0000	19.0300	18.3594	0.6706
1.0000	18.2900	18.3594	-0.0694
0.6700	18.0700	17.8742	0.1958
CHISQR =	0.70091E+03	SUM ABS(DIFF) =	75.635
FORTRAN STOP			

## SOLAR TERRESTRIAL INTERACTIONS

GALEN MCKINLEY

This summer, I worked on an ongoing project to produce a database of all the data collected by neutron monitors at stations all over the world during solar Ground Level Events (GLE's).

A GLE is often the result of a powerful solar flare that greatly increases the number of solar protons hitting the surface of the Earth. There have been 52 such events between February 1942 (Event #1) and June 1991 (Event #52) which have been recorded by 122 various stations. The ways in which the stations have recorded these data and the entirety of their reports vary widely. Therefore, it is important to establish a computerized database that is in a standard format, that is easy to understand, and that is quick to access via electronic mail and by computer programs for analysis.

By standardizing and simplifying the data, we are making it accessible to scientists who are now able to study GLE's more effectively and learn more about the sun and solar effects on the Earth.

To help establish this database, I entered and processed some miscellaneous data from various events. However, I mostly updated entire events to ensure that they were as complete as possible before they were moved from the CDC CYBER 750 to the VAX 8650. To do my tasks, I used a

ZENITH PC as a terminal emulator for these two computers.

I worked with several different types of files on the CYBER and VAX.

An E-file contains raw, unprocessed data that have been entered directly from the reports sent to us by the 122 various stations. In a complete file, there are uncorrected counts, pressures, and pressure corrected counts for all the time intervals desired for the specific event. However, incomplete files are still processed and included in the database because they can still be very informative and useful.

(See Example #1)

A C-file is an E-file that has been processed by computer programs written by Louise Gentile. It includes the counts per second and the percentage increases that are useful to the scientist because they show the increased levels of solar particles during an event. (See Example #2) The percentage increase is also plotted by the computer to give a visual representation of the increased flux during an event. (See Example #3)

A NTP file contains station information and scale factors for the raw data. These files are needed to process the data because they hold information that the computer programs use to change the raw data in an E-file to the counts per second and percentage increase of the C-file. They also contain information that is used to make the headers that top each E- and C-file. These headers tell the scientist where a station is located on the globe, its altitude, and other information that makes studying the data more effective and productive. (See Example #4)

The catalog lists the data we have received from the stations for each event, shows which data has and has not been entered, and gives the

station information used in the NTP files.

The event folders are where we store the station reports that are sent to us for each event. The event notebooks are the books in which the hard copies of the E- and C-files, and the plots are kept for reference.

Updating an event is a process that includes many steps to insure that the event is as complete as possible once it has been updated. We want to get rid of any problems or mistakes that were not resolved when the huge task of entering fifty years of data was first undertaken.

First, I would check the catalog against the NTP file to make sure that there were no discrepancies so that the catalog and the headers would be consistent. Then, I would go through the event folder and the event notebook to make sure that no new data needed to be entered into the E-files. I would enter whatever data need to be added and talk with Louise Gentile, Jack Campbell, or Peggy Shea to work out any other problems with the data. Once there were no more problems or unentered data, I would remove the old headers and reprocess the E-file. I would print out the E-file, C-file, and plot. Then, after they were checked by Louise, I would take out the old file in the event notebook and replace it with a new one. The last step in this process was to move the updated files to the VAX where they will be permanently stored and will be accessible to scientists via electronic mail.

This summer, I also used data from the GLE database during a project to analyze data collected for Events #15-#51 at the Oulu station

in Finland. I worked with Nick Vickers to find the onsets of these events. The onset is the time period in which the first sign of increased solar protons is found. First, I calculated the point at which a sharp increase can no longer be considered noise in the data. To do this, I found the counts per second at the baseline of the event. Then, I multiplied this number by the seconds in the interval I was examining. Then, I took the square root of this product. The number I arrived at is called the standard deviation of the data, or the sigma. Thirty percent of all randomly generated data will be under this level in terms of a percentage increase. However, ninety eight percent of all noise will be under three sigma. So I multiplied the sigma for each interval of each event by three and compared it to the percentage increases for the event that were recorded at Oulu. I chose an onset at a time where the percentage increase was above three sigma and where it stayed above three sigma for several intervals. Nick also compared the percentage increases to the three sigma and decided where he thought the onset occurred. Nick and I then discussed our results and chose an onset that made sense to us both. Our work will be used in a paper written by Louise Gentile and other scientists that will be delivered to the Cosmic Ray Conference in Dublin, Ireland in August 1991.

The project of producing this extensive database of GLE data is not yet finished for many reasons. There is an enormous amount of data to be acquired, entered, and processed. Although much of these data have been added to the database, there is much more to do. Also, there are

many problems with the data we have. Often times, we cannot interpret the data, or insufficient data have been provided, or station information is incorrect. More of these problems must be resolved before the project is complete. Once it is complete, all that will need to be done is to enter new data from new events to keep the database up-to-date and useful for scientists' study of GLE's.

06/24/91

MTWASHNGTN LATITUDE 44.30 LONGITUDE 288.70 ALTITUDE 1909 M  
 MTWASHNGTN INSTRUMENT IGY NEUTRON MONITOR  
 MTWASHNGTN STANDARD PRESSURE 23.80 INHG COEFFICIENT -25.00 % / INHG  
 MTWASHNGTN PRE-INCREASE BASELINE TIME INTERVAL 590716 220000-240000 UT  
 MTWASHNGTN PRE-INCREASE AVERAGE COUNTING RATE COUNTS PER SECOND  
 MTWASHNGTN TIME INTERVALS 7200  
 MTWASHNGTN SCALE FACTORS 64.

STATION	YYMMDD	SEC	TIME (UT)	CODE	UNCORR. PRESS.	CORR. % INC.
			INTERVAL	TD	COUNTS (INHG)	COUNTS
MTWASHNGTN	590716	7200	000000-020000	00	1642.	24.15
MTWASHNGTN	590716	7200	020000-040000	00	1646.	24.15
MTWASHNGTN	590716	7200	040000-060000	00	1652.	24.13
MTWASHNGTN	590716	7200	060000-080000	00	1661.	24.12
MTWASHNGTN	590716	7200	080000-100000	00	1656.	24.11
MTWASHNGTN	590716	7200	100000-120000	00	1678.	24.11
MTWASHNGTN	590716	7200	120000-140000	00	1678.	24.12
MTWASHNGTN	590716	7200	140000-160000	00	1688.	24.12
MTWASHNGTN	590716	7200	160000-180000	00	1691.	24.10
MTWASHNGTN	590716	7200	180000-200000	00	1698.	24.09
MTWASHNGTN	590716	7200	200000-220000	00	1724.	24.08
MTWASHNGTN	590716	7200	220000-240000	00	1739.	24.07
MTWASHNGTN	590717	7200	000000-020000	00	1758.	24.07
MTWASHNGTN	590717	7200	020000-040000	00	1799.	24.06
MTWASHNGTN	590717	7200	040000-060000	00	1838.	24.06
MTWASHNGTN	590717	7200	060000-080000	00	1850.	24.04
MTWASHNGTN	590717	7200	080000-100000	00	1879.	24.05
MTWASHNGTN	590717	7200	100000-120000	00	1847.	24.05
MTWASHNGTN	590717	7200	120000-140000	00	1806.	24.05
MTWASHNGTN	590717	7200	140000-160000	00	1809.	24.04
MTWASHNGTN	590717	7200	160000-180000	00	1794.	24.03
MTWASHNGTN	590717	7200	180000-200000	00	1772.	24.02
MTWASHNGTN	590717	7200	200000-220000	00	1696.	24.01
MTWASHNGTN	590717	7200	220000-240000	00	1632.	23.99
MTWASHNGTN	590718	7200	000000-020000	00	1556.	24.00
MTWASHNGTN	590718	7200	020000-040000	00	1552.	23.99
MTWASHNGTN	590718	7200	040000-060000	00	1546.	23.99
MTWASHNGTN	590718	7200	060000-080000	00	1514.	23.97
MTWASHNGTN	590718	7200	080000-100000	00	1550.	23.97
MTWASHNGTN	590718	7200	100000-120000	00	1582.	23.98
MTWASHNGTN	590718	7200	120000-140000	00	1614.	23.99
MTWASHNGTN	590718	7200	140000-160000	00	1628.	23.97
MTWASHNGTN	590718	7200	160000-180000	00	1632.	23.97
MTWASHNGTN	590718	7200	180000-200000	00	1638.	23.96
MTWASHNGTN	590718	7200	200000-220000	00	1670.	23.95
MTWASHNGTN	590718	7200	220000-240000	00	1698.	23.93

\*

\*\*\*\*\*

E07MTWS 06/24/91

EXAMPLE #1 : AN E-FILE

06/24/91

MTWASHNGTN LATITUDE 44.30 LONGITUDE 288.70 ALTITUDE 1909 M  
 MTWASHNGTN INSTRUMENT IGY NEUTRON MONITOR  
 MTWASHNGTN STANDARD PRESSURE 23.80 INHG COEFFICIENT -25.00 % / INHG  
 MTWASHNGTN PRE-INCREASE BASELINE TIME INTERVAL 590716 220000-240000 UT  
 MTWASHNGTN PRE-INCREASE AVERAGE COUNTING RATE 16.53 COUNTS PER SECOND  
 MTWASHNGTN TIME INTERVALS 7200  
 MTWASHNGTN SCALE FACTORS 64.

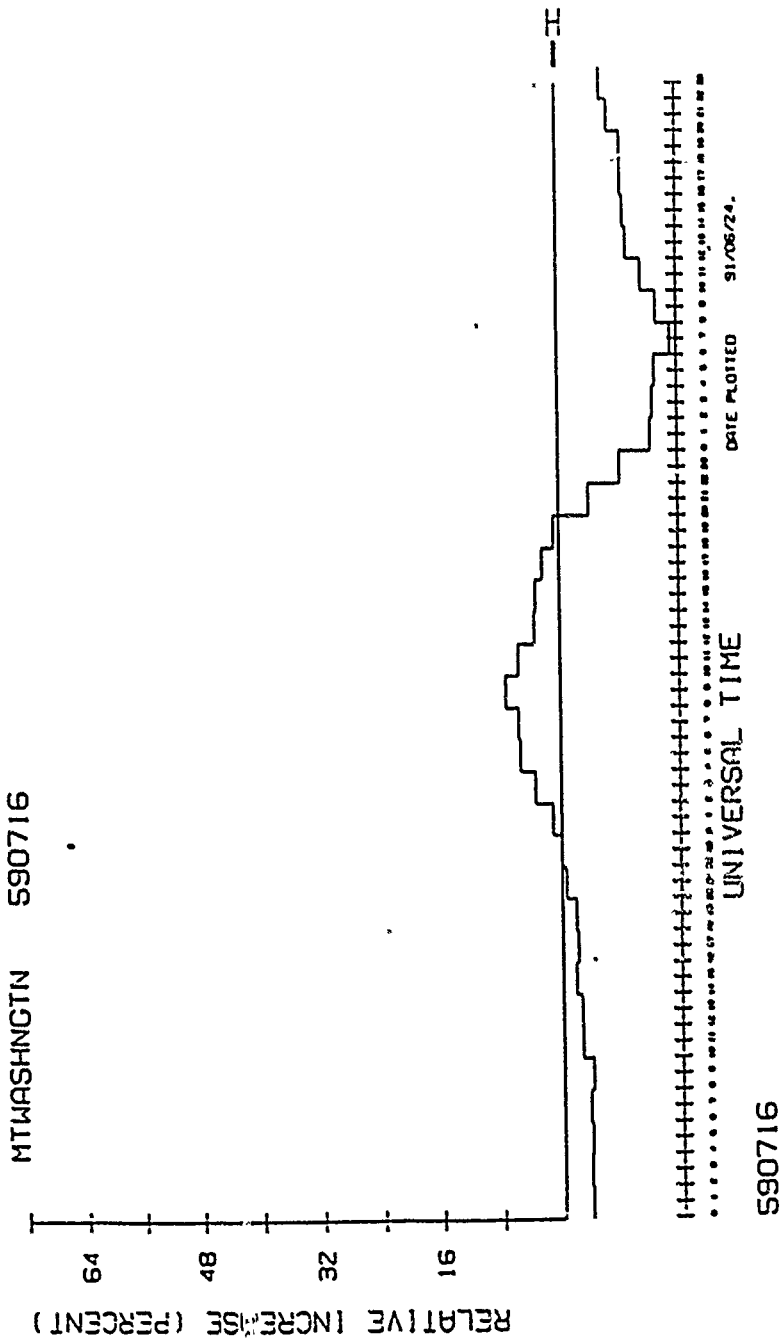
STATION	YYMMDD	SEC	TIME (UT)	CODE	UNCORR.	PRESS.	CORR.	% INC.
			INTERVAL	TD	C/S	(INHG)	C/S	
MTWASHNGTN	590716	7200	000000-020000	00	14.60	24.15	15.93	-3.6
MTWASHNGTN	590716	7200	020000-040000	00	14.63	24.15	15.95	-3.5
MTWASHNGTN	590716	7200	040000-060000	00	14.68	24.13	15.93	-3.6
MTWASHNGTN	590716	7200	060000-080000	00	14.76	24.12	15.97	-3.4
MTWASHNGTN	590716	7200	080000-100000	00	14.72	24.11	15.88	-3.9
MTWASHNGTN	590716	7200	100000-120000	00	14.92	24.11	16.12	-2.5
MTWASHNGTN	590716	7200	120000-140000	00	14.92	24.12	16.13	-2.4
MTWASHNGTN	590716	7200	140000-160000	00	15.00	24.12	16.25	-1.7
MTWASHNGTN	590716	7200	160000-180000	00	15.03	24.10	16.20	-2.0
MTWASHNGTN	590716	7200	180000-200000	00	15.09	24.09	16.23	-1.8
MTWASHNGTN	590716	7200	200000-220000	00	15.32	24.08	16.44	-.5
MTWASHNGTN	590716	7200	220000-240000	00	15.46	24.07	16.53	.0
MTWASHNGTN	590717	7200	000000-020000	00	15.63	24.07	16.72	1.1
MTWASHNGTN	590717	7200	020000-040000	00	15.99	24.06	17.07	3.3
MTWASHNGTN	590717	7200	040000-060000	00	16.34	24.06	17.41	5.3
MTWASHNGTN	590717	7200	060000-080000	00	16.44	24.04	17.46	5.6
MTWASHNGTN	590717	7200	080000-100000	00	16.70	24.05	17.76	7.4
MTWASHNGTN	590717	7200	100000-120000	00	16.42	24.05	17.46	5.6
MTWASHNGTN	590717	7200	120000-140000	00	16.05	24.05	17.07	3.3
MTWASHNGTN	590717	7200	140000-160000	00	16.08	24.04	17.05	3.1
MTWASHNGTN	590717	7200	160000-180000	00	15.95	24.03	16.89	2.2
MTWASHNGTN	590717	7200	180000-200000	00	15.75	24.02	16.64	.7
MTWASHNGTN	590717	7200	200000-220000	00	15.08	24.01	15.88	-3.9
MTWASHNGTN	590717	7200	220000-240000	00	14.51	23.99	15.21	-8.0
MTWASHNGTN	590718	7200	000000-020000	00	13.83	24.00	14.52	-12.2
MTWASHNGTN	590718	7200	020000-040000	00	13.80	23.99	14.46	-12.5
MTWASHNGTN	590718	7200	040000-060000	00	13.74	23.99	14.39	-12.9
MTWASHNGTN	590718	7200	060000-080000	00	13.46	23.97	14.04	-15.1
MTWASHNGTN	590718	7200	080000-100000	00	13.78	23.97	14.37	-13.1
MTWASHNGTN	590718	7200	100000-120000	00	14.06	23.98	14.71	-11.0
MTWASHNGTN	590718	7200	120000-140000	00	14.35	23.99	15.03	-9.1
MTWASHNGTN	590718	7200	140000-160000	00	14.47	23.97	15.10	-8.7
MTWASHNGTN	590718	7200	160000-180000	00	14.51	23.97	15.14	-8.4
MTWASHNGTN	590718	7200	180000-200000	00	14.56	23.96	15.14	-8.4
MTWASHNGTN	590718	7200	200000-220000	00	14.84	23.95	15.40	-6.8
MTWASHNGTN	590718	7200	220000-240000	00	15.09	23.93	15.57	-5.8

\*

\*\*\*\*\*

C07MTWS 06/24/91

EXAMPLE #2 : A C-FILE



EXAMPLE #3 : A PERCENTAGE INCREASE PLOT

EVENT #	07	590716	2200000	2400000	INSTA STPRESS.	UNIT	COEF	TIME	INTERVALS	SCALE FACTORS
STA. NAME		LAT	LONG	ALT						
ALMA-ATA-A	43.25	76.92	808	IGY	920.00	MB	-0.72	7200		16.
BERGEN	60.40	5.32	0	IGY	1010.00	MB	-	3600		
BERKELEY	37.86	237.70	70	IGY	750.00	MHHG	-0.96	7200		16.
BUENOSAIRES	-34.60	301.52	0	IGY	760.00	MHHG	-0.943	7200		64.
CAPE SCHMIDT	60.87	100.51	0					7200		
CHICAGO	41.83	272.33	200	IGY	750.00	MHHG	-0.96	7200		16.
CHURCHILL	58.75	265.91	38	IGY	1004.00	MB	-0.73	3600	900 600	64.
CLIMAX	39.37	253.82	3400	IGY	504.00	MHHG	-0.97	3600		128.
COLLEGE	64.06	212.17	91	IGY	745.00	MHHG	-0.94	7200		32.
DEEP RIVER	46.10	282.50	145	IGY	1000.00	MB	-0.693	3600		30.
ELSWORTH	-77.72	318.87	91	IGY				7200		32.
HELISS	80.62	56.25	20	IGY	1000.00	MB	-0.74	7200		16.
HERMANUS	-34.42	19.22	26	IGY	1015.00	MB	-0.765	7200		16.
HERSTMONCE	50.88	0.33	23	IGY	1014.00	MB	-0.77	7200		80.
HOBART	-42.90	147.33	18	IGY				7200		256.
HUANCAYO	-12.03	284.67	3400	IGY	518.00	MHHG	-0.96	3600		64.
INVERCARY	-46.50	168.37	0	IGY	1000.00	MB	-0.704	3600		100.
IRKUTSK	52.47	104.03	433	IGY			-0.74	7200		16.
JUNGFRUIJ	46.55	7.98	3550	IGY	482.00	MHHG	-0.96	3600		100.
KERGUCLEN	-49.35	70.22	33	IGY	750.00	MHHG	-1.00	7200		100.
KIEL	54.33	10.13	33	IGY	755.00	MHHG	-1.05	7200		10.
KODAIKANAL	10.23	77.48	2343	IGY	770.00	MB	-0.72	7200		32.
LAE	6.73	147.00	0	IGY	1000.00	MB	-0.72	3600		12.8
LEEDS	53.83	358.42	100	IGY	753.20	MHHG	-0.91	7200		12.8
LINCOLN	40.82	263.32	350	IGY	729.20	MHHG	-0.96	7200		16.
LINDAU	51.60	10.10	140	IGY	740.00	MHHG	-1.005	7200		10.
LOHNICKY-A	49.20	20.22	2632	IGY	550.00	MHHG	-0.943	7200		64.
MAKAPUJ	21.30	202.35	100	IGY	750.00	MHHG	-0.96	7200		32.
MAKERERE	0.34	32.56	1196	IGY	876.70	MB	-0.76	7200		80.

EXAMPLE #4 : AN NTP FILE

# TEMPERATURE, KINETIC ENERGY, AND INTERNAL ENERGY DEPENDENCES AND ISOTOPIC EFFECT FOR THE REACTION OF Cl<sup>-</sup> WITH CH<sub>3</sub>Br

John S. Paschkewitz, High School Apprentice Program  
A. A. Viggiano, R. A. Morris, Mentors

*Phillips Laboratory, Geophysics Directorate, Ionospheric Effects Division (LID),  
Hanscom AFB, MA 01731*

## Abstract

Rate constants for the reactions of Cl<sup>-</sup> with CH<sub>3</sub>Br and CD<sub>3</sub>Br have been measured as a function of reactant ion/neutral average center-of-mass kinetic energy ( $\langle K.E.c.m. \rangle$ ) at several temperatures using the Variable Temperature Selected Ion Flow Drift Tube (VT-SIFDT) apparatus. Rate constants were found to show identical negative temperature and kinetic energy dependences ( $T^{-0.8}$  and  $\langle K.E.c.m. \rangle^{-0.8}$  for the Cl<sup>-</sup> + CH<sub>3</sub>Br reaction,  $T^{0.9}$  and  $\langle K.E.c.m. \rangle^{-0.9}$  for Cl<sup>-</sup> + CD<sub>3</sub>Br) and showed little if any internal energy dependence. Rate constants for Cl<sup>-</sup> + CD<sub>3</sub>Br were slightly greater than those for CH<sub>3</sub>Br at low  $\langle K.E.c.m. \rangle$ , but at high  $\langle K.E.c.m. \rangle$ , there was no isotope effect within experimental uncertainty.

## Introduction

Nucleophilic aliphatic substitution reactions, especially of the nucleophilic bimolecular substitution or S<sub>N</sub>2 type, are a well-studied but still interesting class of chemical reactions. S<sub>N</sub>2 reactions, such as the Cl<sup>-</sup> + CH<sub>3</sub>Br reaction studied in this

experiment, are believed to involve displacement of a nucleophile by a stronger nucleophile as shown in Figure 1. The reaction mechanism involves backside attack by the stronger nucleophile, resulting in an inversion of configuration, much like the flipping outwards of an umbrella in a gale, and the displacement of the weaker nucleophile.<sup>1, 2</sup>

The rate at which the S<sub>N</sub>2 reaction proceeds is affected primarily by temperature and steric factors. Electron affinities have little effect since any electron withdrawal or release by any of the substituents has the same effect on both the reactants and the transition state.<sup>1</sup> Like many reactions, however, the S<sub>N</sub>2 reaction is affected by temperature change, which affects the total energy of the reactants. The total energy is the sum of the translational energy and the rotational and vibrational modes of internal energy. However, the population of each mode of internal energy may have a different effect on the reaction rate.<sup>3</sup>

The vibrational modes of internal energy were of particular interest in the reaction Cl<sup>-</sup> + CH<sub>3</sub>Br → Br<sup>-</sup> + CH<sub>3</sub>Cl ( $\Delta H = -30$  kJ/mole). It was expected that the "umbrella" and C-Br stretch modes of vibration would affect the reaction rate. By using the Variable Temperature Selected Ion Flow Drift Tube (VT-SIFDT) to vary internal energy at a fixed collision energy, internal energy dependences could be derived.

## Experimental

Measurements for this experiment were carried out on the Variable Temperature Selected Ion Flow Drift Tube (VT-SIFDT) at Phillips Laboratory, Hanscom AFB (see Figure 2). Detailed descriptions are given by Graul and

Squires,<sup>4</sup> Smith and Adams,<sup>5</sup> and Viggiano *et al.*<sup>6</sup> The VT-SIFDT produces ions, uses a flowing inert carrier gas to carry them through a flow tube into which a reactant gas or gases are injected, and uses a quadrupole mass filter and particle detector to determine products. The VT-SIFDT also allows for a greater degree of versatility than flowing afterglow or Selected Ion Flow Tube (SIFT) reactors due to its temperature variability and expanded energy range.<sup>5</sup>

Positive or negative ions are produced using a high pressure (0.1-1.0 Torr) ion source. These ions are focused into a low pressure ( $10^{-4}$  Torr) quadrupole mass filter using a series of electrostatic lenses. A 6" diffusion pump is used to maintain low pressure in the quadrupole chamber.<sup>6</sup> After mass analysis, the ions pass through another series of lenses to optimize ion current in the flow tube.<sup>5</sup> Because the flow tube operates at high pressure (0.5 Torr), a venturi inlet is used to inject the ions into a fast-flowing helium buffer exhausted to a high-capacity Roots blower pumping the flow tube. The venturi inlet consists of a 2 mm wide ion entrance aperture surrounded by an annular slit which expels helium carrier gas at high velocity, creating a venturi effect and allowing the ions to pass from a region of low pressure to one of high pressure.<sup>4</sup>

The flow tube itself is a stainless steel tube 1 m in length with a 7.6 cm outside diameter. To allow for variable temperature (85-550K) operation, the flow tube is surrounded by a copper jacket connected to resistive heaters for heating, and a series of copper tubing heat exchangers brazed to the jacket through which liquid nitrogen can flow for refrigeration. The helium carrier gas is preheated or precooled using copper tubing brazed to the jacket. Resistance temperature detectors are attached to the jacket in various locations to monitor the temperature. The entire flow tube is surrounded by a vacuum box which acts as a Dewar-type

insulator, and the tube is wrapped in foil to minimize heat transfer by infrared radiation.<sup>6</sup>

Ion kinetic energy can be controlled by means of a drift tube mounted inside of the flow tube. The drift tube is made of 60 stainless steel rings, 0.1 cm apart and connected electrically by external resistors. Voltage is applied to the resistor chain, which in turn applies a potential to each ring, generating a uniform electrostatic field along the axis of the flow tube and allowing a broader energy range for ion interaction with the reactant gas. Ion flight times are determined by applying pulses to two of the rings and measuring the flight times using a digital time of flight unit connected to a multichannel analyzer. Ion velocity is determined by dividing the difference between the two flight times by the distance between the two rings, and the drift velocity at given field is determined by subtracting the ion velocity at zero field from the ion velocity at the given field.<sup>5, 6</sup>

The average kinetic energy in the ion-neutral center-of-mass system,  $\langle KE_{cm} \rangle$ , in the drift tube is derived from the Wannier formula<sup>7</sup> as

$$(1) \quad \langle KE_{cm} \rangle = \frac{(m_i + m_b)m_n v_d^2}{2(m_i + m_n)} + \frac{3kT}{2}$$

where  $m_i$ ,  $m_b$ , and  $m_n$  are the masses of the reactant ion, buffer gas, and reactant neutral, respectively;  $v_d$  is the ion drift velocity; and  $T$  is the temperature. The first term in the formula is the energy supplied by the drift field, and the second term is the thermal energy. This formula is an excellent approximation of the ion energy at low ion energies.<sup>8, 9</sup> At energies approaching 1 eV the formula is still good to within

$\pm 10\%$ . The neutral reactant temperature under the conditions of the present experiments is the same as that of the buffer gas.

The detection system is made up of an ion-sampling orifice, a lens system to focus ions into a quadrupole mass filter, and an ion detector-amplifier. The orifice is located in the center of a molybdenum disc located at the apex of a cone forming part of the quadrupole/ detection system housing. The orifice is very small (0.2 mm in diameter) to insure that a 6" diffusion pump connected to the chamber can keep the pressure below  $10^{-4}$  Torr. After passing through the mass filter, the ions are converted into electrons in a channel electron multiplier. The electron signal pulses are amplified and counted on a pulse counter.<sup>5</sup>

One of the primary goals of the SIFT technique is to determine the rate constant, k, for the generalized reaction:



The ion count rate of  $A^+$  is monitored as a function of the flow rate of B in the flow tube so k is defined by the first order rate equation

$$(3) \quad \frac{d[A^+]}{dt} = -k[A^+][B]$$

In SIFT experiments,  $[B] \gg [A^+]$ , so equation 3 can be integrated to give:

$$(4) \quad k = \frac{V_i S}{z}$$

where S equals the slope of the plot of  $\ln [A^+]$  against  $[B]$  and z is the reaction length. Average ion velocity ( $v_i$ ) is determined by the procedure described earlier, and  $[B]$  is function of the flow rates of B and the buffer gas and the pressure in the flow tube. The value of z depends on the mixing time for the reactant neutral which is added through several reactant gas inlet ports.<sup>5</sup> The ports are rings measuring 4

cm in diameter with 8 small (0.4 mm) holes pointing upstream.<sup>6</sup> The finite mixing time of the reactant gas added through the injectors results in an end correction to the reaction length, which must be accounted for in the computation of the rate constant.<sup>5</sup>

The Cl<sup>-</sup> + CH<sub>3</sub>Br reaction in this experiment was investigated at 207 K, 300 K, and 545 K, and with varying amounts of potential on the drift tube (0-215V) at each temperature. The source gas for the Cl<sup>-</sup> was Freon-12. CH<sub>3</sub>Br was obtained from Matheson and was 99.5% pure. The CD<sub>3</sub>Br reaction was run under similar conditions, using 99% isotopically pure gas from Cambridge Isotope Laboratories. The helium carrier gas was 99.997% pure.

The reproducibility of the rate constants is typically  $\pm 4\%$ , but can be as high as  $\pm 8\%$  in the worst case (in which the ion signal is very low or the measured ion decay is small). A standard error propagation analysis was carried out to determine the relative and absolute accuracies of the data. Sources of error are the above reproducibility, 8%, and measurement of: temperature, 2%; pressure, 1%; ion flight time, 3%; He flow rate, (relative, 1%; absolute, 2%); neutral reactant gas flow rate, (relative, 3%; absolute, 15%). These errors lead to overall uncertainties of  $\pm 10\%$  for relative error and  $\pm 18\%$  for absolute error. Relative error is the uncertainty in the ratio of two data points. Final relative and absolute uncertainties are  $\pm 15\%$  and  $\pm 25\%$ , respectively, to account for systematic errors not treated in the above.<sup>6</sup>

The isotope effect, or the ratio of the CH<sub>3</sub>Br and CD<sub>3</sub>Br rate constants, can be determined with much greater accuracy. By conducting two experiments, one with CD<sub>3</sub>Br, the other with CH<sub>3</sub>Br , under equal conditions, all experimental factors in determining the rate constants are equal and thus only random error enters into the

determination of the isotope effect. The only factor which is not the same is the gas correction factor, or GCF. The ratio of the GCF's for CH<sub>3</sub>Br and CD<sub>3</sub>Br can be determined with an uncertainty of only  $\pm 2\%$ . The random error and error in the GCF determine the total error.

## Results

The rate constants of the reactions of Cl<sup>-</sup> with CH<sub>3</sub>Br and CD<sub>3</sub>Br are shown in Figure 3 as a function of <K.E.<sub>c.m.</sub>>. For the Cl<sup>-</sup> + CH<sub>3</sub>Br reaction, the rate constants decrease with increasing <K.E.<sub>c.m.</sub>> and temperature, and all of the rate constants fall on one curve regardless of temperature. The CD<sub>3</sub>Br reaction rate constants are slightly larger than those for CH<sub>3</sub>Br at low <K.E.<sub>c.m.</sub>>, but are equal within uncertainty to the CH<sub>3</sub>Br results at higher energies.

Table 1 gives the isotope effect as a function of temperature. The isotope effect appears to remain constant as a function of temperature (within uncertainty). Table 2 gives efficiencies as a function of temperature. The efficiencies were computed by dividing the true rate constant by the theoretical maximum rate constant, which is a function of the neutral reactant's dipole moment and polarizability.

Table 1:

Temperature (K)	k CD <sub>3</sub> Br/k CH <sub>3</sub> Br
207	1.24 ( $\pm .0495$ ) e-11
303	1.25 ( $\pm .0367$ ) e-11
538	1.13 ( $\pm .0838$ ) e-11

**Table 2:**

Temperature (K)	efficiency CD <sub>3</sub> Br	efficiency CH <sub>3</sub> Br
207	.015 (1.5%)	.012 (1.2%)
303	.012	.010
538	.009	.008

A plot of rate constants versus total energy is given in Figure 4. The data points do not fall on one curve, but the data for each temperature fall on separate curves. Rotational and average vibrational energies were computed in order to determine total energy. Rotational temperature in a drift tube has been shown to equal  $(3/2)kT$ , where  $k$  is the Boltzmann constant. Vibrational energy was determined by

$$(5) \quad \sum_n h\nu_n pop(n)$$

where  $pop(n)$  is the population of the vibrational state,  $\nu_n$  are the vibrational frequencies, and  $h$  is Planck's constant.<sup>3</sup>

### Discussion and Conclusions

The rate constant for the Cl<sup>-</sup> + CH<sub>3</sub>Br reaction was found to be proportional to T<sup>0.8</sup>, and the rate constant for Cl<sup>-</sup> + CD<sub>3</sub>Br was found to be proportional to T<sup>0.9</sup>. Kinetic energy dependences were identical to these temperature dependences. For each reaction, all of the rate constants fall on one curve, which suggests that there is no internal energy dependence. The separation of the data by temperature in the total energy plot suggests that there is no single total energy dependence. It therefore also suggests that there is no effect due to rotational or vibrational energies, and it can be concluded that neither the "umbrella" or C-Br stretch modes

of vibration had any significant effect on the reaction rate. Since the rate constants for the  $\text{CD}_3\text{Br}$  and  $\text{CH}_3\text{Br}$  reactions do differ (allowing for uncertainty) at low  $\langle \text{K.E.}_{\text{c.m.}} \rangle$ , it can be concluded that there is an isotope effect at these energies.

A comparison to previous results from Caldwell *et al.* is given in Figure 5. There is a discrepancy at higher temperatures, suggesting that Caldwell's results may be in error.<sup>10</sup> The error may be due to the greater probability of large error inherent to Caldwell's apparatus. For the isotope effect, the present data give a nearly identical ratio (1.22 vs 1.25) to that published by Gronert *et al.*<sup>11</sup>

In summary, the  $\text{S}_{\text{N}}2$  reaction of  $\text{Cl}^- + \text{CH}_3\text{Br}$  exhibits negative temperature and kinetic energy dependences and an isotope effect at low  $\langle \text{K.E.}_{\text{c.m.}} \rangle$  upon substitution of  $\text{CD}_3\text{Br}$  for  $\text{CH}_3\text{Br}$ . However, there is no internal energy effect due to vibrational or rotational modes of internal energy.

## Figure Captions

1. Reaction mechanism for the reaction  $\text{Cl}^- + \text{CH}_3\text{Br} \rightarrow \text{Br}^- + \text{CH}_3\text{Cl}$  ( $\Delta H = -30$  kJ/mole).
2. Schematic of the Variable Temperature Selected Ion Flow Tube (VT-SIFDT)
3. Rate constants for  $\text{Cl}^-$  reacting with  $\text{CH}_3\text{Br}$  and  $\text{CD}_3\text{Br}$  as a function of <K.E.c.m.>. The present results for the  $\text{CH}_3\text{Br}$  reaction are shown as solid circles, solid squares, solid diamonds, and solid triangles for data obtained at 207 K, 300 K, 538 K, and 564 K, respectively. The present results for the  $\text{CD}_3\text{Br}$  reaction are shown as open squares and open triangles for data at 300K and 564 K, respectively. Data points at 207 K for the  $\text{CH}_3\text{Br}$  reaction are connected by a solid line. Data points at 300 K for the  $\text{CH}_3\text{Br}$  reaction are connected by a dashed line. Data points at 300 K for the  $\text{CD}_3\text{Br}$  reaction are connected by a dotted line. Note that temperatures similar for the different sets of data are represented by similar symbols, i.e., solid symbols as compared with open symbols.
4. Rate constants for  $\text{Cl}^-$  reacting with  $\text{CH}_3\text{Br}$  and  $\text{CD}_3\text{Br}$  as a function of average total energy. The present results for the  $\text{CH}_3\text{Br}$  reaction are shown as solid circles, solid squares, solid diamonds, and solid triangles for data obtained at 207 K, 300 K, 538 K, and 564 K, respectively. The present results for the  $\text{CD}_3\text{Br}$  reaction are shown as open squares and open triangles for data at 300K and 564 K, respectively. Data points at 207 K for the  $\text{CH}_3\text{Br}$  reaction are connected by a solid line. Data points at 300 K for the  $\text{CH}_3\text{Br}$  reaction are connected by a dashed line.

Data points at 300 K for the  $\text{CD}_3\text{Br}$  reaction are connected by a dotted line. No uncertainty is given.

5. Comparison of the rate constants for  $\text{Cl}^-$  reacting with  $\text{CH}_3\text{Br}$  as a function of  $\langle \text{K.E.c.m.} \rangle$  and for those from Caldwell *et al.*<sup>10</sup> The present results for the  $\text{CH}_3\text{Br}$  reaction are shown as solid circles, solid squares, solid diamonds, and solid triangles for data obtained at 207 K, 300 K, 538 K, and 564 K, respectively. Data points at 207 K for the  $\text{CH}_3\text{Br}$  reaction are connected by a solid line. Data points at 300 K for the  $\text{CH}_3\text{Br}$  reaction are connected by a dashed line. Data obtained by Caldwell *et al.* are shown as circled plusses, and connected by a dotted line.<sup>10</sup>

## References:

1. R. Morrison and B. R., *Organic Chemistry* - (Allyn and Bacon, Inc., Boston, 1973).
2. J. Cason, *Principles of Modern Organic Chemistry* - (Prentice-Hall, Inc., Englewood, NJ, 1966).
3. W. Moore, *Physical Chemistry* - (Prentice-Hall, Inc., Englewood, NJ, 1972).
4. S. Graul and R. R. Squires, Mass Spectrom. Revw. 7, 263 (1988).
5. D. Smith and N. G. Adams, Adv. At. Molec. Phys. 24, 1 (1988).
6. A. A. Viggiano, R. A. Morris, F. Dale, J. F. Paulson, K. Giles, D. Smith and T. Su, J. Chem. Phys. 93, 1149 (1990).
7. G. H. Wannier, Bell. Syst. Tech. J. 32, 170 (1953).
8. L. A. Viehland and R. E. Robson, Int. J. Mass Spectrom. Ion Processes 90, 167 (1989).
9. L. A. Viehland, A. A. Viggiano and E. A. Mason, J. Chem. Phys. submitted (1991).
10. G. Caldwell, T. F. Magnera and P. Kebarle, J. Am. Chem. Soc. 106, 959 (1984).
11. S. Gronert, C. DePuy and V. Bierbaum, J. Am. Chem. Soc. 113, 4009 (1991).

**Figure 1: S<sub>N</sub>2 Reaction: Cl<sup>-</sup> + CH<sub>3</sub>Br → CH<sub>3</sub>Cl + Br<sup>-</sup>**

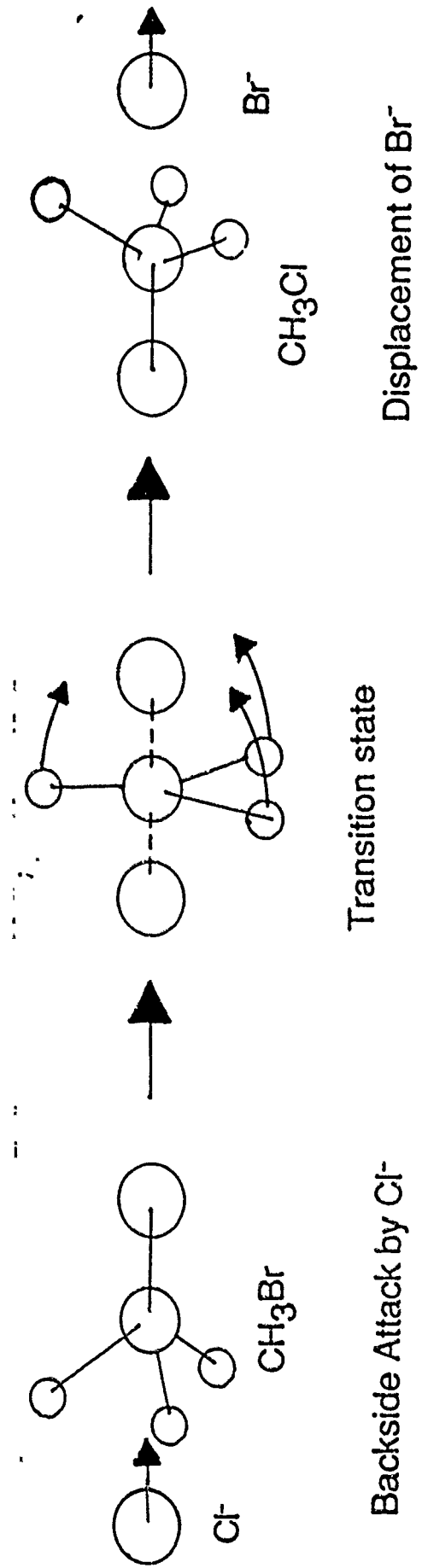


**Figure 2: The Variable Temperature Selected Ion Flow Drift Tube (VT-SIFDT)**

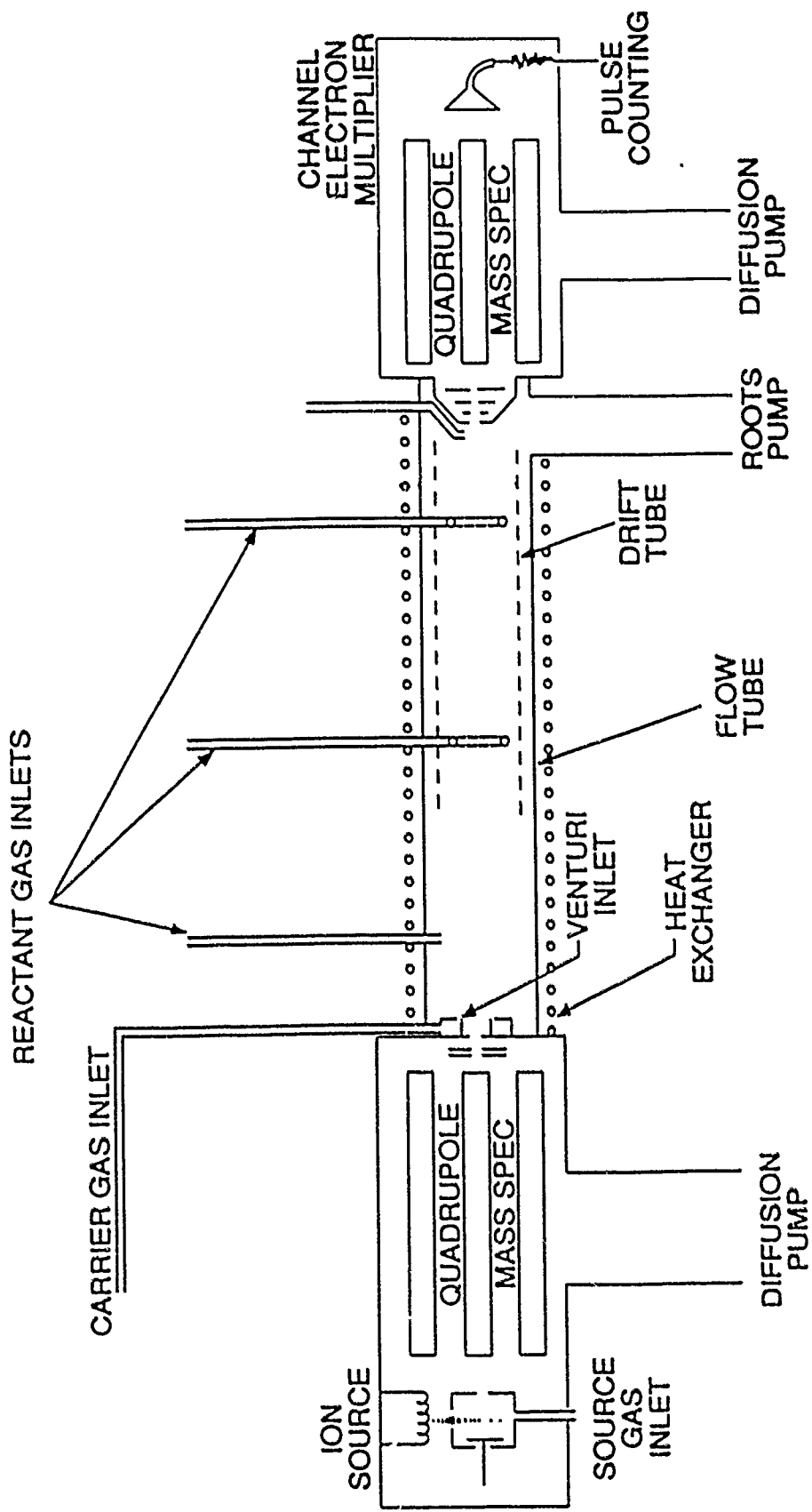


Figure 3

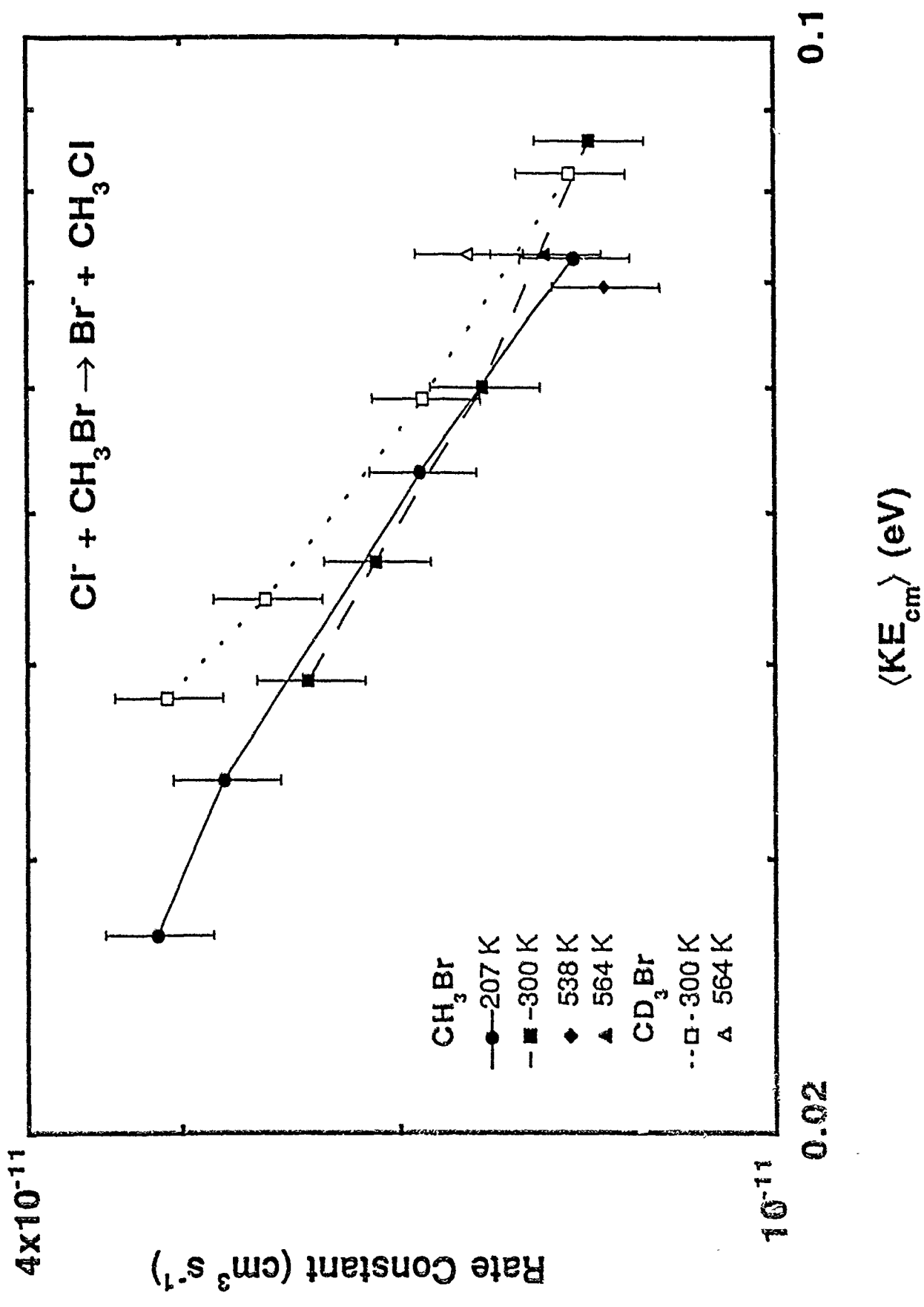


Figure 4

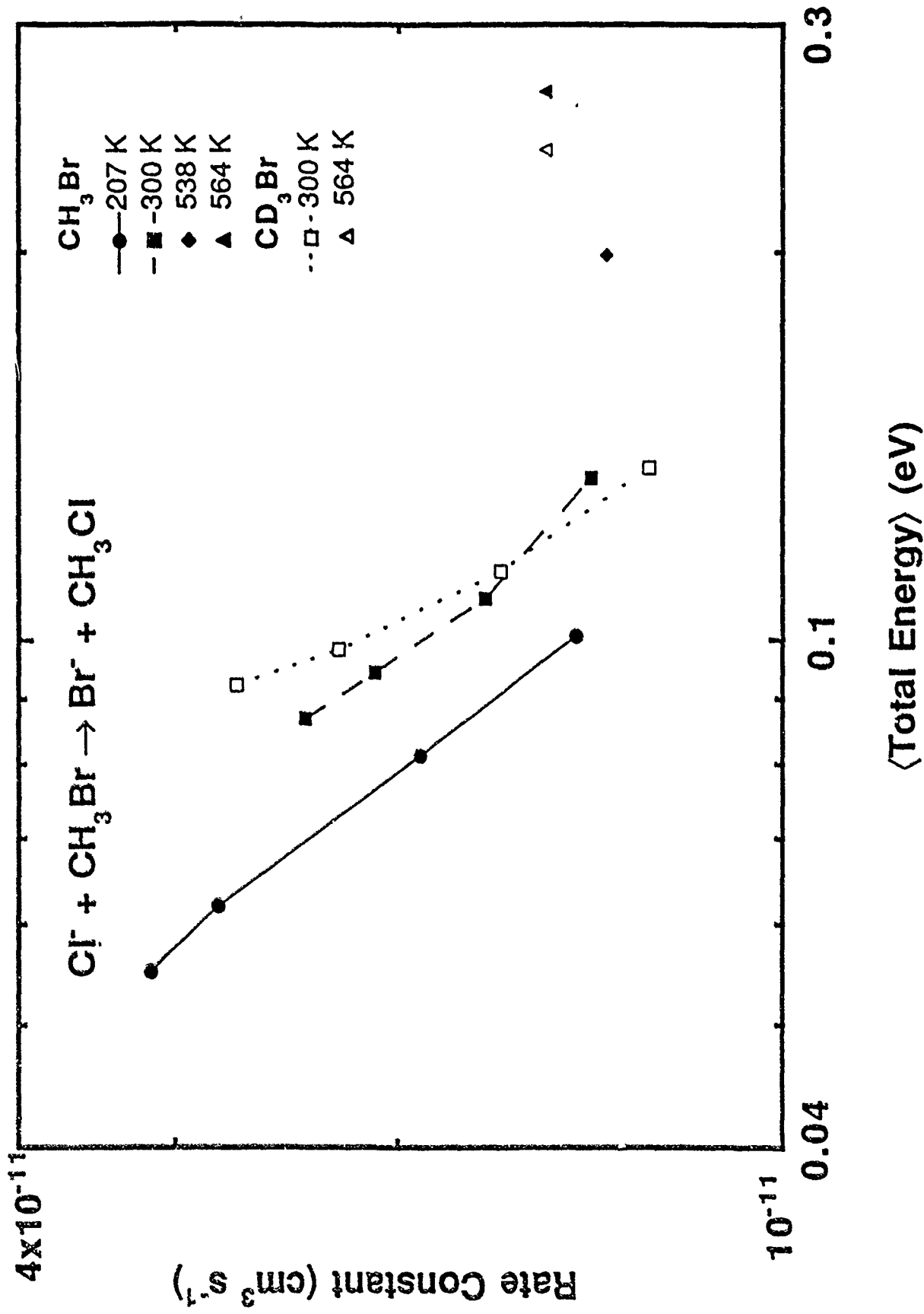
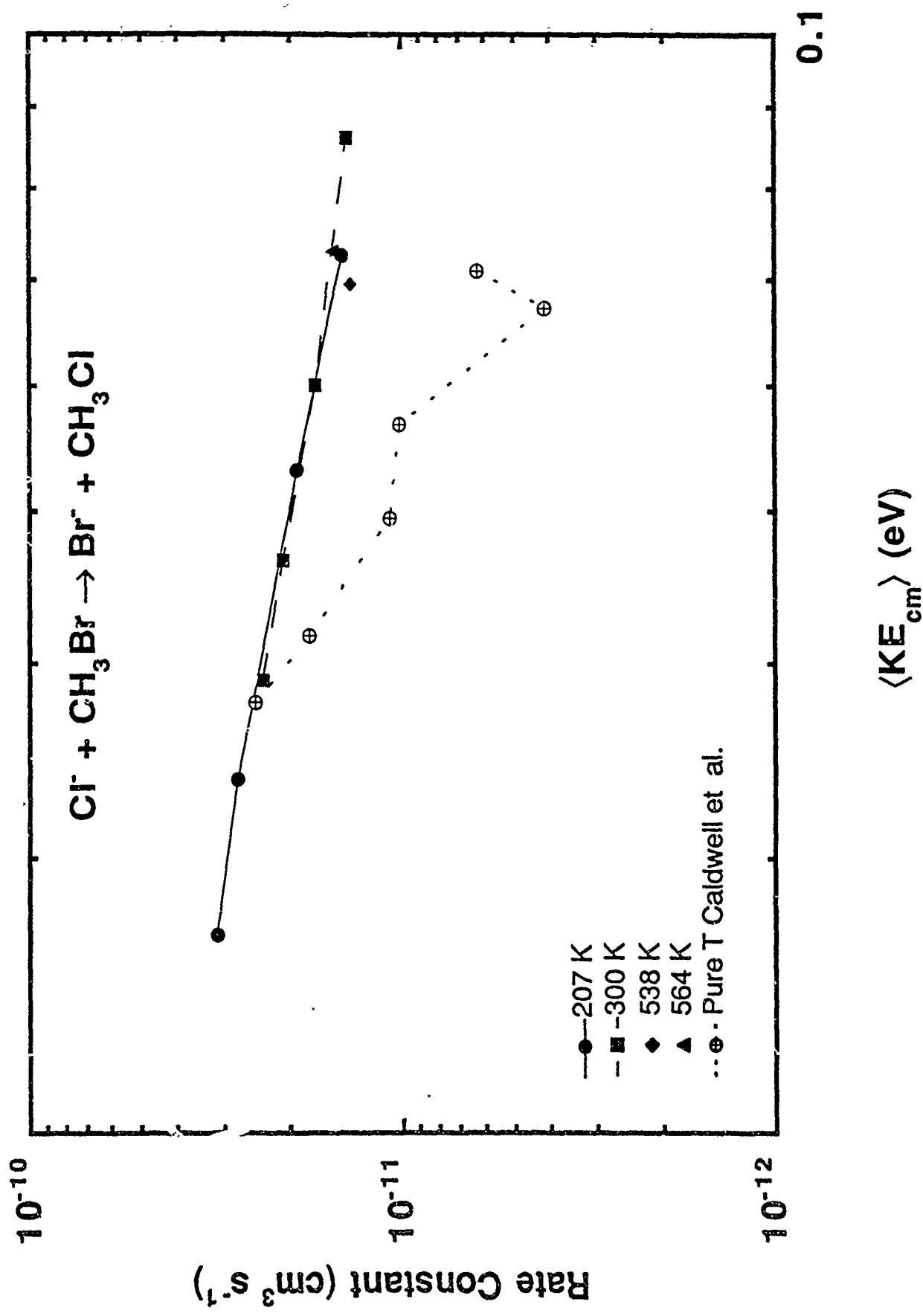


Figure 5



RESEARCH & DEVELOPMENT LABORATORIES  
1991 HIGH SCHOOL APPRENTICESHIP PROGRAM  
RESEARCH PAPER: FINAL REPORT

IONOSPHERIC EFFECTS ON RADIO SIGNALS

JEFFREY M. ROTH

AUGUST 21, 1991

Acknowledgements

I am very appreciative to the people at GL who have taken their time to let me work with them. I would like to thank Gregory Bishop, for selecting me to work with him and for giving me a taste of what bureaucracies are like; Charley Andreasen, for explaining everything to me, advising me how to get along in the 'real world', and also telling interesting stories; Elizabeth Holland, for keeping me up to date on everything and helping me to learn Fortran and how to understand procedure files; and Andy Mazzella, for helping me to become acquainted with the computers. I am thankful to these people, who have shown me what it is like to be an engineer.

Abstract

My work term this summer has been at the Ionospheric Applications Branch of the Geophysics Laboratory on Hanscom

AFB, Massachusetts. The work I have completed in the eight weeks has dealt mostly with the use of computers. This has included processing and analyzing ionospheric data, modifying and debugging system software, and producing various plots of ionospheric conditions.

### Introduction

Due to the intricacies of today's communications, surveillance, and tracking systems, both military and nonmilitary alike, calibrations must be done to take into account the irregularities of the ionosphere. Parts of this region of the upper atmosphere contain highly ionized gases in the plasmic state, due to intense solar radiation. These free-flowing ions, electrons, and neutral particles make up approximately five percent of the ionosphere, causing the region to be only slightly ionized. Because the ionosphere is created mostly by the sun's radiation, TEC, or total electron content, values follow a daily cycle, peaking in the afternoon, and sinking to lows in the night. See figure 1. These TEC values are one focal point to the work done here at the Geophysics Laboratory, and consist of the measurement of electrons contained in a volume with a base of one square meter at the Earth's surface and a height at the 'top' of the ionosphere. This 'top' of the ionosphere is vaguely defined as 1000 km. Its base is considered to be an elevation of roughly 50 km. While between these two areas, an ionosphere technically exists, the region of greatest impact and ionization is usually between 300 and 350 km. Figure 2 shows these general characteristics as a profile.

Ionospheric research, as stated above, is important to systems which must propagate radio waves through the atmosphere. Whether it be a navigation, communication, or ranging system, the ionosphere, if not taken into account, can seriously impair its performance. The problems associated with the ionosphere include deterioration of tracking, imaging, and detection, signal loss, ranging errors, and radio wave refraction and distortion. Because at least one of these effects is usually present, it has been necessary to create ionospheric models which can predict ionospheric activity fairly accurately . Though certain models do exist, one of the major projects here at the GL is to develop a version that can predict activity much more precisely.

### Discussion

In efforts to create a successful model of the ionosphere it is necessary to be able to analyze data from it. Presently, there are four stations that collect ionospheric data for use at GL. These are Thule, Greenland; the Shetland Islands, U.K.; Austin Research Laboratories, at the University of Texas at Austin; and GL, here at Hansom. From these stations we receive raw data, usually in the form of 10" magnetic tapes, but also in chart form. This data is gathered from Global Positioning Satellites, GPS, that emit radio waves. Figure 3 is a chart of about 4 hours of raw data from Shetland for February 27 of 1991. On this chart there are 4 bands of data. The top line is called L1 band and the second to top is called L2 band. These operate at L-band radar frequencies of 1.5 GHz and 1.2 GHz, respectively. The bottom two

bands are measures of TEC. They are called Absolute TEC and Relative TEC. These two bands are fairly alike, only they do not appear so because the ratio of the Relative TEC's scale to the Absolute TEC's scale is 10:1.

In order to plot this raw data we had to do two things. First, it had to be processed through programs to produce data files that the plot programs could access. And secondly, we had to create files that contained the azimuth and elevation of each individual satellite which passed overhead. At this point we could plot data from the different sites.

One type of plot, shown in figure 4, is a pass file. It is simply the graph of a single GPS satellite that passed over Shetland. In it there are three lines. The 'noisy' one is Absolute TEC, and the one which tracks it is Relative TEC. The lowest line is Vertical TEC, which is Relative TEC computed to be directly overhead. Because Relative TEC is simply a value of electron content between the satellite and the receiver, as the satellite approaches the horizon and the angle of elevation decreases, this value increases because the line connecting the two bodies is passing through more ionosphere. Vertical TEC takes this into account and computes the electron content at a fixed elevation of 90 degrees. The two other curves of "x's" and "+"s map the azimuth and elevation of the satellite respectively.

Another type of plot obtained from the same data is shown in figure 5. This is a 24 hour plot of Vertical TEC of six or so satellites, also shown with their azimuth and elevation. Note the daily cycle of ionospheric activity shown in this plot, in

which the TEC peaks around early afternoon and is lowest at times with no daylight.

A plot that uses a different type of data is illustrated in figure 6. This output is from 4 channel GPS data from Shetland. Because Shetland has a special receiver, called a 4-Channel Receiver, they can track four space vehicles at once. As a result, there are four 24 hour Vertical TEC plots on one page, compared to only one as shown before. Although some are missing, the vertical lines on this plot separate different satellite passes. The satellite number is given on the horizontal axis.

The plotting method for creating graphs like the previous three is not very complicated, if each individual program works correctly to do its part. This was not the case when I began working, however. Many of the plotting programs contained errors and 'bugs' which needed to be worked out. This required quite a bit of time, considering how large these programs are, but after much time we did get them to produce correct graphs.

### Results/Conclusion

From my work here at GL this summer, I feel I have learned a wealth of knowledge about operating computers. I have become familiar with computer systems which I previously had never used. I have learned to use the Cyber 180-860 and Vax 9201 mainframe computers, along with NOS, the Network Operating System of the building networks. I have also learned to use the CFSS, Central File Storage System, also called Masstor, which is a large file storage mainframe. From modifying the plot programs I have even acquired another computer language,

Fortran 77, which I did not know before. Because PC's are used here as terminals, I have become familiar with them, along with MS-DOS, Microsoft's® Disk Operating System, and various other programs such as cassette tape backup software, and SigmaPlot®, a graphing program by Jandel®.

Though I have had previous experience on Macintosh computers, I have never learned to use PC's or mainframes, and am grateful that I have had a chance to do so. To me, the experience I have learned this summer is very valuable, and I know it will help me not only in college, but also for the rest of the work I do in high school.

### Bibliography

1. G.J. Bishop, J.A. Klobuchar, S. Basu, J.R. Lynch, D.S. Coco, C. Coker, "Measurement of Trans-Ionospheric Effects Using Signals from GPS," Proceedings of 1990 IES Symposium on the Effect of the Ionosphere on Radiowave Signals and System Performance, May 3, 1990.
2. Liebowitz, Ruth P., "Ionospheric Models for the Air Weather Service," Historical Brief, Air Force Geophysics Lab, Hanscom AFB, MA, October 1990.
3. Bishop, Gregory J., "Introduction to Ionospheric Effects on SBR," March 1987, Air Force Geophysics Lab, Hanscom AFB, MA.
4. Klobuchar, John A., "Ionospheric Effects on Earth-Space Propagation," Environmental Research Paper, Dec. 27, 1983, Air Force Geophysics Lab, Hanscom AFB, MA.
5. Inada, Maki, "Ionosphere - Total Electron Content," USAF-Universal Energy Systems High School Apprenticeship Program Final Report, Air Force Geophysics Lab, Hanscom AFB, MA, August 8, 1989.

# **FIGURES...**

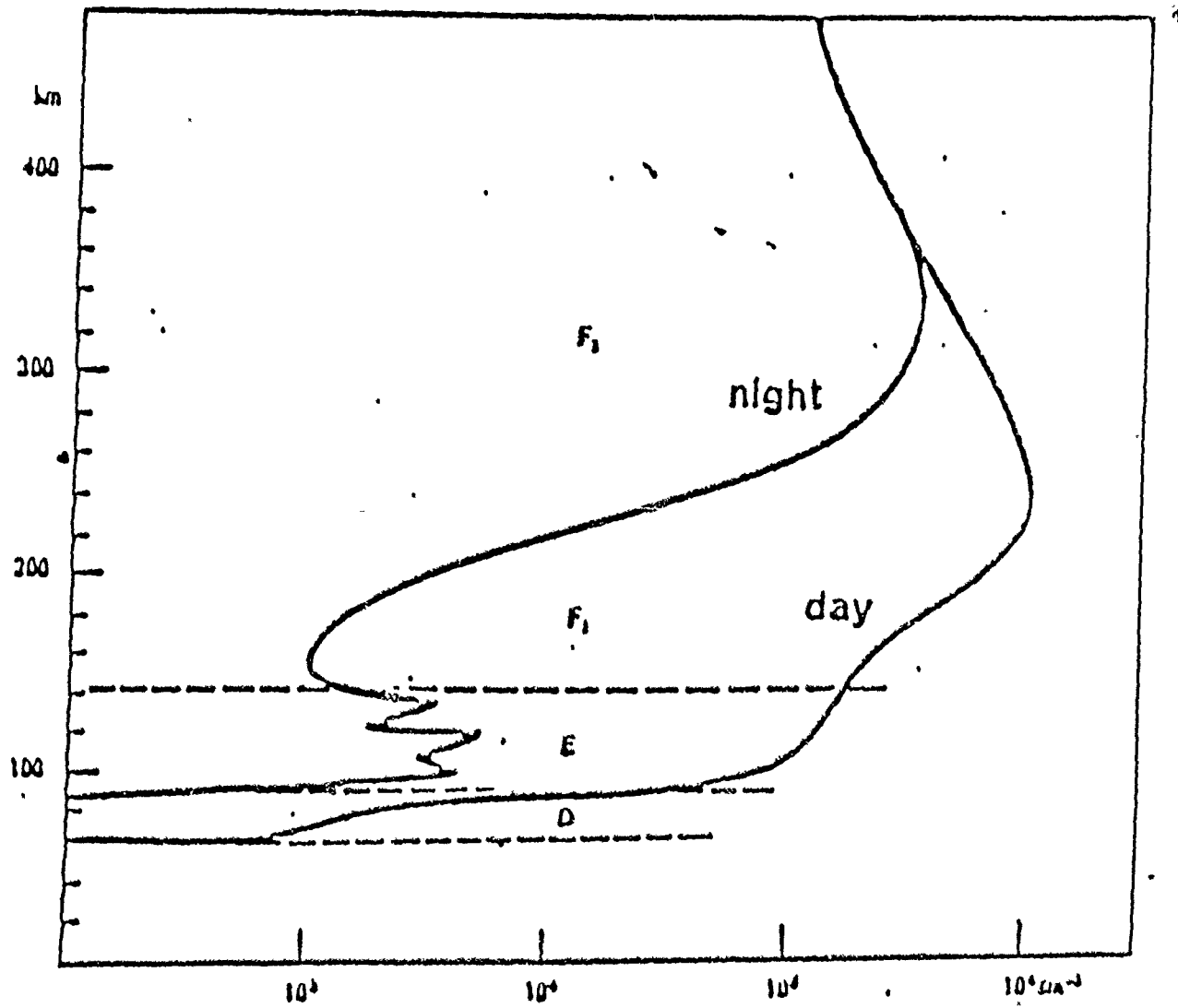


Figure 1: Typical Diurnal Variation in Ionospheric Electron Density Profile.

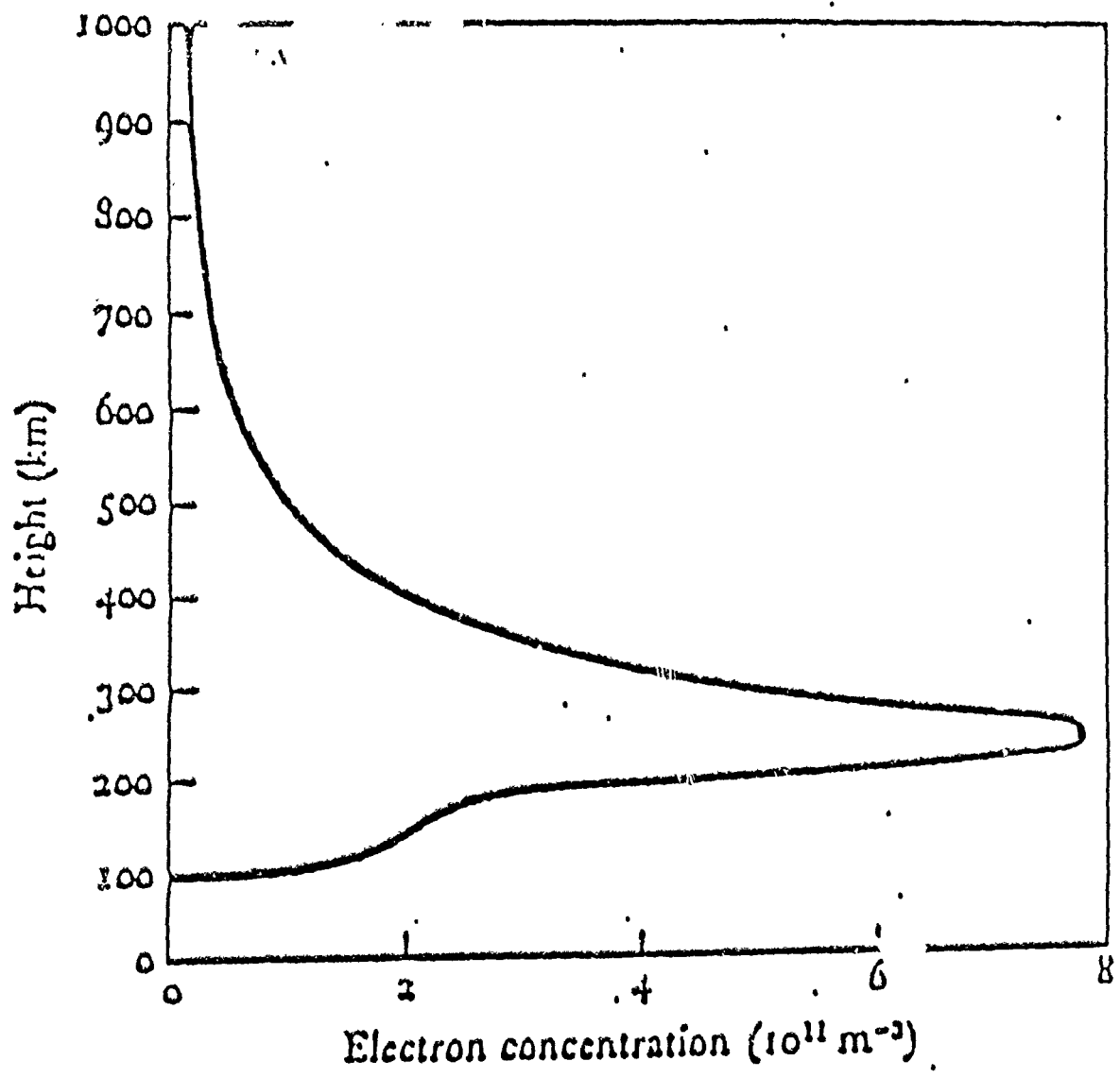


Figure 2: Typical Electron Density Profile of the Ionosphere.

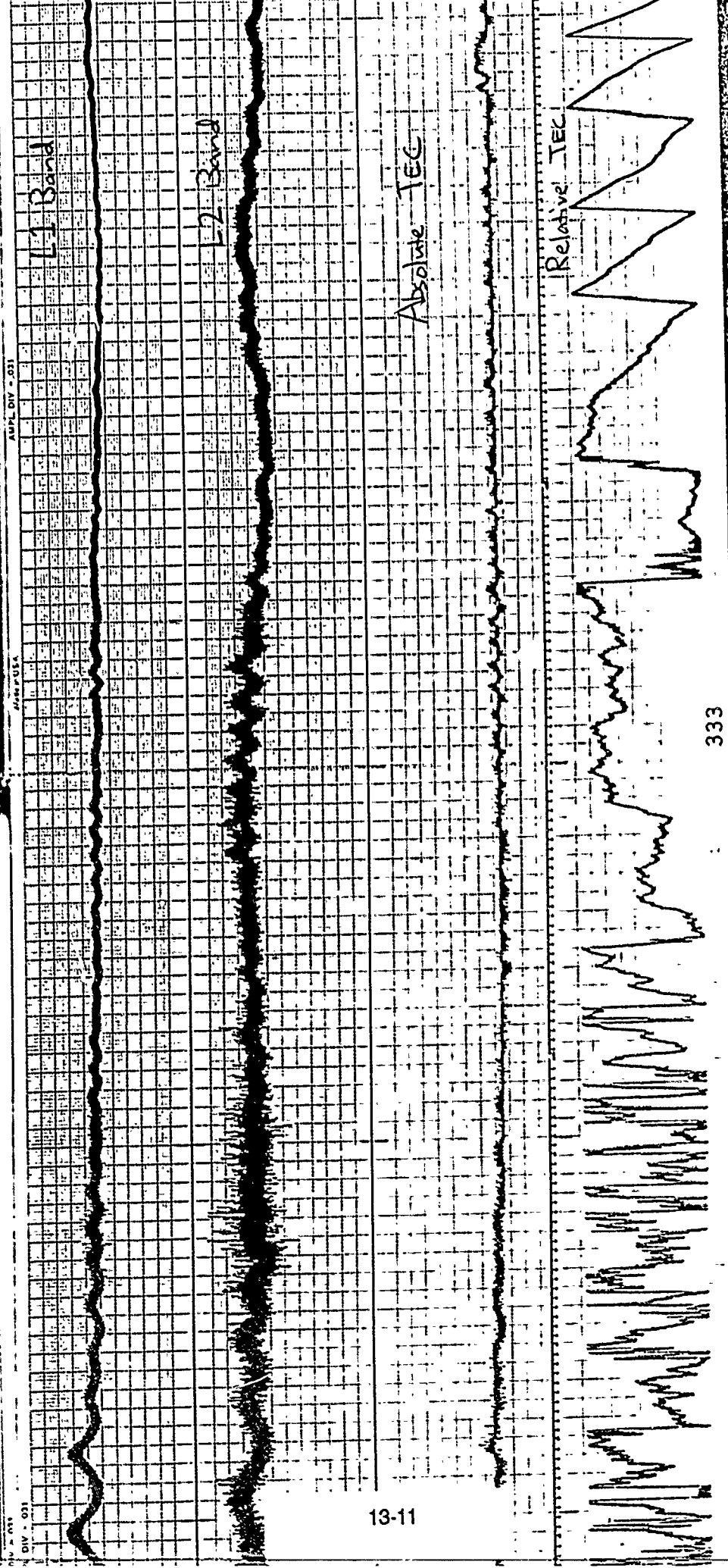


Figure 4: GPS Pass File.

PASS FILE : 4

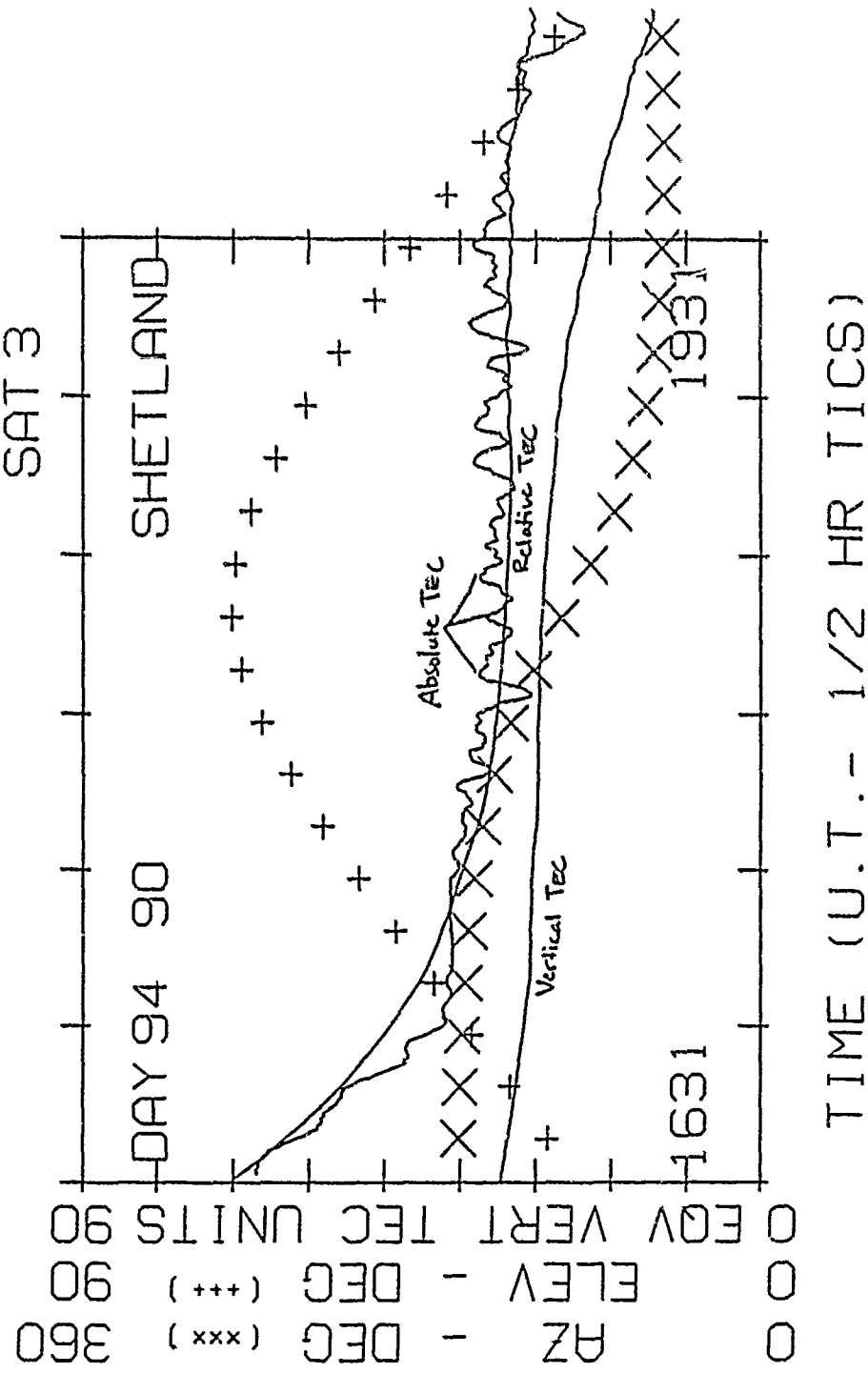
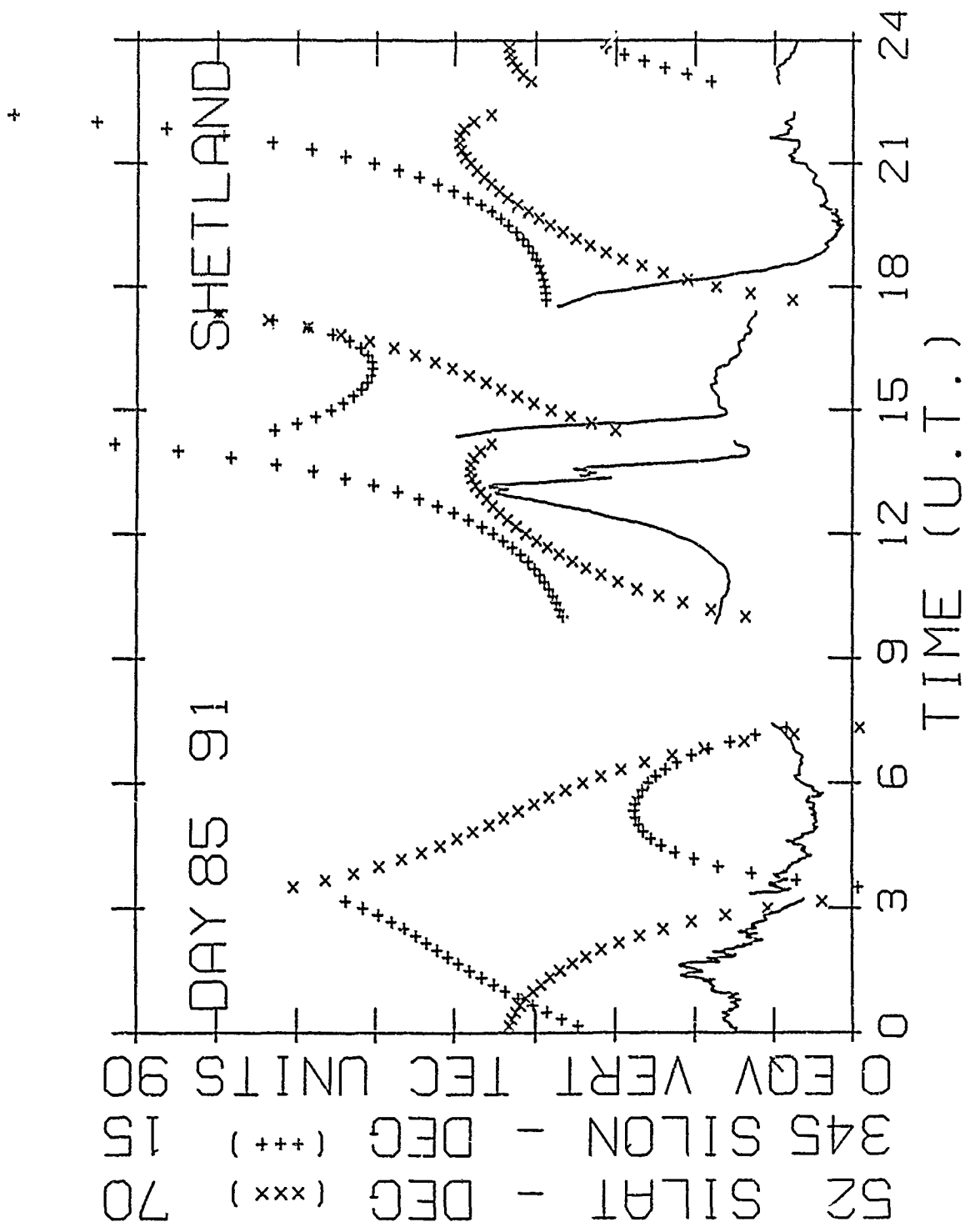
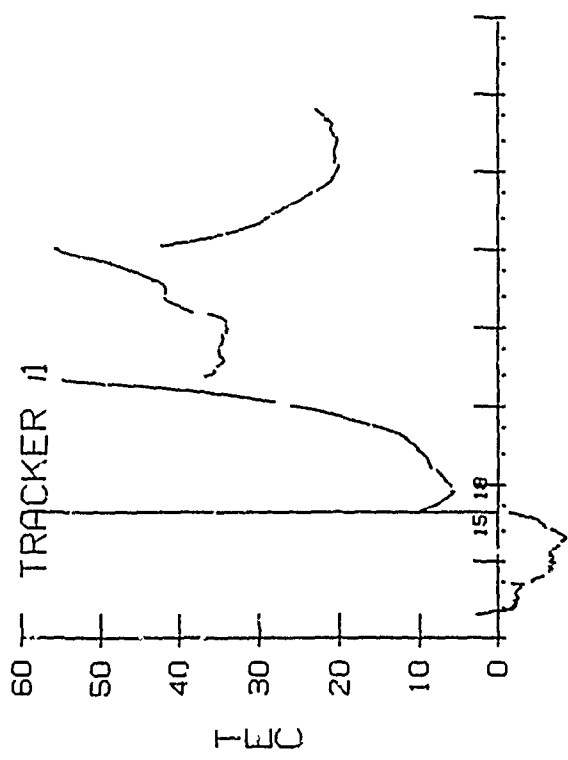


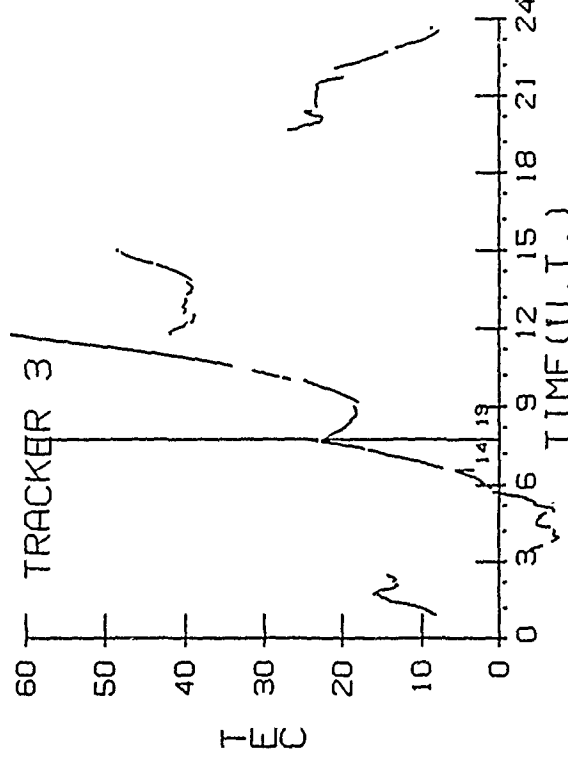
Figure 5: 24-Hour GPS Plot.



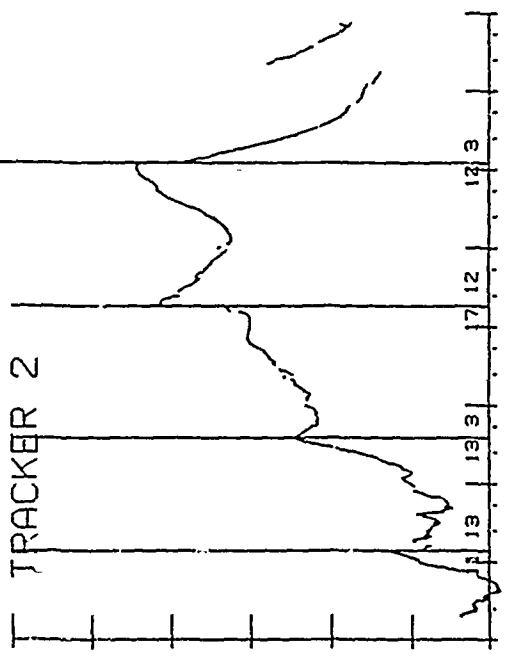
F-FILE T1-4100 A-CHANNEL TS ADJUSTA SMMCAT  
 B-FILE 082  
 R-FILE T1-4110 GPS SHETLAND 1991 DATA  
 STPLAT= 60.16 STPLON= -1.15



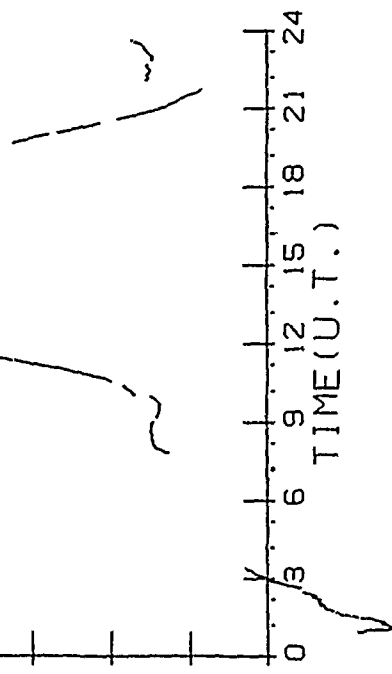
TRACKER 1



TRACKER 3



TRACKER 2



TRACKER 4

Figure 6: 4-channel GPS Data from Shetland.

FINAL REPORT 1991

BY: Paul K. Swietek

This summer I spent my time working in Atmospherics Sciences Division at the Air Force Geophysics Laboratory located at Hanscom A.F.B, Massachusetts. I performed what could be called odd jobs than doing any kind of research. These tasks included computer observations of weather stations across the country; updating fax weather charts and copying HIRAS data on magnetic tape to optical disks.

Task 1 was the weather observations that I did only for my own interest and no other purpose. The observations were brought up by entering the stations three letter identification number and the current time in GMT. The data from these stations included temperature; dewpoint; pressure; wind speed and direction visibility; observed weather and cloud cover. Other commands could bring up the current radar soundings from across the country to observe and track thunderstorms. Weather advisories were also able to be brought up. Twenty-four and thirty-six hour forecasts were available. They predicted temperature; dewpoint; winds precipitation and cloud cover. The command could connect stations of equal temperature, dewpoint, precipitation and pressure.

The second of my jobs was to post the current fax charts that predicted the weather to come and listed some of the current situations and weather from the day before. These charts included 200/500/700/850 millibar analysis, the 00,12,24,36 and 48 hour model runs. Each of those runs consisted of a 500 mb and 700 mb and surface charts. The 500 mb was heights and vorticity

the 700mb predicted precipitation. The surface displayed the predicted locations of the low and high pressure areas. The surface analysis chart showed the current weather across the country. It displayed high and low temperatures and dewpoints at selected cities, high and low pressures, fronts and the warm and cold fronts. The maximum and minimum temperature charts listed the previous days temperatures. The radar summary displayed the radar soundings and came out several times a day. The last chart displayed the previous days precipitation accumulation. These charts were used for weather briefings given by the scientists on Monday, Wednesday and Fridays.

My last topic was to transfer data on magnetic tape to an optical disk. This disk could hold 5 one inch magnetic tapes which would facilitate loading of the data. This data would later be sent to the CRAY2 computer in Texas.

This summer turned out to be quit disappointing in that the things I did were quit simple and a waste of time. No research work was performed and it wasn't uncommon for me to have nothing to do for several hours each day as my mentor never had any thing for me to do.

# POLARIZATION OF LASER LIGHT IN A DOUBLE PHASE CONJUGATE MIRROR EXPERIMENT

Mara L. Collins

*Phillips Laboratory, Nonlinear Optics Center of Technology, PL/LTN,  
Kirtland Air Force Base, New Mexico 87117-6008*

The project I was involved with was in a lab working with ways to enhance output power from a laser and to synergistically combine beams from two or more lasers. In an experiment involving varying angles to optimize power from phase conjugation two beams of horizontally polarized laser light are required. Using two lasers and various optical equipment including Faraday optical isolators, a broadband polarizing beamsplitter cube and a retardation plate, we achieved two beams of horizontally polarized light crossing in a crystal of barium titanite conducive to phase conjugation.

## I. Introduction

A phase conjugate mirror uses nonlinear optical effects to reflect a beam exactly back along the path of propagation regardless of the angle with which the beam hits the phase conjugate mirror and of arbitrary distorters along the beam path. The phase conjugate wave or the returning beam will be free of distortion because any distortion in the path the phase conjugate mirror will be "undone" on the return trip. The phase conjugation we studied, with the double phase conjugate mirrors, is the combination of two mutually incoherent beams of light in a crystal of barium titanite ( $\text{BaTiO}_3$ ), which acts as a double phase conjugate mirror. The nature of the atomic structure of the crystal is such that it forms a refractive index grating within the crystal resulting from the interference patterns of the two beams combining. As the two beams interact each is sent back along the optical path of the other. In our set-up a pellicle beam splitter along the path of the light deflected a portion of the light into a detector connected to an analog to digital converter and a personal computer that measured the power of the beam and hence the reflectivity of the phase conjugation. In order to achieve phase conjugation it was necessary to make sure both beams entering the crystal were horizontally polarized. The polarization of light is a measure of the angle of the light wave with respect to a horizontal and vertical set of axes in a plane perpendicular to the direction of propagation. This angle can be seen as having a horizontal component and vertical component. Because a beam of light is made up of many waves it can, in a manner of speaking, have several polarizations, though it is not considered polarized light. If the waves making up the beam of light all have the same polarization the light is polarized.

The optical instruments we used in our set-up included two lasers, the beams of which each traversed a similar path to reach the crystal. Two lasers had to be used so that the beams would be incoherent with each other.

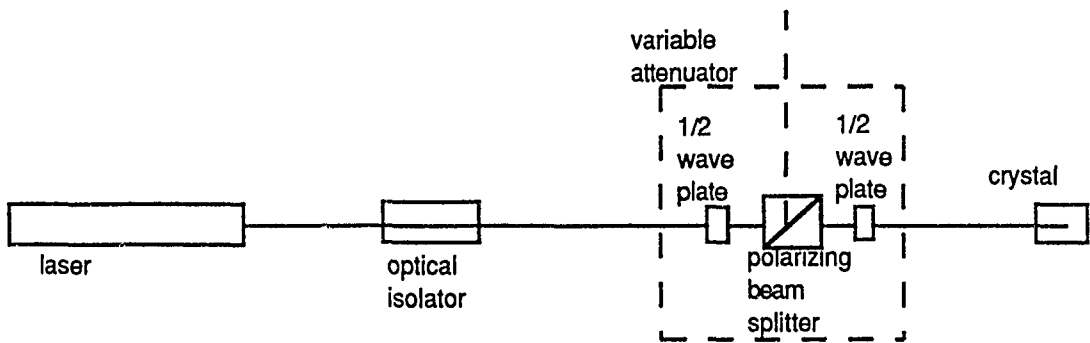
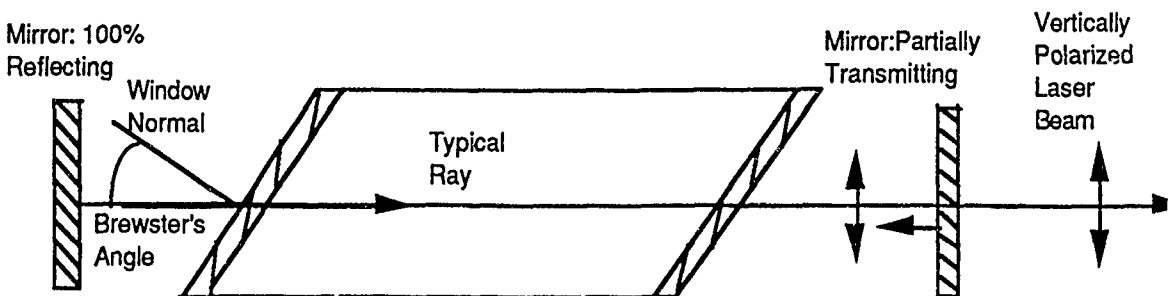


**Figure 1: Path of Beam to Crystal**

## II. Discussion

Light coming out from a laser is already polarized because of the way the laser works. A laser consists of three different components: a pump, a resonator, and the laser medium. The pump provides energy, exciting the laser medium, in the case of our experiment with a HeNe laser, helium and neon, causing stimulated emission of light. The resonator is the chamber in which the process takes place, and is made up of two aligned mirrors. One mirror has close to 100% reflectivity, the other slightly less. Between the mirrors are two Brewster windows which by a carefully adjusted angle of incidence allows full transmission of light polarized in one direction while rejecting light of another polarization. As light traverses between the two mirrors it acquires the desired polarization because light of the other polarization is not transmitted. Because the HeNe laser is small and portable enough to easily be rotated in its stand the angle of polarization can also be adjusted easily.



Brewster's Angle: Equal to  $\tan^{-1}$  of  $n_2/n_1$

**Figure 2: Functional Diagram of Laser**

Because optical feedback, light retracing its optical path back into the laser, causes instability in the laser, an isolator is used for feedback extinction. The isolator uses the Faraday effect, in which the polarization of light passing through a magneto-optically active medium in a magnetic field is rotated. This rotation is nonreciprocal, or independent of the direction of propagation of the light, depending only on the Verdet constant of the medium, the strength of the magnetic field, and the length of the path through the magnetic field, according to the equation  $q = vhl$ , where  $q$  represents the angle of rotation,  $v$  represents the Verdet constant,  $h$  represents the strength of the magnetic field and  $l$  represents the length of the path through the medium in the magnetic field. Using this principle, an optical isolator operates by having incoming light from the laser pass through a polarizer, pass through the Faraday rotator and then pass through another polarizer allowing close to 100% transmission of the light. The feedback passing through the second polarizer first, then the rotator and then the first polarizer should have close to 100% extinction of the light.

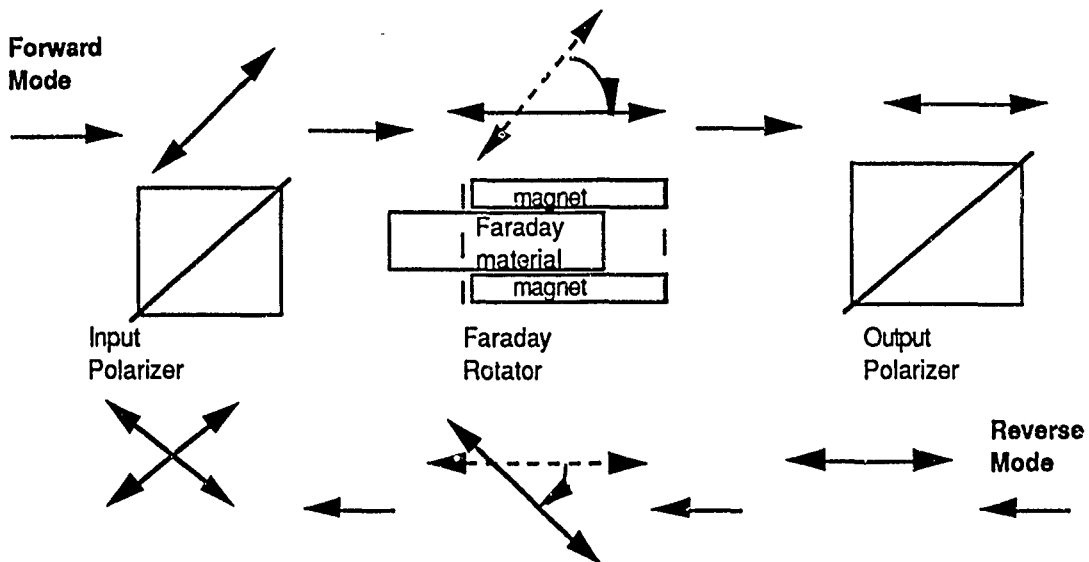
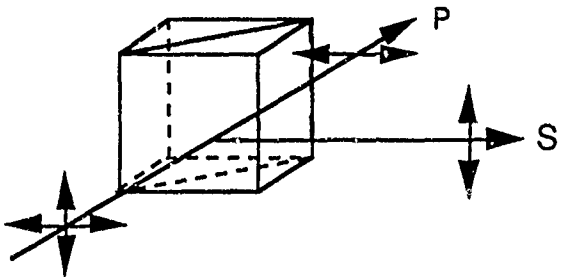


Figure 3: Operation of Faraday Optical Isolator

To measure the amount of polarization as the light reached the crystal a broadband polarization beamsplitter cube was placed in the path of the beam so that the horizontally polarized light was sent into a detector connected to a voltmeter. The wave pattern of light falling on any surface, like a vector, can be split into two components, one perpendicular to the plane of incidence and one in the plane. The one perpendicular is considered vertically polarized, or p-polarized, the one in the plane horizontal, or s-polarized. At a critical angle the vertical polarization has close to zero reflection, so for light hitting certain surfaces, for example the surface of a lake or the edge of a prism, the horizontally polarized light will be reflected and the vertically polarized light will be transmitted. The broadband polarization beamsplitter cube is a pair of coated prisms cemented together to form a cube, in which the diagonal reflects the horizontally polarized light and permits the vertically polarized light to pass through unimpeded. Broadband refers to the fact that the beamsplitter cube is effective through a range of many wavelengths such as the visible spectrum.



**Figure 4: Broadband Polarization Beamsplitter Cube**

Initially we used a mirrored surface as an attenuator, but, due to unacceptable losses, we adapted to a variable attenuator system in which the broadband polarization beamsplitter cube was used in conjunction with a retardation plate. The attenuator is used as a way to reduce and control the power reaching the crystal. . The crystalline structures making up wave plates are birefringent; that is, they have different refractive indices with differently polarized light. The atomic structures of the crystals result in different resonant frequencies along different axes, a "fast" axis and a "slow" axis. By retarding the wave frequency of one component of the light a wave plate can rotate the polarization of the beam. In general, a retardation plate causes a difference between the phase shifts along each axis or a retardation of  $\Gamma = 2\pi f(n_{\text{slow}} - n_{\text{fast}})L/c$ . In this equation,  $n_{\text{slow}}$  refers to the index of refraction of the slow axis and  $n_{\text{fast}}$  refers to the index of refraction of the fast index. In a half-wave plate,  $\Gamma = \pi$ , or half a wave. The slow axis of a half-wave plate retards one component of the light so that it is 180 degrees out of phase with the fast component. This results in the plane of the wave being rotated by twice the angle the axes of the wave plate make with the vertical and horizontal axes of the light. To form a variable attenuator in a set-up requiring horizontally polarized light the horizontally polarized light is sent through the half-wave plate rotating it to be vertically polarized. The light is then analyzed by the broadband polarization beam splitter cube, transmitting the vertically polarized light to another half-wave plate where it is rotated back to horizontal polarization. To change the amount of light passing through the variable attenuator, the half-wave plate can be rotated so

that the light it transmits is not wholly vertically polarized, so that some of it will be deflected in the polarization cube before it is rotated back to normal.

Between the optical isolator and the crystal the beam passes mirrors, lenses, and pellicle beam splitters which can affect the polarization a small amount. However, the amount of alteration of the polarization is not significant with the HeNe laser. The pellicle beam splitter is a five micron thick plastic membrane stretched over a metal frame. Because it is extremely thin it eliminates secondary reflections making them coincident with the original beam. Because when light hits the pellicle some light passes straight through and some is reflected, the pellicle is used for beam sampling.

In our final set-up as shown in Figure 5, the light sources are two HeNe lasers. As the beam is transmitted through the crystal's photorefractive gratings, the phase conjugate of the opposite beam is formed and sent back along each path. At the pellicle the returning beam is deflected and sent through a pinhole and a neutral density filter to a detector. The pinhole is placed so that only the phase conjugate beam would be measured by the detector. The neutral density filters are used to attenuate the beam to the range of detector sensitivity. Measurements were made using photodetectors, a BIOPAC MP100 analog to digital converter and an Apple Macintosh SE/30 computer.

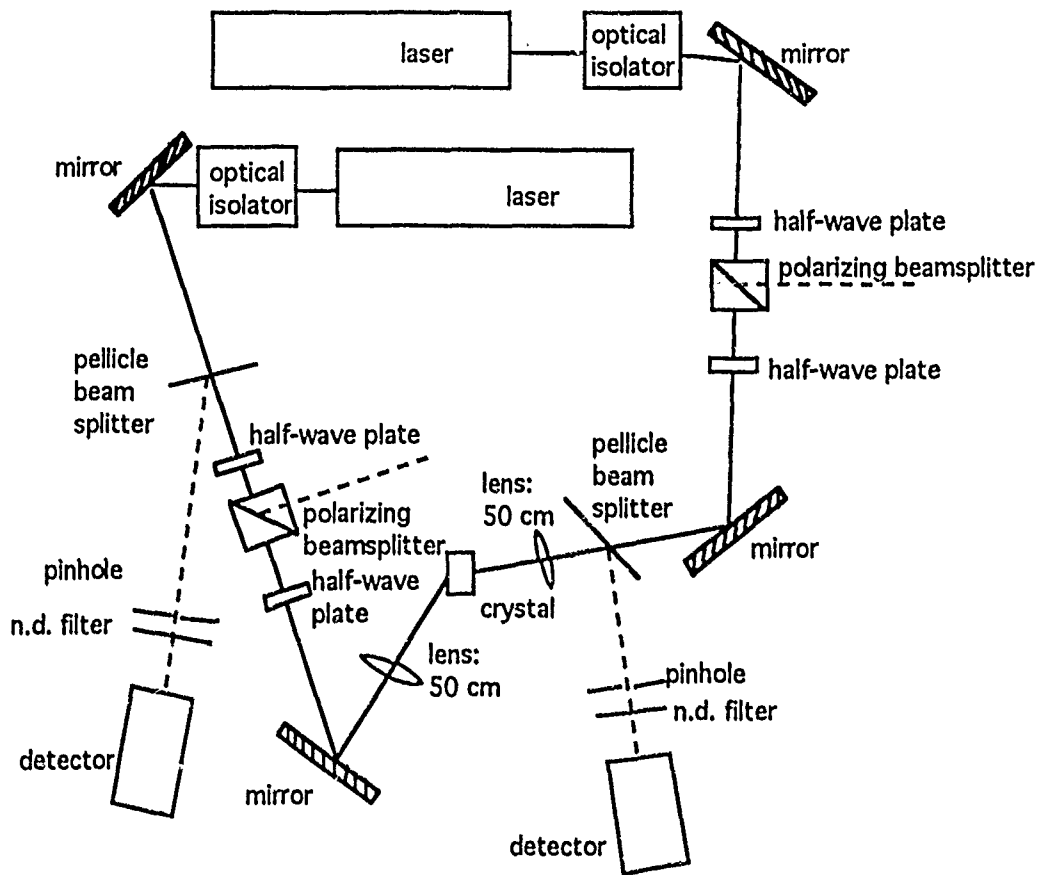
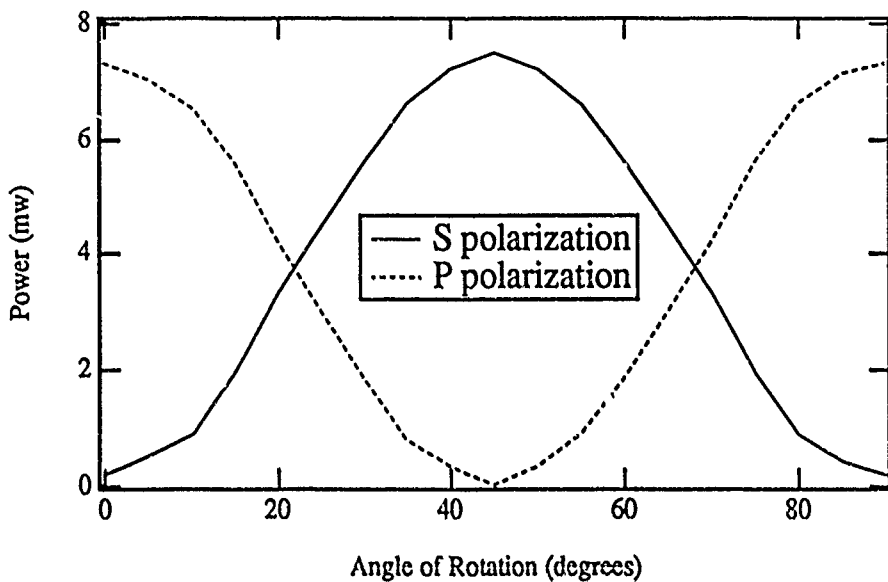


Figure 5: Schematic of Final Set-up

### III. Results

The graph in Figure 6 of the change in polarization of light as it passes through a half-wave plate rotated through 90 degrees shows that the polarization changes completely or is rotated 90 degrees when the wave plate is rotated only 45 degrees. This is because the half-wave plate retards the slow component of the polarization so that it is 180 degrees out of phase with the fast component, which describes a plane-polarized wave making an angle  $\theta$  on the opposite side of the fast axis so that the original plane wave is rotated through  $2\theta$ .



**Figure 6: Polarization of Light Passing through Rotated Half-Wave Plate**

The graph in Figure 7 shows the change in the polarization of the light as it passes through a Faraday optical isolator with the second polarizer removed while the amount of the Faraday material in the magnetic field is changed. The distance in millimeters refers to the distance between the knob, which is being rotated outward, and the body of the isolator. This knob controls the amount of Faraday material in the magnetic field, increasing the amount of Faraday material in the field as it is rotated outward. When the knob is approximately 10 mm from the body of the isolator the change in the polarization reverses. This indicates that the amount of the rotator rod in the magnetic field is no longer increasing, but rather decreasing.

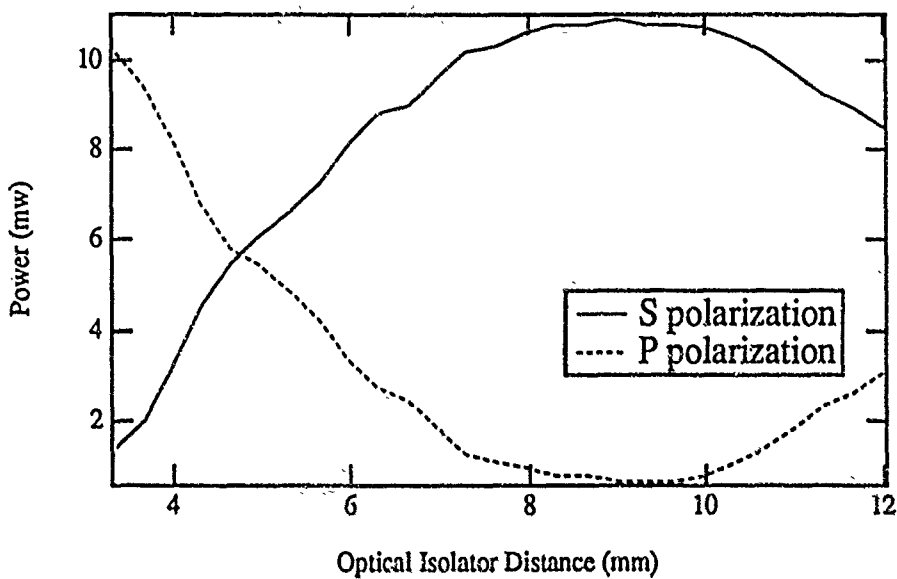


Figure 7: Polarization of Light through Faraday Rotator Optical Isolator

#### IV. Conclusion

With the correct optical equipment one can easily manipulate the polarization of light. The final set-up of the experiment had the desired polarization for phase conjugation. In addition, polarized light with certain optical equipment has other applications, like controlling the power of the light reaching the crystal as shown with the variable attenuator. We demonstrated the use of a half-wave retardation plate showing that the angle of polarization of light is rotated by twice the angle the plate is rotated. For the Faraday rotator we demonstrated that the angle of the polarization of the light can be controlled directly by changing the amount of Faraday material in the optic path in the magnetic field.

#### References

1. J. Feinberg, Physics Today, pp. 46-52, Oct. 1988
2. M. Gruneisen, E. Seeberger, J. Mileski, and K. Koch, Opt. Lett. **16**, 596 (1991)
3. Newport Catalog, "Precision Laser & Optics Products", 1989
4. OFR Catalog "Isolators '91 (Faraday Rotators)"
5. Pedrotti and Pedrotti, Introduction to Optics, Prentice Hall, 1987

HSAP FINAL REPORT

Eric Eidson

ABSTRACT:

This paper is an outline of the eight week High School Apprenticeship Program (HASP) and the steps taken to interface Neural Network programs into the University of New Mexico's KHOROS Graphical Signal Processing environment. I also discuss my experiences in installing a Logitech Hand-Held scanner and Microsoft Windows 3.0 on a PC.

I first came to the Phillips Labs at Kirtland Air Force Base as part of my High School Internship program to learn more about computers. The Phillips Lab is an Air Force Laboratory for research in space and missile technologies. I worked at the Lab's Super Computer Center which has a large array of computers including a Cray2. My mentor, Captain Steven Anderson, leads a research effort to combine pattern recognition, neural processing, signal processing and satellite autonomy. I enjoyed my work so I applied to the HASP program and got a position with my previous mentor. The main goals for the duration of the HASP program, were to learn the FORTRAN programming language, gain some experience with UNIX, participate in some of the team projects, and benefit intellectually and personally from the HASP experience itself.

The ongoing team project is to create a research tool which "...supports the signal processing research using pattern recognition and classification techniques [which] does not require domain expertise for the application engineer in neural computation."<sup>1</sup> To create part of this research tool, we integrated existing FORTRAN Neural Network programs with KHOROS which was "originally created as a research tool for image

processing..."<sup>2</sup> The KHOROS environment has been designed so that it can be modified to fit the changing needs of the user. The Neural Network programs and the KHOROS system were written in different languages, and had different systems of user interaction. The FORTRAN Neural Network programs had a menuing system for the user interaction, and KHOROS, written in C, had a graphical user interface. My role in interfacing the Neural network programs involved dividing the FORTRAN programs into separate subroutines which could be called by a program written in C.

The main part of each Neural Network program held the entire menuing system and branching structures. When the programs were run, the menu would present nine options, which were identified by numbers 0 through 8. When a valid option was picked, the program would branch to the correct loop identifier. The loop would perform the option selected (including some input or output), and subsequently loop back to the "Menu display" section. The original code is shown below in pseudocode form (Pseudocode allows us to write out what a particular line in the actual code is doing):

```
Main Program Section
    Display Menu
    Read in a number
    If number < 9 and > -1 then
        branch to right option

        Option 1: Do option one
                    branch to Display Menu
        Option 2: Do option two
                    branch to Display Menu
        ...

```

In the code that I wrote, in pseudocode form, the menuing system was divided into subroutines as follows:

```
Main Program Section
    Display Menu
    Read in a number
    If number < 9 and > -1 then
        call right subroutine
    branch to Display Menu

    Subroutine Option-1
        Do code for option 1
    end subroutine

    Subroutine Option-2
        Do code for option 2
    end subroutine
    ...

```

The "Display Menu" section has been replaced with a program in C, so it displays a graphical menu which can be used with KHOROS. Replacement of the "Display Menu" with a program in C is simpler with my code, whereas in the original code, such replacement would require the entire replacement of all code, including the "Display Menu" and all the "Options."

The FORTRAN Neural Network programs were written with COMMON statements, which allow different subroutines to share and change memory locations. At the time, I did not know any compatible C statement that could pass memory location(s) to a FORTRAN COMMON list, so I replaced them with argument lists. Replacement of the COMMON statements reduced the size of the executable program considerably, possibly because the compiler was better equipped to optimize argument lists. Passing argument lists also offers the advantage of allowing a programmer to identify the parameters a subroutine will utilize.

Some of the subroutines performed more than one distinct operation. They would do input and output, as well as actual data operations. For example, consider the original code in pseudocode form:

```

Set threshold in another subroutine
Subroutine Data-input-and-operations
    Open data file
    Read in value of X and Y
    Begin loop for Y number of times
        Begin loop for X number of times
            Read in value from data file and put it
            in xin
            If xin is greater than threshold then
                assign xin the value of 1
                else assign xin the value of 0
            Put xin in a one-dimensional array
        End loop (For X)
        call Another_data_operator
        call Yet_Another_data_operator
    End loop (For Y)
End subroutine

```

The pseudo-subroutine performs three distinct operations. It opens a file, inputs values which are then compared to a threshold. Then other subroutines are called, and they perform other operations on the data. I divided the original FORTRAN code into three separate, one-operation subroutines. As a result, the code is more modular, more portable, and easier to read and understand. Consequently, it is easier to document and maintain. Additionally, the division of the subroutines would allow KHOROS to choose the desired operation to perform.

The first of the three subroutines is classified as an input subroutine:

```

subroutine data_input
    Open data file
    read in value of X and Y
    start loop for Y number of times
        start loop for X number of times
            read in a value from data file
            and put it in xin
            put xin in a two-dimensional array (X by 200)
        end loop (for X)
    end loop (for Y)
end subroutine

```

Other changes to the Neural Network programs, while not necessary to interface the programs to KHOROS, increased the readability of the code. Consider:

```
type 0001
0001 format('This is line one.')
      type 0002
0002 format('This is line two.')
```

And the replacement:

```
type 0001
0001 format('This is line one./
-           'This is line two.')
```

We join all the extra type/format statements to get one type and one format statement. The format statement can hold up to sixteen extra lines. Consider also:

```
if (Is_it_on .eq. true) type 0003
0003 format('Status is ..... ON')
else type 0004
0004 format('Status is ..... OFF')
```

Which is replaced by:

```
type 0003
0003 format('Status is ..... ','$);
if (Is_it_on .eq. true) print *,* 'ON'
else print *,* 'OFF'
```

The change makes clear, at a glance, that only one status line will be displayed.

Prior to the completion of my role in the team project, I used a tutorial book and the experience of some other members of the team to learn FORTRAN. Also, I took a three day seminar on UNICOS, which is the Cray 2 implementation of the UNIX operating system. This brought me to the point where I had a solid FORTRAN foundation to build upon. When I finished the modification of the Neural Network programs, I started to learn C.

In learning C, I examined basic operations, operators and input and output. I wrote basic counting programs in C and examined a program that determined the readability of a document, using an algorithm based on word count, sentence count and syllable count (number of syllables determined by multiplying the number of vowels by 0.86).

In addition to learning computer languages, I installed a Logitech Hand-Held scanner on my mentor's UNYSIS 80386 microcomputer. I had one significant problem during the installation, which I discuss here. The software was loading for the scanner but it was not configured correctly for the SuperVGA video card. After trying different SuperVGA configurations on the scanner, I attempted to re-install the UNYSIS system software for the SuperVGA card, and found that there was no free address space in the section of memory which is required by the SuperVGA video card. It was later determined that a communication card was using an overlapping address section of memory. When the attempt to change the memory locations for both the communication card and the SuperVGA card failed, we configured the scanner for an EGA card. The problem with this solution is it increases the graininess of the picture. Later, we hope to find a solution so that we can use the scanner in SuperVGA mode.

I also installed Windows 3.0 on the UNISYS 80386 system, but because we still had not solved the conflicting memory problems for the SuperVGA card and the Communication card, we were only able to use it in VGA mode, not SuperVGA mode. The installation program for Windows 3.0 also had a conflict with QEMM, a window/memory management program, so we removed the

QEMM driver. Currently, the system is up, and Windows resides somewhere in the lower end of twelve megabytes of extended memory.

I have accomplished the goals set at the beginning of the HASP program by helping interface Neural Network programs into KHOROS and learning FORTRAN and UNIX on the way. Additionally, I have learned some documentation skills, when I reported the changes I made to the Neural Network programs. I have also learned some C, and I am eager to learn some more. When I encountered problems, I used the Scientific Method to solve them. I hypothesized the causes of the problem and then I proposed solutions to the problem. Also, I consulted other people for their opinions. When the proposed solutions failed, I proposed others, including seemingly less preferred solutions.

QEMM driver. Currently, the system is up, and Windows resides somewhere in the lower end of twelve megabytes of extended memory.

I have accomplished the goals set at the beginning of the HASP program by helping interface Neural Network programs into KHURCS and learning FORTRAN and UNIX on the way. Additionally, I have learned some documentation skills, when I reported the changes I made to the Neural Network programs. I have also learned some C, and I am eager to learn some more. When I encountered problems, I used the Scientific Method to solve them. I hypothesized the causes of the problem and then I proposed solutions to the problem. Also, I consulted other people for their opinions. When the proposed solutions failed, I proposed others, including seemingly less preferred solutions.

Bibliography

1. Anderson, S. A. et al. "Neural network environment for signal processing and pattern recognition of large scale data." *Proceedings of the Second Workshop on Neural Networks: Academic/Industrial/NASA/Defense, WNN-AIND 91:* 483 (1991)
2. Williams, Carla S. and John R. Rasure. "A Visual Language for Image Processing." *1990 IEEE Workshop on Visual Languages, Skokie, Illinois (October 4-6, 1990):* 86

FINAL REPORT FOR THE HIGH SCHOOL APPRENTICESHIP PROGRAM

EXPERIMENTING WITH FRACTALS AND CAREERS

Eric L. Engberg

Apprentice # 725

## Abstract

My work at Kirtland Air Force Base was multileveled, as were the benefits. Throughout my work period I made a point of being curious about what people did for their living, if they could tell me. My goal in this was to gain an understanding of what a broad range of careers in the scientific field entailed. This experience was unique to working in the laboratory. On a more specific level I wanted to learn as much as I could about fractals, and how this new area could be utilized to have real world applications, especially for the Air Force.

## Introduction

My first few weeks on the job were a slow period of learning. My mentor, Captain Edward Carmona, was a computer scientist and I had almost no experience in programming. We had daily tutorials in the programing language C and I used a program called Reflex to type Captain Carmona's numerous references into a database and print out a report. Both were useful experiences, but once I finished the database and demonstrated competence in Turbo C, Captain Carmona and I determined that although I still would not be able to do his work, it was time to choose a project of my own. Thinking about this I remembered an excellent lecture on fractals by Heinz-Otto Peitgen who had visited my school in the Spring of 1991. Fractals were an area I knew little about, but they were fascinating, and I had excellent computers to implement them on. The decision was simple. My work was from then on to be focused on fractals.

## Discussion

My work entailed a great deal of library research. Time and difficulty levels allowed me to read: Chaos, by James Gleick, An

Introduction to Fractals and Chaos, by John W. Haussmann, LT, USN, Fractal-Based Image Compression I and II, by R.D. Boss and E.W. Jacobs, bits and pieces of The Beauty of Fractals and The Science of Fractal Images by Heinz-Otto Peitgen, and A Better Way to Compress Images, by Michael Barnsley and Alan Sloan. This literature contained more information than I could understand, but I learned a great deal, certainly enough for my project.

Using this knowledge, Captain Carmona helped me to write a program in Turbo C that would use Iterated Function System codes to create fractal images. The program works by taking a random pixel's coordinates, multiplying them by the IFS code matrix values, and then placing a new pixel at the transformed coordinates. We devised a way to place the transformation values in a data file to run the program, but I decided it was more beneficial to run the fractals from code inside the program. This allowed for more of a demonstration-like program that anyone knowing how to run a program could use and made it more simple to see how the programs worked.

I began by using values of known structures I read out of an article or text. These transformations produced professional fractal images like the spleenwort fern, a fractal tree, a Sierpinski Triangle, and a square, but I wanted to do more than follow a fractal cookbook.

I experimented with self-devised transformation values, and through trial and error tried them out to see what kind of image they would produce. Some created strange pictures, others

caused the computer to lock up and I had to reboot. This taught me value of saving all my work quite often, and certainly before an untried run.

During this time, I was also working on my goal of understanding many different careers. As I was leaving one evening I asked a man who worked in the hall on my way out, what exactly did he do? I was pursuing my quest for knowledge about different jobs. He worked for Cray, and he was one of the people who kept the Cray running when something broke down. On other occasions I talked to a graduate student from MIT who was simulating plasma particles on the Intel Supercomputer, and an engineer doing microwave shots.

### Results

The results of my search of possible careers are that I did learn a lot about various careers, but I still haven't found exactly what I would like to go into as an adult.

The results of my project are much more successful. I have two programs of fractal demonstrations displaying 40 fractal images 33 of which I designed the IFS code myself. I think all of these are interesting images that have at least a mathematically artistic value.

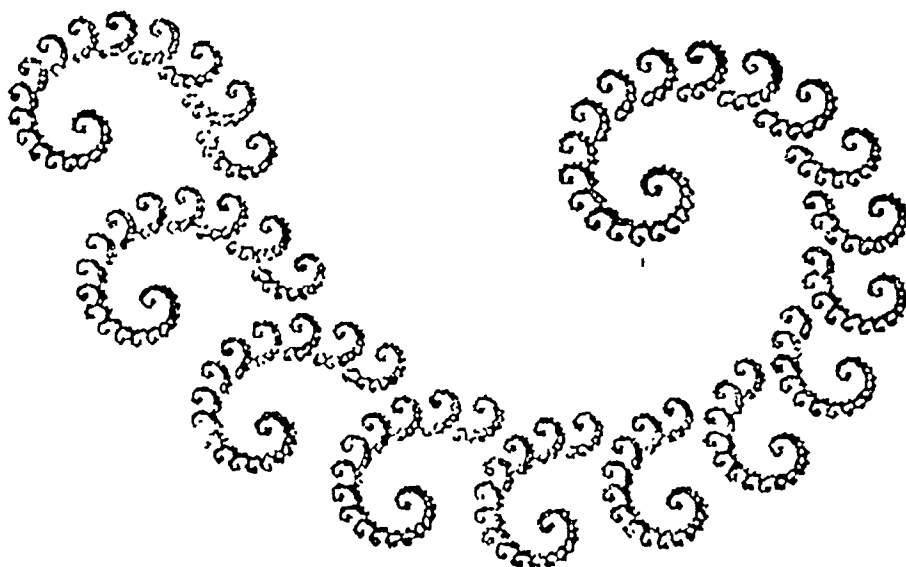
Here are a few sample IFS codes for their images:

Paisley Spiral

2 transformations

100,000 points

	a	b	c	d	e	f	p
$f(0)$	.85	-.31	.31	.85	1	-10	.8
$f(1)$	-.3	0	0	-.3	10	-1	.2



Spleenwort Fern

4 transformations

100,000 points

	a	b	c	d	e	f	p
$f(0)$	0	0	0	.16	0	0	.01
$f(1)$	.2	-.26	.23	.22	0	1.6	.07
$f(2)$	-.15	.28	.26	.24	0	.44	.08
$f(3)$	.85	.04	-.04	.85	0	1.6	.85



Starship (Briarpatch) Original 2 transformations 30,000 points

	a	b	c	d	e	f	p
$f(0)$	.9	2	0	-.6	.5	.6	.6
$f(1)$	-.3	.33	0	.9	1	-.2	.4

Fiber Original 3 transformations 60,000 points

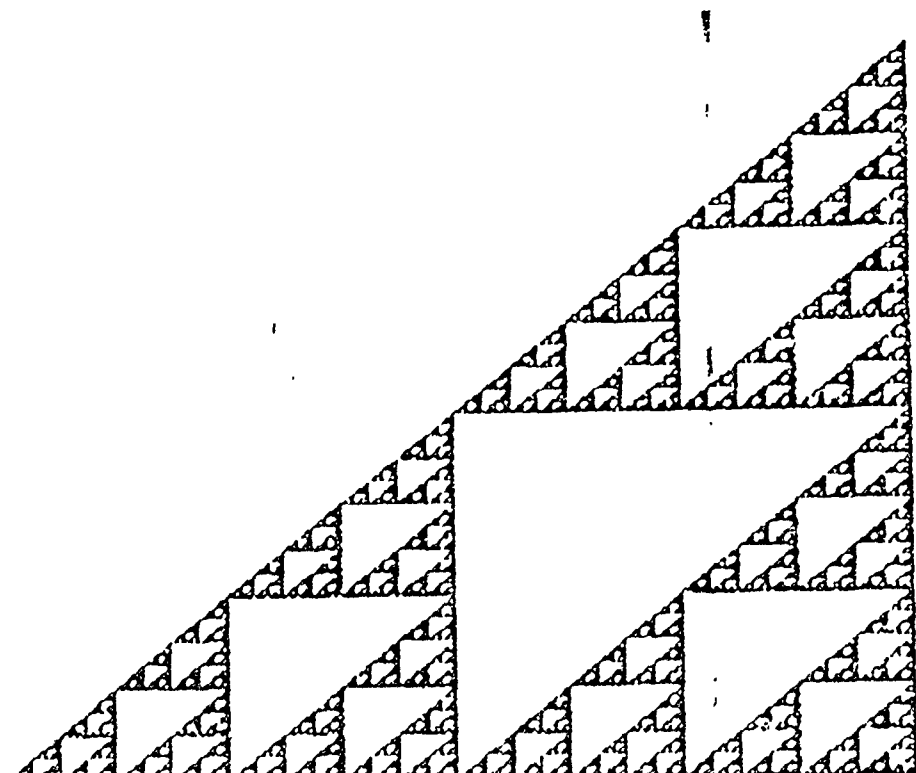
	a	b	c	d	e	f	p
$f(0)$	-.5	.3	0	-.6	.4	.1	.4
$f(1)$	-.2	.4	0	.9	0	-.42	.2
$f(2)$	.25	-.35	.42	.69	0	-.69	.4

Differentiated Curve Original 2 transformations 6,000 points

	a	b	c	d	e	f	p
$f(0)$	-.5	.3	0	-.6	.4	.1	.7
$f(1)$	.2	.4	0	.9	0	.2	.3

Sierpinski Triangle 3 transformations 9,000 points

	a	b	c	d	e	f	p
$f(0)$	.5	0	0	.5	0	0	.33
$f(1)$	.5	0	0	.5	1	0	.33
$f(2)$	.5	0	0	.5	.5	.5	.34



To view these IFS codes they can be easily implemented into the array values of the C program at the end of this paper.

I learned more about how IFS and Recurrent IFS (RIFS) codes can be utilized for image compression than I could put into practice, I lack the computer science skills. However, E.W. Jacobs and R.D. Boss seem to have the issue quite nearly figured out. "The need for data compression is not new," they say, and fractal techniques can achieve staggering compression ratios of 10,000 to 1. It seems that if these techniques were used wherever possible, a lot of memory would be saved. I recommend more research in the area.

#### Conclusion

I have learned what I wanted to learn at Kirtland Air Force Base. Fractals were an exciting area of research and I have learned how to program in Turbo C and how to use Reflex for a database. I have a good program for fractal demonstrations, and hopefully fractals will help with image compression.

I have also spoken with many people in different fields and gotten a good idea of what it is like to work in a scientific field. Science is a particularly good field because scientists are always required to continue learning, otherwise technology gets ahead of them. The High School Apprenticeship Program was a very good experience.

## Appendix

### C Program for Fractals In Graphics Mode

(Array values for Paisley Spiral)

```
void DoFractal(void)

    int h, w, color=15;
    int m, j, i, k;
    float a[2], b[2], c[2], d[2], e[2], f[2], p[2];
    float n, x, y, newx, newy;
    float pk, xscale, yscale, xoffset, yoffset;

    m=2;

    for (i=0; i<=m; i++)
    {
        a[0]=.85;
        b[0]=- .31;
        c[0]=.31;
        d[0]=.85;
        e[0]=1;
        f[0]=-10;
        p[0]=.8;
        a[1]=- .3;
        b[1]=0;
        c[1]=0;
        d[1]=- .3;
        e[1]=10;
        f[1]=-1;
        p[1]=1           /*Probalities are added*/
    }

    xscale=65;
    yscale=40;
    xoffset=120;
    yoffset=120;

    x=0;
    y=0;

    for (n=1; n<100,000; n++)
    {
        pk = (float) rand()/32767;
        if (pk <= p[k])
            k=0;

        else
            k=1;

        newx = a[k]*x + b[k]*y + e[k];
        newy = c[k]*x + d[k]*y + f[k];
        x=newx;
        y=newy;

        if(n>10)
            putpixel(x*xscale + xoffset, y*yscale + yoffset, color);
    }
```

SUMMER APPRENTICESHIP IN THE CHIEF GEOLOGIC RESPONSE SECTION, KAFB

Matthew Firstenburg - Civil Engineering Assistant

The eight week High School Apprenticeship Program was spent at Kirtland AFB in Albuquerque, New Mexico. These eight weeks were spent obtaining data to be used in testing designed to formulate a theory on the microstructural properties of soil. This data was obtained using the Cue-2 image processing system. This system was used to view individual particles to determine their areas, perimeters, aspect ratios, and compactness. These four properties will later be used to formulate the theory on their microstructural properties. Another project worked on during the summer involved use of the Movias motion analysis system. This system is used in the analysis of subterranean detonations in a division wide project, Halfspace. Movias allows for manipulation of films taken of subterranean detonations to create graphic representations of the displacement of the soil and rock used. These graphs include values of velocity, displacement, energy, and momentum, and are used by geologic analysts to develop theories on effects of subterranean detonations on underground structures, wiring, and shelters.

The Cue-2 image processing system is used to obtain data crucial to the development of microstructural theories to be used in future testing. This testing will consist of the compaction of rocks contained in a specimen container. These rocks will be tracked throughout the loading process, and the rotation, disintegration,

displacement, and fracture of these rocks will be recorded. A simplistic two-dimensional analysis was done initially to discover problems that may be encountered in future three-dimensional tests. This two-dimensional analysis was performed on the Cue-2 system. This system consisted of an x-ray light, an incandescent light, a high resolution video camera, and a Gateway 2000 486 computer which ran the Cue-2 program. One problem was to determine the significance of rock orientation in the container. Because no data was taken on the initial setup, it was attempted to show that the orientation of the rocks had no impact on test results.

The Cue-2 system helped to show this. A rock was placed on the x-ray light, which allowed for a distinct outline of the rock for computer analysis. This analysis consisted of thresholding to make a binary image of the rock, analyzing the image to find the area, perimeter, compactness, aspect ratio, and the angle between the major and minor diameters, and then performing statistical analysis that would allow comparisons to be made between different rocks and different orientations. Because none of the rocks were the same size, the area was used to match rocks of comparable size. Other variables were those considered relevant to the project.

The thresholding of the image was done manually by specifying the range of grey levels that would be converted to black. Any grey levels outside of this range would be colored white. Initially a regular light was used for illumination, but because of the shadow produced, proper results could not be obtained. This problem was solved by placing the rocks on the x-ray light. This produced a clear outline of

the rock, and allowed for better thresholding. There was still a very light shadow on the side of the rock not in direct line of the overhead light. This was solved by obtaining a ringlight system which evenly illuminated the light from above.

Initially the x and y distances for the camera were calibrated using an object with known dimensions. This object was then placed on the measuring surface, and the calibration subprogram was run. The camera was far enough away that the height of the rocks didn't cause any error in the program calculations of area and perimeter. The perimeter and area were calculated by the computer according to the precalibrated pixels. If some inner part of the rock was not highlighted during the thresholding process, then it would not be included in area calculations. Such holes could be filled and the area could be corrected for accurate data. These values for area and perimeter could then be used to calculate the compactness by dividing the perimeter by the area.

The Cue-2 program analyzed the binary images created and calculated the area, perimeter, and Ferret's diameters at various angles. These diameters were then used to calculate the aspect ratio, which is the minor diameter divided by the major diameter. However, the problem with this aspect ratio is that of the rock were very oddly shaped, perhaps like a semicircle, then the aspect ratio would calculate higher than it actually is. For this reason Martin's radii were used. Martin's radii take the length measurements from the center of mass to the edge of the object at various angles. However, the program couldn't yet be altered to be able to take measurements at

increments any smaller than 45 degrees, and therefore the system could not yet provide the most accurate possible aspect ratios. The program will have to be improved to take measurements at increments of at least 1 degree.

In the initial data collection, seven batches of 25 rocks each were used. Three orthogonal views were taken and the previously mentioned variables were to be calculated for three views, x, y, and z, of each rock in each batch. The program had a few problems that did not allow for the most accurate measurements of the variables desired. The lighting was one problem. It was extremely difficult to obtain images with no shadows. This eventually led to inaccurate data taken and once solved, required that all data and images be recalculated. This data will eventually be statistically analyzed and will be used to determine the importance of particle orientation. The fact that only 25 rocks were used from each batch also causes some concerns as to statistical analysis in the future. Although the error encountered in the collection of data was under 3 percent, thus providing acceptable values, only time will tell if the data will be sufficient for the development of desired theories.

The main goal of this project is to develop a generalized theory that will allow the accurate modeling of rotation, disintegration, displacement, and fracture of particles. This preliminary work must be completed before any other testing can be accomplished.

A much smaller part of the High School Apprenticeship Program was spent working on the Movias motion analysis system. Movias consists of a Gateway 2000 486, an 8mm film projector, and a specialized projection

screen. From tests done out in the field, usually at what is known as "The Ranch," films are made and sent to the person in charge of converting these films into graphs and charts. These films are then transformed from a visual explosion into a series of more informative graphs and charts.

The first step in the transformation is to load the film onto the Movias device. This device is a projector that plays the film onto a digitizing board. This board is used to plot points for use in graphic illustration. The projector allows the user to advance and rewind the film at any necessary rate and interval. The films come from the Ranch at an area designated for the Halfspace project. Each film consists of a face on view of a vertical cross section of the underground test bed. This section shows from one to three detonations, aligned vertically. These are detonated at preset intervals, usually about 5 milliseconds. The latest film consisted of three detonations, precisely 5 milliseconds apart, and it was filmed at a rate of 10,000 frames per second. The film is then advanced to the frame beginning the first detonation, and as the displacement of earth increases, this increase is digitized.

The process of digitizing is extremely complex. A file is first made on the 486, and an initialization set up is performed. This consists of titles, frame rates, advance rates, film speed, fiducial point locations, and the number of points that will have their displacement digitized. Then digitizing is begun. The digitizing itself is the point where things get interesting. The most efficient points to digitize must then be decided upon. This involves analyzing

the film and then deciding which points on the film to begin digitizing. The points must be chosen carefully due to the fact that many of them are eventually blown completely out of camera range. About seventy points are digitized per frame on the average. This means a digitization of approximately seventy points per frame for a minimum of four hundred frames. This makes for quite a large task.

Once the digitizing process is completed, it is time to convert the raw data into graphs and tables. To access the graphing capabilities, the file must first be transformed in space. This aligns the two fiducial marks, determined during the initialization process, for each frame. At this point the graphing menu can be entered, where there are twelve different choices for the x and y axis values. These include position, displacement, acceleration, momentum, and energy.

These graphs are the final output products and are sent to others to be analyzed. It is during this further analysis that theories are developed and questions are answered. Without the graphic representations offered by the use of the Movias system, many of these theories would be left undeveloped, and many of these questions would be left unanswered.

## TEM STAGE COLLECTORS, LDEF SAMPLES, AND A SUMMER AT KIRTLAND AIR FORCE BASE

Russell Grubbs, High School Apprentice

Abstract - My high school apprenticeship was very successful. The design for the TEM (transmission electron microscope) was completed and its construction is in progress. The objective of the TEM Stage collectors will be to collect vaporized space craft materials. We will then be able to know how space craft material changes over time and distance. The actual experiment will be performed in October, most likely at Los Alamos National Laboratories. The one problem with the design is that it will have to be rescaled. This is because the dimensions are too large for the vacuum chamber. In order for the experiment to be accurate it requires a smaller device. Robert Roybal's original draft was drawn to a certain scale and he wanted to continue using the same measurements. The gearing system still needs to be developed. The LDEF (Long Duration Effects Facility) samples were partially characterized and the lab recently purchased a camera which will finish the job and check the work that has already been completed. This summer I increased my knowledge of computers because I had access to them daily. Finally, I learned how to perform most of the tests described in the Introduction.

Introduction - This summer I was assigned three projects. I was to observe and learn as much as possible about how a laboratory

functions, document the topography of samples, and to design a series of TEM stage collectors. Our lab functioned in the following manner: each person worked on their own individual research projects. This work would be interrupted by someone requesting an evaluation of a sample. Samples usually consisted of materials that had been subjected to stress and had failed. I observed these samples being characterized five different ways.

The most common way that a sample was viewed was with the scanning electron microscope (SEM). The procedure to do this was as follows: the sample was mounted to a superconductive material which acted as a slide, coated with the same material, and then placed in the SEM. The reason for the superconductive material is so that the sample does not become charged by the electron beam and give an incorrect signal. By using the SEM, one is able to know the topography of a sample. The image from the SEM can be transferred to a computer (SUN) where it can be identified. The unknown sample becomes identified when transferred because as the electrons strike the sample, characteristic x-rays are given off (similar to a finger print). The computer matches the unknown x-ray with the closest known substance. By transferring the image it can be saved and manipulated more easily. Consequently certain things such as distance between two points and a printout of the object can be obtained.

X-ray defraction is another way to determine an unknown. It utilizes the same concept above but in this particular tests compounds are listed for the unknown and not simply elements as

with the SUN. This machine was extremely easy to use as was the SEM. The only procedure needed was to turn it on with a switch. A computer collected all the data. The operator only needed to decide which compound matched the unknown. A CD-ROM was connected to the computer with all possible compounds and their x-ray defraction graphs. It can be difficult to decide which compound matches the unknown. The units on the graph from the CD-ROM did not match the units obtained during the test. During my apprenticeship, the lab bought a plotting program. I suggested that we format both graphs into the new program. The new program had the power to align both graphs to the same units and identifying the unknown sample became easier.

The three other tests that our lab performed were more specialized and were only used when an individual project required them. These tests included a tensile test, hardness test, and chemical analysis. The tensile test was use to determine how much pressure a sample could withstand. It was performed as follows: place the sample in the hydropic clamps, attach wires (strain gauges) to the sample that would lead to a computer, and then apply the pressure to the sample. The strain gauges allowed the computer to collect such information as stress, load, and, of course, strain. The machine, called an MTS tensile test, would draw a graph that would check the data collected by the computer. The results gathered by the computer would be changed into useable data using the plotting program mentioned earlier. I was unable to observe the hardness test because the machine was broken. The chemical

with the SUN. This machine was extremely easy to use as was the SEM. The only procedure needed was to turn it on with a switch. A computer collected all the data. The operator only needed to decide which compound matched the unknown. A CD-ROM was connected to the computer with all possible compounds and their x-ray defraction graphs. It can be difficult to decide which compound matches the unknown. The units on the graph from the CD-ROM did not match the units obtained during the test. During my apprenticeship, the lab bought a plotting program. I suggested that we format both graphs into the new program. The new program had the power to align both graphs to the same units and identifying the unknown sample became easier.

The three other tests that our lab performed were more specialized and were only used when an individual project required them. These tests included a tensile test, hardness test, and chemical analysis. The tensile test was use to determine how much pressure a sample could withstand. It was performed as follows: place the sample in the hydropic clamps, attach wires (strain gauges) to the sample that would lead to a computer, and then apply the pressure to the sample. The strain gauges allowed the computer to collect such information as stress, load, and, of course, strain. The machine, called an MTS tensile test, would draw a graph that would check the data collected by the computer. The results gathered by the computer would be changed into useable data using the plotting program mentioned earlier. I was unable to observe the hardness test because the machine was broken. The chemical

microscope. A change in crystal structure of the vapor should be noticed.

The objective of this experiment is to redefine the Air Force's Repetitive Pulse Phenomenology Program, RPLP, code. This code was established using only one collector. The code has several inconsistencies. For example, the RPLP code treats the vapor as a continuum and it is not known if the vapor can be classified. The revised experiment will correct these inconsistencies and possibly a new code will be developed. The new code will provide a better understanding of how the vapor changes over time and distance.

Another application of these collectors could be to help produce more carbon 60. "Regular" carbon is shot with a laser and after a series of changes becomes C-60. These collectors could help gain more C-60 than the present method. C-60- is important to future developments in medicine and other research. Applications of C-60 include a possible cancer cure and higher quality plastics. Due to the scarcity of C-60 it is very expensive. Therefore, research is often limited.

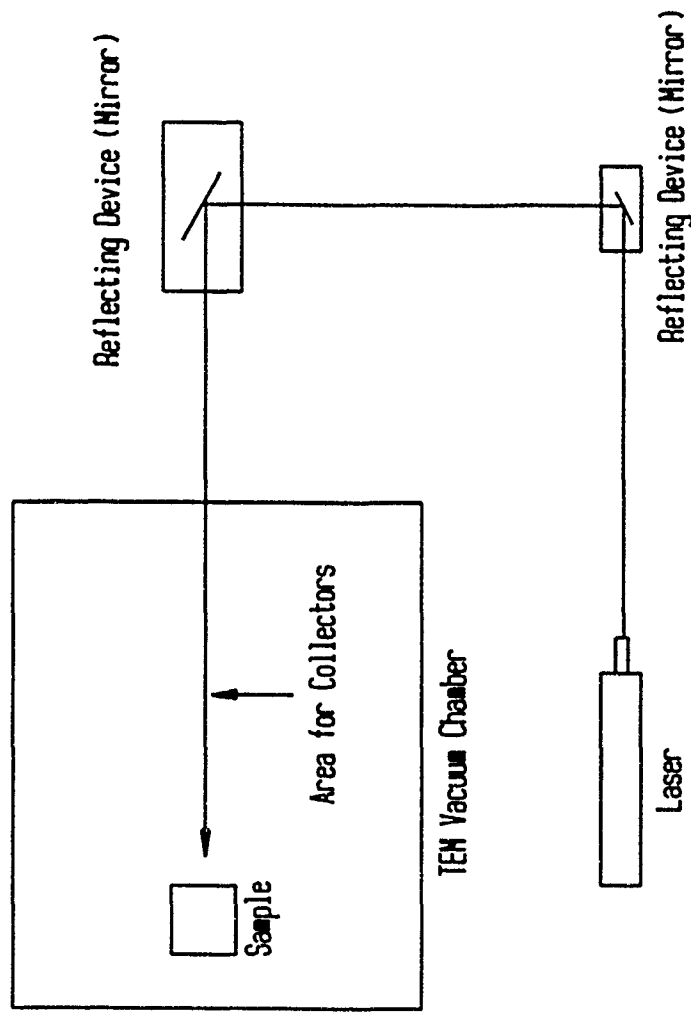
The design that I have created has several advantages. First, the collectors are treated as a group and not as individual collectors. The collectors can be rotated at the same time to the next position. This idea allows there to be a given amount of readings (6) at the same position. The collectors, therefore, do not have to be changed between shots and results from the same experiment can be checked. Also, the design is simple and easy to build and operate. During my first draft I tried to stack the grids (which are inside a collector)

instead of using a rotating disc. The rotating disc makes hiding each grid as easy as a rotation instead of trying to move each individual grid. The reason that each grid must be hidden is because after it has collected it's vapor it would become contaminated with the vapor from another shot if it is exposed.

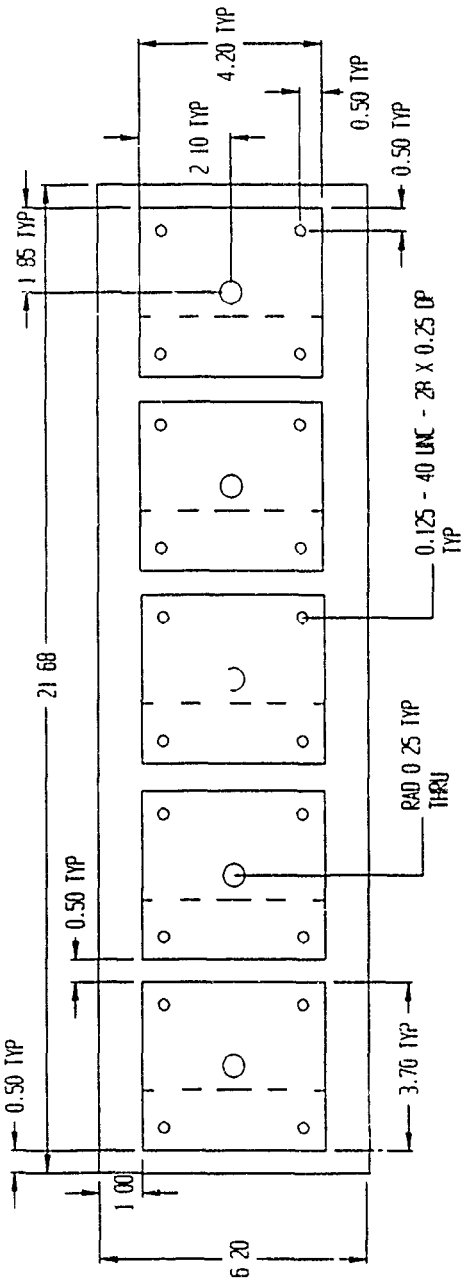
Results - The results of my summer are shown in the drawings included. The drawings include Mr. Roybal's original collector, the experiment design, my abstract idea of the collectors, a sketch, and the mechanical drawing of the collectors. The gearing is yet to be finalized and the stage is not yet built. The shot and collection will be done in October.

Conclusion - This summer I was part of two actual research projects. It was very confusing walking into the middle of these projects because I did not understand what was trying to be accomplished. The objective of the experiments is to develop better space craft materials. I hope that the drawings and the text of this paper show the reader how this will be done. The language of the TEM experiment is very hard to understand. A collector holds a disc which holds six TEM grids. Five collectors are lined up one after the other. The general idea drawing (abstract) is not to scale. After becoming familiar with the ideas and the language of the experiment and my co-workers I was able to learn how a lab functioned and how research is conducted.

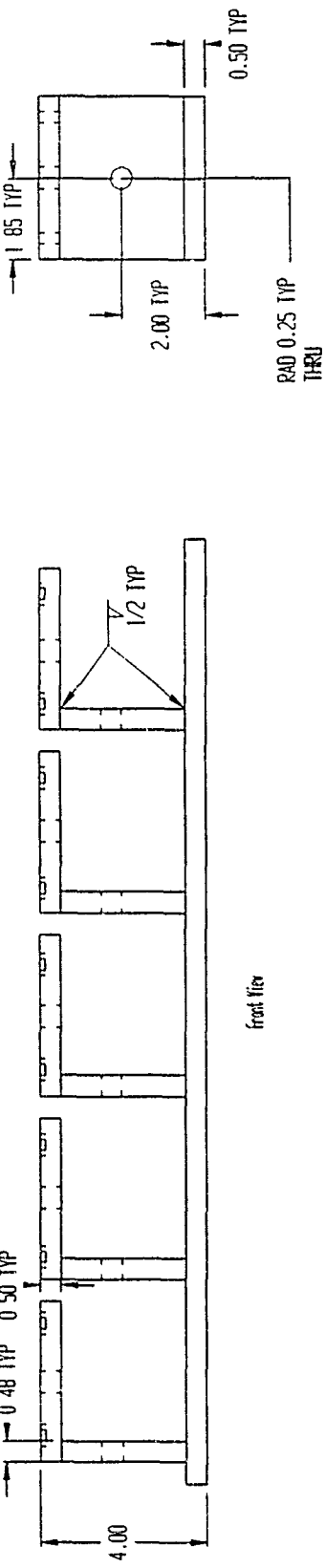
## Experiment Design



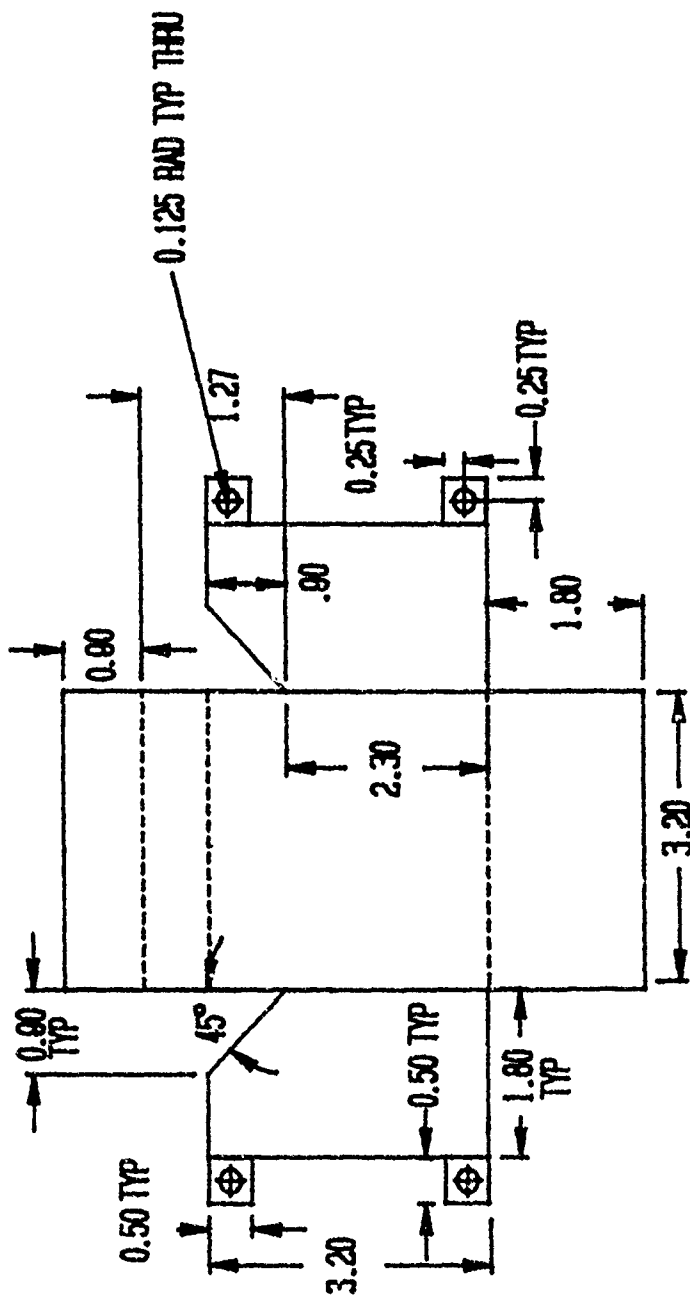
Mechanical Drawing of IEM Stage Collectors  
(Top, Front, and Side Views)



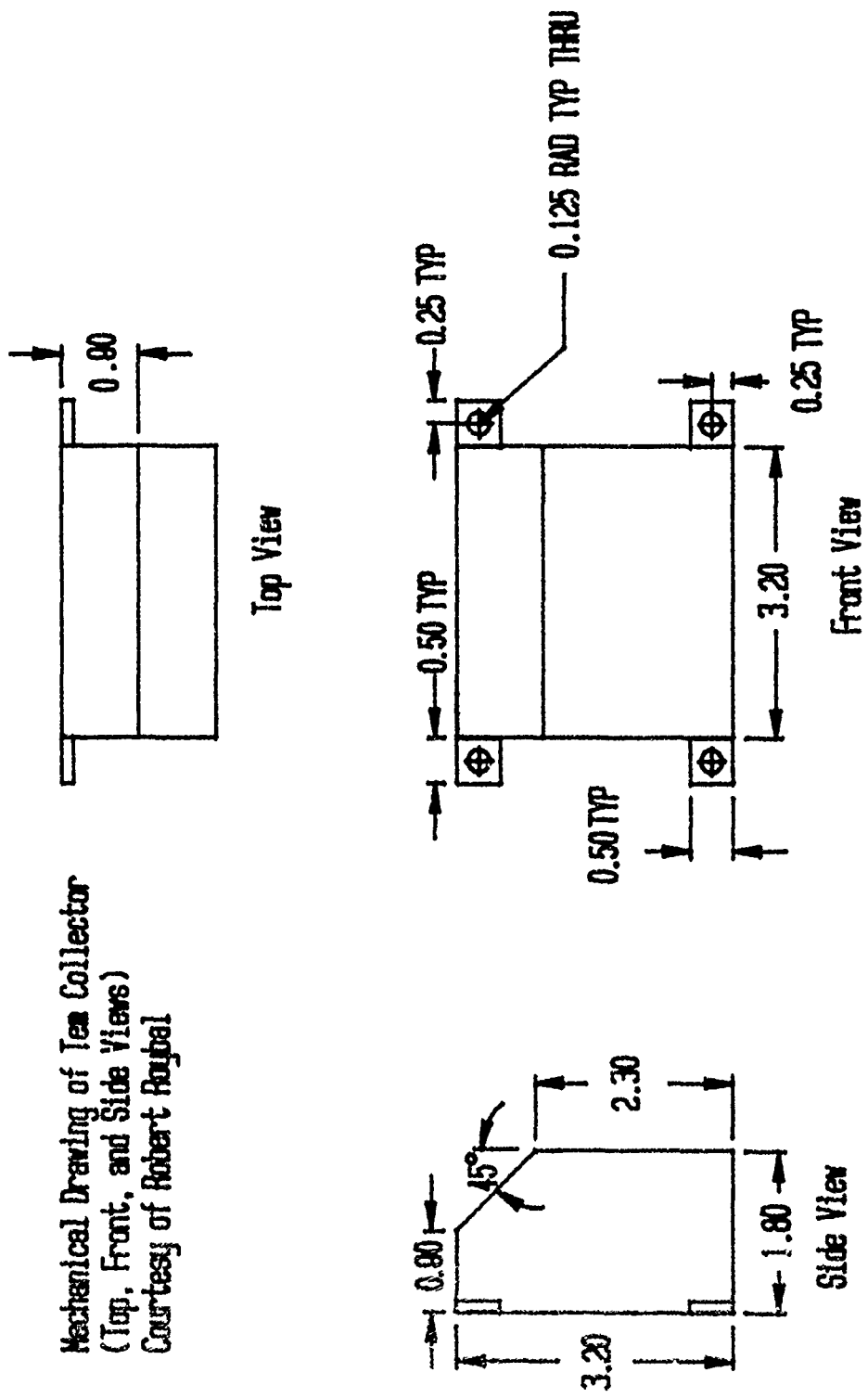
Front View



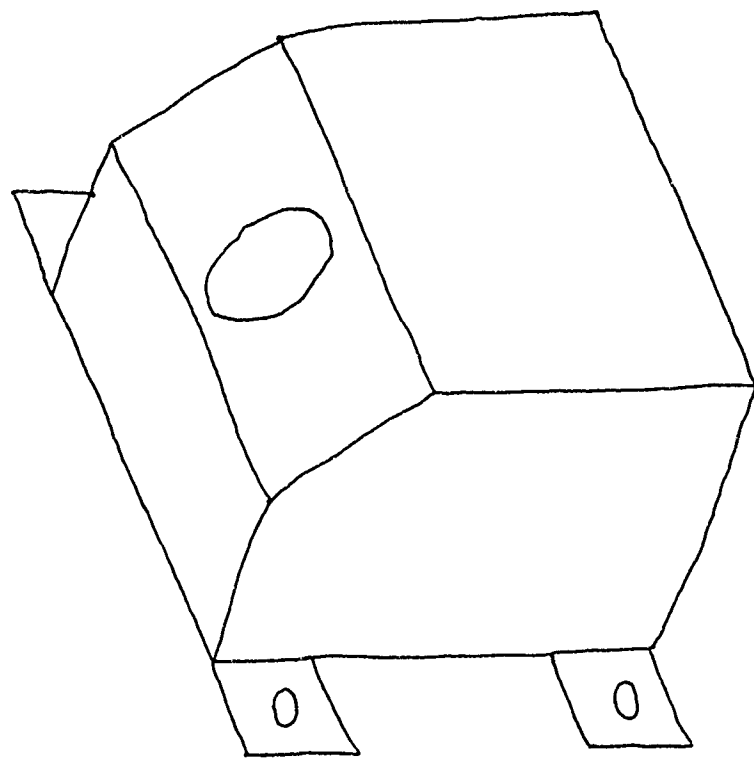
'Layout' of TEH Collector  
Courtesy of Robert Rojbal



Mechanical Drawing of Tea Collector  
(Top, Front, and Side Views)  
Courtesy of Robert Raybal

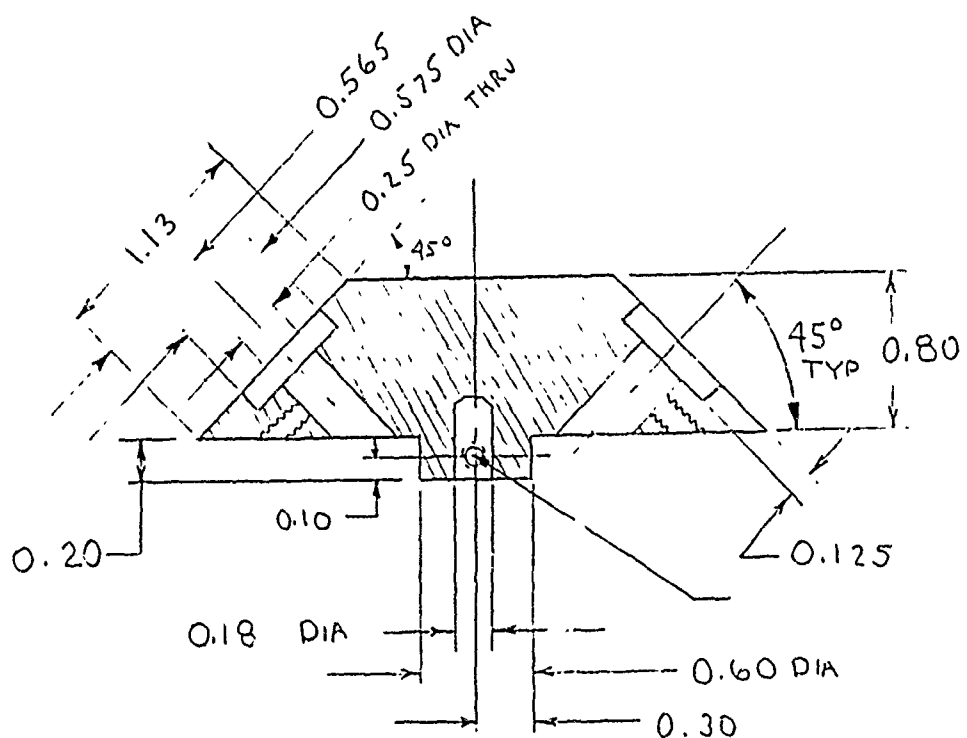
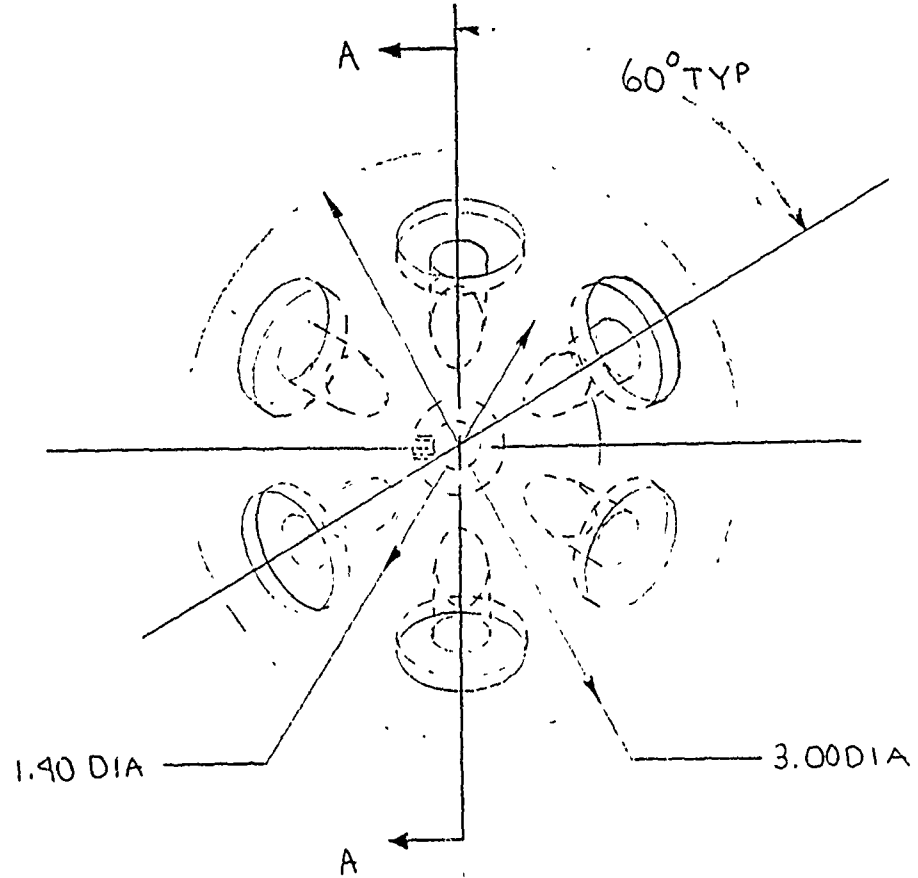


Shield, TEM Collector Holder  
Courtesy of Robert Rajpal



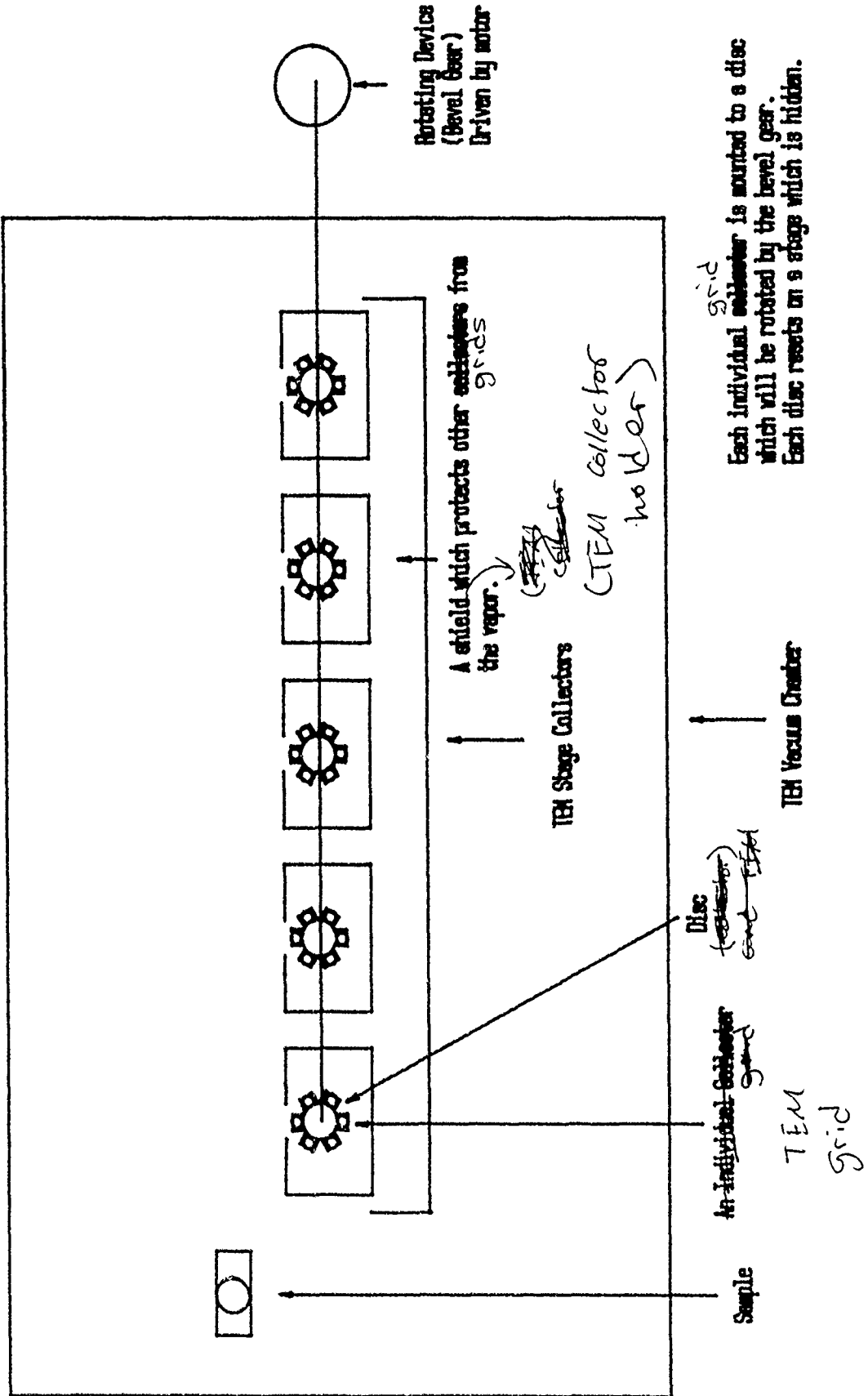
STAGE TEM SAMPLES

AMADA  
22-141 50 SHEETS  
22-142 100 SHEETS  
22-144 200 SHEETS



MATERIAL: STAINLESS STEEL

## General Concept of TEM Stage Collectors Design



Note : note to

Scale

## ADVENTURES IN HIGH ENERGY

by Brad L. Karmiol      Apprentice

### ABSTRACT

This summer I worked on various projects, and rarely by myself. On the first day I discovered that there was another high school student working in the same building as I was, and our mentors decided that it would be easier for them if he and I worked together. Brian Rizzoli and I spent the rest of the summer working together on projects ranging from upkeep of laboratory equipment to acquisition of data captured on film. Our biggest project, however, was the development of a program that would digitize these data images from the film, and then the actual digitization of many data images using this program.

### INTRODUCTION

The experiment, "Marauder," being conducted in our building is a high energy plasma experiment. Basically, argon gas is injected into a toroidal chamber which is then subjected to high voltage, forming a high energy plasma. This plasma moves upward in the chamber, and then is pumped out of the chamber. All of this occurs in a matter of milliseconds, and data is captured by polaroid pictures of oscilloscope traces. It is through these pictures that the scientists can map the

magnetic field, examine toroidal structure, check the height reached, and view other information. However, it is easier to store, compare, and manipulate the data when it is a digitized image on the computer. Brian and I were given the task of writing a program that could digitize and aid in the manipulation of these images, and then using this program to do exactly that.

#### PROBLEM DISCUSSION

The program was originally written in GW-Basic, as Quickbasic was not available to us at the time. This presented a large problem for me, as I knew little about programming in Basic. Therefore Brian was the main programmer while I would test the program to identify the bugs and suggest ways to make the program more user-friendly. Our first hurdle was learning how to use the Summa Graphics Pad, which is what we were going to use to actually digitize the images to the computer. That was fairly simple, as was setting up the menus in our program. The most difficult step was translating the points that we entered into the Summa Graphics Pad into screen coordinates, and then scaling the screen coordinates to properly align each particular image. This took some complicated math and a good deal of time.

From there we put in image manipulation aids such as sorting the data by  $x$ -value, scaling it, and interpolating it. We were then able to remove all of the bugs, and we had a fully functioning program. Therefore we began digitizing images. After digitizing about 300

images, we decided to go back and try to make our program faster. The scientists wanted us to interpolate each digitized image to 500 points, and this took about ten minutes. We were able to dramatically increase the speed of our interpolation, from ten minutes down to about 25 seconds. We then accelerated the program even more by changing from a bubble sort to a shell sort. After this we wrote the program in Quickbasic so that we could compile it, and finally I wrote most of the manual which accompanies our program. The manual and a printout of the program follow this report as figures one and two, respectively.

### RESULTS

Our work produced the digitization, proper scaling, interpolation to 500 points, and saving to disk of about 300 data images, as well as a user-friendly, expedient program that the scientists can use to digitize their images. We also produced a simple manual to instruct the scientists on how to use the program. Some of the images we digitized and manipulated were included in Captain Carl Sovinec's final report (figure three), and the rest are being analyzed by the scientists with whom we worked (figure four).

### CONCLUSION

My first days in the high energy plasma building left me somewhat

overwhelmed. Although my mentor assured me that I would acclimate quickly, I was slightly fearful of all the new things to learn. Almost immediately I found ways to help the scientists with whom I worked and this bolstered my confidence. By the end of the summer I had aided in the production of a program that will help the scientists conduct their experiment. While I put a lot of work into this summer, I got a lot out of it. I gained scientific experience, and spent a summer in the "real world." I met many great people and made many new friends. I hope that I will be in the High School Apprenticeship Program again next summer, so that I have the opportunity to repeat these experiences and enjoy new ones.

#### ACKNOWLEDGEMENTS

I would like to thank Dr. James Degnan for making sure that I was kept busy, Dr. Dave Price for sharing his computer and software, Jerry Baca for being friendly, Mike Martin for being a helpful instructor, and Brian Rizzoli for making the teamwork of the program so enjoyable. Finally, I would like to thank Dr. Sue Englert for being a great second mentor and a caring, patient friend.

APPENDICES - FIGURES

"Summa Graphics Pad Integration at Digitization" - Figure 1 - Manual

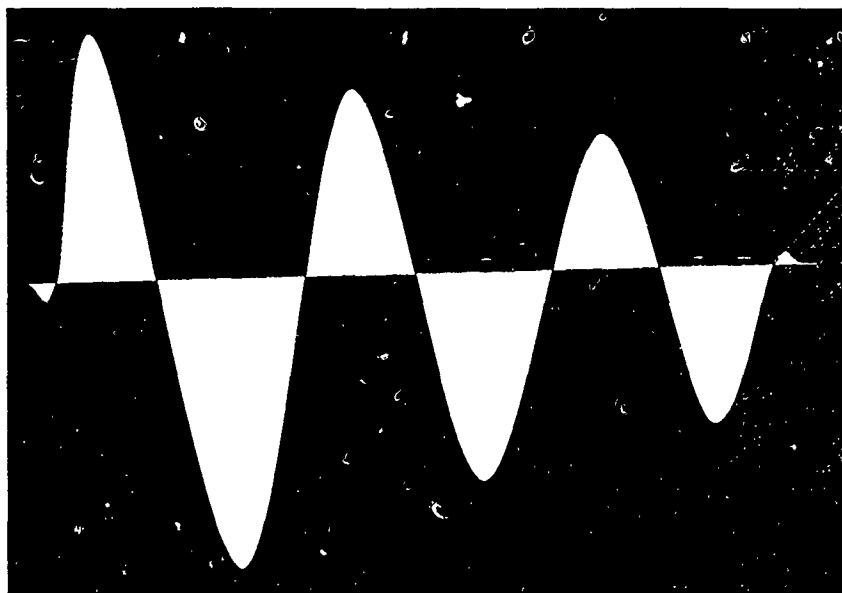
"Summa Graphics Pad Integration and Digitization" - Figure 2 - Program

Large Graphs - Figure 3 - Images from Captain Sovinec's Final Report

Small Graphs - Figure 4 - Digitized Field Mapping Shots

Figure 1

## Summa Graphics Pad Integration and Digitization



By Brian Rizzoli and Brad Karmiol

### **Setting Up the Sketch Pad**

To begin using the Summa Graphics Sketch Pad for digitization, make sure the graphics pad is correctly configured for your computer and for digitization. Instructions concerning configuration and pad setup are found in the Summa Graphics Sketch Pad instruction manual.

### **Setting Up the Program**

On the enclosed disk, you will find the following programs:

SUMMA.EXE  
SUMMA.BAS  
SINE.DAT  
SINE.TST

If you are using a disk drive, format a disk on which to keep your digitized files. **FORMAT A:.** After the disk has formatted, replace the Summa Digitizing program disk in the drive.

If you are using a hard drive, copy summa.exe and summa.bas over to any directory on the hard drive. **COPY A:SUMMA.\* C:.** Next, make a new directory from the C: path. This is the directory in which you will save all your digitized files. The defaults for the digitizing program are to the path **C:\SHOTS\.** For ease of use, it is recommended that you create your directory with this name. **C:MD SHOTS.** Finally, copy the files SINE.DAT and SINE.TST to the directory you have just created. **COPY A:SINE.\* C:\SHOTS\.** It is a good idea to keep the sine files in your files directory since the program may call on the sine files as examples.

### **Loading the Program**

To load the Summa Graphics digitizing program from disk, type **A:SUMMA** and press the enter key.

To load the program from hard drive, type **C:SUMMA** and press enter.

### **Opening Menu**

After the program loads, you will be presented with an opening menu. Here you will decide the way the Summa Graphics Pad will accept data or you can view a previously stored picture. To select the desired option, press the space bar until your choice is highlighted in red. Press the enter key.

**Single Point Selection :** This option will allow you to digitize your image point by point.

The graphics pad will only accept the points that you choose by clicking the mouse.

The points you click will immediately be connected by lines. It is not necessary to digitize the points in the correct order since you can sort the data by x values.

**Selective Stream by Button :** This is probably the best option for digitizing an image. The graphics pad will accept single points like the single point mode, but will now also accept a constant flow of points when you hold down the button. This option allows for fluid curves and point by point selection.

**Continuous Stream Selection :** For this option you do not need to press any mouse buttons. Instead, simply place the mouse on the pad and the pad will accept a steady flow of points. Be careful, however, because the pad will continue to accept points even when the mouse is a quarter inch above the pad. This feature makes removing the mouse from the pad quite difficult. Another disadvantage of the continuous stream mode is the fact that it is extremely difficult to place the mouse correctly over the image without choosing unwanted points.

**Show Saved Data :** This option allows the viewing of previously saved data. You are asked to specify the drive and directory. If you are using a floppy disk to save your data, place the disk in the drive and type in the corresponding drive name. If you are using a hard drive, type in the path and directory set up for digitized images following the example. The default path is C:\SHOTS\|. Pressing the enter key without typing a drive or directory will send you to the default path.

Next, a directory of the path or drive you have specified will be printed to the screen. Type in the desired file and hit enter. (NOTE : The directory will only print the files that end with .DAT. Make sure you name all your digitized files this way!) If the file you have typed is found in the path or drive, the image is drawn to the screen.

Initially, the image is scaled to the screen size. To receive an accurate view, choose 'S' for scaling. Type in the appropriate coordinates of the image and the graph will be redrawn. A feature of scaling is the ability to zoom in to a particular region of the graph. When asked for the corners of the graph, type in the coordinates of a box which would surround the portion of the graph that you want to view.

## **Prepare to Digitize**

After choosing the mode you want the Summa Graphics Sketch Pad to accept points, you will be asked to place your graph on the graphics pad, and place the device at the lower left hand corner. Place your image on the Summa pad. Try to line it up well, and it is recommended that you tape the image to the pad. Select the lower left hand corner by placing the crosshairs of the mouse on this point and clicking any of the four buttons on the mouse. Do likewise for the lower right and upper right corners.

## **Digitize**

Now, as the program will request, you should draw or trace your graph with the mouse in a manner befitting your chosen mode (Single Point, Selective Stream, or Continuous Stream). Any of the buttons on the mouse will register to the pad. When you are finished, press 'Q' and click your mouse on any point on the pad. The final point, the

one after you pressed 'Q', will not be including with the other points that you have just entered.

## **Final Menu**

The final menu is operated in the same manner as the opening menu.

**Exit :** Exit will take you out of the program. If you have digitized an image but not saved it, the data will be lost forever.

**Digitize Another :** Digitize another will return you to the opening menu. If you have not saved your digitized image, the data will be lost.

**Scale & Interpolate Data :** Scale and interpolate data will allow you to scale the image from the pad's coordinates to the actual coordinates of the graph. You will be asked to give the coordinates of the lower left corner, upper right corner, and the data origin. Type in the appropriate numbers when requested. You are then given the option to interpolate the data. If you choose to do so, you can interpolate five to 1000 points. When you are asked if you want the points printed to the screen, choosing NO will give a graphic representation and choosing YES will give a numerical representation of the graph. The graphic representation in interpolation is scaled to the screen size. For an accurate view of the graph, choose show current data from the final menu. When you are finished scaling and interpolating, you will return to the final menu.

**Sort :** Sort will sort your data points along the x-axis and then return you to the final menu. Sort is helpful in both single point and selective stream modes. If, when tracing the graph, you see you have missed a point, select those points before you exit to the final menu. The graph will appear incorrect because the points have been connected, but this is all right. In the final menu, sort will correctly place these points and the graph will be fixed. If you try to sort data that has two X values for one Y value, the graph will reflect this tracing error.

**Show Current Data :** Show current data will allow you to view the image that you are

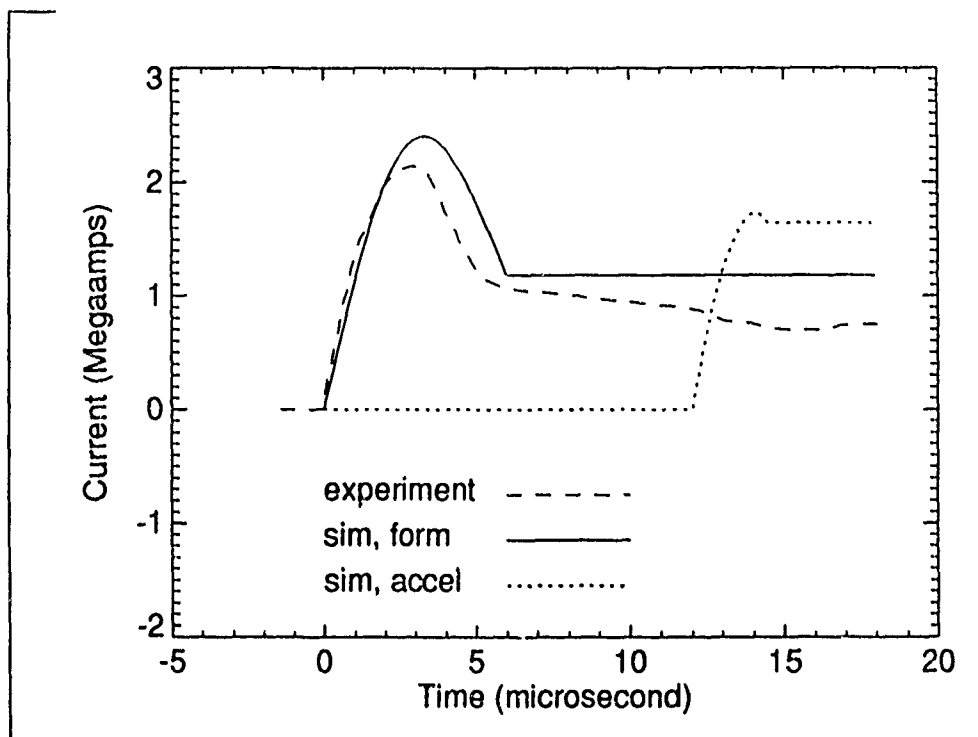
currently working with, and then return you to the final menu. The image shown will be scaled to the screen size. Select 'S' to scale and type in the appropriate values.

**Save Data :** Save data will allow you to store your data on floppy disk or within your hard drive. You will be asked for the drive and directory in which you want to save the file. The default, by pressing return, is C:\SHOTS\ . Next you will be asked for a file name. The name can be up to eight characters long and must end in the

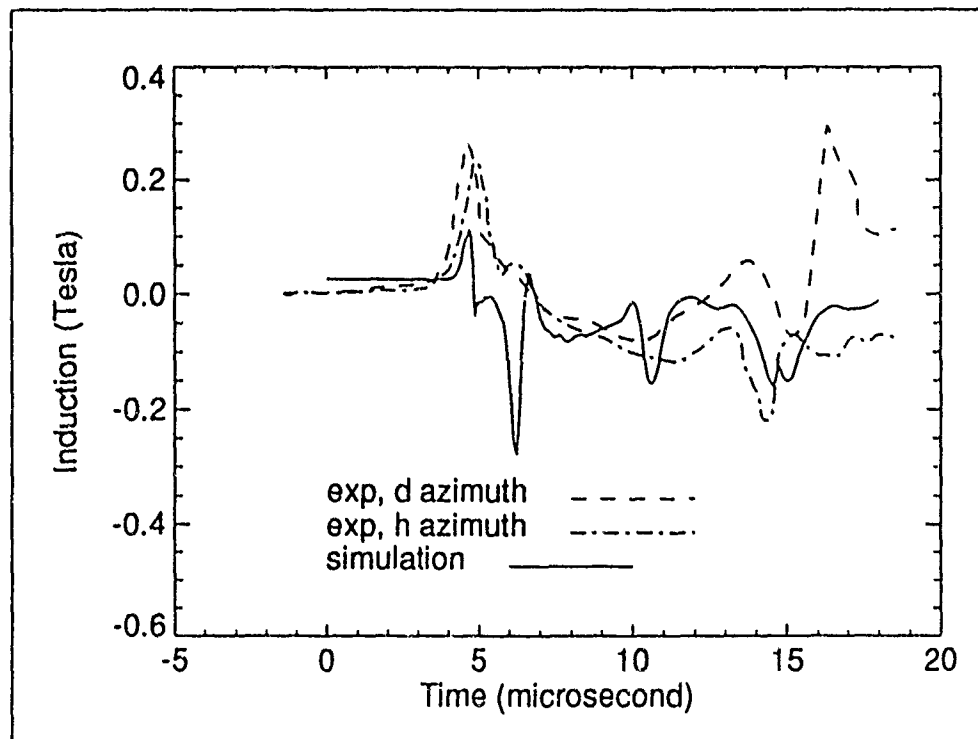
extension .DAT. If you fail to add the extension, the file will not show up on the directories within the program, but they will still be saved. If you type in a file name that already exists, you will be asked if you want to overwrite the old file. After you are done saving your file, the program will return to the final menu.

**Show Saved Data :** Show saved data works the same as in the opening menu. If you want to show saved data, it will not overwrite any data you are currently working with.

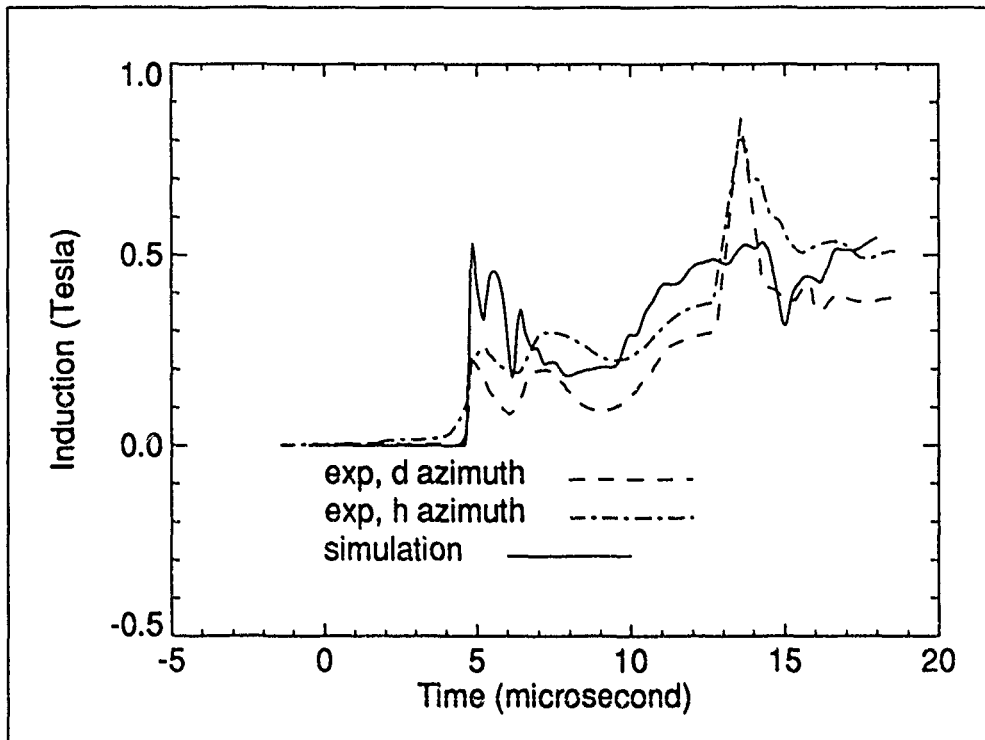
EXAMPLES OF DIGITIZED EXPERIMENTAL DATA PLOTTED  
TO COMPARE WITH SIMULATED DATA



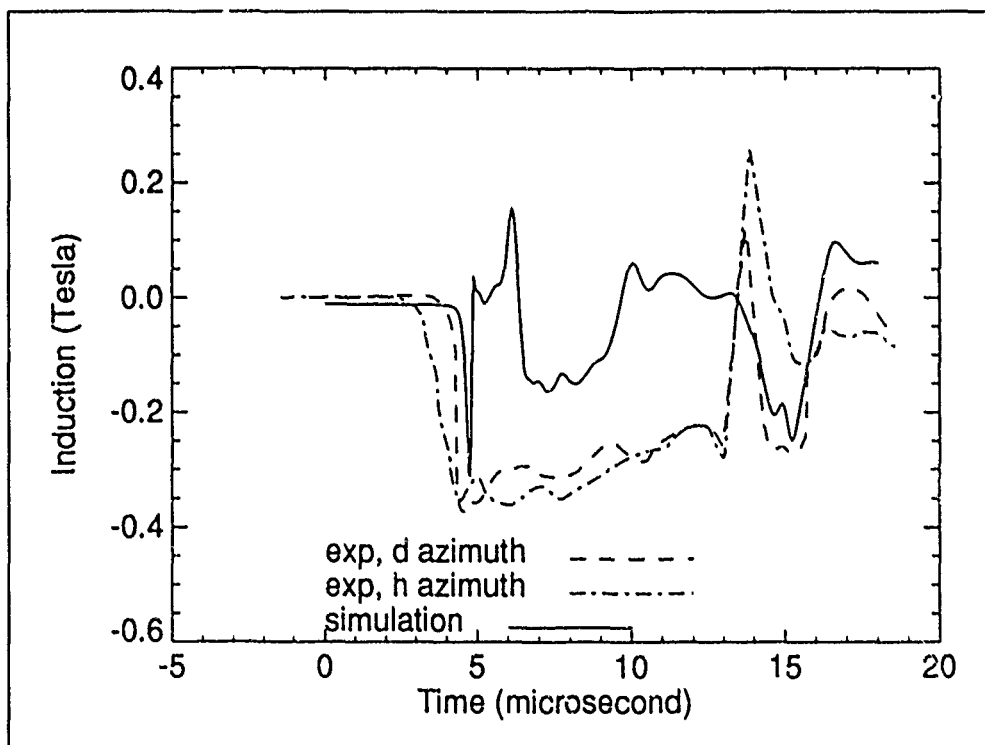
Circuit current from the two-circuit simulation and experiment.



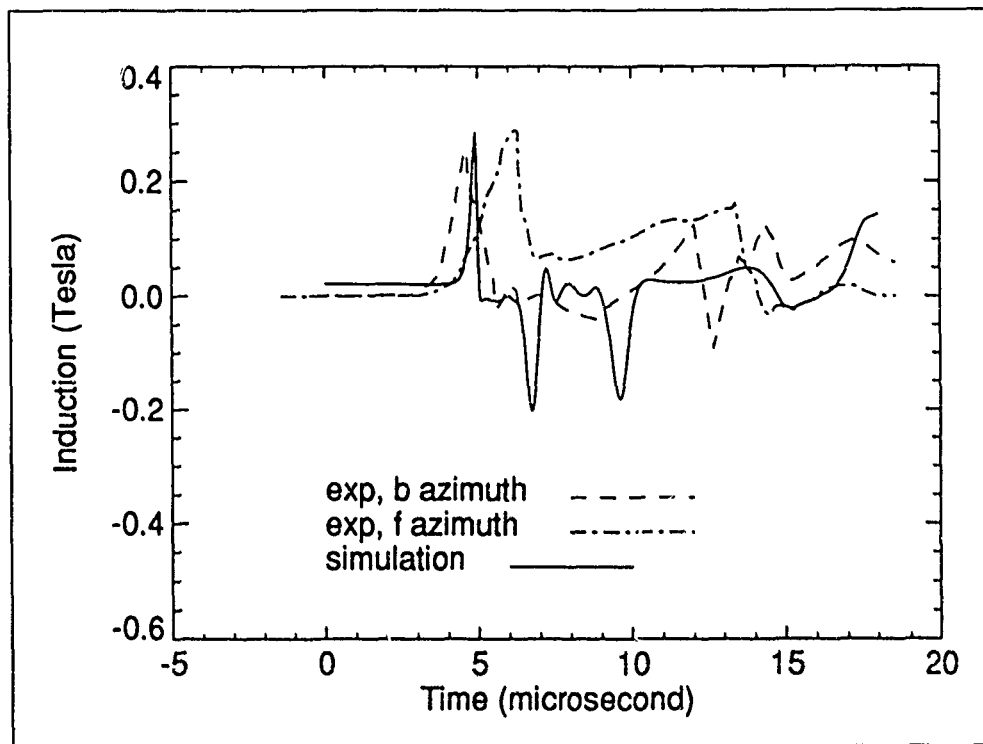
Radial magnetic field 13 cm above the gun--two-circuit discharge.



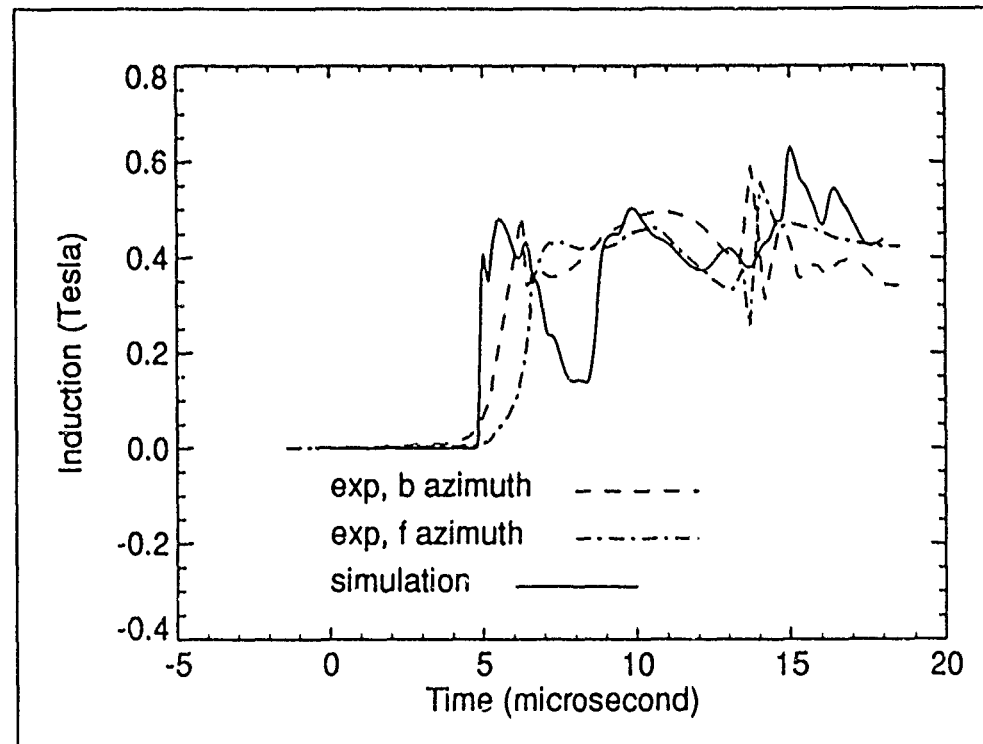
Azimuthal magnetic field 13 cm above the gun--two-circuit discharge.



Axial magnetic field 13 cm above the gun--two-circuit discharge.



Radial magnetic field 19 cm above the gun--two-circuit discharge.



Azimuthal magnetic field 19 cm above the gun--two-circuit discharge.

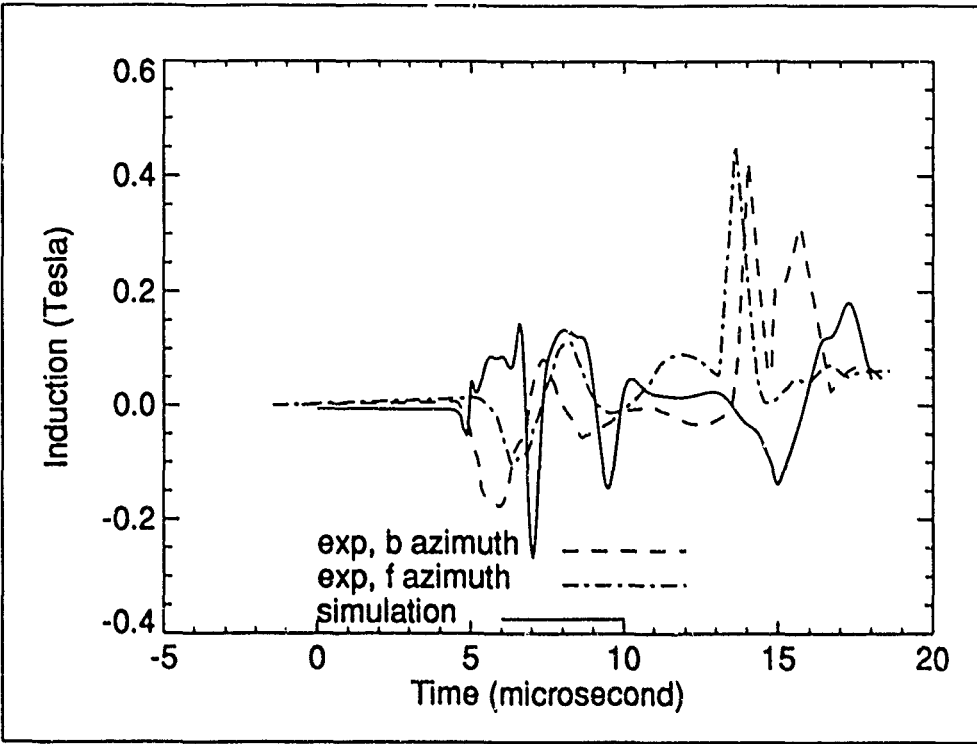


Figure 26. Axial magnetic field 19 cm above the gun--two-circuit discharge.

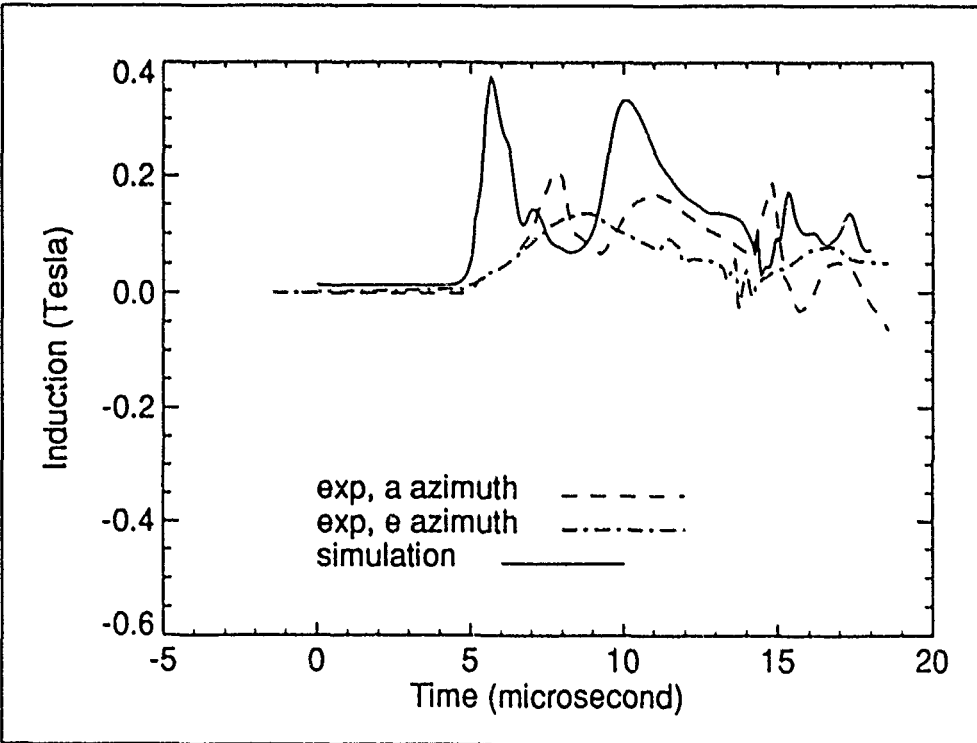
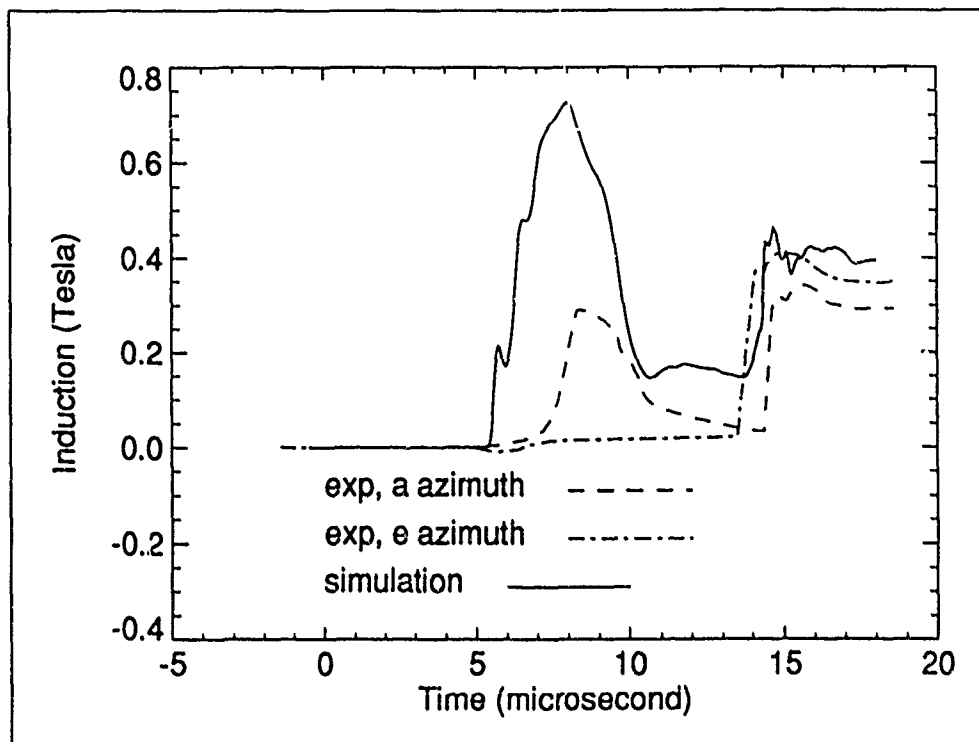
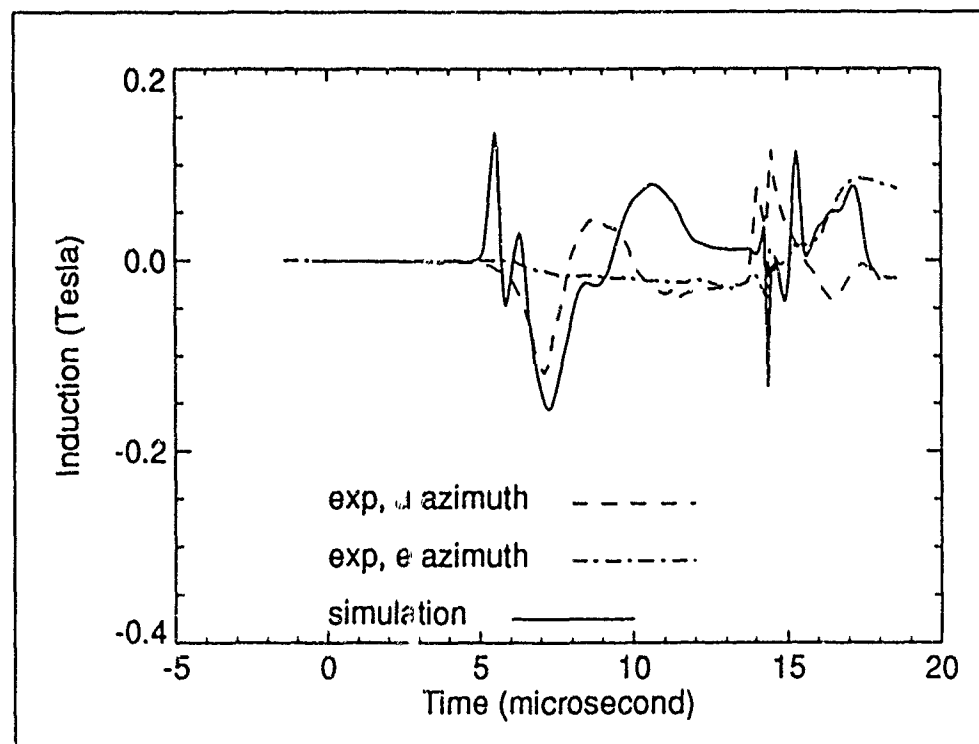


Figure 27. Radial magnetic field 33 cm above the gun--two-circuit discharge.



Azimuthal magnetic field 33 cm above the gun--two-circuit discharge.



Axial magnetic field 33 cm above the gun--two-circuit discharge.

(APPENDICES ON FILE AT RDL.)

COMPARISON OF SEISMIC REFRACTION AND BOREHOLE DATA WITH DIFFERENT COMPUTER INTERPRETATION PROGRAMS TO DETERMINE A SUITABLE SITE FOR PILE TESTING.

Kerim Martinez

ABSTRACT

The Hayman Igloo test site at UTTR in Utah was characterized to determine if the area was suitable for pile testing. The subsurface was investigated for two geological parameters. The site was determined to have an adequate water table for testing (10 - 15 ft depth). The bedrock layer was investigated for the presence of the second parameter, a 30 to 70 ft depth. Before a site could be determined the best possible data interpretation method had to be found. Geophysical and geological subsurface investigation techniques were compared. Refraction interpretation and graphic interpolation computer programs were also compared. Two refraction programs, Seisview and SIPT, and a Surfer mapping program with a kriging interpolation technique were utilized. Each method provided a different view of the data. Two suitable test sites were determined by combining the topographic and 3-D results. The subsurface investigation and computer programming techniques were combined to produce the best possible interpretation and representation of data for studies with near-surface parameters.

## 1.0 INTRODUCTION

Site characterization is the first process in any full-scale explosive test. The primary work responsibility of the Geodynamics Section is the characterization of subsurface materials and the study of subsurface exploration methodology. Both geophysical and geological techniques of subsurface investigation are employed for the fulfillment of site characterization. The investigation and subsurface profiling of the geology is the basic anatomy of this report.

The Shock Physics Division has been tasked to select and characterize a test site for pile testing. The proposed test is designed to determine the survivability and vulnerability of structures founded on piles located in a saturated environment. Several possible test sites were evaluated by GS in Utah. The proposed test sites are located in the Utah Test and Training Range (UTTR). The subsurface evaluations were conducted at various locations, however, only the findings of one location are studied in this report due to the significant amount of testing conducted at UTTR.

The geology of the proposed test sites must meet certain requirements. The two primary requirements are bedrock and water table information. The determination of a bedrock depth and the composition of the hard layer are important parameters. The bedrock layer must be able to support the weight of a pile or a pile group. A pile is a long slender object designed to channel the weight and stress of a structure into the surrounding geology. According to the designed pile parameters, the bedrock layer must be no less than 30 feet deep and no more than 70 feet deep. The significance is that the pile is designed for end bearing capacity and must rest on steady geology to function successfully as a close simulation of a real existing foundation plan. The second requirement is the determination of the subsurface's saturation. The designation of the saturation is the investigation of the water table. The water table is the upper limit of the geology which is wholly saturated with water. The desired depth of the water table is around 5 feet, however, a measurement with at least 10 feet more depth is acceptable because of the eventual leveling excavation of the pile test site. The Air Force wants to understand more thoroughly the concept of piles and their possible uses in military facilities. Some of the military facilities may be located in areas with high saturation and a shallow bedrock layer. The results from the testing would provide adequate information on this subject.

This report focuses on the site characterization aspect of the pile project. The report is structured as to produce two distinct objectives. The first is the eventual determination of a test site. The second is to determine

the methodology that would provide the best information for all site characterizations with similar geological parameters. The subject of piles is discussed to give the reader an understanding of the eventual application of the results. An extensive explanation of the field and computer methodology is also given. The methodology is an integral part of the results, and in some respect, they are the results.

## 1.2 OBJECTIVE

The main objective of this report is to select a suitable site for a full-scale high explosive test of pile foundations utilizing different investigation methods. The success of the objective depends on the fulfillment of two major factors. First, the determination of the most reliable and efficient method of subsurface investigation, as it pertains to pile testing. There are two major methods for exploring the subsurface. The two methods are geophysical exploration and drilling and sampling exploration. Seismic refraction surveying was chosen as the geophysical method. Borehole drilling and sampling was chosen for the geological technique. After testing, the results from both refraction testing and borehole drilling will be compared to determine which method best provides the information necessary for properly assessing the site for pile testing.

The second major factor is the computer interpolation of both the borehole and the seismic refraction data. The initial results produce a specific characterization of the subsurface. Due to the large area proposed for the pile test (200 foot diameter) for pile testing, a broader scope of the subsurface must be acquired. Through the utilization of computer interpolation programs the data can be generalized by means of innovative data estimation techniques. The second objective is to determine which computer interpolation program combined with a subsurface exploration technique produces the best method for establishing test sites with near-surface parameters.

## **2.0 METHODOLOGY - FIELD TESTING AND COMPUTER PROGRAMMING**

The initial subsurface investigation conducted at the UTTR test site was a seismic refraction survey. In order to understand the data a thorough understanding of the refraction method and analysis must be obtained. A seismic refraction survey is a geophysical approach to subsurface exploration. Refraction studies are an innovative, cost efficient technique for investigating unknown subsurface characteristics. There are two major geophysical techniques used in subsurface seismic exploration. Reflection is a process where the measured ray is reflected back to the ground surface after contacting a subsurface layer. Refraction is a process where the measured ray is refracted along the layer boundary before it returns to the surface.

The seismic refraction survey was conducted between April 2-5, 1991. The investigation was conducted at two possible pile test locations. This report concentrates on the results of subsurface tests at site 2, near the Hayman Igloo test site (figure 1). The straight lines indicate the locations of the various refraction arrays.

The seismic refraction technique consists of measuring the travel times of compressional waves generated by an impulsive energy source to points of various distances along the ground surface. Refraction is the deflection from a straight path undergone by an energy wave on passing from one medium into another where the velocities differ. A disturbance through elastic media propagates through two distinct waves. First, compression waves in which the deformations of the medium consist of alternating compression and refraction, commonly known as "primary" or p-waves. P-waves are compressional body waves which have the highest velocity of seismic waves. As the p-wave travels through the subsurface, it moves each particle it traverses in a direction colinear with the direction of propagation (Lankston 1989). The second wave is shear. For the purpose of refraction surveying the p-wave is desired. It is easier to detect than the shear wave because the p-wave arrives first.

The subsurface characteristics are measured in velocity. The physical property of subsurface materials which is measured is the rate at which acoustic wave energy propagates through various mediums of the subsurface (Lankston 1989).

The rate of propagation in a designated medium is called the velocity of the medium. It is the measurement of the p-wave as it travels through the subsurface. In physics, velocity is a vector quantity. In geophysics velocity is used to denote the scalar quantity speed or the rate at which p-wave energy is propagated through a subsurface medium (Lankston 1989). It is important to note that seismic velocity is not a determination of the density of the subsurface geology, but the velocity is dependent on the density. The velocity at which p-waves travel are important in determining layer characteristics.

The critical angle of refraction is fundamental in the process of seismic refraction surveying. HuySEN's principle states that in a homogeneous medium, waves expand from a source as expanding spheres. Every point on a wave front is the source of a new wave that moves away from it. The raypath or p-wave is the first arriving signal and perpendicular to the wave front. The geometrical aspect of refraction is the critical refraction of the ray at the velocity contrast boundary (Lankston 1989). The critical refraction or angular deviation a ray undergoes depends on the ratio of transmission velocities of the two materials, represented by Snell's Law. The foundation of seismic refraction lies in the critical incidence and Snell's Law.

The interpretative process allowed a variety of aspects which contributed to the overall analysis. Sometimes it was necessary to model the data. A form of ray tracing was utilized to model the p-waves. It generates raypaths by obeying Snell's Law of velocity contrast boundaries. Time, distance, and velocity relationships were used to calculate the travel time along each segment of the raypath (WES 1979). A problem associated in a single source refraction test is the inability to distinguish two-layer cases from multi-layer cases and the existence of dipping (sloping of the layer). The field testing correction for this problem was the implementation of two shot points for each array with one on each side of the geophone spread. The two datasets were compared to determine the characteristics of the subsurface layers. In this survey the two-shot method was required due to the necessity of a two-target boundary investigation, the water table and bedrock.

The second subsurface exploration technique utilized at the UTTR site was

drilling. The process consists of drilling into the subsurface with a mechanical device. The purpose is to acquire subsurface data on soil characteristics. The types of results generated by drilling which were utilized in this report include the establishment of water table and bedrock depths, the soil samples, and the blow count number associated with standard penetrometer testing. Drilling is a process utilized primarily by the geological and civil engineering community. The results are actual data which provide specific information on the condition of the subsurface layers. However, the expensive nature of drilling does not allow the implementation of a large, dense test setup. Occasionally, this obstacle may deprive the investigator of a reliable general description of a large area designated for pile testing, but not included in the subsurface characterization process. However, the proposed utilization of computer interpolation of the data from the scattered borehole locations is designed to compose a general characterization of subsurface layers.

The drilling and sampling of the subsurface was conducted at site 2, at the Candy Mountain Site in the Lakeside Range in Hill Air Force Base's UTTR. The borehole testing was conducted between May 29, 1991 and June 7, 1991. The locations of the boreholes are shown in figure in relation to the refraction survey. Dames & Moore of Salt Lake City was the geotechnical contractor for the borehole testing. The contractor provided the equipment and personnel to operate the machinery and supply geological expertise. The proposed drilling method layed out a plan to drill a maximum of 70 ft at each location (70 ft being the maximum depth possible for pile testing). The main purpose was to acquire the depth to rock. The additional features included the verification of saturation at a certain depth and sampling and soil analysis of subsurface materials.

The SIPT refraction program was utilized to interpret the seismic survey results. SIPT is a sesimic refraction inverse modelling program for time share terminal computer systems. SIPT is an interactive Fortran computer program enhance by James Scott of the U.S.G.S. Scott modified an earlier program and produce a more effecient interpretation technique.

SIPT models the subsurface layer characteristics with a cross-sectional

representation. The program accepts as input the travel times of the geophones and characterizes the layers in a delay-time method. A ray tracing method was used where the computed travel times in the model are compared against the recorded travel time measurements (Scott et al 1972). Ray tracing determines the true position of points of entrance and emergence of rays refracted along each layer while taking the dipping and layer thicknesses into account (Scott et al 1972). The program simulates its own wave propagation and compares the computer results with the real data model. The model is corrected for discrepancies using delay-time and ray tracing.

Seisview is the one of the interpretative programs utilized to produce graphic results of the seismic refraction survey. Seisview is a program specifically designed for seismic refraction studies. It was employed to provide an alternative view of the data. The two refraction programs do have some similarities. However, Seisview has a very different approach in the interpretation process.

The Seisview program contains many facets which produce informative results for the user. Seisview accepts both single and multi-channel refraction records. Seisview also accepts both single shot and stacked refraction data. The program provides the user with a computer view of the data in a wiggle trace of variable area mode. It is also capable of automatically picking the first-break arrival points. However, for this effort the manual picking method was chosen to exclude any chance of error associated with undesired disturbances which may have occurred during seismic testing, e.g. wind, weather, movement by personnel on the surface.

In the interpreting process, Seisview supplies a variety of different functions. The layer thickness and velocities are calculated from the time-distance plots based on manually picked first-break arrival points. The interpretation of dipping and horizontal layers was accomplished by Seisview's ability to utilize both forward and reverse profiles. The layer velocity was interpreted through the process of regression. Regression is a functional relationship between two or more correlated variables. The variables are empirically determined from the data. The determined variables were utilized to predict values of one variable when given the values of others. Regression is

a function that yields the mean value under the condition that one or more independent variables have specified values.

The third computer program utilized was Surfer. Surfer is an efficient program designed by Golden Software Inc. to produce both two and three dimensional high resolution graphics. Surfer is an ideal program for the presentation of data, whether it may be in a small or large volume dataset. Surfer consists of topographic and three-dimensional graphic features which concisely display seismic results in a visually attractive manner. The program was utilized to interpret the borehole results and display the interpolation of both the seismic refraction and borehole data in a cartographic manner.

The Surfer program is divided into three main parts: GRID, TOPO, and SURF. The GRID function allows the user to create a regularly spaced grid through a choice of different parameters and mathematical operations. The regularly spaced grid consists of a rectangle constructed of rows and columns. At each individual intersection of the rows and columns GRID interpolates the (Z) value. The generated grid is now available to be presented in either a two or three-dimensional graphic representation.

### 3.0 COMBINATION OF SEISMIC REFRACTION AND BOREHOLE TOPOGRAPHIC AND RESULTS

3-D

The combination of the seismic refraction and borehole data was conducted to achieve the best possible representation of the bedrock layer. The datasets were combined in the same grid file. The limited amount of borehole data presented a major difficulty. The borehole data must be weighted because of the comprehensive kriging method. Therefore, the refraction array datasets were deleted by 3 geophones data points on each side of the array (6 total). The 24% depletion of the datasets do not seriously undermine the refraction data's presentation because the data at the end of the array is considered as unreliable information.

The combination plots display interesting results about the suitability of the site. The map of the Seisview and borehole data is shown in figure 2. The contour lines represent the area within the 30 to 70 ft depth range. The primary method of comparison was the study of the borehole locations within the bedrock parameters. The combination plot show that 10 of the 13 borehole locations are within the parameters. The Seisview plot shows all 13 borehole locations within the parameters. The borehole map shows 9 of the 13 borehole locations within the parameters. The SIPT and borehole map is shown in figure 3. The map has a slightly smoother character as compared to the SIPT map. The plot show 7 of the 13 borehole location within the parameters. The SIPT map revealed that only 2 of the 13 borehole locations were within the parameters. The objective of finding a medium between the datasets was accomplished. From the combination maps a reasonable approximation of suitable pile sites can be made.

#### 3.1 COMBINATION OF SEISMIC REFRACTION AND BOREHOLE 3-D RESULTS

The 3-D representation of the seismic refraction and borehole data was conducted. The premise was to compare the surface maps with the others to search for both similarities and discrepancies. The 3-D surface map of the SIPT and borehole data is shown in figure 4. The decline in depth from the SE to the NW is less rigid. The non-exaggerated 3-D surface map of the Seisview and borehole

data is shown in figure 5. The shaded portion represents the area within the bedrock parameters. The 3X exaggerated 3-D surface map is shown in figure 6. There is a distinct difference in the range of depth. The short borehole bedrock depth (BH4, BH10) protrudes the Seisview plot upward to form a mound like structure. A S 60° W view of the same plot is shown in figure 7. The plot displays a somewhat more rippled layer from the SW perspective. This process allows the investigator to view the data in any way which will produce the best results.

### 3.2 SITE SUITABILITY FOR PILE TESTING

The final determination of this effort is the selection of a site suitable for pile testing. A 3-D surface map is ideal for presenting the data, characterizing the layer, and determining site suitability. However, a topographic map is used for the final presentation because of its simplicity when applied to the field. The final determination of site suitability is shown in figure 8.

The final map was constructed by comparing all of the topographic maps of the bedrock layer. The 30 to 70 ft depth parameters from each plot were overlapped on each other on one map. The dark shaded portion represents the area suitable for pile testing with a high degree of certainty. The area incorporates 8 of the 13 borehole locations. The probable existence of a 30 to 70 ft depth parameter is represented by the line shaded area. The area has a reasonable chance of meeting the pile testing specifications. The entire area incorporate 11 of the 13 borehole locations. There are two recommended sites for conducting pile testing. The first is the area within the borehole locations BH5, BH9, and BH10. The second is within the borehole locations BH8, BH1, and BH11. The two areas meet both the water table and bedrock parameters.

#### 4.0 CONCLUSIONS

- 1) Two definitive areas were established as suitable for pile testing. They include the area between the borehole locations BH5, BH9, BH10, and the area between BH8, BH1, and BH11.
- 2) The SIPT program is reliable for near-surface interpretation of the first parameter (water table depth). The second parameter (bedrock) interpretations were inconsistent and had a lot of variation. However, the program did present the structural characteristics of the bedrock which is necessary for finding a suitable site.
- 3) The Seisview program is reliable in determining the water table and bedrock parameters. However, the straight line representation of the data muffled a variety of rippling and dipping characteristics that the SIPT program offered.
- 4) The Surfer topographic and 3-D programs presented the data in an informative and useful manner. The topographic maps provided a reliable view of the subsurface which made the site characterization process easier. The 3-D map provided an excellent perspective of the subsurface. The graphics programs proved their worthiness in areas of geologic study.
- 5) The seismic refraction survey provided an abundance of data which was essential in characterizing the subsurface. If processed through an appropriate program, the refraction results accurately assess the subsurface for a near-surface characterization study.
- 6) The borehole drilling provided an excellent view of the soil composition in addition to determining the water table and

bedrock parameters. The utilization of the graphic program to present the data enhanced the quality and usefulness of the results.

- 7) Combining the borehole and refraction results proved to be the best method of presenting the data.
- 8) If the Hayman Igloo test site is designated as the test area then a concentrated borehole analysis of the two suitable test sites is recommended.
- 9) Utilizing two subsurface investigation techniques with two interpretation programs is a reliable method for obtaining the best possible characterization of a possible test site with near-surface dual parameters.

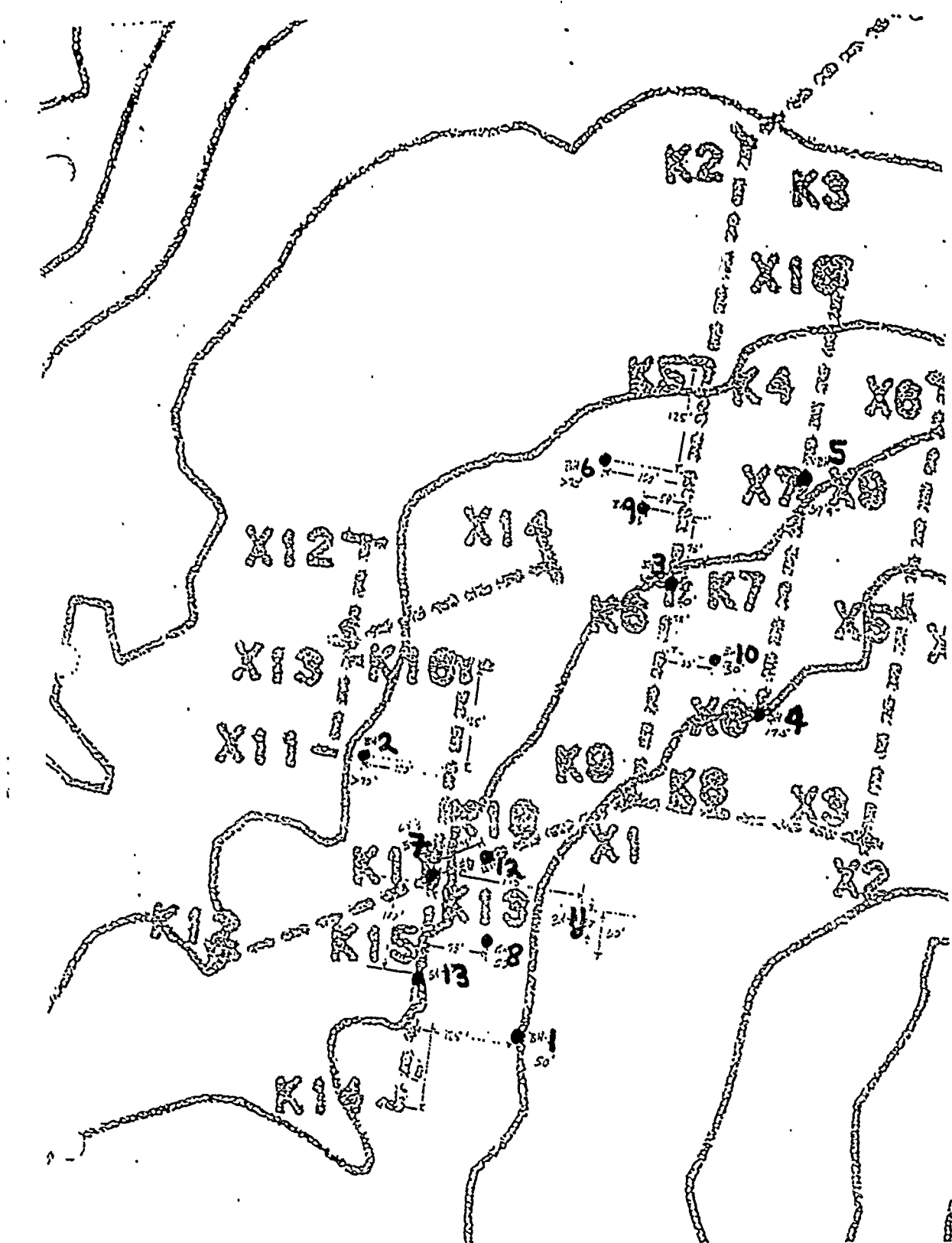


Figure 1 Borehole locations in relation to the seismic refraction arrays (Boreholes represented by dark black filled circles).

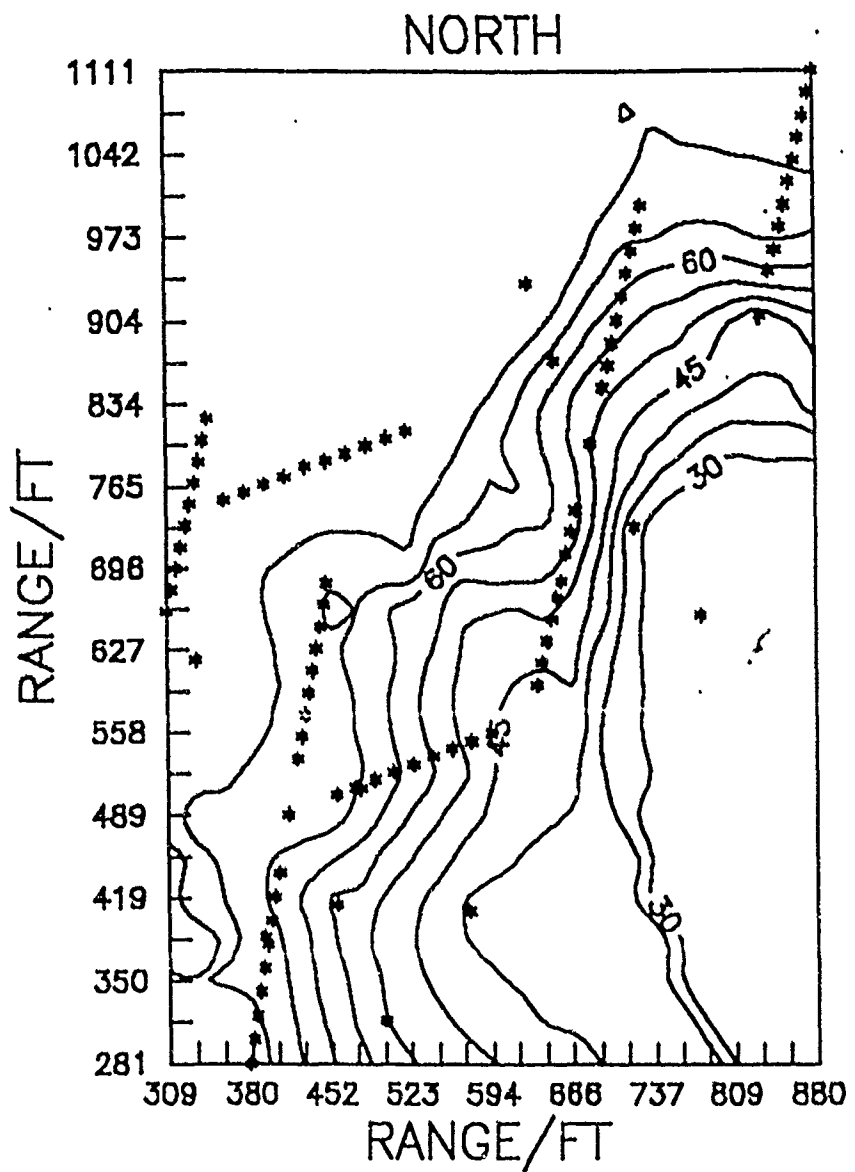


Figure 2 Topographic map of Seisview and borehole bedrock depths with 30 to 70 ft parameters.

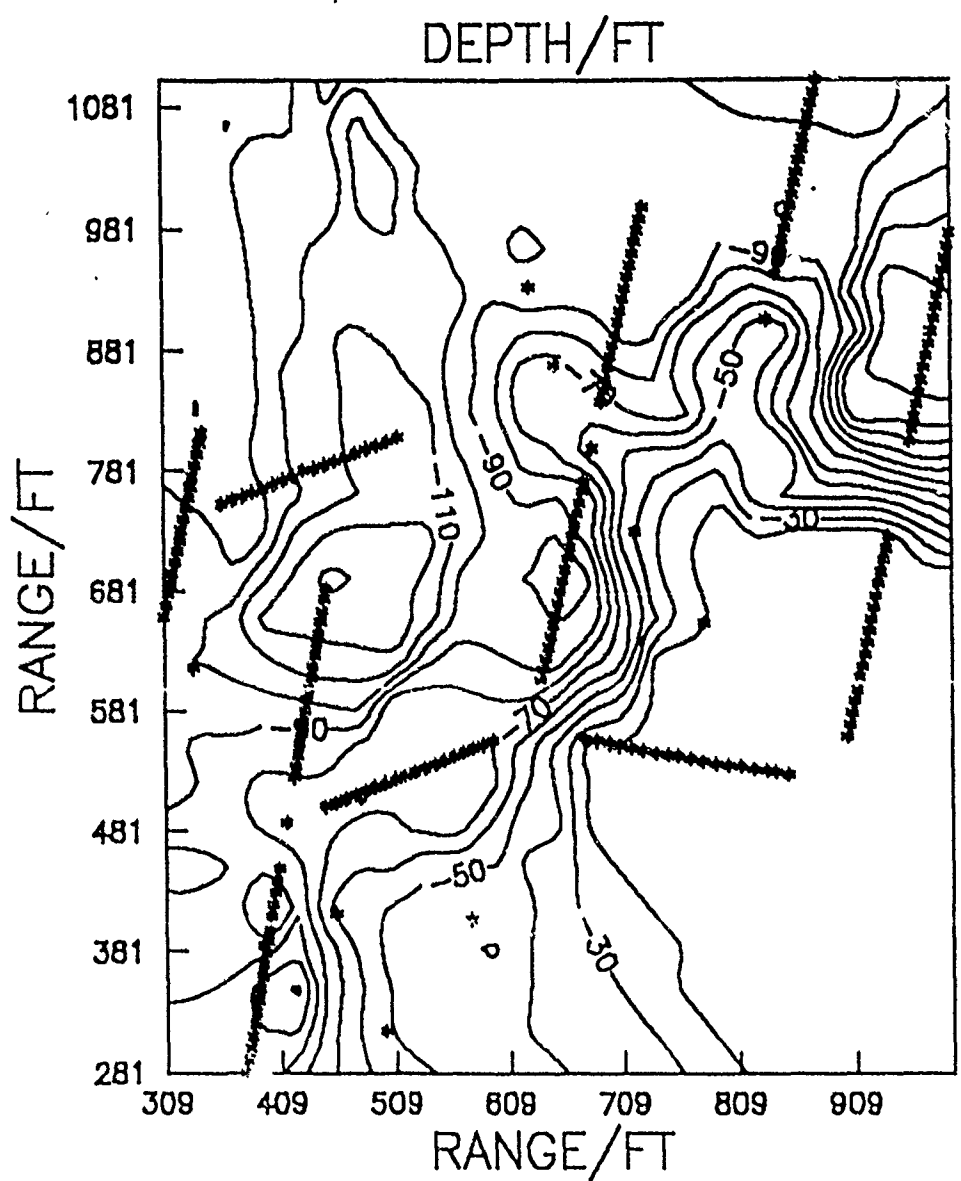


Figure 3 Topographic map of SIPT and borehole bedrock depths.

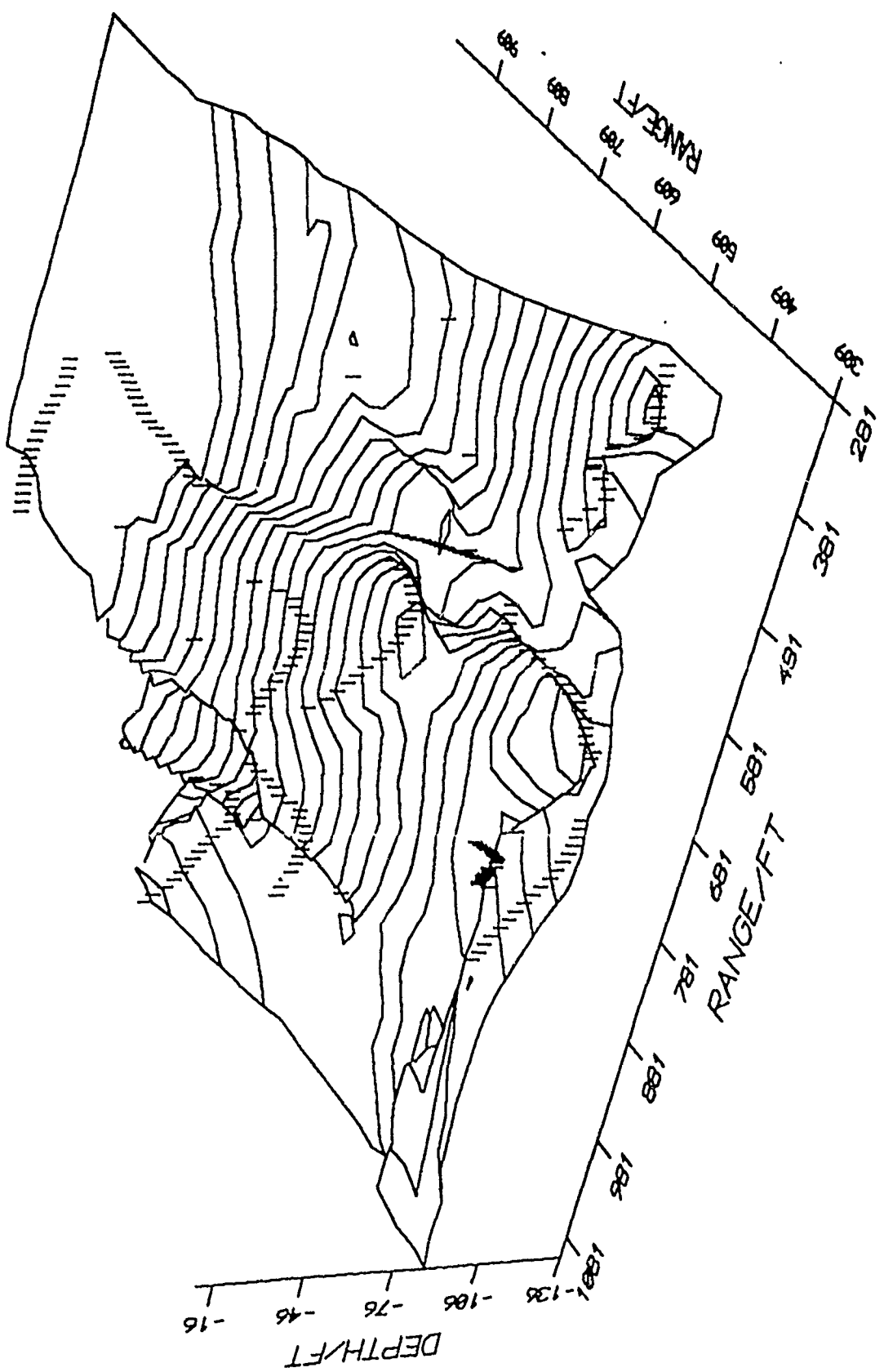


Figure 4 Three-dimensional map of SIPT and borehole bedrock depths in a N 60° E direction (Z scale = 3X).

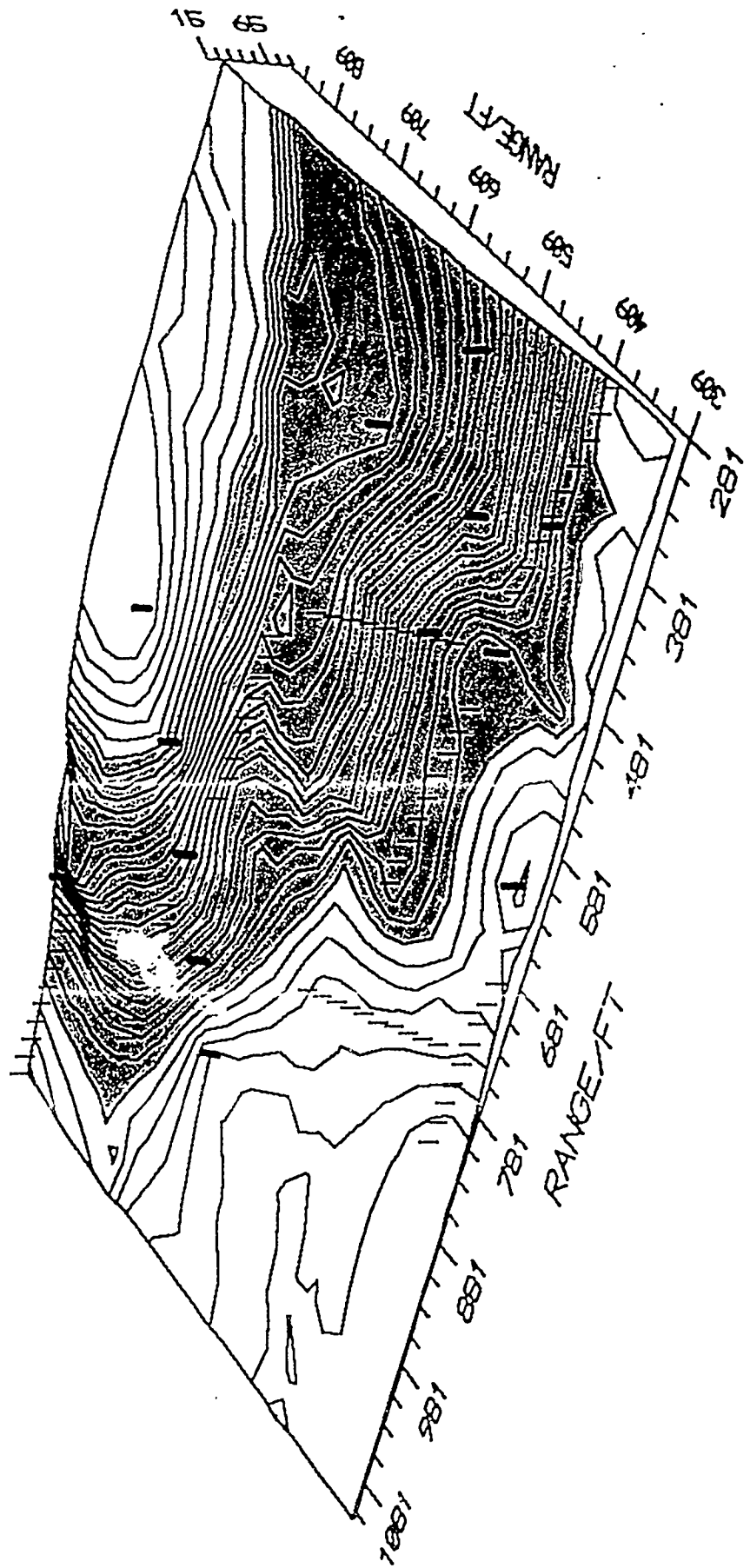


Figure 5 Three-dimensional map of Seisview and borehole bedrock depths in a N  $60^\circ$  E direction (Z scale = X).

SIESVIEW/BOREHOLE BEDROCK MAP

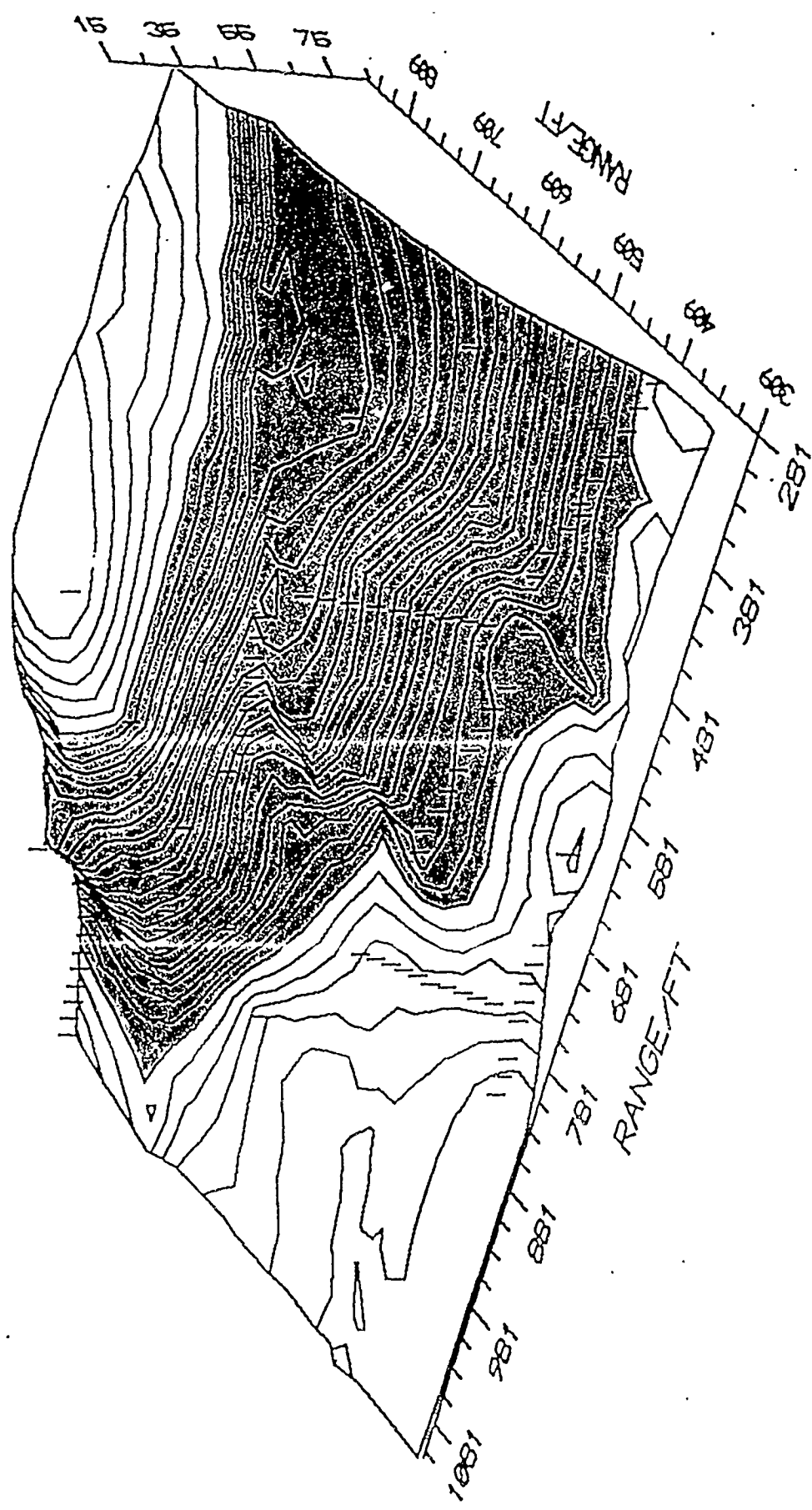


Figure 6 Three-dimensional map of Seisview and borehole bedrock depths in a N 60° E direction (Z scale = 3X).

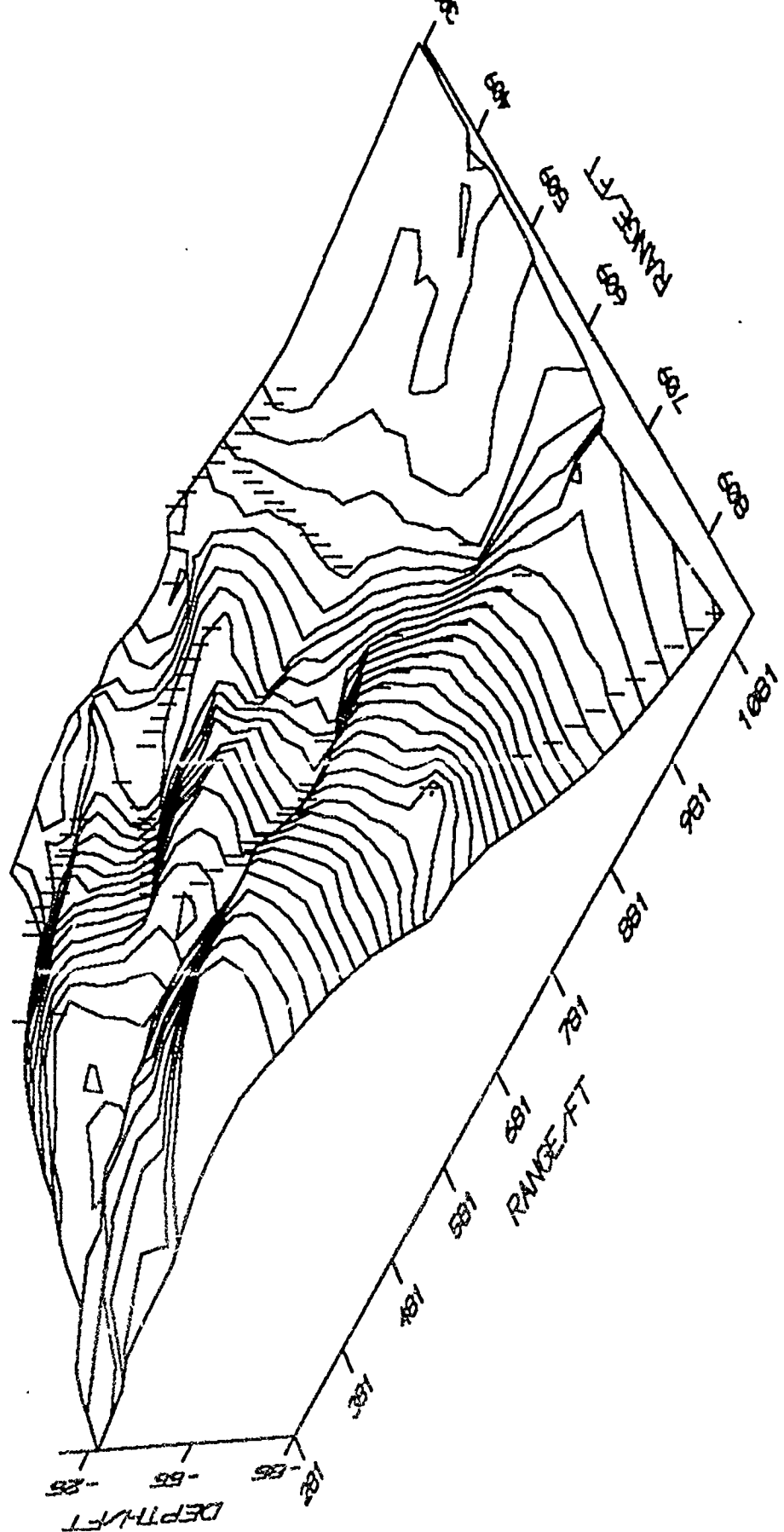


Figure 7 Three-dimensional map of Seisview and borehole bedrock depths in a S 60° W direction (Z scale = 3X).

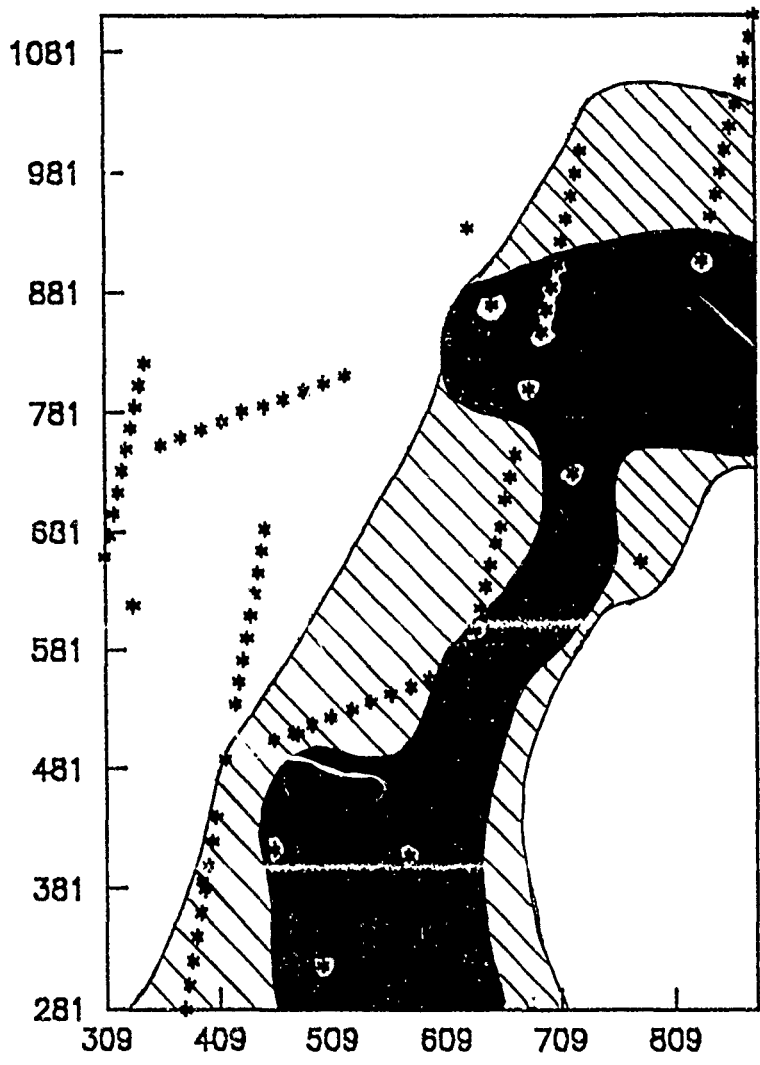


Figure 8 Final determination of a suitable pile testing areas.

LIST OF REFERENCES

1. Corson, William, Capt. USAF, "Survivability of Structures founded on Piles in Saturated Soil," Draft technical report, Phillips Laboratory, KAFB, NM, January 1991.
2. Corson, William M., John J. Gill, Keith H. Maxwell, John N. Thomas, Paula J. Jackson, Charlie Wayne, "Survivability of Structures founded on Piles in Saturated Soil," technical report, Phillips Laboratory, KAFB, NM, 1991.
3. Dames & Moore, "Report Geotechnical Investigation Lakeside Range, UTTR Hill Air Force Base, Utah for Kirtland Air Force Base," Salt Lake City, Utah, June 19, 1991.
4. EG&G Geometrics, "Operating Manual: Model ES-2415, 24-Channel Signal Enhancement Seismograph," Sunnyvale, Calif.
5. --- "Seisview: Seismic Refraction Processing Software," User's Manual, Geometrics, Inc., Sunnyvale, Calif, 1986.
6. Golden Software, Inc., "Surfer: version 4," reference manual, Golden, Colorado.
7. James, Robert C., Glen James. Mathematics Dictionary, Van Wostrand Company, New York, 4th edition, 1976.
8. Lankston, Robert W., "High Resolution Refraction Data Acquisition and Interpretation," Geo-Comp-Graph, Inc., Fayetteville, AR, 1988.
9. --- "The Seismic Refraction Method: A Viable Tool for Mapping Shallow Targets into the 1990s," Geophysics, Vol 54, no. 12, December 1989. pgs. 1535-1542.
10. Scott, James H., Benton L. Tibbetts, Richard G. Burdick, Computer Analysis of Seismic Refraction Data," U.S. Department of the Interior, Bureau of Mines, 1972.
11. Scott, James H., "SIPT - A Seismic Refraction Inverse Modelling Program for Timeshare Terminal Computer Systems," U.S. Department of the Interior Geological Survey, Denver, Colo., 1977.
12. Waterways Experiment Station, "Seismic Refraction Surveying," U.S. Army Corps of Engineers, Appendix B, May 1979.

EXPERIMENT VERSUS THEORY - MARAUDER AND MACH 2

Kirtland Air Force Base  
Phillips Laboratory  
High Energy Plasma Division  
Albuquerque, New Mexico

A Final Report Presented to  
AFOSR Summer Research Program  
Research and Development Laboratories

by

Brian D. Rizzoli

July 21, 1991

## Acknowledgments

First of all, I would like to thank the AFOSR Summer Research Program and the USAF for providing this outstanding program. I would also like to thank Mike Martin for showing me the mechanical side of the experiment, Jerry Baca, for not only his expertise in data acquisition, but also for allowing me the constant use his computer, and finally, I would like to thank my mentor, Dr. Sue Englert for all of her help and support.

## General Description of Project

Working at the High Energy Plasma Division I was exposed to two different types of research - experimental and theoretical. I was given tasks that involved the testing and cleaning of the Marauder components as well as collecting data in a control room. I was also given the project of writing a program that would allow the numerical digitizations of Marauder oscilloscope photographs. The oscilloscope data would be stored in a computer to compare with the theoretical data being simulated.

## Detailed Description of Project

The Marauder experiment was designed to create a compact toroid of plasma that could be accelerated to high speeds, condensed, and released. The power necessary to create the toroid was generated from a huge layout of power banks named the Shiva Star. Marauder was set in the center of a "star" of six arms in order to channel the massive amounts of energy needed for the project directly to the chambers.

Marauder eventually will consist of a formation chamber, an acceleration chamber, and a compaction chamber. While I was at the lab, only the formation and acceleration chambers were constructed.

The formation chamber contained sixty high speed nozzles that released argon gas into a vacuum. A magnetic field was generated to hold the shape of the toroid, and then energy was applied to the argon gas. A consistent and well formed plasma toroid was created after much effort. The amount of energy, amount of gas, angle of the nozzles, size of the chamber, effects of the magnetic field, and many other variables were constantly reworked to create a workable toroid.

The acceleration chamber was a path for the toroid to take after formation. The chamber contained a magnetic field to keep the toroid in place, and the top of the

chamber was sealed by a thick plastic disc to contain the toroid after acceleration. The engineers were designing a compaction chamber to be placed over the acceleration chamber.

The Marauder experiment was maintained by Maxwell contractors and a few Air Force personnel. I worked with the maintenance and cleaning of Marauder for a number of weeks. During this time, I helped take apart Marauder, clean the chambers with alcohol and freon, assemble the data links for probe data, make various parts from inventory materials, replace nozzles, set the chambers under vacuum, check for leaks, align a laser, and reassemble Marauder. Marauder was completely taken apart three times during my stay; once for routine cleaning, once due to the explosion of a glass probe within the chamber, and once because a technician dropped a small copper sealing strip into the formation chamber.

Marauder was fired approximately twice a week, leaving the other three days for examination of the data by both experimental and theoretical personnel. On the shot days, I worked in the control room for data acquisition - mainly consisting of pulling oscilloscope film and fixing computer settings. Before firing the energy banks, every oscilloscope was checked for the correct initial settings. Three test shots were fired to make sure Shiva Star was working correctly. Each time Marauder fired, every

photograph had to be labeled according to the probe of which it corresponded, the date, and the shot number. If everything went well (meaning no electrical arcing or , we completed approximately ten shots a day.

I was not working with Maruader, my mentor had me write a program that would allow the digitization of the photographs. The data would then be used by others to determine how close a computer simulation was to the Marauder experiment. The computer simulation was called MACH 2 because it simulated high speed plasma in two dimensions.

In writing my digitization program, I was to convert a drawing/sketch pad to a digitization pad. The building had a number of Summa Graphics Sketch Pad's that they had previously ordered, but never used. The sketch pad manual described the conversion process for digitization and detailed every command that could be sent to the sketch pad. However, because the pad was designed for drawing, specifics on digitization were not given.

My mentor asked that the program I would write be written in BASIC on an IBM compatible machine. She wanted to be able to scale the data, interpolate the data, sort the data, save the data, and retrieve the saved data. Taking this information, I constructed a program skeleton of my ideas - basically a simple flow chart of the main subroutines I would need. I was also given a program

called DIGIT3.5.BAS DIGITIZER ROUTINE. This program attempted to use the Summa Graphics Sketch Pad for digitization, but was very poorly written, had terrible screen colors, and many routines simply did not work. I was, thankfully, able to salvage specifics on opening a communication line to the sketch pad.

The actual writing of the program was a tedious challenge. The interpolation subroutine took the longest to write as it took the greatest math calculations. I started with a two dimensional interpolation routine I found in a book of numerical recipies, but quickly discarded it because it was not suited for the program. Finally, I wrote my own interpolation routine that relied only on linear interpolation for the calculations. While the routine was initially very slow - up to ten minutes per graph, the speed improved to less than thirty seconds after the program was compiled. To further improve speed, I replaced the bubble sort I had been using with the fast and efficient Shell sort.

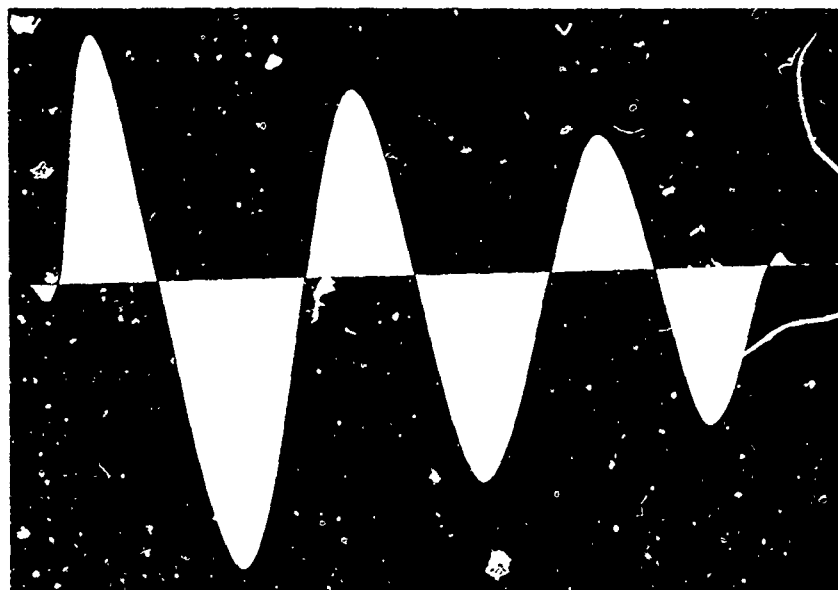
With the program in working order, my mentor asked me and another student in the program to digitize two hundred and fifty oscilloscope photographs. Working with my own program helped immensely in finding errors and places for improvement. The data generated from my program was used in the MACH 2 simulation program and in various graphs comparing simulation and experiment data.

The final program included a menu driven approach to choices, error handling, a zooming feature, a sample digitized graph, all of my mentor's specifications, and an instruction manual. The program, which I named Summa Graphic Pad Integration and Digitization, will be used until new computerized oscilloscopes replace the current photograph oscilloscopes.

## Conclusions

The AFOSR Summer Research Program provides valuable work experience as well as an exciting summer job. My exposure to a scientific research group has provided insights on both career opprotunities and academic possibilities. The Summer Research Program has left me with experience, memories, and many new friends.

# **Summa Graphics Pad Integration and Digitization**



(See 'BRAD KARMIOL.)

**By Brian Rizzoli and Brad Karmiol**

EXAMPLES OF DIGITIZED EXPERIMENTAL DATA PLOTTED  
TO COMPARE WITH SIMULATED DATA

(See 'BRAD KARMIOL.)

(APPENDICES ON FILE AT RDL.)

## HOLOGRAPHY

Dawn Vernooy

The purpose of this summer research project was to construct a quality hologram. By building several holographic set ups, and using interferometric and holographic theory, fringe patterns are created and then "photographed" to form a hologram. The included paper provides an historical background of holography, a theoretical background , a geometrical description, and the experimental account of my project.

### 1 Introduction

#### 1.1 What is holography?

The use of a lens to image an object is one of the oldest principles in optics and photography. However, in 1948 Gabor<sup>1</sup> introduced a two-step imaging process in which an intermediate record, containing the information necessary to recreate the image, is made. The two-step imaging process consists of two elements: recording and reconstructing. First, the interference patterns which exist when an object field (Fresnel or Fraunhofer diffraction pattern of the object) are allowed to interfere with a reference field (usually a plane or spherical wave that is at an angle with respect to the object beam), and are then

photographed. The resulting record of interference patterns obtained in the first step are called a hologram after the greek word *holos*, meaning "the whole"<sup>2</sup>, because it contains information involving both the amplitude and phase of the light being reflected off the object. The second step, reconstruction, consists of placing the recording medium into a coherent beam of light, which therefore generates the image of the object known as the reconstructed image, of which there are two types: real and virtual. A real image is one that appears on the opposite side of the recording medium from the source, and needs no additional focusing devices to record a focused image. A virtual image is one that appears in the same side of the recording medium as the source, and additional focusing devices are needed to detect a focused image. The entire procedure is known as holography.

## 1.2 Historical Background

Holography was first introduced by Gabor and investigated in an attempt to evade obstacles limiting the resolving power of electron microscopes<sup>3</sup>. Gabor suggested a two-step photographic imaging process in which the hologram was recorded with electron wavelengths and then reconstructed with wavelengths in the visible region<sup>4</sup>. Since the intermediate phase in this two-step process was "a recording by the square-law detector"<sup>5</sup>, a means of retaining the necessary phase information was to be assimilated into the process<sup>6</sup>. This was accomplished by a method which was already known through the work of Zernike<sup>7</sup> in the phase contrast microscope and Young's double split experiment, in which a coherent beam of light is separated and then

allowed to interfere with itself to be recorded on film before the actual recording process. The result is an interference pattern which stores the amplitude and phase information necessary to recreate the image of the original object. On the basis of this principle, the first step of the Gabor process can best be described as the recording of the interference pattern between diffracted light from an object and a coherent beam. The reconstruction in the Gabor two-step process was accomplished by then illuminating the properly processed hologram with the same or different coherent illumination and once again recording the radiation field in a plane removed from the hologram. This particular process, however, was limited by the intensity of the incident illumination, the photographic processing, and undesired noise called the conjugate image<sup>4</sup>. The conjugate image was formed with the same amplitude and opposite phase shift and appeared as a disturbing background when the reconstructed focused image was viewed.

Thus, following the work of Gabor, the early efforts of many investigators<sup>5</sup> to eliminate the extraneous image in wave-front reconstructions were not very successful. In all their work, a suggestion of Gabor's was not pursued. He had recognized the possibility of eliminating the conjugate image, as we can note from the following quotation:

"But it is very likely that in light optics, where beam splitters are available, methods can be found for providing the coherent background which will allow the better separation of the object planes, and more effective elimination of the effects of the 'twin wave' than the simple arrangements which have been investigated."<sup>6</sup>

However, with the development of the laser, very intense coherent quasi-monochromatic beams of light became readily available, bypassing the

limitations of the thermal source, and hence provided the coherent background requirements necessary for extending techniques for removing the extraneous image.<sup>11</sup> In addition to separating the extraneous image, objects which could otherwise not easily be used in the original Gabor systems, such as objects with a dark background and continuous-tone objects, could now be imaged using holography.

## 2 The Geometric Model

### 2.1 Two-Source Interference

Inherent to the geometrical model is the understanding of how two sources of continuous waves, emitting at the same frequency, interfere in space. This phenomenon can be easily demonstrated by dropping pebbles in a pool of water. Such patterns can be simulated by the superposition of two identical sets of concentric circles where the radial difference between the circles is one wavelength (Figure 1)<sup>12</sup>. Assuming that the white areas denote constructive interference, and the dark areas denote destructive interference, tracing either set results in a set of hyperbolas. Figure 2<sup>13</sup> represents constructive interference patterns illustrating the set of hyperbolas. Along the zero order, all intersecting circles have a constant radial difference of zero, and along the nth order, the difference is  $\lambda n$ . In between the orders of maxima are hyperbolas representing the minima (not shown in Figure 2), where the wave amplitude is always zero in spite of the fact that waves of two sources of disturbances are continually passing through.

Figure 1. Sets of Concentric Circles

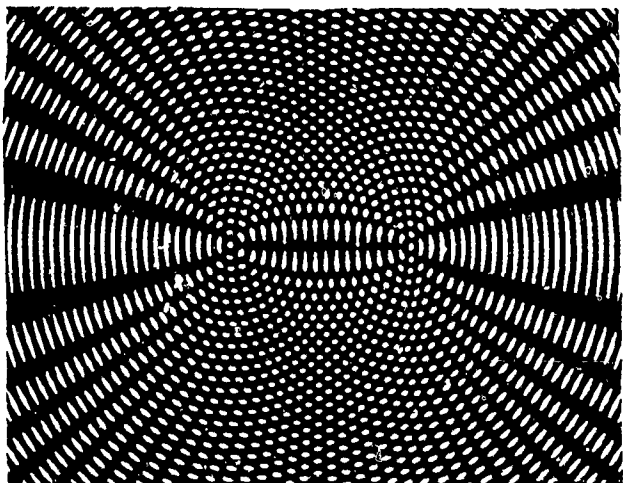
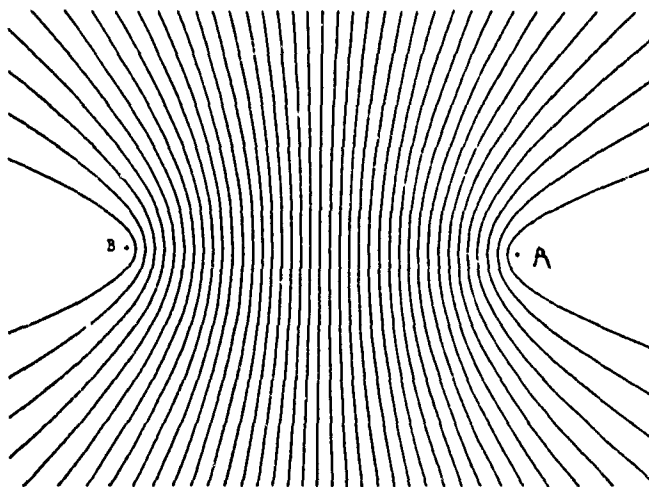


Figure 2. Set of Hyperbolas (Constructive Interference)



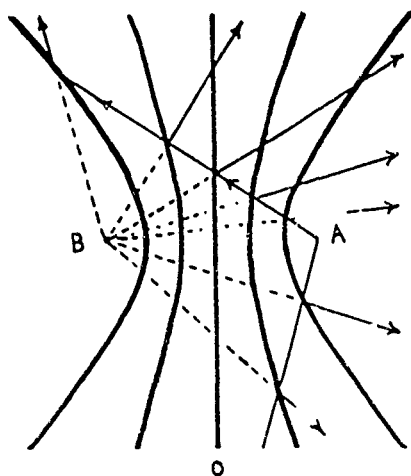
If the two sets of concentric circles on Figure 1 were made in separate transparencies, they could be moved relative to one another to observe whole sets of hyperbolas relative to the position of the two sources. This demonstrates the interference patterns made by the Michelson interferometer and Young's double slit interference patterns<sup>11</sup>.

## 2.2 The Model

Characteristics of these hyperboloids are used to demonstrate properties of recording media necessary to create a hologram (Figure 3); the zero order, which perpendicularly bisects the line connecting the two sources, will be used as an example. If this plane were a mirror, any ray of light originating from source A would be reflected in such a manner as to appear to come from source B. Thus, B would be the virtual image of A. Consider an order other than zero and think of it as though it were a hyperbolic mirror. Any ray of light originating from source A would once again appear as if it were coming from source B. In both cases, a single assertion can be made:

"A ray of light arriving from source A will be reflected by any portion of any hyperbolic surface in such a direction as if it were generated by source B."<sup>15</sup> A more mathematical statement is that "The tangent on any point of a hyperbola bisects the angle formed by the two radii through that point."<sup>16</sup>

Figure 3. Phenomenon of the Hyperbolas



A statement of the geometrical description of a hologram can be verbalized as follows: Assume all hyperboloidal surfaces that represent

the interference maxima are partially reflecting surfaces. When a hologram is made, the volume throughout the recording medium contains a linear superposition of many hyperboloidal sets of partial mirrors, each set created by the interference between the reference beam and light from a point on the object, thus creating a hologram. When it is viewed, each set reflects light from the reference beam and forms an image of an object point.

### 2.3 Applications of the Model

#### 2.3a The Virtual Image

Figure 4 shows the optical case of two-beam interference in three dimensional space. Assume that the two sources are emitting at the same constant frequency and a recording medium is placed at a point shown. Since the usual thickness of the recording medium, such as a photographic film plate, is approximately  $10\lambda$ , the interference patterns recorded inside the emulsion represent sections of hyperboloidal surfaces of many different orders. Suppose that after processing, these surfaces become partially reflecting mirrors (as well as partially transmitting and absorbing). By illuminating the film with source A only, at the original relative positions (Figure 5), some of the light is transmitted directly through these partial mirrors, some is absorbed, but the rest is reflected in such a way as to appear as if they are coming from source B. Therefore, if the observer looks in the direction of source B through the processed film, he sees the virtual image of B.

Figure 4. Two-Beam Interference in Three Dimensional Space

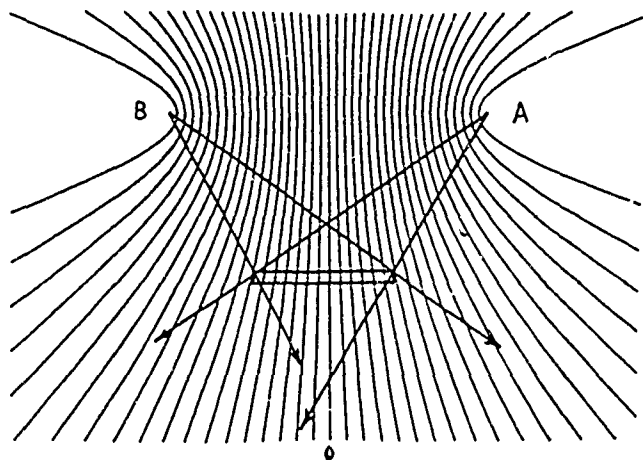
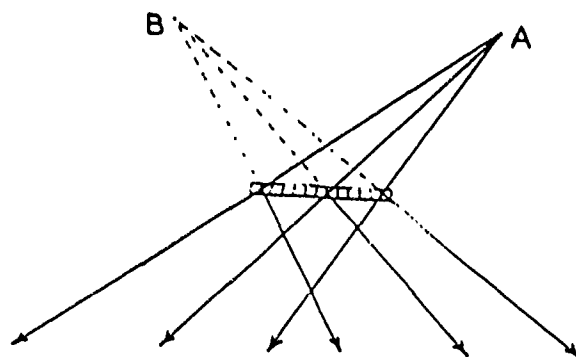


Figure 5. Reconstruction of a Virtual Image

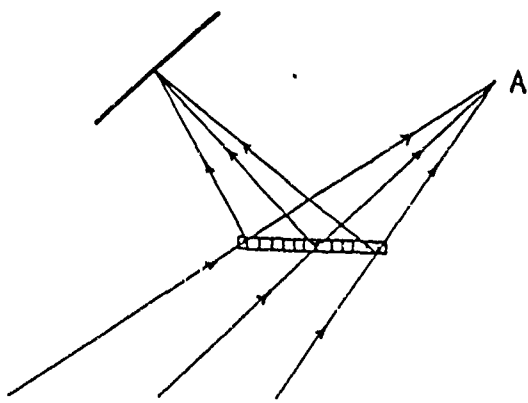


The light from source A can be called the reference beam and the light from source B can be called the object beam. If more than one point source is located in the vicinity of B, each source will form a unique hyperboloid set with source A, and the film will record all of them. Upon illuminating the processed hologram with only source A, each set will reflect light in such a way as to recreate the virtual image of all its object points.

### 2.3b The Real Image

Take the hologram from Figure 5 and illuminate it in a backward direction by focusing the beam of light back toward source A (Figure 6). The reflected light from the hyperboloidal mirrors will focus at B so that if a screen were present, there would be a real image of B on the screen.

Figure 6. Reconstruction of a Real Image



### 2.3c Redundancy

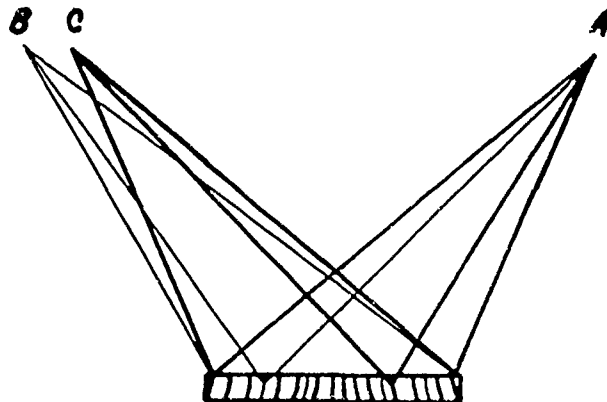
It is well known that if a hologram is broken up into pieces, each piece will give a complete perspective of an original scene. Since every elementary volume in the hologram was formed with light from a complete perspective of the scene, each of these elementary volumes will produce a complete perspective. In other words, the size of the film used to form a hologram is independent of the size of the scene. In fact, for the purpose of projecting a real image on a screen with a laser beam, it is desirable to select a narrow area by using an undiverged beam so that area covered does not exceed a few millimeters in diameter<sup>11</sup>. In this case, the real image consists of small rays at

angles relative to one another. This increases the depth of field, allowing a focused image over a long distance along long beam paths to form a real image.

### 2.3e Dynamic Range

Not only the locations of all the points on an object are reproduced on the hologram, but their relative intensity as well. Suppose the scene consists of sources B and C with B having the same intensity as A but with C being less intense than A (Figure 7). Assume the mirrors formed between A and B are of higher reflectivity than those formed between A and C, due to the difference in fringe visibility.

Figure 7. Comparison of Intensities



When this processed hologram is illuminated by A, points B and C are recreated by the reflected light from these surfaces in correspondence with their original intensity. Thus, a hologram can recreate total variations from faintly illuminated areas to glares.

### 2.3f Noise

As is true of all information transmission systems, the output always has noise added to it. Besides the so-called grain noise of the photographic film, which is due to the scattering of light by the particles in the film, another source is intermodulation noise. In Figure 7, not only are there interference patterns between A and B, and A and C, there is also a pattern formed between B and C (not shown). The latter pattern forms a set of hyperboloids that also intersect throughout the volume of the film but of much lower spatial frequency (fewer lines per millimeter across the surface of the film. This results in the scattering of light in arbitrary directions when the hologram is illuminated with the reference beam alone. When the scene consists of three dimensional objects, every pair of points on the object creates an unwanted interference pattern. Therefore, the larger the object and the closer it is to the film plane, the more serious the interference noise becomes.

### 2.3g Beam Ratio

To help minimize the effects of the intermodular noise, practical holography requires that the reference beam be of a higher intensity than any point from the object. In practice the intensity ratio, as measured by using a diffuser in front of a light meter, between the reference and the object beams varies from 1 to 1 to 10 to 1 for transmission nolograms", the type so far discussed. This allows the mirrors to form between the reference and points on the object to be generally of higher reflectivity than those forms between any pair of

points on the object. Also, the noise can be further minimized by having the smallest angle between the reference beam and any object beam to be greater than the largest angle formed by a pair of points on the object. This assures that the minimum spatial frequency formed by the object and the reference beam is greater than the spatial frequency noise. When the hologram is illuminated, the intermodulation noise is diffracted to angles always smaller than the signal desired. In this way, even though the noise cannot be eliminated, it can be isolated.

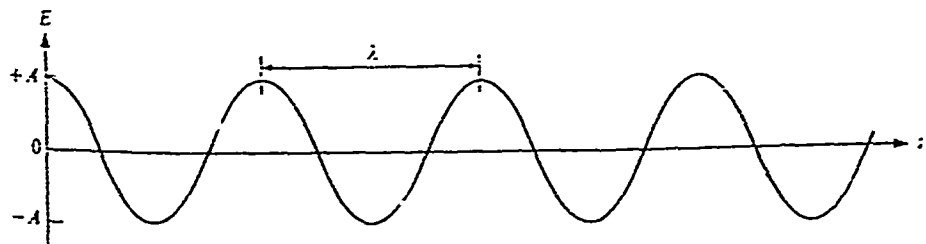
### 3 Coherence

The spatial and temporal coherence of the light plays an essential role in making a good hologram. For the reference beam and object beam to interfere, the light must be coherent. Interference and coherence are the experimental and theoretical aspects of the same phenomenon. Coherence theory is the statistical description of radiation, expressed in terms of correlation functions. As spatial interference is the oldest and simplest example of correlation between light beams, coherence theory was developed first as a description of "interference". Only recently have other correlation effects, such as temporal coherence become of interest. Although coherence is a measure of the correlation between two radiation fields, the term has been extended to apply to the light source, which is said to be coherent if all beams are highly correlated; for example a laser. Temporal coherence (Figure 8)<sup>19</sup> can be described as follows: for a given position in space, the amplitude and phase of a light wave is correlated to the amplitude and phase of a light wave at the same position in space but at

a different time.

Figure 8. Temporal Coherence of a Light Wave

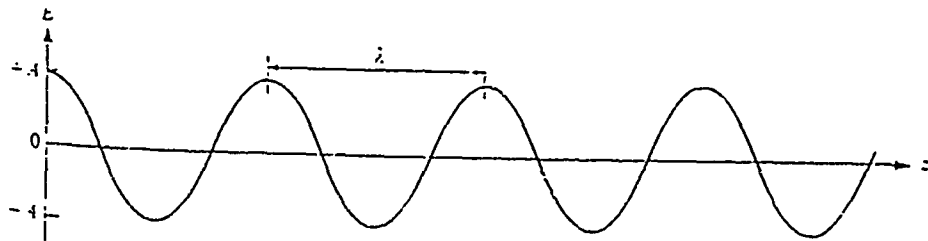
$$\psi = A \sin(kx \pm \omega t)$$



Spatial coherence (Figure 9)<sup>21</sup> can be described as follows: for a given time, the amplitude and phase of a light wave is correlated to the amplitude and phase of a light wave at a different point in space at the same time.

Figure 9. Spatial Coherence of a Light Wave

$$\psi = A \sin(kx \pm \omega t)$$



#### 4 Experimental Account

4.1 Purpose: By researching the theoretical background of holography, and exploring the experimental aspects of this concept, I have constructed several types of holographic layouts desiring to obtain a

acceptable hologram.

4.2 Hypothesis: Since Set Up I, the multiple-beam reflection hologram, would produce the more pronounced interference patterns and is more mathematically precise than the other set-ups. Set Up I should produce a better quality hologram.

4.3 Procedure: Set up<sup>12</sup> of the optical elements:

1. Define the optical axis.

- a. Mount the laser on the optical table<sup>13</sup>
- b. Make the beam straight and level by defining a certain point on a beam block and adjusting the beam so it remains at that point when interrupted at fixed intervals on the table by the beam block.

(Note that every time a new optical element is introduced into the system, the beam has to be checked to determine if it has remained on the defined optical axis.)

2. Align the microscope objective so that it interrupts the beam at the defined optical axis.

3.<sup>14</sup> Adjust the pupil so that the maximum amount of light is emitted.

4. Insert the collimating lens so that its distance from the pupil is its focal length, and the beam remains a constant size when interrupted by the beam block at various points on the table.

5. Insert the iris to adjust the diameter of the beam and block out any extraneous light.

6. Insert the shear plate at a 45 degree angle to the beam; if fringes appear on the beam block, the light waves can be

rendered collimated.

7. Introduce the beam splitter into the system.
8. Place flat mirrors in the new, created beam path, and adjust so that the beam is directed to the film plane.
9. Place the object in the other beam path.
10. Equate the paths of the reference beam and object beam.
11. Determine the angle between the reference beam and object beam<sup>25</sup>.
12. Make the beam ratio 10 to 1, using a detector to measure the intensities. To decrease the intensity of the reference beam, use a neutral density filter.
13. Turn out the lights.
14. Carefully open the case and insert the film plate in to the holder/developer (emulsion side toward the setup). Close the lid and put the cover on the film box<sup>26</sup>. Close the door of the case.
15. Open the door where the laser is and expose<sup>27</sup> the film for the allotted time (1 to 6 seconds)<sup>28</sup>. Close the door.
16. Open the door by the film, place light proof plates over glass windows in holder, take out the holder, and close the door.
17. Develop the film
  - a. Pour the developer in the top of the holder.
  - b. Wait five minutes and drain the developer.
  - c. Pour in the fixer, wait five minutes and drain.
  - d. Pour in the wash, wait ten minutes, and drain.
  - e. Allow the film plate to dry for fifteen minutes.

18. Illuminate the film with the laser.

#### 4.4 Results

##### Set Up I

Trial	Object	Exposure	ND Filter	Results
1	gold ring	4 sec.	yes	no fringe only dark, opaque circle
2	gold ring	1 sec.	yes	some fringe visible, middle of circle still opaque
3	gold ring	1 sec.	no	opaque circle
4	gold ring	shorter than 1 sec., successive on/off	no	visible fringe, but no hologram is reconstruct- ed

##### Set Up II

Trial	Object	Exposure	ND Filter	Results
1	gold ring	1 sec.	no	opaque
2	gold ring	successive on/off	no	many fringes visible, but streaks appear across the film

### Set Up III

Trial	Object	Exposure	ND Filter	Results
1	gold ring	successive on/off	no	visible fringes, but no hologram could be reconstruct- ed

2	gold ring	successive on/off	no	ring was moved closer to the film, but no change from trial 1
---	-----------	----------------------	----	--

#### 4.5 Conclusion

Even though a hologram could not be produced, I do feel that my experiment was of a success. I have gained an extensive knowledge of laser physics, holographic theory, and the skill of working with optical equipment in a laboratory. I found that my third, and most simple set up, produced the best results in that the fringe patterns were most pronounced. Although I could not determine what was causing the hologram not to form, some variables I would change in my project would be: using a lower wattage laser, a shutter system to control the exposure time, and a different optics bench (the table I was using could have had a vibration problem).

## Bibliography

Born, Max and Wolf, Emil. Principles of Optics. London: Pergamon Press, Ltd., 1959.

DeVelis, John B. and Reynolds, George O. Theory and Applications of Holography. Reading: Addison-Wesley Publishing Company, 1967.

Dyson, J. and Haine, M.E. "A Modification to Gabor's Proposed Diffraction Microscope", Nature. vol. 161 (1950) p. 315-316.

El Sum, H.M.A. Reconstructed Wavefront Microscopy. Phd. Thesis, Stanford University, November, 1952.

Gabor, D. "A New Microscope Principle", Nature. vol. 161 (1948), p. 777-778.

Gabor, D. "Diffraction Microscopy", Journal of Applied Physics. vol. 19 (1948), p. 1191.

Guralnik, David B. Webster's New World Dictionary of the American Language. New York: Warner Books, Inc., 1984.

Jeong, Dr. Tung H. and Lodge, Francis E. Holography Using a Helium-Neon Laser. Bellmawr: Metrologic Instruments, Inc., 1978.

Leith, E.N. and Upatneiks, J. "Reconstruction of Wavefronts and Communication Theory", Journal of the Optical Society of America. vol. 53 (1962) p. 1377.

Melles Griot Optics Guide, 1988.

Newport Optics Guide, 1990.

O'Shea, Donald C., Callen, W. Russell, and Rhodes, William T. Introduction to Lasers and Their Applications. Reading: Addison-Wesley Publishing Company, 1978.

Smith, Howard M. Principles of Holography. New York: John Wiley and Sons, 1969.

Steele W.H. Interferometry. London: Cambridge University Press, 1983.

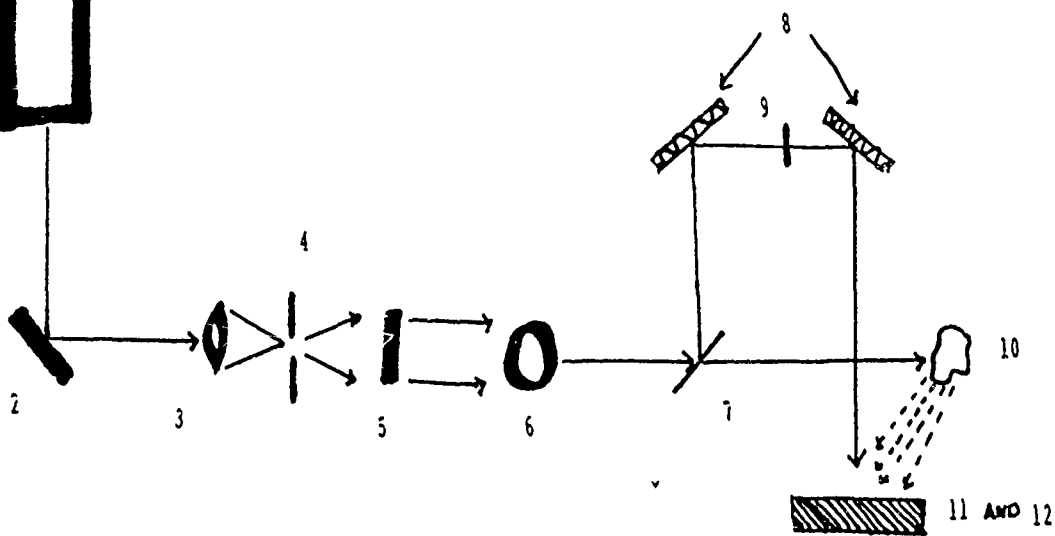
Strong, John. Concepts of Classical Optics. San Francisco: W.H. Freeman, Inc., 1958.

1. M. Born and E. Wolf, Principles of Optics (London, 1959) p. 319
2. D.B. Guralnik, ed., Webster's New World Dictionary of the American Language (New York, 1984) p. 289
3. D. Gabor, "A New Microscope Principle", Nature, vol. 161, p. 777-778 (1948)
4. D. Gabor, "Diffraction Microscopy", Journal of Applied Physics, vol. 19, p. 1191 (1948)
5. Howard M. Smith, Principles of Holography, (New York, 1969) p. 3
6. Ibid., p. 5
7. John Strong, Concepts of Classical Optics (San Francisco, 1958) p. 490
8. M.E. Haine and J. Dyson, "A Modification to Gabor's Proposed Diffraction Microscope", Nature, vol. 161, p. 315-316 (1950)
9. H.M.A. El Sum, "Reconstructed Wavefront Microscopy", Phd. Thesis, Stanford University, November, 1952
10. E.N. Leith and J. Upantnieks, "Reconstructed Wavefronts and Communication Theory", Journal of the Optical Society of America, vol. 53, p. 1377 (1962)
11. Donald O'Shea, W. Russel Callen, and William T. Rhodes, Introduction to Lasers and Their Applications (Reading, 1978) p. 7
12. diagram taken from Holography using a Helium-Neon Laser, Metrologic Instruments, Inc., p. 10
13. Ibid., p.10
14. John Strong, p. 425
15. Francis A. Jenkins and Harvey E. White, Fundamentals of Optics (New York, 1957) p. 305
16. M. Born and E. Wolf, p. 326
17. John B. De Velis and George O. Reynolds, Theory and Application of Holography (Reading, 1967) p. 128
18. Dr. Tung Jeong and Francis E. Lodge, Holography Using a Helium-Neon Laser (Bellmawr, 1978) p.11
19. W.H. Steele, Interferometry (Cambridge, 1983) p. 5
20. Donald O'Shea, W. Russel Callen, and William T. Rhodes, p. 7

21. Ibid., p. 7
22. See the Appendix for a diagram of the various layouts and detailed descriptions of their components.
23. The table is floating on pneumatic legs and covered by a light-proof case.
24. Step after number two is applicable to Set Ups numbers II and III. Steps that are applicable to all layouts begin again at step thirteen.
25. the equation used to find this is:  $\sin \text{obj.} + \sin \text{ref.} / \lambda = n$  lines/mm (my angle was 30°), taken from Newport Optics Catalog, p. M-9
26. In Set Up III, the film is first put into a neutral density filter holder and then put into the holder/developer after being exposed to avoid light aberration caused by the glass plates in the front and back of the film holder.
27. Allow the laser to be on for at least fifteen minutes before using it to expose the film.
28. Dr. Tung H. Jeong and Francis E. Lodge, p. 29

## APPENDIX

## Set Up I



1. Laser	7. Beam Splitter
2. Beam Director	8. Flat Mirrors
3. Microscope Objective	9. Neutral Density Filter
4. Pupil	10. Object
5. Collimating Lens	11. Film Holder/Developer
6. Iris	12. Film (KODAK 649 F, 4x5in.)

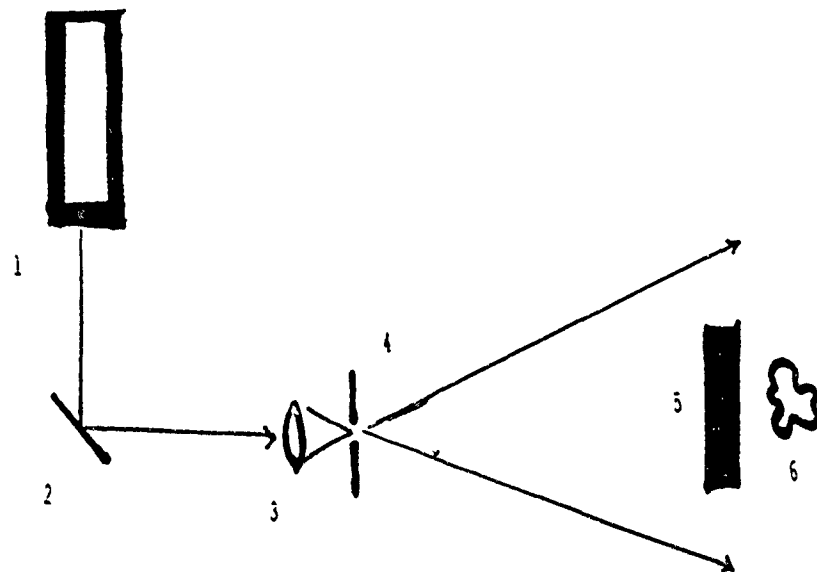
Object Beam 2000 lines/mm, sensitivity

2000 lines/mm, sensitivity

= 900 ergs/cm --with helium

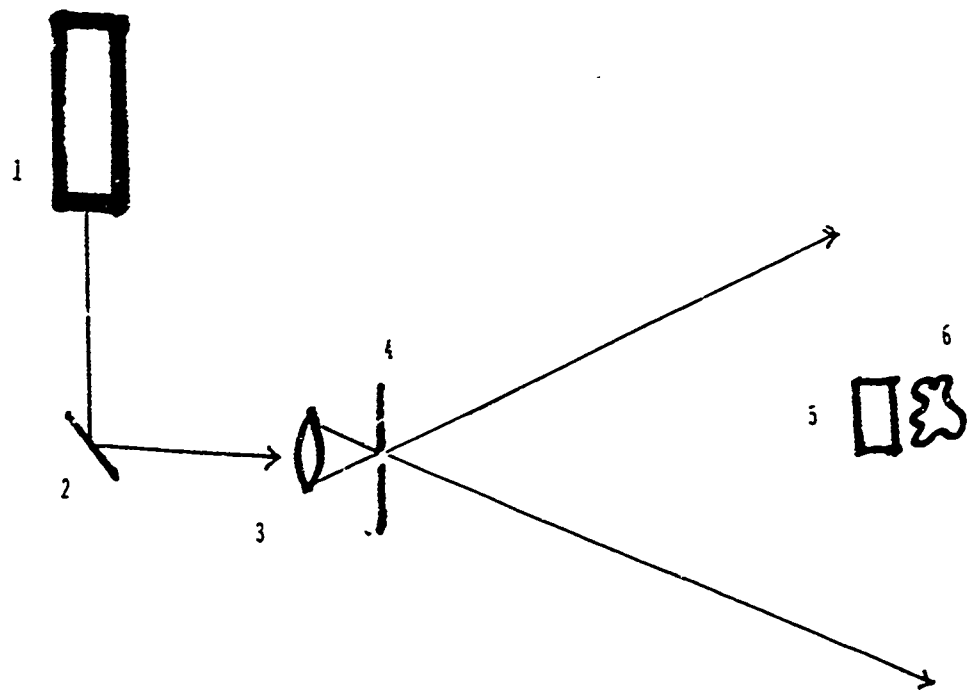
<sup>1</sup> Newport Optics Catalog, p. 18-9

Set Up 11



1. Laser	3. Pupil
2. Microscope Objective	4. Film Holder/Developer
5. Object	

Set Up III



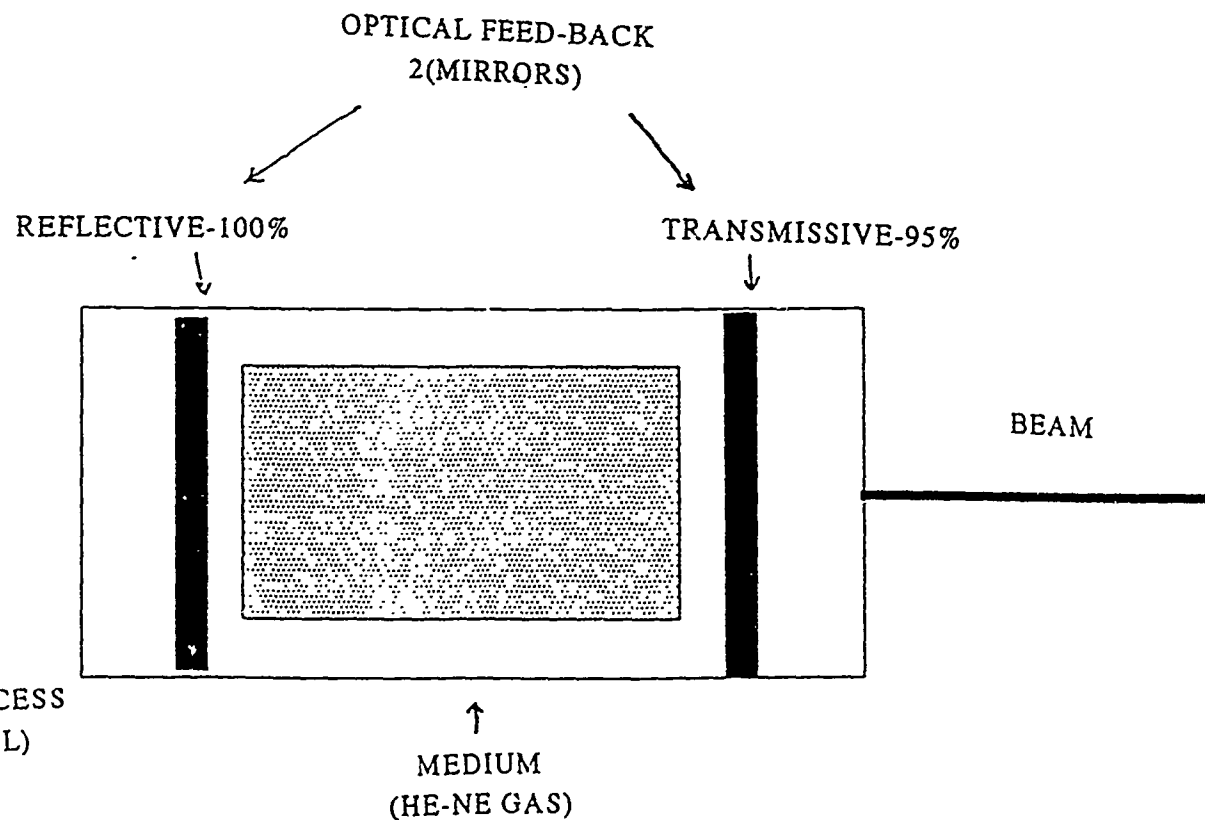
1. Laser	4. Neutral Density Filter
2. Microscope Objective	holder (film holder)
3. Pupil	5. Object

## Descriptions of Components

### The Laser:

The light source used in making the hologram is a 20mW, Class III Helium-Neon continuous-wave laser (Figure 1) that transmits at a wavelength of 632.8 nm. A laser is used because it is a monochromatic and coherent light source that is easily filtered and collimated as opposed to white light.

Figure 1. A Helium-Neon Laser



### The Spatial Filter:

The spatial filter is composed of two basic optical instruments: a microscope objective (Figure 2)<sup>1</sup> and a pupil. The microscope objective focuses the light so that only the central, strongest mode if light passes through the pupil. The pupil blocks out nearly all of the spatial noise. Therefore the purpose of the spatial filter is to "clean up" the laser beam, so that it

<sup>1</sup> Newport Optics Catalog, p.1-16

resembles a uni-phase spherical wave emitted from a point source of light. It provided a safe, convenient way to remove random fluctuations from the intensity profile of a laser beam created by spatial noise (Figure 3)<sup>3</sup>. In this set up a 10x microscope objective and a 25 micron pupil are used<sup>4</sup>.

Figure 2. The Microscope Objective

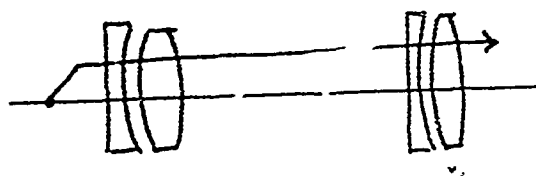
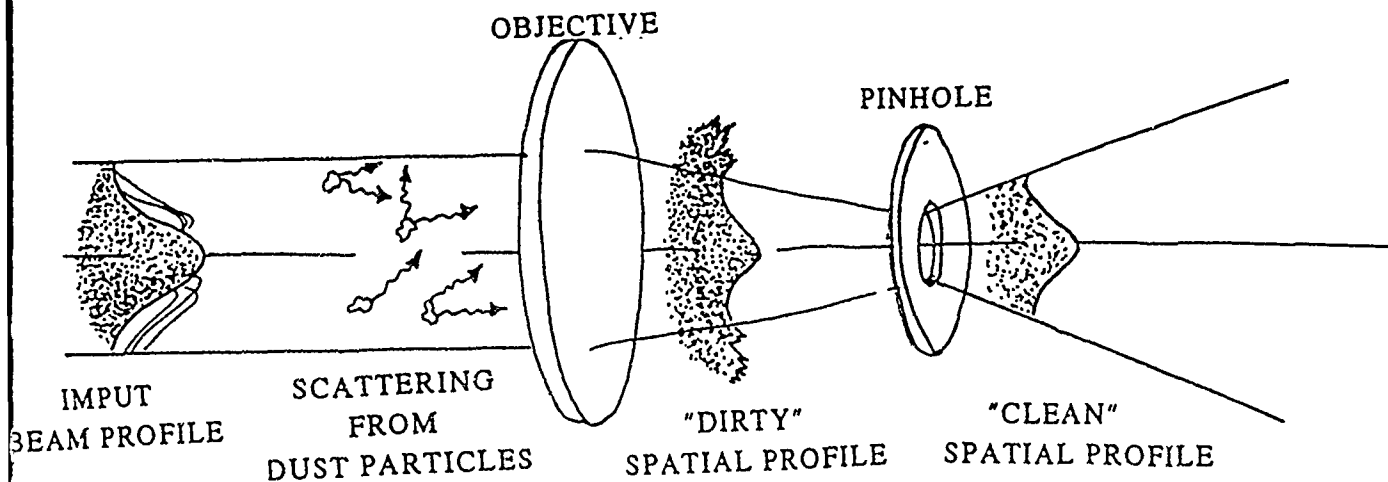


Figure 3. The Spatial Filter



<sup>3</sup> Ibid., p. I-16

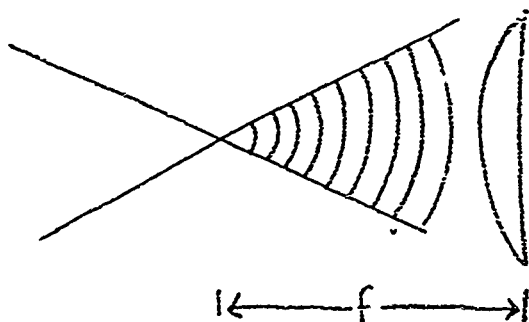
<sup>4</sup> The Newport Optics Catalog suggests the use of a 25 micron microscope

pupil with a 10x

#### The Collimating Lens:

The collimating lens (Figure 4) is a single plano-convex with a focal length of 49.2 cm. It terminates further divergence of the laser beam emitting from the pupil, rendering the light waves parallel.

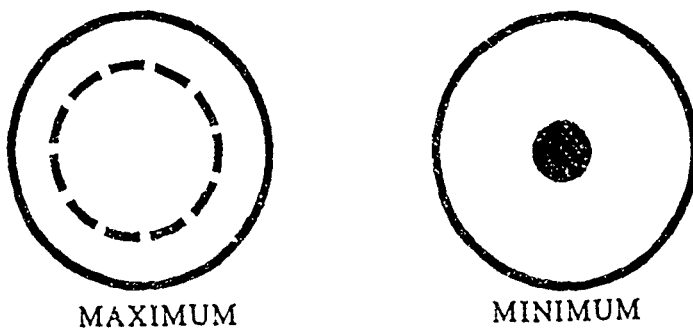
Figure 4. The Collimating Lens



#### The Iris Diaphragm:

The iris (Figure 5) reduces or expands the beam's diameter while keeping the energy per unit area constant. The iris used in this set up has an aperture that ranges from 28mm to 15mm.

Figure 5. The Iris Diaphragm



#### The Plate Beam Splitter:

The plate beam splitter consists of a thin (1mm) plate of optical crown glass on each side of which is deposited a different type of coating. The first surface is coated with an all-

SURFACE QUENCHING OF SINGLET DELTA OXYGEN ON A  
90% NICKEL/10% COPPER ALLOY

Evan Werkema

**ABSTRACT:**

Data are presented which represent the  $O_2(^1\Delta)$  quenching rates and deactivation efficiencies for samples of 90% nickel / 10% copper alloy demonstrating varying degrees of aging.

**INTRODUCTION:**

The chemical oxygen-iodine laser (COIL) is a laser that is pumped chemically rather than electrically. It makes use of oxygen in the first electronically excited state, known as singlet delta ( $O_2(^1\Delta)$ ). Singlet delta has a life span in a vacuum of around 45 minutes, remarkably long for an excited species. It also happens that the energy of  $O_2(^1\Delta)$  is slightly higher than that of excited iodine ( $I^*$ ), the lasing medium of the COIL.  $I^*$  is a species with a very short life span which loses its energy by the emission of near-infrared light. When  $O_2(^1\Delta)$  and ground state iodine ( $I_2$ ) are brought together, the excited oxygen rapidly gives up its energy to the iodine. The iodine first dissociates to I atoms, then forms  $I^*$ , which quickly re-releases the energy as infrared light. This is the basis of the COIL. Because of its long life span,  $O_2(^1\Delta)$  can be generated remotely by chemical means and sent into the laser. The advantage of this chemically pumped laser is that it does not require the large electrical power supplies that conventional lasers do.

Since it must be generated and premixed with  $I_2$  outside of the laser cavity itself, the excited oxygen for the COIL must pass over several surfaces prior to entering the laser cavity. Although  $O_2(^1\Delta)$  (hereafter referred to as  ${}^1\Delta$ ) has a long life span in a vacuum, it can be rapidly deactivated (quenched) by contact with other materials. Two

kinds of quenching can occur: homogenous and heterogenous. In homogenous quenching,  $^1\Delta$  is deactivated by the ground state oxygen ( $^3\Sigma$ ) or other molecules present in the gas phase. In heterogenous quenching,  $^1\Delta$  is deactivated by the solid wall surfaces it contacts. Depending on the wall materials, much  $^1\Delta$  can be lost over short distances. Therefore, it is important for the flow tube materials to be such that they do not quench a significant portion of the excited oxygen before it reaches the laser. The purpose of the research performed was to test what degree of quenching might be expected from a 90% nickel/10% copper alloy as a potential material for use in the COIL. It was part of an ongoing research effort at Phillips Laboratories to test various metallic and non-metallic surfaces that could come in contact with  $^1\Delta$  in the COIL.

#### EXPERIMENTAL:

The following setup was used to test the quenching effects (see Figure 1). A flow of very pure oxygen (Airco Specialty Products Ultrapure grade, 99.993%) was established in a tube. The flow was then split through a discharge-bypass system. The discharge path was channelled through a microwave generator (Ophthos Instruments, Inc.), which activated a very small portion of the oxygen to the  $^1\Delta$  state (the low concentration of  $^1\Delta$  will be important later). The bypass path was unaltered, flowing only ground state oxygen ( $^3\Sigma$ ). Flow rates through the two paths were separately controlled by two Unit Instruments, Inc. mass flow controllers (model no. UFC 1000) such that, when the two paths were recombined downstream, the concentrations of  $^1\Delta$  and  $^3\Sigma$  in the flow tube could be varied independently. This control was necessary in order to maintain a constant initial concentration of  $^1\Delta$  at various pressures.

Before the paths were recombined, the bypass flow passed through a tube coated with mercury oxide (HgO). The microwave generator, in addition to creating  $^1\Delta$ , also created a minute quantity of  $O_2(^1\Sigma)$  (the

next higher activation state of oxygen) and atomic oxygen.  $^1\Sigma$  rapidly deactivates to  $^1\Lambda$  or  $^3\Sigma$ , but atomic oxygen has to be removed chemically. The HgO coating in the tube reacted with the atomic oxygen, removing most of it from the system.

Once the two paths were recombined, the oxygen entered the test section of the setup.  $^1\Lambda$  is constantly undergoing radiative decay, and as it does so, it emits infrared light of a characteristic wavelength (about  $1.268\mu$ ). The intensity of the light emitted by the flow of oxygen at any given point is proportional to the concentration of  $^1\Lambda$  present at that point. To determine the quenching effects of the Ni/Cu alloy test section, measurements of the light emitted by the flow were taken immediately before and immediately after passing through a 0.2m length of Ni/Cu tube one inch in outside diameter. This was accomplished by attaching Teflon blocks fitted with observation ports to the ends of the tube. The upstream block was then connected to the flow from the discharge-bypass system, and the downstream block to a vacuum system. The observation ports consisted of Plexiglas windows oriented perpendicular to the flow direction and an apparatus to support a fiber optic cable. Opposite the windows, aluminum coated reflectors were positioned inside the blocks so that the amount of light passing out of the window was maximized. During the execution of the experiment, a flexible fiber optic cable fitted with a collimating lens (Oriel Corp. glass fiber optic system, ca 62% transmitting at  $1.27\mu$ ) would be connected to the upstream block to read the initial signal, then switched to the downstream block to read the quenched signal. Devices to measure pressure (MKS Baratron Pressure Transducer No. 22BH8, 0-10 Torr) and temperature (Omega thermocouple) information were also attached at each port, since these conditions also affect  $^1\Lambda$  quenching rates and must be included in the calculations. Owing to the low signal emitted and the potential for light leaking in from outside, all data collection was performed in darkness.

The light signal sent down the fiber optic first passed through a chopper set at 24.9 Hz (EG&G Parc No. 194A), which modulated the signal, and then through a narrow band pass filter set at  $1.268\mu$  (48% peak transmission, FWHM  $0.008\mu$ ).  $1.268\mu$  is the wavelength emitted by the  ${}^1\Delta$ , so all other wavelengths were removed by the filter. The signal from the filter was then sent into an intrinsic germanium detector (Applied Detector Corporation model no. 403LL, responsivity  $7 \times 10^{10} \text{V/W}$ , NEP  $10^{-16}$ ), which converted the optical signal into an electrical signal. This signal then passed into a lock-in amplifier (Stanford Research Systems No. SR510). A voltage signal from the chopper representing the chopper frequency was also sent into the lock-in, thus permitting phase sensitive detection of the  ${}^1\Delta$  emission.

The amplified voltage signal from the lock-in then passed through an analog to digital (A/D) converter and into a Zenith 248 computer. The data acquisition software was designed to take 2000 measurements from the voltage signal over a given time period, then calculate the average signal, and store the average to a data file on a disk. Normally, data would be taken over a range of pressures between 1 and 7 Torr. For a given pressure, the fiber optic probe would be positioned in the upstream port and the computer instructed to take a set of data, average the signal, and store the result. This is the signal representing the initial  ${}^1\Delta$  concentration. Then the probe would be moved to the downstream port and a new set of data would be taken. This was the signal representing the quenched  ${}^1\Delta$  concentration. This process would be repeated several times until enough data had been collected for a particular pressure (usually around 4 sets of upstream and downstream points). Then the pressure would be changed, keeping the initial concentration of  ${}^1\Delta$  constant using the separate flow controllers mentioned earlier. The constant concentration was necessary in order to be able to compare the quenching effects at two different pressures.

The collected data would then be manipulated using a series of

programs designed to calculate the rate constant for the disappearance of  ${}^1\Delta$  ( $k_{\text{obs}}$  observed or  $k_{\text{obs}}$ ) and the quenching efficiency ( $\gamma$ ) of Ni/Cu. A detailed description of the data acquisition software is given in a recent report [1].

#### RESULTS/ANALYSIS

The graph of ( $k_{\text{obs}}$ ) vs. pressure (Figure 2) shows the results of the tests on Ni/Cu.  $K_{\text{obs}}$  represents the overall rate constant for the disappearance of  ${}^1\Delta$ , and is given by the linear equation

$$k_{\text{obs}} = k_q[{}^3\Sigma] + k_w \quad (1)$$

where  $k_q$  is the gas phase quenching rate constant and  $k_w$  is the wall quenching rate constant [2]. The fact that the concentration of  ${}^1\Delta$  is so low to begin with ( $[{}^1\Delta]/[{}^3\Sigma] < 0.001$ ) permits the assumption that  $[{}^3\Sigma]$  is proportional to gas pressure in the system, and thus the use of pressure on the graph instead of  $[{}^3\Sigma]$ .

$K_{\text{obs}}$  is related to the change in  ${}^1\Delta$  concentration by the linear approximation

$$[{}^1\Delta]_0 / [{}^1\Delta] \approx 1 + (k_{\text{obs}})t \quad (2)$$

where  $[{}^1\Delta]_0$  is the initial concentration of  ${}^1\Delta$  and  $[{}^1\Delta]$  is the concentration at time  $t$ .

Two Ni/Cu tubes were used during the course of the study. The first was scrubbed with a wire brush on the inner surface and acid cleaned to remove paint spots. This resulted in a partial removal of the oxide coating that forms naturally with time. The second was sandblasted to remove the oxide coating completely. On the graph, July 9 and July 31 represent the scrubbed tube, the others represent the sandblasted tube. The scrubbed tube was stored open to the air from

July 9 to July 31, hopefully completing the oxidation of the exposed areas. The sandblasted tube was stored under vacuum between runs from July 12 to July 19, and under oxygen from July 20 to July 22.

Theoretically, the slopes of the graphs ( $k_q$ ) should all be slightly positive, since in Equation 1, increased pressure should mean increased  $k_{obs}$ . But upon inspection, the results for the sandblasted tube, in particular July 12 on, seem to indicate a negative gas quenching rate! Since this is unrealistic, some other mechanism must be causing greater quenching at lower pressures. The most probable explanation has to do with radial diffusion. The theoretical model for these experiments assumed that ' $\Delta$  concentration was uniform across the diameter of the tube. If there was very high quenching at the walls, however, ' $\Delta$  concentration at the walls of the flow tube would be lower than at the center. Since radial diffusion is slower at higher pressures, the radial diffusion effect would be less pronounced at high pressures, hence the negative slope in  $k_{obs}$ . The high  $k_w$  (y-intercept) also indicates a very high quenching rate. This behavior is most likely due to the reactivity of the exposed metal surface. As the surface oxidized with time, the slope of  $k_{obs}$  vs. pressure increased and  $k_w$  decreased. The results for the scrubbed tube, where less of the oxide coating was removed, showed positive slopes for  $k_{obs}$  vs. pressure.

Another factor which might have affected the data was an increasing quenching rate over the course of a day's runs possibly due to the surface adsorption of a slight amount of  $O_2$ . This weakly bonded  $O_2$  would have escaped overnight when the system was left in vacuum. If this was the case, however, the effects were masked by the error due to the fact that the present computational model cannot account for radial diffusion.

For purposes of comparing Ni/Cu to other materials, a quantity called the quenching efficiency ( $\gamma$ ) is calculated.  $\gamma$  is equal to the probability that any particular collision between a molecule of ' $\Delta$  and

the wall will result in a deactivation. The gamma for an oxidized Ni/Cu surface like that of the scrubbed tube on July 31 has a  $\gamma$  equal to about  $2.8 \times 10^{-4}$ . This value is not much different from the results obtained earlier by others for the individual elements copper ( $\gamma=2.1 \times 10^{-4}$ ) and nickel ( $\gamma=2.6 \times 10^{-4}$ ), but is somewhat higher than Pyrex ( $\gamma=3.2 \times 10^{-5}$ ) or Inconel (a 76% Ni, 15% Cr, 8% Fe alloy,  $\gamma=8.8 \times 10^{-5}$ ) [3].

#### CONCLUSION

The results of the tests seem to indicate that the 90% nickel, 10% copper alloy could be expected to behave similarly to pure copper and nickel in terms of quenching efficiency. This would make it inferior to both Pyrex and Inconel in terms of maintaining a concentration of  $O_2(^1\Delta)$  over the distance from the chemical generator to the laser. These results seem to be consistent with the materials' relative activities and abilities to resist corrosion as well. It also appears that oxidized Ni/Cu surface appears to maintain a  $^1\Delta$  concentration better than a pure metal surface.

The difference between the  $\gamma$  for Ni/Cu and the other metal materials may seem small. Yet even small differences have an effect upon the efficiency of the chemical laser.

Other factors also play a role in choosing a wall material, such as the size of the laser and the application for which it is to be used. It is possible that the durability and strength of the material may be important in addition to how well it maintains  $^1\Delta$ . These are subjects for future study.

REFERENCES:

- (1) E. Werkema, P. Whitefield, and R. Crannage, Data Acquisition and Analysis Software Documentation:  $O_2(^1\Delta)$  Surface Quenching Experiment, submitted for publication Laser Digest, August, 1991.
- (2) R.F. Heidner, III, J. Photochem., 25 229 (1984).
- (3) R. Crannage, E. Dorko, and P. Whitefield, Surface Deactivation Efficiencies for  $O_2(^1\Delta)$  Quenching on a Range of COIL-Related Materials, Part 1. J. Phys. Chem., submitted September, 1991, and references therein.

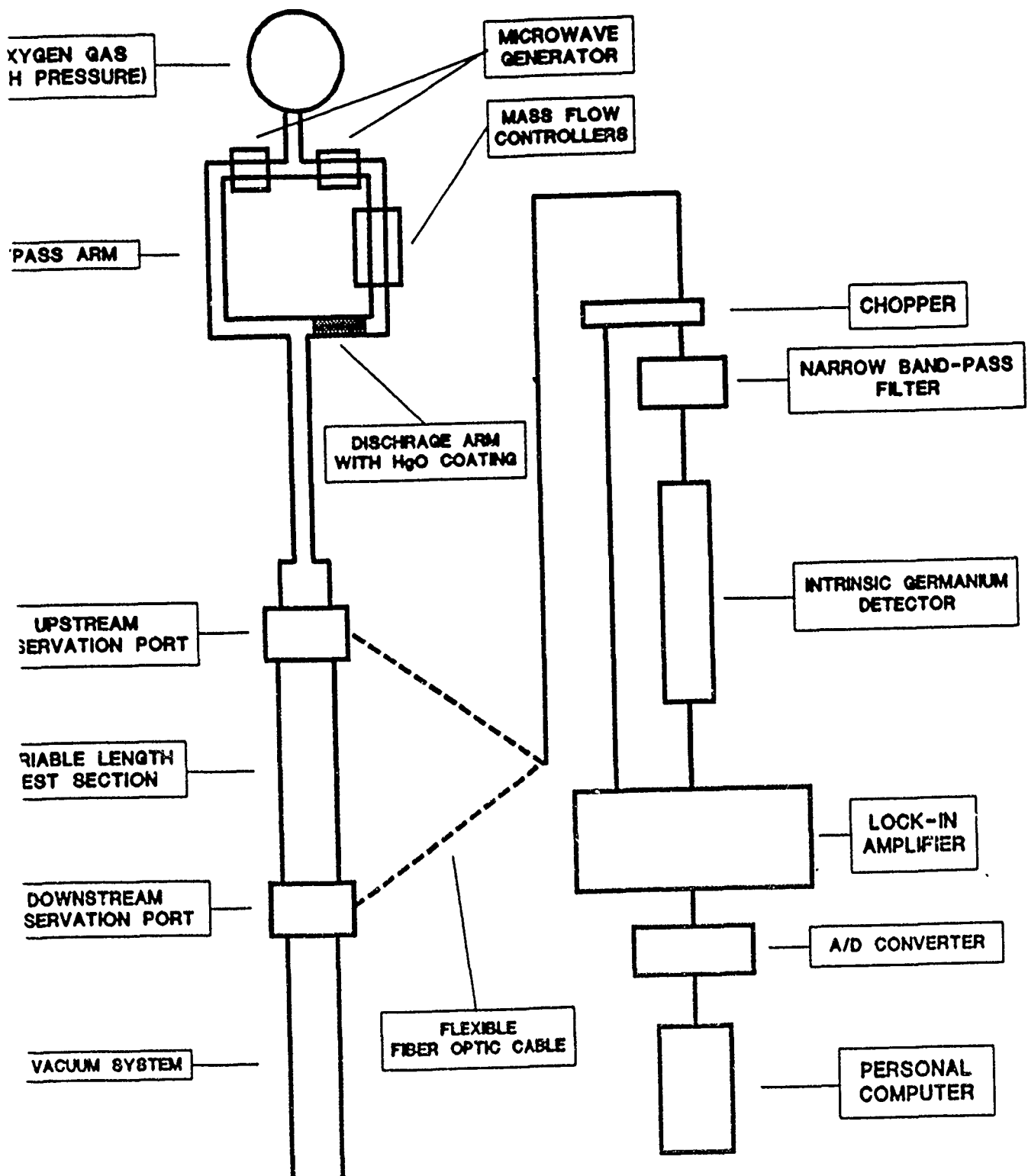


Figure 1: Experimental Setup

# Kobs vs Pressure

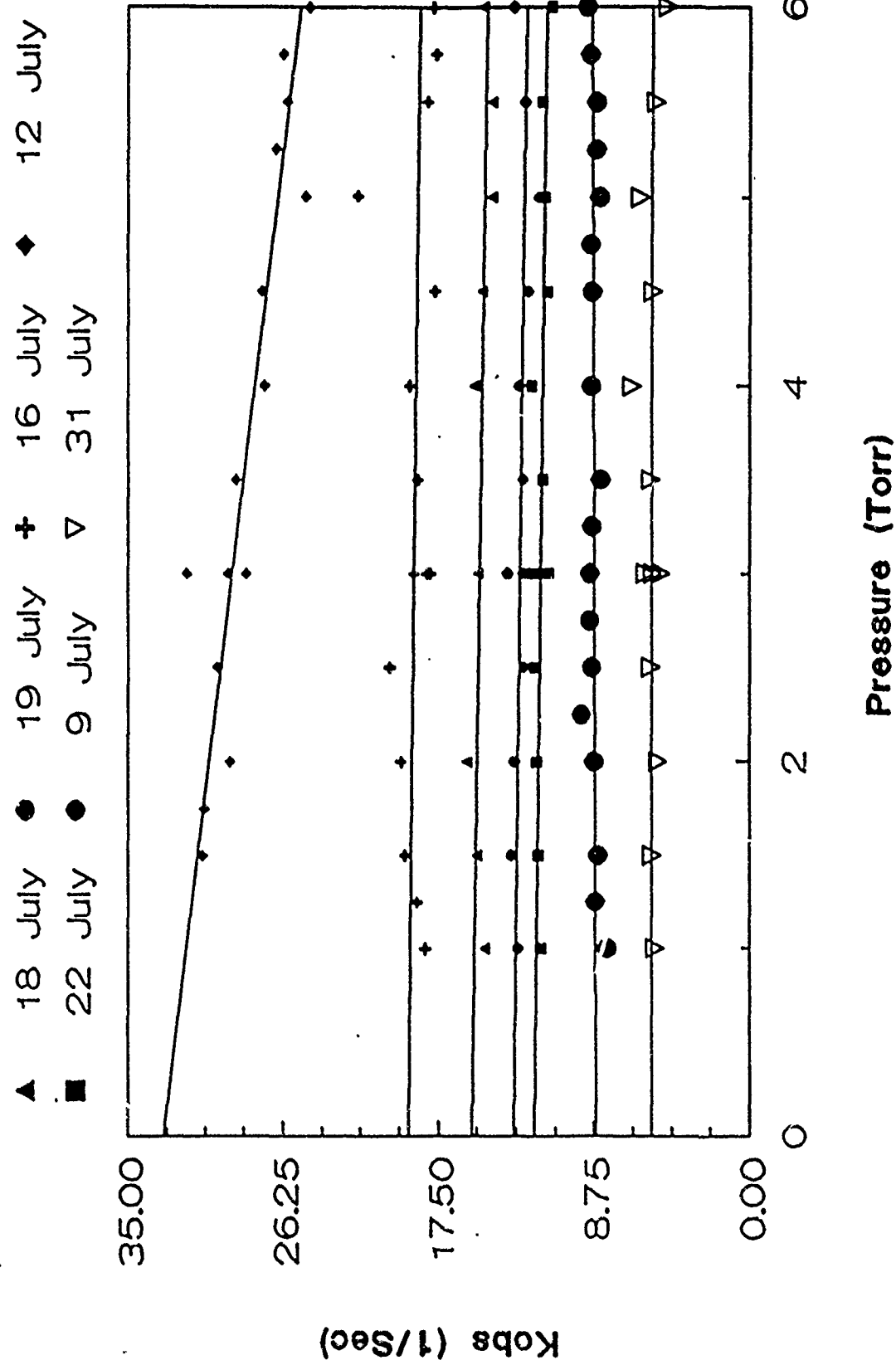


Figure 2:  $K_{ob}$  vs. Pressure Graph

KINETICS OF HYDROXYL RADICAL PHOTODEGRADATION  
OF 2-BUTANONE (METHYL ETHYL KETONE)  
UNDER SIMULATED ATMOSPHERIC CONDITIONS

Jennifer Brewer

Abstract

The relative OH reaction rate from the simulated atmospheric oxidation of 2-Butanone has been measured. Reactions were carried out at  $297 \pm 2\text{K}$  in a 100-liter FEP Teflon<sup>®</sup> film bags. Hydroxyl radicals were generated in the bag by the photolysis of ethyl nitrite in zero-air. The rate constant measured for 2-Butanone was  $2.8 \pm 10^{-11} \text{ cm}^3 \text{ molecule}^{-1} \text{ sec}^{-1}$ . The rate constant obtained for 2-Butanone was placed on absolute basis with the absolute rate constant of  $2.56 \times 10^{-11} \text{ cm}^3 \text{ molecule}^{-1} \text{ sec}^{-1}$  for propene, the reference organic used.

Introduction

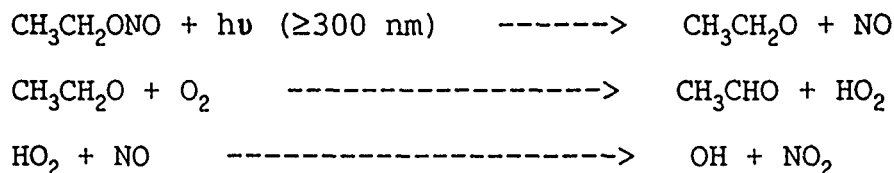
The Air Force uses a variety of volatile organic compounds (VOCs) for the cleaning and painting of aircraft and in a number of other industrial operations. All of these VOCs have strict federal, state, and local ceilings on allowed emission levels. A thorough, fundamental knowledge

of the atmospheric physical and chemical transformation which these compounds can undergo is essential to accurately assess their environmental fate and effects. Such scientific knowledge will ultimately help the Air Force ascertain the relative contribution of VOC emissions from various Air Force operations to the overall air quality problems in a given urban area.

The atmospheric photochemical reactivity of simple VOCs is largely controlled by their reactions with various trace-level chemicals such as  $\text{NO}_x$ ,  $\text{O}_3$ , and OH, with the OH radical playing the most important role.<sup>1</sup> As part of my Summer Research Program, and ongoing Air Force research to characterize the atmospheric transformations of VOCs and address their potential environmental impact, I report herein the results of kinetic studies on the OH photodegradation of 2-Butanone under simulated atmospheric conditions.

### Experimental

Hydroxyl radicals were generated in Teflon<sup>\*</sup> bags by the photolysis of ethyl nitrite in air<sup>2</sup>:



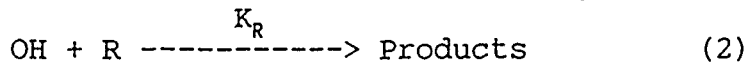
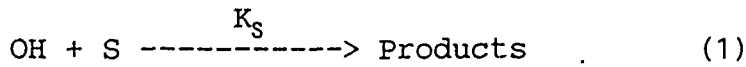
The ethyl nitrite was prepared by the dropwise addition of 50% sulfuric acid into an ethanol-saturated solution of sodium nitrite. The ethyl nitrite produced was swept out of the reaction flask by a stream of high purity nitrogen, passed through a saturated NaOH trap to remove traces of  $H_2SO_4$  dried by passage through a trap containing calcium chloride, and collected in a trap at 196K (refrigerating unit inside a methanol resevoir). The purity of the ethyl nitrite was confirmed by GC/MS and FT-IR analysis. The ethyl nitrite was stored in the dark at 193K. 2-Butanone (Aldrich Chemical Company, Inc.) and propene (Aldrich Chemical Company, Inc.) were both research grade and rated 99% pure. Experiments were carried out at  $297 \pm 2$ K and atmospheric pressures 754 to 768 Torr. Irradiations were carried out in 100-liter, 2 mil FEP Teflon<sup>®</sup>-film bags, surrounded by six 40-watt sun lights (Westinghouse F40). These lights provided UV radiation in the 300-450 nm region. The bag and the lamps were housed inside an aluminum box, with a fan at the top of the box to maintain a constant temperature inside the bag. In this work, propene was chosen as the reference compound. Measured amounts of the reference compound and a VOC were flushed from a Pyrex<sup>®</sup> receptacle into the Teflon<sup>®</sup> bag by a stream of zero-air during the bag loading process. The reference compound and the VOC sample were allowed to mix for 4 hours before taking initial sample ( $S_0$ ) and reference

(Ro) GC responses. These compounds were quantitatively monitored by gas chromatography with flame ionization detection, using a fused silica capillary column (Supelco SpB-5 15m, 0.53 mm ID). The ethyl nitrite and NO (which was added to quench any secondary reactions which might occur due to O<sub>3</sub> formed in photolysis process) were admitted into the chamber via a sampling port on the side of the chamber. The reactants were allowed to mix for 30 minutes prior to irradiations. Maximum irradiation time was 225 seconds, with an initial 90-second irradiation, followed by others at 15-second intervals. Under the above experimental condition, in the absence of CH<sub>3</sub>CH<sub>2</sub>ONO and NO, the reference compounds and VOC sample compounds were photochemically stable, i.e., they showed no observable photolysis.

The initial concentrations of reactants in the Teflon bag were as follows:

$$[2\text{-Butanone}]_0 = 1 \text{ ppm}_v, \quad [\text{propene}]_0 = 1 \text{ ppm}_v, \\ [\text{CH}_3\text{CH}_2\text{ONO}]_0 = 10 \text{ ppm}_v \text{ and } [\text{NO}]_0 = 2.5 \text{ ppm}_v$$

The rate constants for the OH radical reaction with the reference compound and with the VOCs were determined by the relative rate technique.<sup>3</sup> The OH radical generated by the photolysis of CH<sub>3</sub>CH<sub>2</sub>ONO reacts with the reference, R and sample, S as follows:



Assuming that the reaction with OH is the only significant loss process for both reference and sample VOC, it can be shown mathematically that:

$$\ln \frac{[S_o]}{[S_t]} = \frac{K_s}{K_R} \ln \frac{[R_o]}{[R_t]} , \quad (3)$$

where the subscripts o and t indicate concentrations at the beginning of the experiments and at time, t, respectively, and  $K_s$  and  $K_R$  representing rate constants for reactions in equations 1 and 2 above.

Plots of experimental data for  $\ln \frac{[S_o]}{[S_t]}$  vs  $\ln \frac{[R_o]}{[R_t]}$

should yield a straight line with a slope of  $\frac{K_s}{K_R}$  and a zero

intercept. Thus, knowing  $K_R$ , the values of  $K_s$  can be calculated from the slope.

Equation 3, above, implies that the initial concentrations of the sample and reference at  $t=0$  are known. In this investigation another approach was used. The decay curve for both the reference and sample were used to calculate the rate constant of the sample, since the decay curve values are independent of the initial concentration. The reference decay curve ( $\ln R_t$  vs time in seconds) gave the slope of the reference,  $-K_R$ , and the sample decay curve

( $\ln S_t$  vs time in seconds) gave the slope of the sample, -  $K_s$ . From equations 1 and 2 it can be shown mathematically that:

$$\frac{-\text{slope reference}}{-\text{slope sample}} (K_R) = K_s \quad (4)$$

At the end of each run, the Teflon<sup>\*</sup> bag was cleaned by filling it with zero-air containing 1 ppm<sub>v</sub> of O<sub>3</sub> and evacuating it while it was being irradiated. This was followed by a similar process, but this time with 1 ppm<sub>v</sub> of NO added. After these irradiations, the bag was filled and flushed twice with zero-air, and then refilled with zero-air and sampled for traces of organic compounds by GC/MS at the end of the above cleaning treatment, no significant quantities of any original compounds or products of irradiations were observed.

### Results and Discussion

Figures 1 and 2 show typical decay curves for Propene (reference) and 2-Butanone (sample), respectively. The plots are a linear least squares analysis of data. Based on equation 4, above, the average relative rate constant for OH<sup>-</sup> (hydroxyl radical) photodegradation of 2-Butanone, under simulated atmospheric conditions, is reported as  $2.82 \times 10^{-12}$  cm<sup>3</sup> molecule<sup>-1</sup> sec<sup>-1</sup>. Published literature results for OH

degradation of 2-Butanone under simulated conditions (4,5,6) range from  $1.15$  to  $4.5 \times 10^{-12} \text{ cm}^3 \text{ molecule}^{-1} \text{ sec}^{-1}$ .

It is generally accepted that the reaction of OH radicals with simple carbonyls proceeds via H-atom abstraction from the C-H bonds. Thus, the OH radical oxidation of 2-Butanone would be expectd to proceed via the same mechanism as above.

Based on relative rate constant of  $2.82 \times 10^{-12} \text{ cm}^3 \text{ molecule}^{-1} \text{ sec}^{-1}$  and OH atmospheric concentration of  $1 \times 10^6 \text{ cm}^{-3}$ <sup>7</sup> the estimated atmospheric lifetime of 2-Butanone is 4.10 days.

FIGURE 1

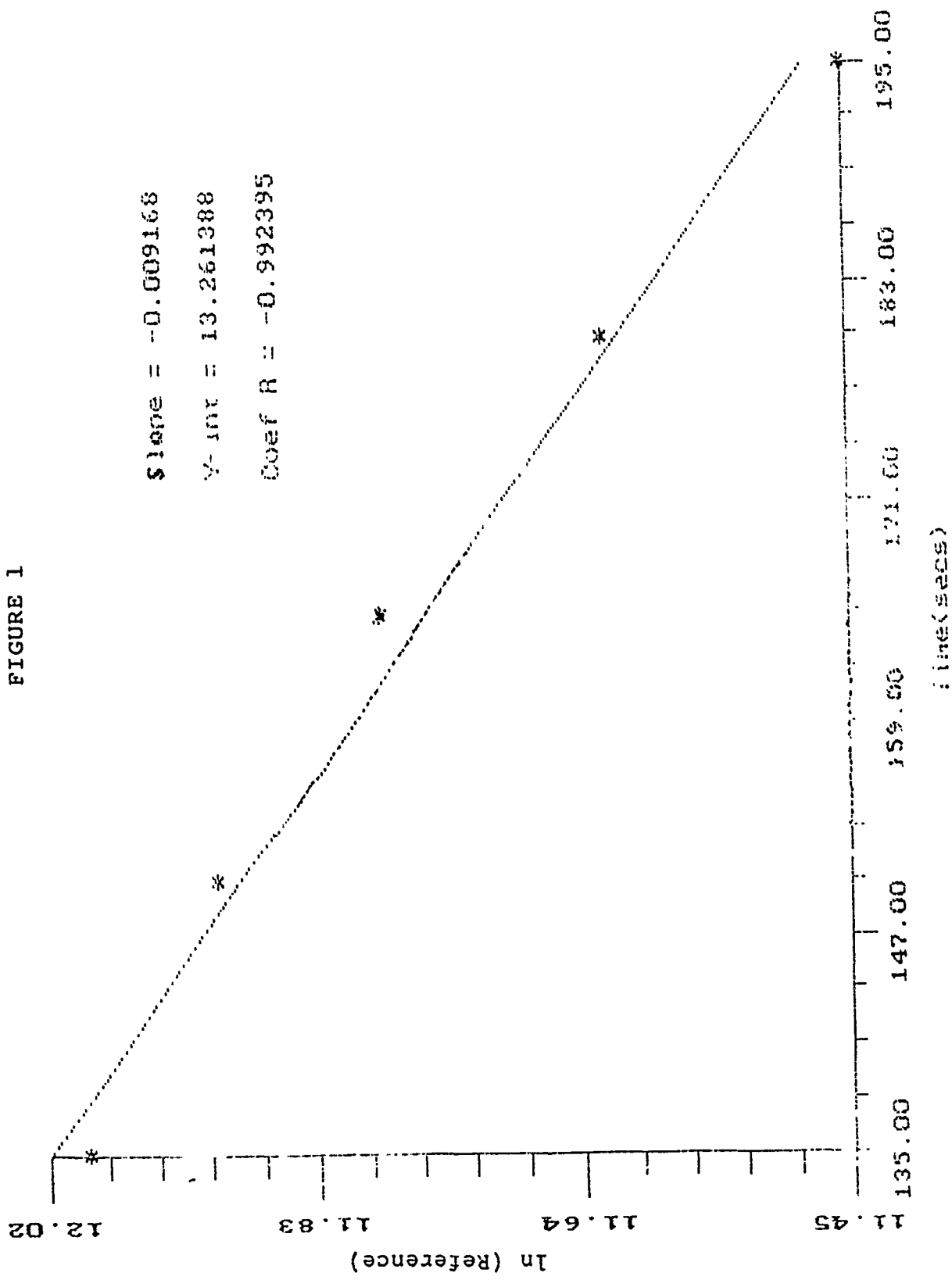
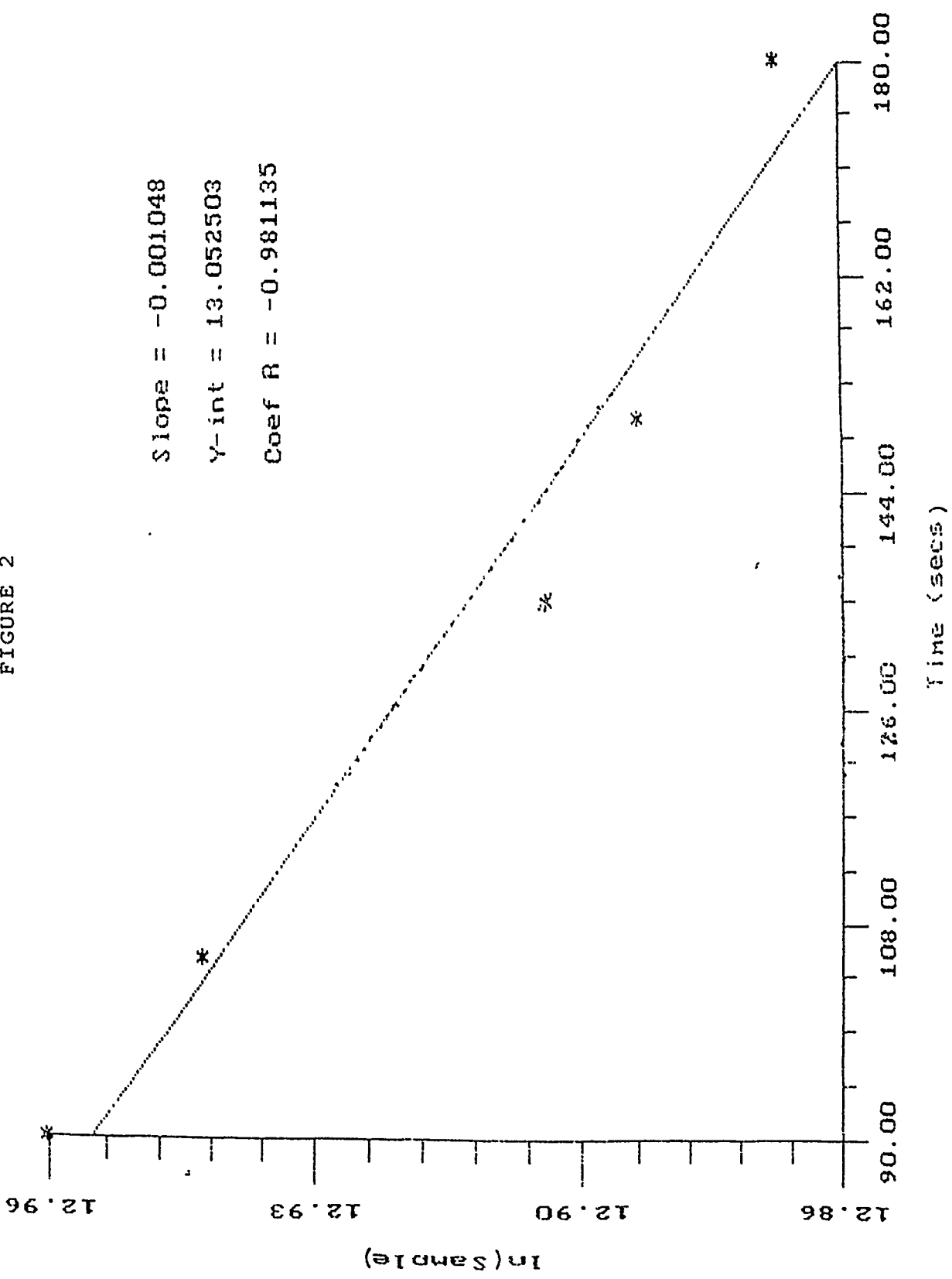


FIGURE 2



## LITERATURE CITED

1. R. Atkinson, Atmos. Environ. 24A (1): pp. 1-41 (1990).
2. R. Atkinson, W. P. L. Carter, A. M. Winer, J. N. Pitts, Jr., J. Air Pol. Control 31 (10): 1090-1092 (1981)
3. R. Atkinson, K. R. Darnall, A. C. Lloyd, A. M. Winer, J. N. Pitts, Jr., Adv. Photochem. II 11, 375-487 (1979).
4. R. Atkinson, Kinetics and Mechanisms of the Gas-Phase Reaction of the Hydroxyl Radical with Organic Compounds, Monograph No. 1, D. R. Lide, Jr., Ed., American Chemical Society, and the American Institute of Physics for the National Institute of Standards and Technology Publication. New York (1989).
5. R. Atkinson, Chem. Rev. 86, 69-201 (1986).
6. H. Niki, P. D. Maker, C. M. Savage, and M. D. Hurley, J. Phys. Chem. 68, 3581 (1978).
7. J. G. Anderson, Geophysics Res. Lett. 3, 165 (1976).

Working at Tyndall Air Force Base

8/30/91

Nirmala Darmarajah

The work I did this summer (1991) at Tyndall Air Force Base, Panama City, Florida, had a great deal of responsibility associated with it. I worked at the Technical Information Center (TIC) in the Air Force Science and Engineering Services Center (AFESC). My mentor was Mr. Andrew Poulis. He showed me the importance and the impact of my work. My job was to enter, into the TIC's cataloguing system, certain records containing Bird Air Strike Hazard (BASH) information. The BASH Team is a group of researchers who monitors and experiments with ways to control bird strikes to airplanes. This issue may seem minor, but about \$20 million dollars or more in damages occur to airplanes each year because of birds being ingested into engines or hitting windshields. Some strikes result in the death of the pilot and possibly the passengers. Since a lot of experimentation is being done to reduce and control bird strikes, it is vital that the scientists have proper and easy access to information concerning their particular experiment. If they cannot easily access pertinent information they may repeat a previously executed experiment. This wastes a great deal of money as well as time. The process in which I put the information into the computer was very efficient and time saving.

First I obtained a record from TIC. The 'records' that I worked with were primarily Bird Strike Committee Europe meetings and the papers presented there. First I would catalogue the actual meeting, by place of meeting and publisher. Then I catalogued each paper presented at the meetings. They were distinguished by title and author. Over the course of the summer

I entered almost 200 records. The first 100 also had abstracts so the researchers didn't have to check out a book and find out that it had little to do with his subject. In addition to cataloguing I also filed reports and conferences on the shelves. I learned to file magazines, check a book out to a person, how to find a book in the computer by using its accession number, and how to edit a record.

This summer was one of the most productive summers I have spent, because I learned the value of cooperation within a closely knit working organization. Everyone's job is important, no matter how small, to keep the organization in well oiled condition.

C.I.A.

PHILIP C. DORCH

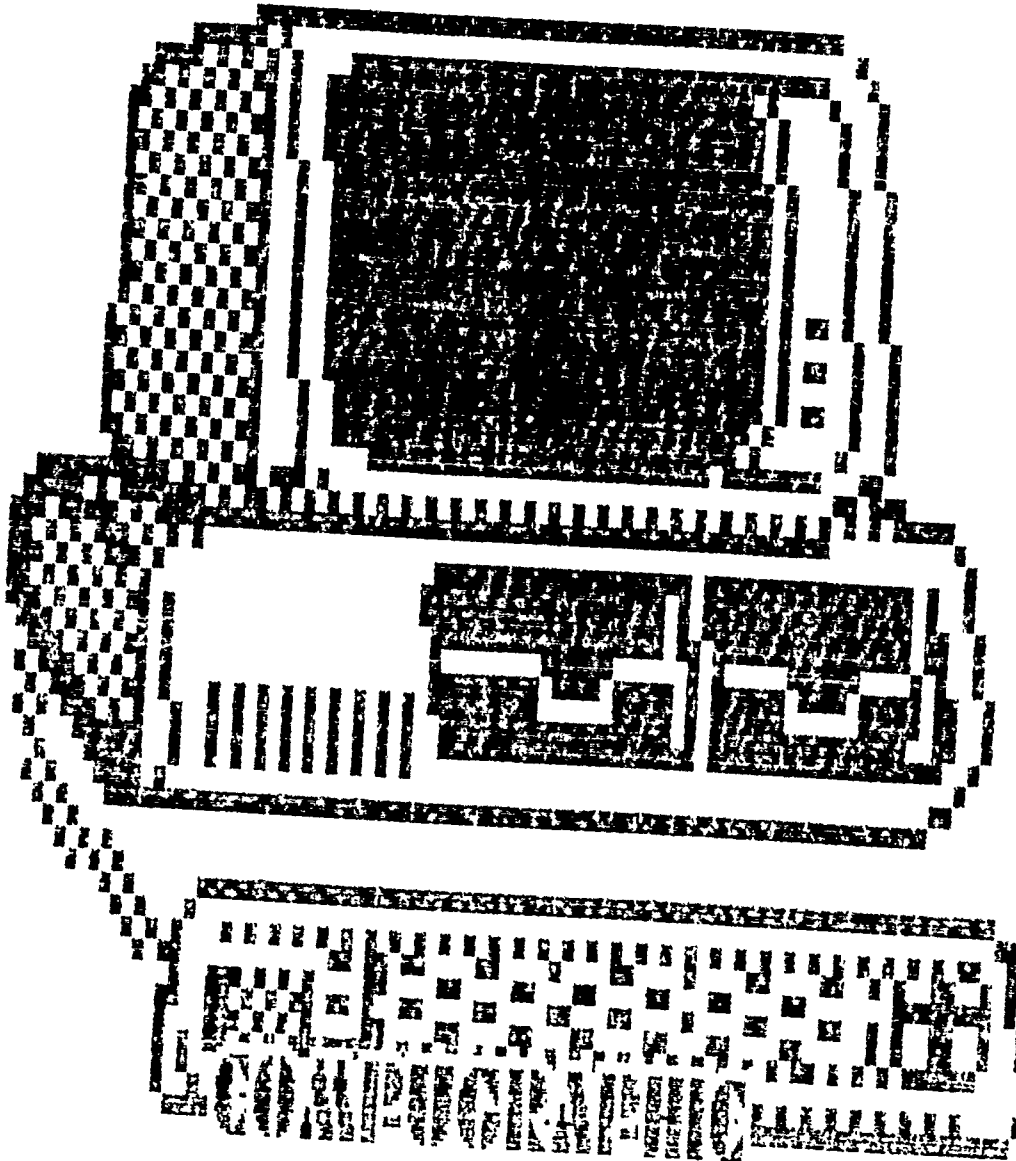


PHOTO BY RAYMOND LEE ROBERTSON FOR THE NEW YORK TIMES

### General Description

A series of tests were conducted on a Compugraphic Integrator in order to find out it's ability at processing top value documents. Each test was conducted under close supervision. The tests consisted of three stages: Draft and Transfer, Typography and Design, Review and Revise. To be able to conduct these experiments, I had to be educated in the proper testing and research procedures required of a personage in my position. I obtained hands-on training for all the equipment which I was to use and spent numerous hours in training. After that, I felt confident that I could perform to the highest of RAXI's standards. We conducted tests and researched this project for about seven weeks. The results of our experiments proved to be important for the Air Force and informative to the public.

Special Thanks To:

Larry Testerman

(Who helped me with my project)

Parry Sullivan

(Who made this job interesting)

Mary Reynolds

(An instructor, friend, and mom)

Teresa Mims

(Who helped me through the hard times - a real honey)

### Problem

The purpose of this study was to test a CGI's (Compugraphic Integrator) capability to produce high performance, high quality material with the potential of mass distribution.

### Detailed Description

Upon arrival at Tyndall Air Force Base, Florida, I was given a general description of what my assignment was to be. I was to work in the Air Force Engineering and Services Center Lab (AFESC) on a project called C.I.A. (Compugraphic Integrators Ability). The project itself consisted of observing, documenting, and testing the Integrator's ability to produce quality documents with superior results.

Instructions on the equipment's use was necessary to proceed with this project. Mr. Parry Sullivan, along with his assistant Ms. Teresa Mims, were the tutors for this task. They instructed the author for three days on the computer. The course consisted of three levels: basic training, the intermediate stages, and the advanced rank. I received hands-on training and in-depth instructions on all the equipment that I would be handling. After my first-rate training was over, I was ready to begin the experiment.

The experiment consisted of three main stages. The first one was under the control of Mr. Larry Testerman and his colleague, Ms. Reynolds. They were in charge of draft and transfer. If the publications required superior design and type they were directed to the Compugraphic Integrator.

Using the CGI for excellant topography and design was the second stage of the experiment. This was headed by Ms. Teresa Mims. We would then produce places for graphics, adjust the topography, and add graphics. This was the

longest and hardest stage of the three. Arranging all the designs and topography to be in just the right place and appear just right was a continuous effort. It required long hours and a lot of work to achieve the final product.

Before the finished product was printed, it went through one final stage, revision and review. The completed product was put on file and transferred to the graphics division of AFESC. They reviewed it, made any final corrections, and added photographs. When they finished checking it, it was ready to be printed and distributed.

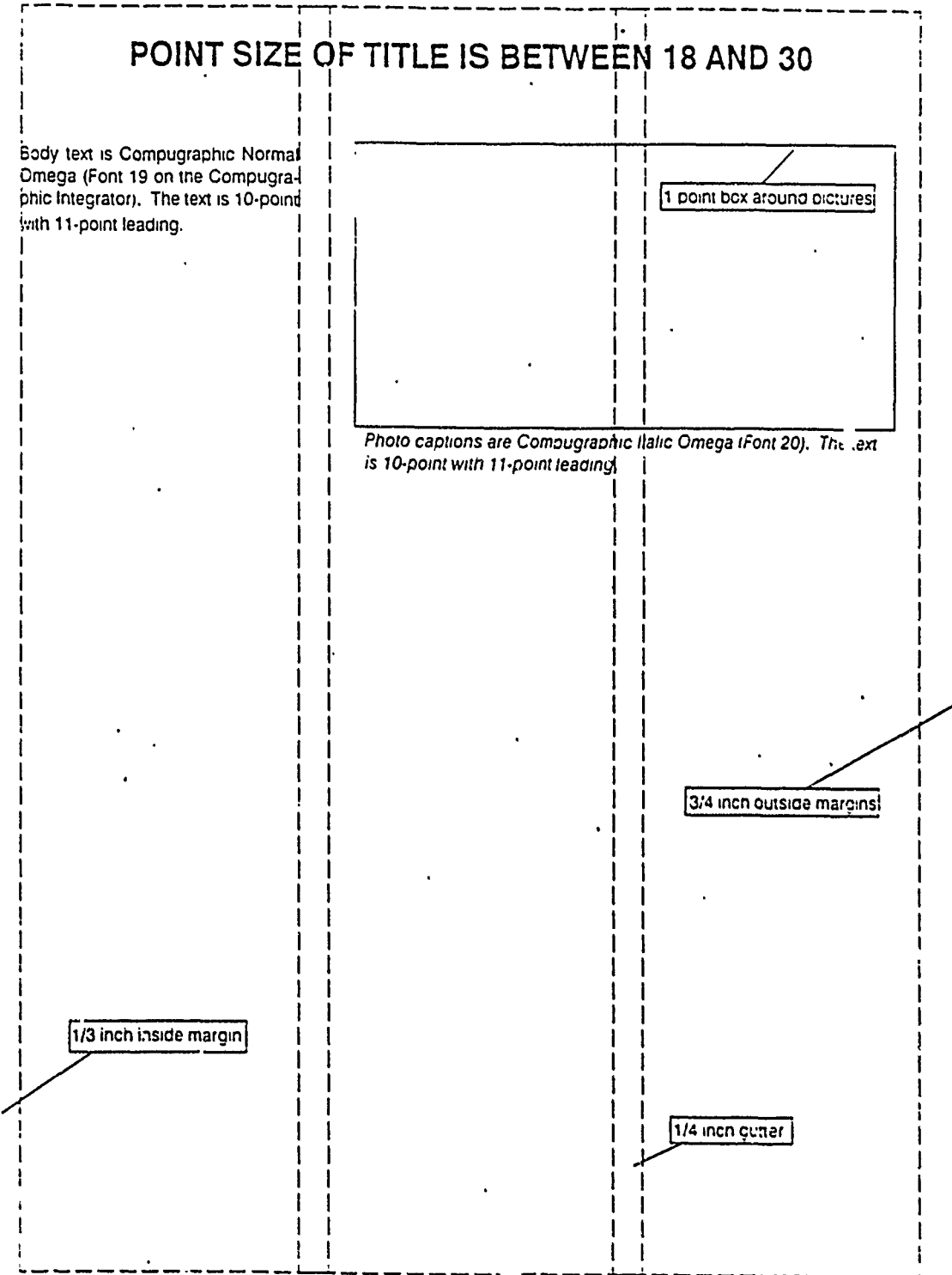
### Results and Conclusions

The Compugraphic Integrator proved its ability to produce high quality documents. The Integrator shows much promise and would be of great value to almost any research laboratory. The Compugraphic Integrator produces high value material, in a short amount of time, with few or no mechanical problems. I Found this project to be exciting and educating. Some of the documents I worked on were UPDATE, ENHANCEMENT TECHNOLOGY, and TECH DATA. This was a great opportunity to see how a part of the AIR FORCE worked, besides flying.

### Other Experiences from the Program

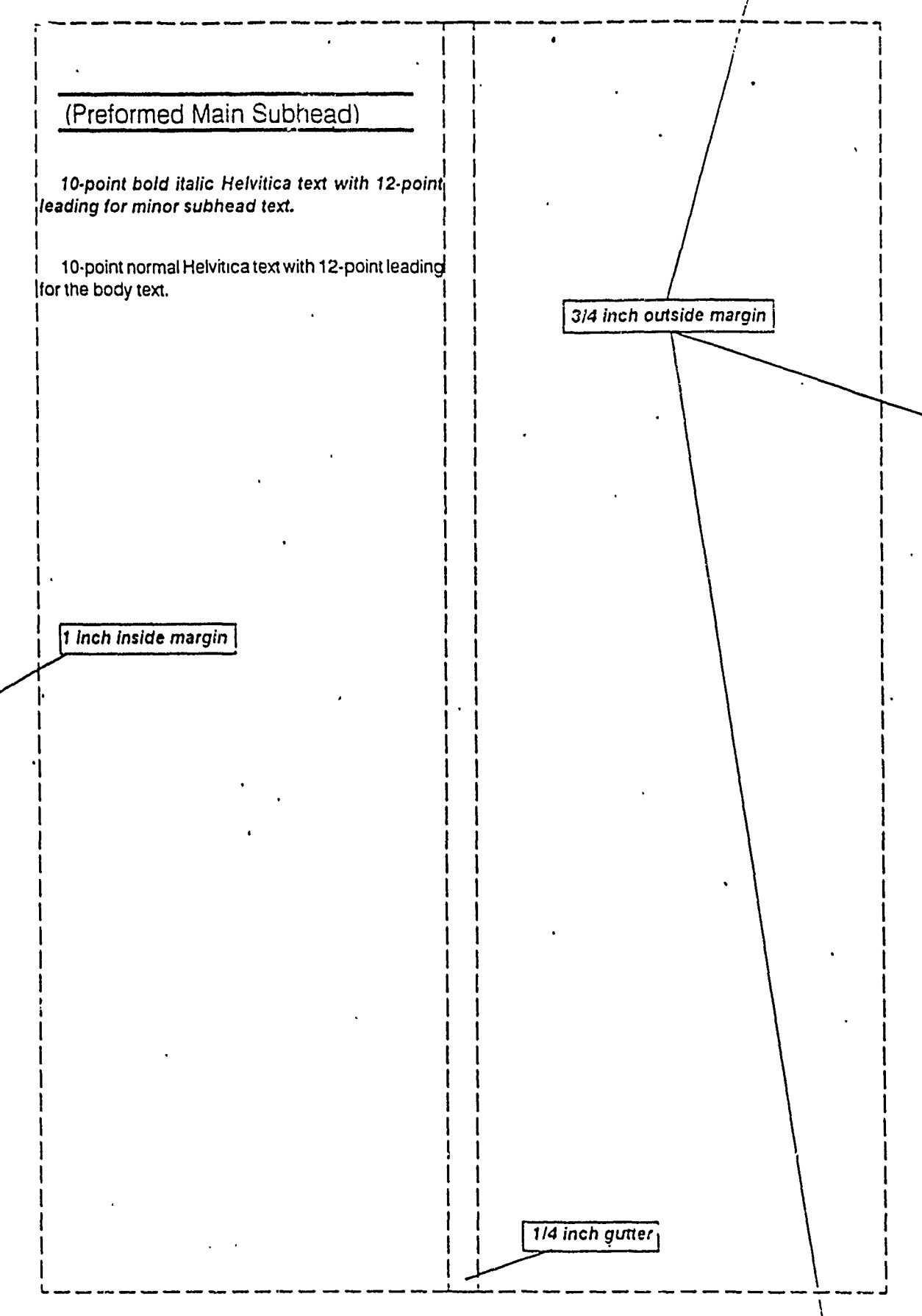
During the summer I was introduced to many aspects of research and engineering in the AIR FORCE. Through the appointment of my mentor, I visited a few other facilities on Tyndall AFB. I was given a detailed tour of the graphics lab at AFESC. I received a trip to the flight which included many lectures on the numerous planes. I went to the military police station and received a tour of their facilities. I also journeyed to all warehouses and supply depots with my associates. The experience and knowledge I have acquired this summer I'll never forget. I truly appreciate all the time and help my colleagues gave me.

Figure 2. Page layout for The Military Engineer



PAGE FOOTER IS COMPUGRAPHIC BOLD OMEGA (FONT21). THE TEXT IS 9-POINT

Figure 1. Page layout for the Technology Area Plan



# *HSAP FINAL REPORT*

JUNE 17 - AUGUST 9, 1991

*RICHARD C. HARTZER*

## HSAP FINAL REPORT

Richard C. Hartzer

This summer, my task as a high school apprentice was to design a program that would use DBase IV databases to print out a list of overdue DTIC summaries. This list will be used to contact the various project officers and inform them of their outstanding summaries. After I finished this program, I worked with Brent Miller barcoding books. With a combined effort, we completed approximately three hundred books.

In the WUIS (Work Unit Information Summary) databases, there are several fields which contain information about the project officer and his task. These databases are delivered to the Air Force Civil Engineering Support Agency where they are processed and entered into the master database. My job was to write a program that would enter this database by way of a query and print out a list of records which had not been updated for a year. This list will be used to notify the project officer of his tardy update. Upon the completion of this program, I worked in the Technical Information Center barcoding books. Barcoding was a tedious task, but the time that will be saved by barcoding far exceeds the time spent working on them.

The DBase IV program is a complex system of databases and utilities. It allows the user to manipulate files and produce queries, reports, and labels. The program I wrote entered a WUIS (Work Unit Information Summary) database and printed the date of the last summary, project title, the

project officer's name, the project officer's rank, and the project officer's office symbol. In order to write this program, I had to become familiar with the DBase IV programming language. But once I had mastered it, the program was written with little trouble.

When activated, my program produces a menu on the screen that gives the operator the choice of printing through the printer or just the monitor. When a selection is made, another menu is activated which gives the operator the choice of printing alphabetically by the project officer's name, or printing by the project officer's office symbol. If the project officer's name is chosen, it prints the listing alphabetically. If office symbol is chosen, another menu appears which lists the various office symbols. Once an office symbol is chosen, the list is printed.

The process of barcoding books required using the Technical Information Center's database to find the item number of the book and replacing it with the number on the barcode. Barcoding allows the librarian to check out books just by scanning the barcode with a light pen instead of wasting valuable time searching for cards and stamping them.

This summer at the Civil Engineering Support Agency has been a productive one. I had a chance to work with computers, and I learned a lot about the technical aspect of the Air Force.

**Long Range Agent Delivery System:  
Summer 1991 Development**

**Prepared By: Thor Johnson (712)  
Submitted To: Research Development Labs and AFCESA/RACF**

The Long-Range Agent Delivery System was designed to launch agent canisters up to 1200 feet in order to extinguish hazardous/inaccessible fires. New Mexico Engineering Research Institute (NMERI) was given the tasks of design, validation, and construction of the prototype.

NMERI's design/validation program was composed of three distinct phases. The Phase I prototype used an air-piston to launch the canisters (Fig. 1). The air piston could launch a fully loaded canister (approx. 15 lbs) 1200 feet when driven by 110 psi. It was found that the air pressure must be increased when using the larger projectile (45 lbs). Beyond 110 psi, the air piston contacted the projectile, resulting in severe damage to both the shell and the launcher. Because this pressure could not fulfill the range requirements, another system was designed.

Phase II revised the design by substituting a fast acting (3ms) butterfly valve and an air chamber for the air piston (Fig. 2). The PGV (Pulsed Gas Valve) system tests indicated that the piston-less system could easily reach 1200 feet at a 40 degree angle of elevation. If the angle was increased to 45 degrees, the maximum range would exceed this figure. Phase III validated the concept of a long-range agent delivery system based on a PGV.

The validation testing necessitated the use of a computerized control system. NMERI chose to use a HP 9825 Data Acquisition/Control Unit for the LRADS controller. The control programs must currently be stored in an off-line computer system that uses the HPIB (IEEE-488) interface bus. The secondary computer that NMERI used was a Hewlett-Packard system running

HP Basic 3.1 or above. The software used for validation is of an elemental nature; it provides functions to operate the relays via menu control, but no "advanced" features were present.

The Long Range Agent Delivery System (LRADS) has been moved to Tyndall AFCESA for further development. Thor Johnson, the summer student, was given the task of improving the LRADS system.

The LRADS system was limited by its accuracy and the time used in the preparation for the next shot. Other problems with the current LRADS system are that it is not fail-safe (the LRADS can fire accidentally) and is unacceptably inconvenient to load. I improved the LRADS software to relieve the inconveniences of loading the shells, and added improved features to the host computer subsystem. The new software is listed in appendix 1. The following hardware improvements can be easily implemented to provide better performance:

1. In order to support multi-tasking, an additional voltmeter must be purchased so that 2 functions can be monitored simultaneously.
2. Because the firing pressure is usually high (greater than 40 PSI), charging time can be reduced by quickly pressurizing the chamber to a high (but only approximate) pressure, then bleeding the chamber pressure down to the desired firing pressure (Fig. 3).
3. It takes 2 to 3 seconds to change the range on the voltmeter, but only a few microseconds to switch inputs. Time is lost in the

switching because many of the circuits on the LRADS system has a different range. The time used in switching ranges can be eliminated by amplifying all inputs so that they have a common range (see Fig. 4 for an example circuit). Electrical noise pickup from the pressure transducer wiring would be greatly reduced if amplified at the transducer (Fig. 5).

4. The Phase III LRADS system suffers from gear slippage in the rapid-loader section. The gear slippage can be eliminated by hypoid or other high-torque gear designs (Fig. 6).
5. Azimuth rotation should be monitored by a take-off on the azimuth motor's gearbox, **not** by the current friction-roller system because the friction take-off exhibits too much slippage, and would be severely crippled in adverse environments (a small film of oil would completely disable the feedback system).

Once these hardware improvements are made, the software will have to be re-written to take advantage of them, or no increase in response time will be noticed.

During testing, it was noticed that the motor and computer power supplies must be operated from separate power supplies unless the power source is far in excess of the surge power ratings, or the computer system will brown-out when either the azimuth or the elevation motor is activated. This was taken int account in the design of the mobile platform.

The mobile platform (Fig. 7) needs to have air and electrical supplies on-board. The proposed air supply is composed of 2 250 cu ft air tanks, each being pressurized to at least 600 psi (the tanks are rated at 2000 psi). Electrical power will be supplied via 2 inverters. An 1800 watt inverter will power the computer/control subsystem, and a 2800 watt (6000 surge) inverter will be used to power the motor drive systems used for positioning the LRADS.

The LRADS system promises to be one of the most useful firefighting concepts available. It provides a simple method for long-range fire extinguishment, and is not limited to any group of agents. The LRADS system will not be obsolete with the development of improved firefighting agents, and therefore has a long effective lifespan.

Figures.

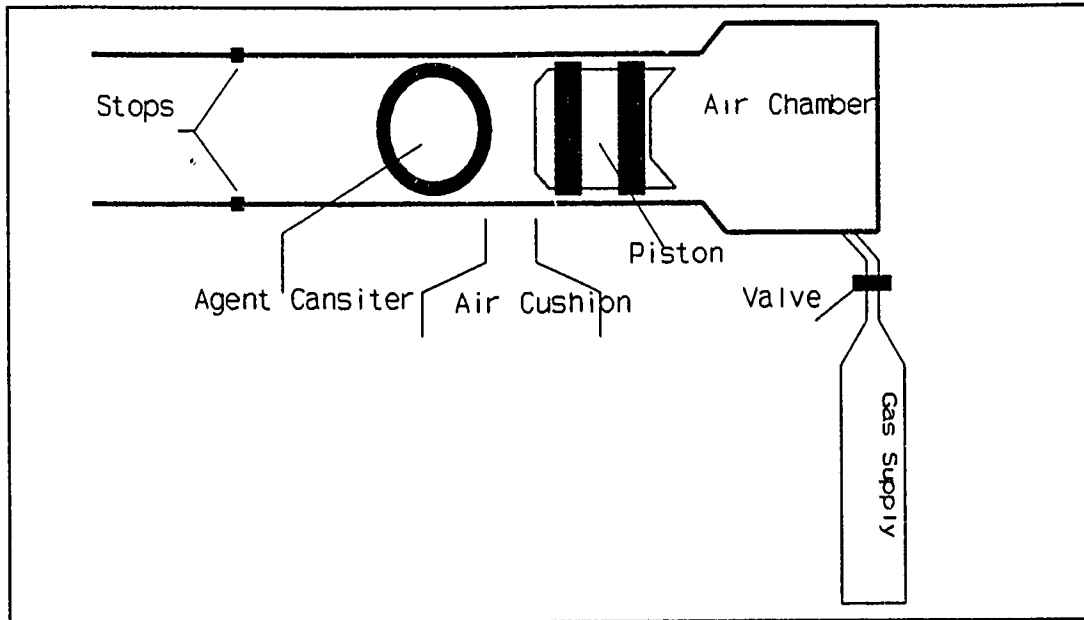


Figure 1. Phase I development.

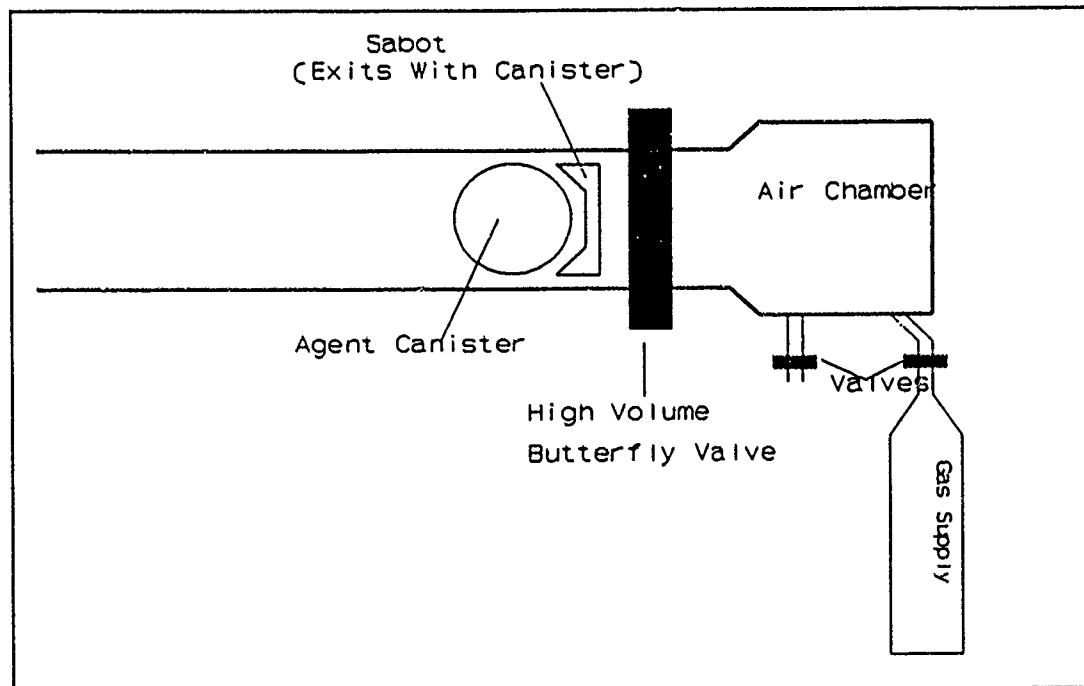


Figure 2. Phase II Air Cannon Development.

## Figures (Cont).

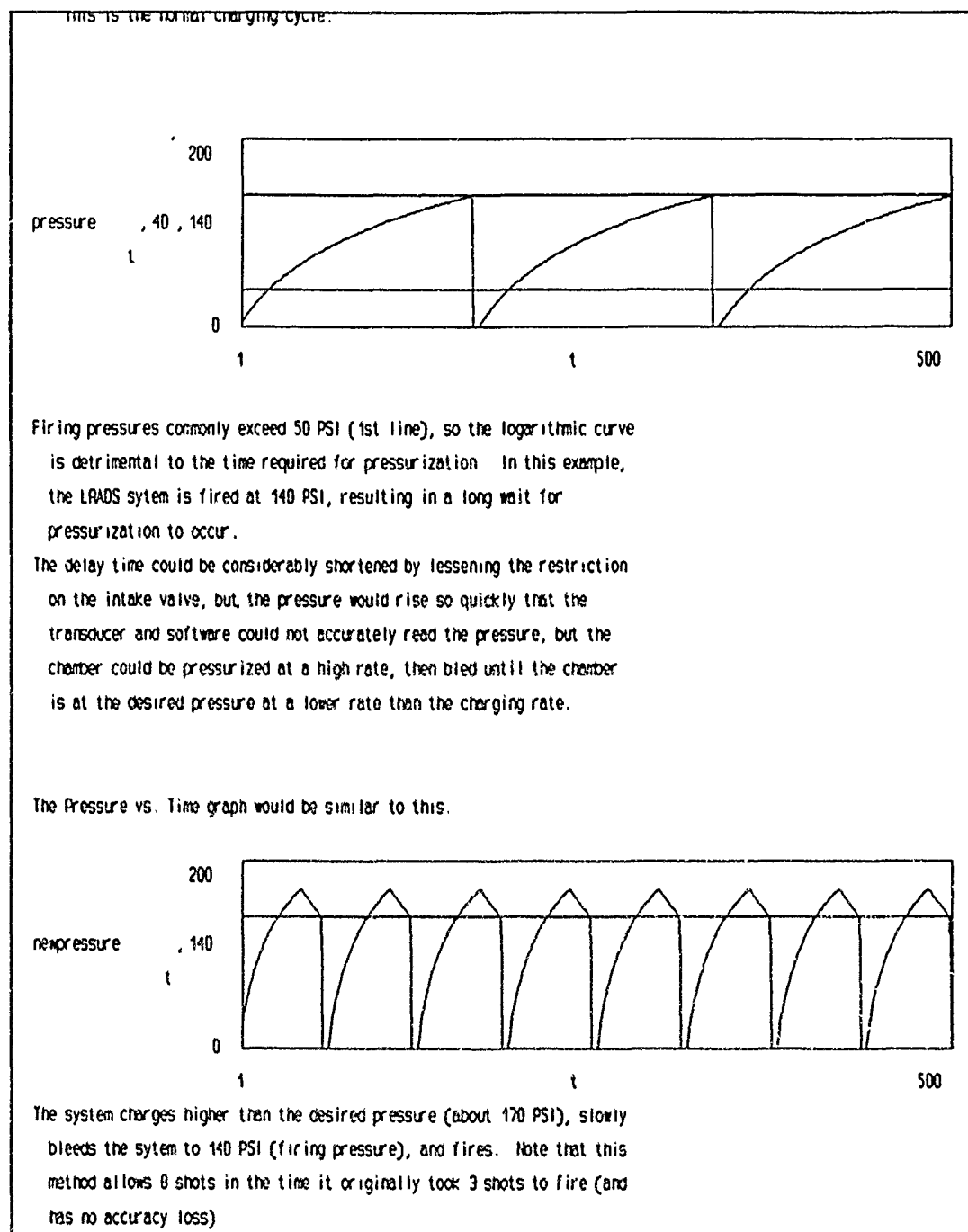
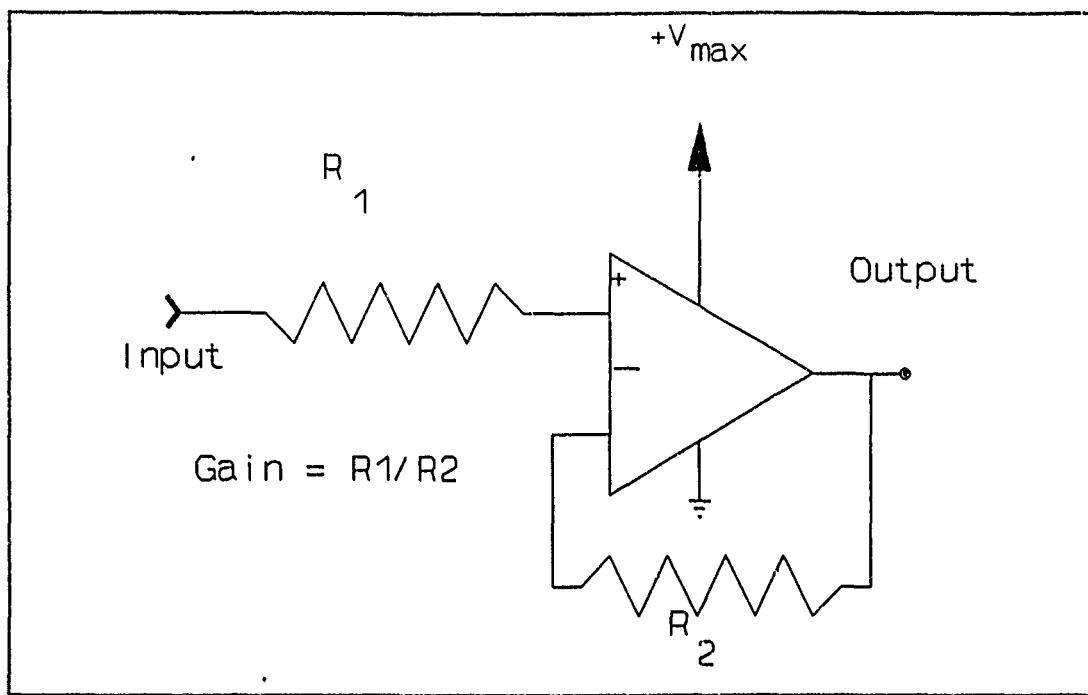


Figure 3. Improved method of pressurizing the chamber.



## Figures (Cont).

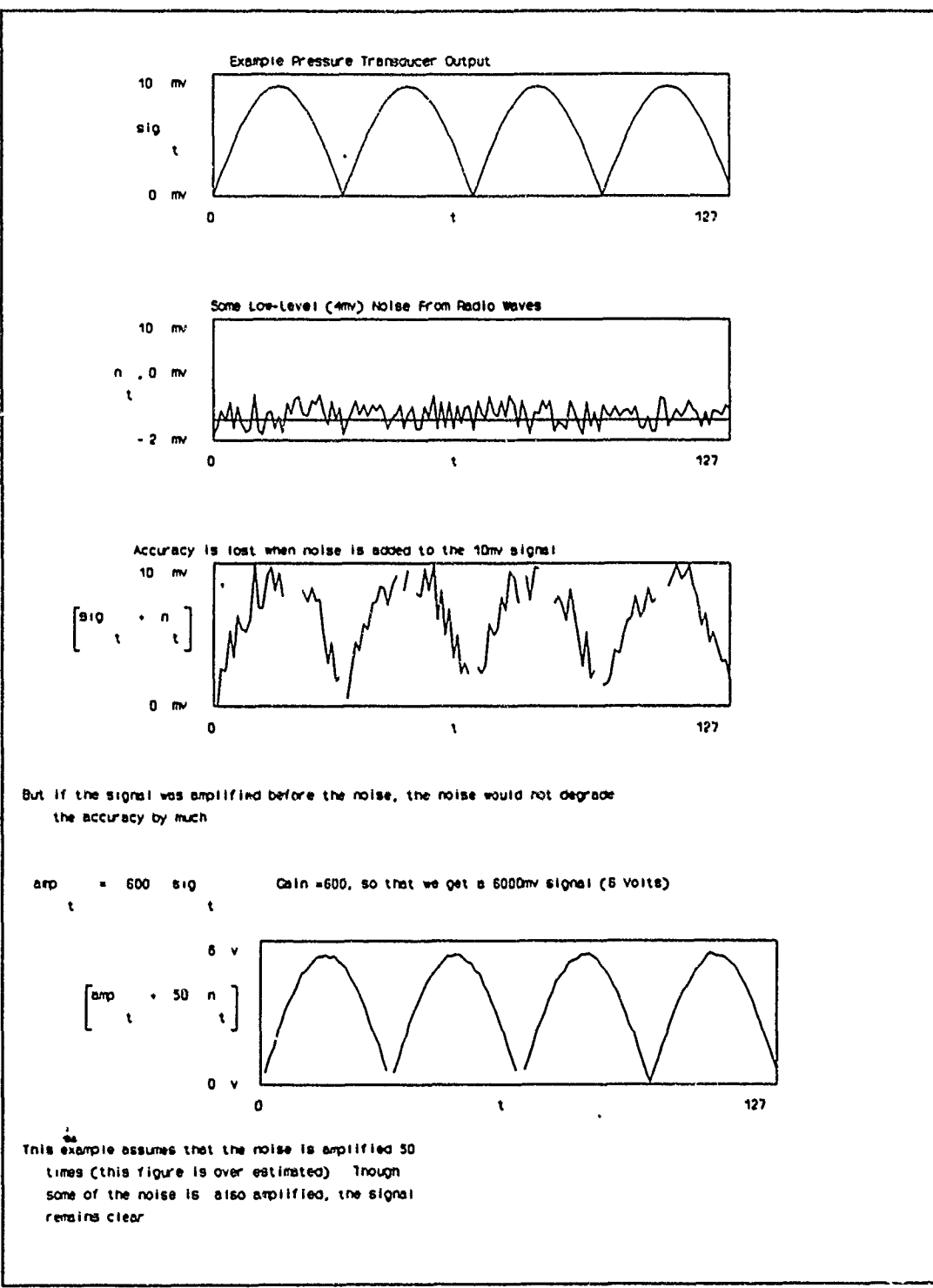
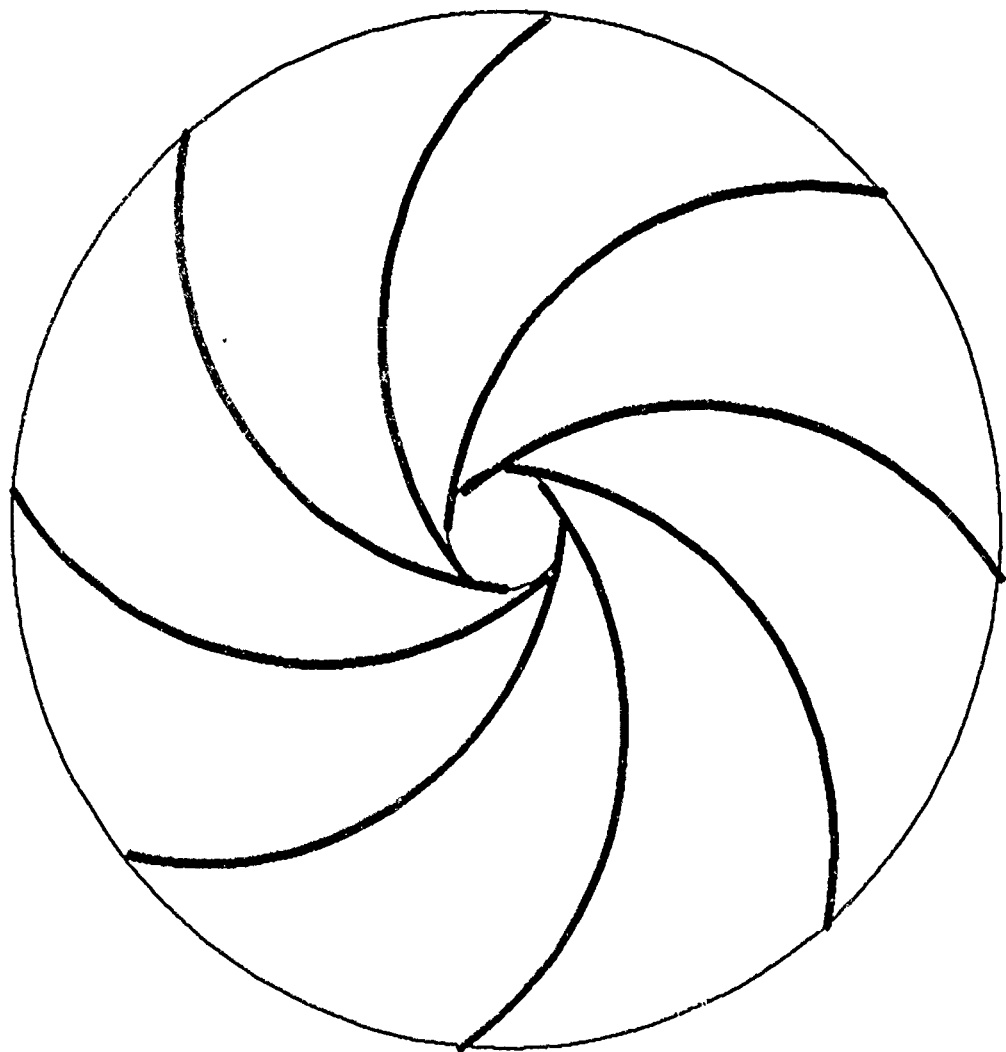


Figure 5. Use of a local amplifier to reduce noise.

Figure 6. Hypoid Gear Mechanism.



(APPENDICES ON FILE AT RDL.)

# **PLASMIDS**

By

Jerome Lindsay  
at

Civil Engineering Laboratory

Plasmids are small circular DNA molecules found inside bacterial cells. Plasmids reproduce every time the bacterial cell reproduces. Once infected, the bacteria will always contain a plasmid. Like all natural DNA plasmids contain a special region in their DNA called an origin of replication. This origin of replication ensures that the plasmid DNA will be replicated by the host cell. One important thing plasmids do is that they often contain genes that make their host bacterial cell resistant to antibiotics which can be extremely useful in genetic engineering.

The first step in obtaining plasmid DNA is to prepare a liquid media that contains billions of cells which contain plasmids. The media gives the cells the all essential nutrients needed to survive.

After a lot of growth is seen on the liquid media the next step is to centrifuge the cells. Centrifuging drives and collects the cells at the bottom of the test tube into a tight pellet. Once finished centrifuging, pour off the liquid media and let cells sit to air dry. Once the cells are dry resuspend them in 700 ul of STET. STET is composed of sucrose, triton X100, EDTA, and Tris. Each part of STET performs a certain task. For example, the sucrose found in STET keeps the cells intact so that the plasmid DNA will come out of the cell gently. Next, the Triton X100 is a detergent that helps break up the cells. The EDTA binds metallic ions which stop any enzymes from degrading the DNA. Finally, the Tris acts as a buffer which prevents change in pH.

After adding the STET vortex test tube briefly and add 50 ul, 5 mg/mL lysozyme. Basically, all the lysozyme does is break up the cell wall.

Next, boil the test tube for 45 seconds. After boiling there will be a white, gooey substance. That substance contains the cell wall, cell membrane, and attached to the cell membrane are the genomic DNA. Immediately centrifuge the test tube. When the centrifuging is done, remove the gooey substance with a toothpick and the remaining liquid will be the plasmid DNA in solution.

Then add equal volumes of isopropanol. The isopropanol takes the plasmid DNA out of solution. Mix the isopropanol by inversion and place test tube in -20°C freezer for 30 minutes.

Once the 30 minutes are up centrifuge the test tube again. Pour off the supernatant and rinse the pellet with 95% ethanol. Centrifuge the test tube again and pour out the ethanol. Then resuspend the pellet in 75 ul of TE. TE is composed of Tris and EDTA. The Tris acts as a buffer and prevents change in pH, while the EDTA stops any enzymes from degrading the DNA. Let the plasmids sit at room temperature for at least 1 hour.

While the plasmids are going into solution a one percent gel can be made up. The gel consists of one gram of agarose, 100 ml of IXTBE buffer and 10ul of ethidium bromide. Only add the ethidium bromide when the gel is cool. Once the ethidium bromide is added let the liquid sit until it turns into a gel.

The final step of isolating plasmids is electrophoresis. The gel has a number of separate wells. In the wells the plasmids are placed and then put into the electrophoresis unit. During electrophoresis an electric current runs through the gel pulling the plasmids from a negatively charged pole to a positively charged pole. The smaller the plasmids the quicker they will migrate to the other pole and the larger the plasmids the slower they move.

# *HSAP FINAL REPORT*

June 17 - August 9, 1991

*Brent Miller*

## HSAP FINAL REPORT

Brent Miller

This summer, my job was in the Technical Information Center, at the Air Force Civil Engineering Support Agency (formerly known as the Air Force Engineering and Services Center). My task included helping Mr. Andrew Poulios compile statistics for the Center's budget. This was accomplished with the help of the Supercalc V Spreadsheet Program. I used the spreadsheet to calculate money spent on different on-line services, books, periodicals, and subscriptions. After my part in this project was finished, I helped to convert part of the library's inventory of books over to a system of computerized "barcodes". This was necessary in order to simplify the checkout and return process of the library. Because of these two tasks, there were few times during this work period that I had nothing to do.

### INTRODUCTION

The statistics that were to be compiled were a part of the Annual Library Report to be done for HQ Military Personnel Center at Randolph AFB. The statistics consist of the prices of books, microforms, subscriptions, periodicals, on-line modem services, etc. bought during that particular fiscal year. The on-line services are used to search for books and bibliographies through the computer modem. My task was to simplify the process of keeping these records.

My other project over the course of this summer was to begin to convert the library over to a system of

"barcodes". The system of barcodes is used because of the accuracy and simplicity of checking books in and out, without cards to deal with. Before, one was forced to enter data into the computer along with keeping track of the cards for the books. Now, the complete task can be completed by scanning the barcode with a light pen.

In order to complete the statistics for the Annual Library Report, I used the Supercalc V Spreadsheet program. The statistics were difficult to set up in a single report because of the complexity of the information. The forms that the information was taken from were often several pages long, unclear, and most of the time, too indepth for a beginner to understand. Mr. Pouli is was helpful in deciphering the forms, but there were times when he was either out of town or busy, therefore leaving me to figure out the forms for myself, or moving over to another temporary project until my questions could be answered. The only easy part of the entire project was the fact that I had worked with spreadsheets the previous summer, but it still was a different program and a more difficult assignment. The statistics won't be completed for quite a while, though, because of the fact that the numbers for the next few months must also be included in the report. This task suited me because it involved having to continually ponder over how to design parts of the program to make sure that they do exactly what I want them to do. The following job was much less exciting, and much more tedious.

The beginning of the barcoding was accomplished by a fellow student and myself over a period of four weeks.

During this period, we barcoded between three and four hundred books. The process involved moving back and forth between the BASIS database and the OLIVE system. The barcoding was done by finding the two records for each book (catalogue and circulation), then changing the itemnumbers and circulation numbers to the barcode number. Different steps in this process required us to be in different parts of the databases, therefore taking a sizable amount of time. Our work, though, saved an enormous hassle for the people who have to check books in and out.

#### CONCLUSION

The experience that I had this summer could not have even nearly been equaled by any other job that I qualified for. The practical lessons I have learned in computers and organization will last me for a lifetime. I honestly hope the projects that I worked on will help the people that I worked so hard for.

# FINITE ELEMENT PRE-PROCESSING, ANALYSIS, AND POST-PROCESSING ON A 3-DIMENSIONAL GRAPHICS WORKSTATION

Jonathan M. Protz

## ABSTRACT

This project uses a Silicon Graphics Personal Iris 4D/35 three-dimensional graphics workstation for finite element analysis by HQAFESC/RDCM at Tyndall AFB, Florida. The project attempts to use the Personal Iris for graphic pre- and post-processing of finite element data. The ADINA series of finite element analysis programs were used. The source code for the software was downloaded from a Cyber mainframe using Kermit protocol and was modified for use on the Personal Iris. The end result was a system which was capable of doing pre- and post-processing. However, there were software conversion problems which prevented using ADINA on the Personal Iris for actual finite element analysis. Also, the ADINA-IN is command based rather than graphic based. There were also major limitations on the ability of the Personal Iris and Cray to communicate. As the project proceeds, these difficulties will be ironed out. One promising option lies in IRIS Explorer graphic-based program development software which could be used to write graphic-based pre-processing and analysis programs that are compatible with ADINA. As these setbacks are overcome, the Personal Iris will become a valuable tool for finite element analysis.

## INTRODUCTION

A major part of the engineering and design process involves experimentation to determine why a problem occurs or whether a proposed solution will work. However, it is not always practical to perform experiments for reasons such as high cost, limited time, or numerous variables. Computer analysis and modeling can provide a practical means of performing tests which would otherwise be impractical. This project deals with computerized finite element analysis being done by HQAFESC/RDCM at Tyndall AFB, Florida.

## PROBLEM

Prior to this project, RDCM did its finite element analysis using ADINA software on a Cray-YMP supercomputer located at Eglin AFB and on a Cyber 830 mainframe computer located at Tyndall AFB. Both are accessed through dial-in modem connections from a dumb terminal or PC. This method is not ideal. Dumb terminal connections limit the user's ability to view and graphically manipulate the complex models generated by the finite element analysis program.

## PROCEDURE

To allow a user to graphically work with finite element data, this project uses a Silicon Graphics Personal Iris 4D/35 graphics. The Personal Iris is to be used mainly for pre- and post-processing of finite element data, although it will also be used for processing small jobs. The Personal Iris is an Unix-based

machine designed for manipulating and animating three-dimensional models in real-time. Currently, it is the only brand of computer that ADINA supports for animation. It is also capable of displaying Postscript images on screen, allowing the user to produce and preview images which can then be sent to a Postscript printer. These properties make the Personal Iris a good choice for pre- and post-processing of finite element data.

In addition to the standard hardware and software, the Personal Iris workstation used in this project is equipped with the following:

\* Hardware

- \* 24 Megabytes RAM
- \* 1.2 Gigabyte Hard Disk Drive
- \* 150 Megabyte 1/4" Tape Drive
- \* Turbo Graphics option
- \* Z-buffer (for in-hardware hidden line removal)
- \* Hayes V-Series Smartmodem 9600

\* Software

- \* Silicon Graphics Software Development Kit
- \* FORTRAN

The Silicon Graphics Personal Iris was set up as instructed in the Personal Iris Owner's Guide. All software was installed. Initial problems with the installation of FORTRAN and the Development Kit were overcome when a manual installation, rather than an automatic installation was done. Once the basic software installation was complete, the Personal Iris was setup for

communicating with the Cyber and Cray.

The Personal Iris was setup for communicating with Cray and Cyber via CDCNET, a distributed communications network controlled by the Cyber. The connection to the CDCNET was made through a Hayes 9600 bps modem connected to serial port #2. The communications software used was C-Kermit. The source code for C-Kermit comes with the 4Dgifts package on the Program Development Kit tape. It was compiled as directed in the "/usr/people/4Dgifts/kermit/README" file. Before C-Kermit could be installed, however, the directory "/usr/local/bin" had to be created. The communications options of C-Kermit were set appropriately in the ".kermrc" file for communicating with the Cyber. A listing of the required setting and of the ".kermrc" file can be found in appendix A. C-Kermit was run in an "xterm" window which was set up to emulate a VT102 terminal. The connection was tested, and a series of script file were written to automatically setup and execute kermit in an "xterm" window. The code for these script files can be found in appendix B.

Once the Personal Iris was set up for communications, ADINA source code was downloaded from the Cyber. The first source code that was downloaded was that of ADINA-PLOT version 4.0. In addition, the source code for a program called "plcomm", which modifies the source code for use on various systems was downloaded. Once the ADINA-PLOTv4.0 and plcomm source-code was downloaded, plcomm was compiled using the "f77" FORTRAN compiler. The ADINA-PLOTv4.0 file was then split into separate subroutines

using the "fsplit" Unix command. Next, a "makefile", which instructs the make command how to compile a program, was made. Here, there were a number of difficulties. The format for a FORTRAN makefile was not the same as the format for a C makefile given in the online manual entry for "make". Through trial and error, the correct format for the FORTRAN makefile was determined. A description of the FORTRAN makefile format can be found in appendix C.

With the makefile written, ADINA-PLOTv4.0 was compiled. Before the program would work correctly, a number of problems had to be fixed. They are as follows:

- \* The -G 3 compiler option had to be used to prevent common block errors.
- \* The subroutines ADTIME and GETDAT had to be rewritten. The rewritten source code to these files can be found in appendix D.
- \* The first line of the subroutine MAIN.f must look as follows:

#### PROGRAM MAIN

- \* Line 56 of the subroutine ASYMB.f must have "W" in place of "N".
- \* The size of the blank common block must be changed from 500000 to a large number such as 3000000.

Once ADINA-PLOTv4.0 was compiled and running correctly, the executable file was placed in the directory "/usr/local/bin/adina". A script file, "ADINAPLOT4\_0", that runs files on ADINA-PLOT was downloaded from the Cray, and placed in the directory "/usr/local/scripts". A plot file was downloaded, and ADINA-PLOTv4.0 on the Personal Iris worked successfully.

With ADINA-PLOTv4.0 operating successfully, ADINA-IN version 3.0 and ADINA-PLOT version 4.0.2, which is capable of doing animation, were downloaded, compiled, and installed. The same corrections needed for ADINA-PLOTv4.0 to run successfully were also needed for ADINA-IN to run, with the exception that line 48, rather than line 56, of the ADINA-IN subroutine ASYMB needed correction. Also, the script file "ADINAIN3\_0" was used in place of the script file "ADINAPLOT4\_0". An ADINA-IN file was downloaded, and ADINA-IN worked successfully.

ADINA-PLOTv4.0.2 was installed following the same procedures as ADINA-PLOTv4.0.2. The same corrections were required, and the extra subroutines of ADINA-PLOTv4.0.2 were added to the makefile. ADINA-PLOT version 4.0 was deleted, and version 4.0.2 was put in its place. ADINA-PLOTv4.0.2 was then compiled and successfully run. With both ADINA-PLOTv4.0.2 and ADINA-IN working correctly, the Personal Iris became fully capable of doing pre- and post-processing of finite element data.

To give the Personal Iris the capability to do finite element analysis calculations in addition to pre- and post-processing, the ADINA program was downloaded from the Cyber. However, unlike the ADINA-PLOT and ADINA-IN source codes, the ADINA source code could not be modified to work on the Personal Iris. As a result, major modifications to the source code were required. As of the time of this report, these modifications have not yet been made. Thus, the Personal Iris cannot yet do finite element analysis in addition to pre- and post-processing of finite element data.

As a last step, to make ADINA-IN and ADINA-PLOT user-friendly on the Personal Iris, an easy to use interface based on interactive script files and the Buttonfly modifiable graphic interface provided with the Personal Iris system software. The Buttonfly interface calls the various interactive scripts, which in turn call the ADINAIN3\_0 and ADINAPLOT4\_0 scripts with the appropriate .in or .plot files as arguments. The Buttonfly interface is called by a script file called "Adina" that is placed in the Workspace. This script file is a modified version of the "buttonfly" script found under the "/usr/demos" directory, and it can be executed by double-clicking its icon. The code for the "Adina" script, the buttonfly ".menu" file, and the interactive scripts are in appendix E.

## RESULTS

The Personal Iris was able to be used for pre- and post-processing of finite element analysis data. Both ADINA-IN and ADINA-PLOT ran successfully. In both cases, the user was able to manipulate his view of the model quickly and easily. ADINA-PLOT version 4.0.2 was capable of animating the models. It was also able to produce Postscript files for output to a Postscript printer.

The attempt to do actual finite element analysis was not successful at the time of this report. The ADINA apparently requires some difficult modifications, however the modifications are not impossible, and ADINA will eventually be operable.

Communications abilities are only moderately successful. File transfers

between the Personal Iris and the Cray cannot be performed directly. The Cray cannot directly transfer files to the Personal Iris because it lacks Kermit communication protocol, and RDCM does not currently have a network connection to the Cray. Files must be transferred from the Cray to the Cyber and then from the Cyber to the Personal Iris. Also, Kermit file transfers are slow, having an effective transfer rate in the area of 1200 bps on a 9600 bps modem.

## CONCLUSION

The Personal Iris is capable of pre- and post-processing finite element data using ADINA-IN and ADINA-PLOT. ADINA-PLOT does provide the ability of graphic post-processing of finite element data. Its animation capabilities are also useful. Although ADINA-IN does provide pre-processing capabilities, they are command based, and it is therefore not as useful as a graphical preprocessor would be. Also, the restrictions of Kermit and modem communications prevent the workstation from using its full potential.

As this project proceeds to reach its full potential, a number of areas will be improved. ADINA will need to be modified to work of the Personal Iris. Also, a graphical pre-processor which is compatible with ADINA will make pre-processing faster and easier. Faster communications that allow the Personal Iris to communicate directly with the Cray, without the use of Kermit, will also be needed. Such communications would enable the Personal Iris to directly work with the analysis programs as they run on the Cray.

One avenue for meeting these needs exists in the new Silicon Graphics program IRIS Explorer. This program, which will be included in the Silicon Graphics 4.0 software upgrade, allows users to create applications involving through point-and-click selection rather than traditional menus. Explorer makes it easy to use the SGI Graphics Library. It would be possible to build a graphic based finite element program set up to be compatible with ADINA and which would allow, among other things, graphically manipulated pre-processing and real time visualization. As these solutions are developed, the Personal Iris will grow to be a valuable tool for finite element analysis.

## **APPENDIXES**

## APPENDIX A

### KERMIT COMM PARAMETERS

C-Kermit, 4E(072) 24 Jan 89, AT&T System III/System V, Communications Parameters:

Line: /dev/ttyd2, speed: 9600, mode: local, modem-dialer: direct  
Bits: 7, parity: even, duplex: half, flow: xon/xoff, handshake: none  
Terminal emulation: 7 bits

Protocol Parameters:	Send	Receive
Timeout:	10	7
Padding:	0	0
Pad Character:	0	0
Packet Start:	1	1
Packet End:	13	13
Packet Length:	90	94
Length Limit:	2048	1024

#### File parameters:

File Names:	converted	Debugging Log:	none
File Type:	text	Packet Log:	none
File Warning:	off	Session Log:	none
File Display:	on	Transaction Log:	none

### ".kermrc" C-KERMIT SETUP FILE

```
set line /dev/ttyd2
set speed 9600
set parity even
set flow xon/xoff
set duplex half
set receive packet-length 94
```

## **APPENDIX B**

### **"Kermitinit" SCRIPT FILE**

```
su root -c "/usr/people/charlie/Kermitscripts/Kermitx"
```

### **"Kermitx" SCRIPT FILE**

```
xterm -e /usr/people/charlie/Kermitscripts/Kermitgo
```

### **"Kermitgo" SCRIPT FILE**

```
/usr/people/charlie/.kermrc  
/usr/local/bin/kermit
```

## APPENDIX C

### FORTRAN MAKEFILE FORMAT

```
pgm_name: list of subroutines as .o files
    f77 *.o [-options] -o pgm_name
subroutine1.o:
< tab >f77 -c [-options] subroutine1.f :
subroutine2.o:
< tab >f77 -c [-options] subroutine2.f :
subroutineN.o:
< tab >f77 -c [-options] subroutineN.f :
```

## APPENDIX D

### ADTIME.f SOURCE CODE

```
SUBROUTINE ADTIME(TIM)
C*----- ADTIME
C
C      TO RETURN THE ELAPSED CPU TIME
C
C          C O M M O N      / C N T R L C /
C          EPS,DEGRAD,NFREAD,NFECHO,NFLOG,NFLIST,NFPORT,
C          1_IERROR,IERRCO,IERRAC,LIMERR,NERRCM,IBATCH,NBSU,
C          2
C          LSTALL,LSTIME,LSTF,LSTDB,LSTM,NFRSAV,NPOSAV,LINPAG,LISKEW
C
C          real tarray(2)
C          REPLACED EXTERNAL REFERENCE TO SECOND WITH UNIX
C          COMPARABLE COMMAND
C
C          EXTERNAL SECOND
C
C          TIM=0.0
C
C          TIM=SECOND()
C
C          TIM=dtime(tarray)
C          RETURN
C          END
```

## APPENDIX D

### GETDAT.f SOURCE CODE

```
SUBROUTINE GETDAT(IDAY,IMONTH,IYEAR)
C*----- GETDAT
C
C      TO RETURN THE CURRENT DATE AS THREE INTEGERS
C      FOR EXAMPLE (15,6,1987)
C
C          C O M M O N      / C N T R L C /
EPS,DEGRAD,NFREAD,NFECHO,NFLOG,NFLIST,NFPORT,
1 IERROR,IERRCO,IERRAC,LIMERR,NERRCM,IBATCH,NBSU,
2
LSTALL,LSTIME,LSTF,LSTDB,LSTM,NFRSAV,NPOSAV,LINPAG,LISKEW
C
C*I GETDAT
CHARACTER*10 DATE,CDATE
C
IDAY=0
IMONTH=0
IYEAR=0
C
C*I GETDAT
C
C
C      CDATE=DATE()
C      READ(CDATE,8020) IYEAR,IMONTH,IDAD
C
C      ADDED THESE UNIX SPECIFIC DATE CALLS
C
CALL IDATE(IMONTH,IDAD,IYEAR)
C
C
GO TO 900
C
800 CONTINUE
IERROR=1
900 CONTINUE
RETURN
C
C*I GETDAT
8020 FORMAT (I4,1X,I2,1X,I2)
END
```

## APPENDIX E

### "Adina" SCRIPT FILE

```
#!/bin/sh  
/usr/demos/bin/buttonfly /usr/people/charlie/adinadata/.menu
```

### ".menu" BUTTONFLY SETUP FILE

```
.backcolor..10 0.0 .10  
.color.0.0 .80 0.0  
.highcolor.0.0 1.0 0.0  
ADINA-IN  
    wsh -C 7,4,3,2 -s 80,24 -f Iris9 -t ADINA-IN -c  
/usr/local/scripts/ad_inquestion  
ADINA  
    .color.0.0 .30 0.0  
    .highcolor.1.0 0.0 0.0  
ADINA-PLOT  
    wsh -C 7,4,3,2 -s 80,24 -f Iris9 -t ADINA-PLOT -c  
/usr/local/scripts/ad_plotquestion
```

## APPENDIX E

### "ad inquestion" INTERACTIVE SCRIPT FILE

```
#!/bin/csh
clear
echo 'The default directory for ADINA-IN'
echo 'files is: ' ~/adinadata
again:
    echo
    echo 'Type in a different directory or <CR> for default'
    set direc=($<)
    if ($direc == "") set direc=~'/adinadata'
if (! -d $direc) then
    echo
    echo 'This is not a valid directory'
    goto again
endif
cd $direc
echo
pwd
echo
ls *.in
morefile:
    echo
    echo 'Type the name of the file you want, <CR> for a new directory,' 
    echo 'or "quit" to quit ADINA-IN'
    set fnm=($<)
    if ($fnm == "") goto again
    if ($fnm == "quit") exit
set fnm=$fnm:r'.in'
if (! -e $fnm) then
    echo
    echo 'This is not a valid file'
    goto morefile
endif
echo
/usr/local/scripts/adinain3_0 $fnm:r
```

## APPENDIX E

### "ad\_plotquestion" INTERACTIVE SCRIPT FILE

```
#!/bin/csh
clear
echo 'The default directory for ADINA-PLOT'
echo 'files is: ' ~/adinadata
again:
    echo
    echo "Type in a different directory or <CR> for default"
    set direc=($<)
    if ($direc == "") set direc=~'/adinadata'
if (! -d $direc) then
    echo
    echo 'This is not a valid directory'
    goto again
endif
cd $direc
echo
pwd
echo
ls *.plot
morefile:
    echo
    echo 'Type the name of the file you want, <CR> for a new directory,' 
    echo 'or "quit" to quit ADINA-PLOT'
    set fnm=($<)
    if ($fnm == "") goto again
    if ($fnm == "quit") exit
set fnm=$fnm:r'.plot'
if (! -e $fnm) then
    echo
    echo 'This is not a valid file'
    goto morefile
endif
echo
/usr/local/scripts/adinaplot4_0 $fnm:r
```

# **HIGH HEAT EFFECTS RESULTING FROM AUXILIARY PROPULSION UNIT**

**BY**

**Chip Summey**

## SUMMER RESEARCH ESSAY

This summer was my first experience working with the Air Force Research and Development Laboratories. I was stationed at Tyndall Air Force Base in Panama City, Florida. Captain Charles Manzione was my head mentor, although my direct mentor who signed my time sheets was Mr. Jim Murfee. The first three or four weeks I was there, I worked with Bill Dass in ARA (Applied Research Associates). There I worked directly in the lab under the supervision of Avery Adcock, the lab manager. While working in the lab, I learned basic civil engineering techniques like sieve analysis and gyratory anylasis. I even had the opportunity to run a few triaxial compression tests in Tyndall's materials testing room.

During the fourth week of my employment, I moved to a different branch, working directly for Mr. Murfee. Dr. Michael McVay, a civil engineering professor from the University of Florida, was working on a summer project dealing with the high heat effects resulting from Auxillary Propulsion Unit (APU) engines operating on jet aircraft concrete parking aprons. An APU engine is the small jet engine (mounted perpendicular to the concrete) used to start the main jet engine. The APU engine runs for five minutes or more. The heat from this engine turns the water in the concrete into superheated steam which cannot escape, thus, causing the concrete to spall like popcorn. My job in this assignment was to assist Captain Sean Childress in modeling this effect on an SGI Iris Workstation. To accomplish this I learned to use both Fortran and the "IDEAS" modeling software.

Participating in this summer research program was probably as beneficial to my education as the whole previous year at high school. Thank you for the opportunity you gave me through this program.

Chip Summey

**AMY THOMAS**

REPORT NOT AVAILABLE  
AT TIME OF  
PUBLICATION